NASA TECHNICAL MEMORANDUM

NASA TM X-3460

NASA TM X-3460



# EFFECT OF WING FLEXIBILITY ON THE EXPERIMENTAL AERODYNAMIC CHARACTERISTICS OF AN OBLIQUE WING

*Edward J. Hopkins and Sam C. Yee*

*Ames Research Center*

*Moffett Field, Calif. 94035*

NATIONAL AERONAUTICS AND SPACE ADMINISTRATION · WASHINGTON, D. C. · MARCH 1977

| 1. Report No. | 2. Government Accession No. | 3. Recipient's Catalog No. |
|---|---|---|
| NASA TM X-3460 | | |

| 4. Title and Subtitle | 5. Report Date |
|---|---|
| EFFECT OF WING FLEXIBILITY ON THE EXPERIMENTAL AERODYNAMIC CHARACTERISTICS OF AN OBLIQUE WING | March 1977 |
| | 6. Performing Organization Code |

| 7. Author(s) | 8. Performing Organization Report No. |
|---|---|
| Edward J. Hopkins and Sam C. Yee* | A-6736 |
| | 10. Work Unit No. |
| 9. Performing Organization Name and Address | 505-11-12 |
| Ames Research Center<br>Moffett Field, Calif. 94035 | 11. Contract or Grant No. |
| | 13. Type of Report and Period Covered |
| 12. Sponsoring Agency Name and Address | Technical Memorandum |
| National Aeronautics and Space Administration<br>Washington, D.C. 20546 | 14. Sponsoring Agency Code |

15. Supplementary Notes

*Project Engineer, ARO, Inc., Moffett Field, Calif. 94035

16. Abstract

A solid-aluminum oblique wing was designed to deflect considerably under load so as to relieve the asymmetric spanwise stalling that is characteristic of this type of wing by creating washout on the trailing wing panel and washin on the leading wing panel. Experimental forces, and pitching, rolling and yawing moments were measured with the wing mounted on a body of revolution. In order to vary the dynamic pressure, measurements were made at several unit Reynolds numbers ranging from $3.3 \times 10^6$/m to $8.2 \times 10^6$/m, and at Mach numbers ranging from 0.25 to 2.0. The wing was investigated when unswept (at subsonic Mach numbers only) and when swept 45°, 50°, 55°, and 60°. The wing was straight tapered in planform, had an aspect ratio of 7.9 (based on the unswept span) and a profile with a maximum thickness of 4 percent chord.

For the design Mach number of 0.95 and the design dynamic pressure of $15 \times 10^3$ N/m$^2$, the pitching- and rolling-moment curves were considerably more linear than at a dynamic pressure of about half the design value. This result substantiates the concept that an oblique wing designed with the proper amount of flexibility can "self relieve" itself of asymmetric spanwise stalling and the associated nonlinear moment curves.

| 17. Key Words (Suggested by Author(s)) | 18. Distribution Statement |
|---|---|
| Wings, oblique<br>Wing flexibility<br>Wings, flow separation | Unlimited<br><br>STAR Category – 08 |

| 19. Security Classif. (of this report) | 20. Security Classif. (of this page) | 21. No. of Pages | 22. Price* |
|---|---|---|---|
| Unclassified | Unclassified | 226 | $7.50 |

*For sale by the National Technical Information Service, Springfield, Virginia 22161

## NOMENCLATURE

The axes systems and sign conventions are presented in figure 1. Lift, drag, and pitching moments are presented about the stability axes system; the side force, rolling moments, and yawing moments are presented about the body axes system. Reference lengths and wing area are given in table 1.

| | |
|---|---|
| $b$ | wing span ($\Lambda = 45°$) |
| $C_D$ | drag coefficient, $\frac{\text{drag}}{qS}$ |
| $C_L$ | lift coefficient, $\frac{\text{lift}}{qS}$ |
| $C_l$ | rolling-moment coefficient, $\frac{\text{rolling moment}}{qSb}$ |
| $C_m$ | pitching-moment coefficient about moment center shown in figure 2, $\frac{\text{pitching moment}}{qS\bar{c}}$ |
| $C_n$ | yawing-moment coefficient, $\frac{\text{yawing moment}}{qSb}$ |
| $Cy$ | side-force coefficient, $\frac{\text{side force}}{qS}$ |
| $c$ | wing chord ($\Lambda = 0$) |
| $c_{\text{root}}$ | root chord ($\Lambda = 0$) |
| $\bar{c}$ | mean aerodynamic chord |
| $L/D$ | lift-to-drag ratio |
| $M$ | Mach number |
| $q$, $Q$ | free-stream dynamic pressure, $N/m^2$ |
| $r$ | body radius |
| $RN/L$ | unit Reynolds number in million per meter |
| $S$ | wing area |
| $(t/c)_{\text{MAX}}$ | maximum wing thickness-to-chord ratio |
| $x$ | chordwise distance along airfoil |
| $x_1$ | axial distance along body from the 57.45 cm longitudinal station |

$x_2, y_1, y_2$ coordinates to define the wing tip (see fig. 2(b))

$z$ vertical distance from the chord plane of the airfoil

$\alpha$ angle of attack, deg

$\Lambda$ sweep angle between a perpendicular to the body axis and the $0.25c$ line of the wing measured in a horizontal plane (right wing tip is forward for positive $\Lambda$'s), deg

# OF WING FLEXIBILITY ON THE EXPERIMENTAL AERODYNAMIC CHARACTERISTICS OF AN OBLIQUE WING

Edward J. Hopkins and Sam C. Yee*

Ames Research Center

## SUMMARY

A solid-aluminum oblique wing was designed to deflect considerably under load so as to relieve the asymmetric spanwise stalling that is characteristic of this type of wing by creating washout on the trailing wing panel and washin on the leading wing panel. Experimental forces, and pitching, rolling and yawing moments were measured with the wing mounted on a body of revolution. In order to vary the dynamic pressure, measurements were made at several unit Reynolds numbers ranging from $3.3\times10^6$/m to $8.2\times10^6$/m, and at Mach numbers ranging from 0.25 to 2.0. The wing was investigated when unswept (at subsonic Mach numbers only) and when swept 45°, 50°, 55°, and 60°. The wing was straight tapered in planform, had an aspect ratio of 7.9 (based on the unswept span) and a profile with a maximum thickness of 4 percent chord.

For the design Mach number of 0.95 and the design dynamic pressure of $15\times10^3$ N/m$^2$, the pitching- and rolling-moment curves were considerably more linear than at a dynamic pressure of about half the design value. This result substantiates the concept that an oblique wing designed with the proper amount of flexibility can "self relieve" itself of asymmetric spanwise stalling and the associated nonlinear moment curves.

## INTRODUCTION

The use of oblique wings on highly maneuverable aircraft (such as military fighters) to improve the aerodynamic efficiency (lift-to-drag ratio) at transonic Mach numbers over that of conventional swept wing designs was experimentally proven in reference 2. Unfortunately, planar oblique wings have the characteristic of developing an asymmetric spanwise distribution of section lift coefficient with a change in angle of attack that leads to asymmetric spanwise stalling of the wing panels and nonlinear pitching-, rolling-, and yawing-moment curves. One method of correcting this deficiency is to bend the wing panels upward to obtain a more nearly symmetrical spanwise distribution of maximum section lift coefficients. In reference 3 it was shown that an impractical wing pivot located near the wing trailing edge is required to trim the rolling and yawing moments induced by wing bending at low lift. For this reason, an alternate method of correcting the asymmetric spanwise wing stall by use of Krüger nose flaps on the downstream wing panel was investigated in reference 4. These Krüger nose flaps were found to provide considerably more linear moment curves, but their use would incur some complexity of operation.

---

*Project Engineer, ARO, Inc., Moffett Field, Calif. 94035

The present investigation was undertaken to explore the possibility of designing an oblique wing with the required amount of flexibility for a specified flight condition so that the deflection of the wing panels would produce a more symmetrical spanwise distribution of section lift coefficients. It was reasoned that if an oblique wing were designed with this proper amount of flexibility for a given lift coefficient that the "self relieving" effect would produce a more symmetrical spanwise wing stall and nearly linear moment curves below this design lift coefficient. Therefore, an aluminum oblique wing was designed with an aspect ratio of 7.9 and a very thin profile (4 percent chord in maximum thickness) to obtain the necessary flexibility. The design point was chosen to correspond to a dynamic pressure of $15 \times 10^3$ N/m$^2$ (or a unit Reynolds number of $6.2 \times 10^6$/m) at a Mach number of 0.95 with the model at an angle of attack of 10°. The matrix-panel method described in reference 2 was used with standard strength-of-material and deflection equations to analyze the wing. Viscosity was not considered in the analysis.

In addition to the design unit Reynolds number of $6.2 \times 10^6$/m, the model was investigated experimentally at unit Reynolds numbers of 3.3, 4.5, and $8.2 \times 10^6$/m throughout a Mach number range from 0.25 to 2.0. Although the main emphasis was related to the determination of the linearity of the pitching-, rolling-, and yawing-moment curves at various dynamic pressures, lift, drag, and side-force results are also presented.

## CONFIGURATION CODE

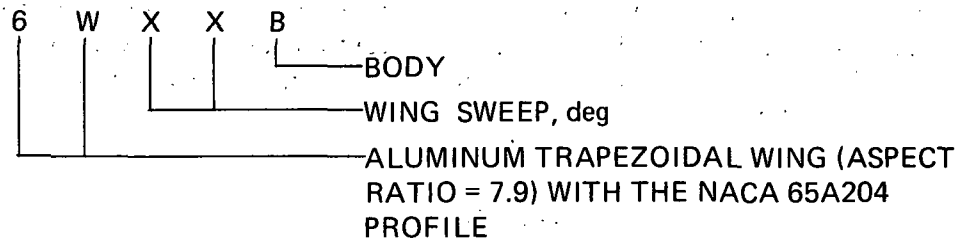


## TEST FACILITY

The Ames 6- by 6-Foot Wind Tunnel is a variable pressure, continuous flow, closed return-type facility. The nozzle ahead of the test section consists of an asymmetric sliding block which permits a continuous variation of Mach number from 0.25 to 2.3. The test section has a perforated floor and ceiling for boundary-layer removal to permit transonic testing.

## MODEL DESCRIPTION

The model consisted of an oblique wing mounted on top of a Sears-Haack body of revolution designed to have minimum wave drag for a given length and volume. With different fairing blocks installed under the wing, the wing could be swept 0°, 45°, 50°, 55°, and 60° (fig. 2(a)). Dimensional details of the body and of the fairing blocks are given in table 3 of reference 1. The wing had

an aspect ratio of 7.9 and straight leading and trailing edges with modified elliptical wing tips (fig. 2(b)). The NACA 65A204 profile shown in figure 2(c) was used along the wing span perpendicular to the 0.25$c$ line. Coordinates for this profile are given in table 2. A planform with straight edges was chosen to approximate the optimum planform for a given area and root bending moment as given by R. T. Jones in reference 5. The wing area was the same as for the elliptical oblique wing (aspect ratio 6), but the wing span was 15 percent greater than that of the elliptical wing in accordance with the Jones concept. The manner in which the straight-tapered planform was derived from the Jones optimum planform and the manner in which latter planform was derived from the elliptical planform are shown in figure 2(d). The wing was made of solid 2024-T3 aluminum and the body was made of stainless steel. The aluminum had an ultimate strength of $49 \times 10^6$ kg/m$^2$, a yield strength of $35 \times 10^6$ kg/m$^2$, and a modulus of elasticity of $7.5 \times 10^9$ kg/m$^2$.

## DATA REDUCTION AND TEST PROCEDURE

The model was sting-supported through the base of the model on a six-component electrical strain-gage balance (fig. 3). Measured axial forces were corrected to a condition corresponding to that of having the free-stream static pressure on the base of the model. Moment data are presented about a center located on the body axis at $0.4c_{root}$ ($\Lambda = 0$) (see fig. 2(a)). Reference lengths and the wing area used in the reduction of the data are given in table 1.

Boundary-layer transition strips (0.1905 cm wide), consisting of a random distribution of glass spheres 0.01905 cm in diameter, were placed on the upper and lower surface of the wing at distances 0.762 cm downstream of the wing leading edge and on the body 2.54 cm behind its tip. Sublimation studies made on the elliptical oblique wing (ref. 1) at wing sweep angles of 0° and 45° indicate that the boundary layer was tripped by the glass spheres near the roughness strips at $\alpha = 0°$ and 10°. Estimates of the required size of roughness strip at other sweep angles and Mach numbers indicate that the chosen size should be adequate.

With the oblique wing swept 45°, 50°, 55°, or 60°, data were generally obtained at Mach numbers of 0.25, 0.4, 0.6, 0.8, 0.9, 0.95, 1.1, 1.2, 1.6, and 2.0. With the oblique wing unswept, data were obtained at only the subsonic Mach numbers. For most Mach numbers, the unit Reynolds numbers covered were as follows: $3.3 \times 10^6$/m, $4.6 \times 10^6$/m, $6.2 \times 10^6$/m, and $8.2 \times 10^6$/m. The angle-of-attack range covered was from −3° to 22°; however, at no time was the product of the lift coefficient and the dynamic pressure allowed to exceed $15 \times 10^3$ N/m$^2$, the design criterion of the model corresponding to an assumed factor of safety of two. For some model and flow conditions the wing tip fluttered so that the angle-of-attack range was restricted and the design criterion was not reached. However, at lift coefficients below this design point, the moment curves should still reflect an improvement in their linearity due to wing flexibility. Angle of attack was indicated by an electrical dangleometer mounted in the support located downstream of the sting. Corrections were applied to the indicated angle of attack for balance and sting deflections.

## RESULTS AND DISCUSSION

The lift, pitching moments, drag, rolling moments, yawing moments, and side force are presented for the oblique wing at various angles of sweep at various Mach numbers in figures 4 through 43. An index of the data figures is presented in table 3. In each figure, to determine the effects of free-stream dynamic pressure changes on the aerodynamic characteristics, data are presented for the following four unit Reynolds numbers: $3.3\times10^6$/m, $4.6\times10^6$/m, $6.2\times10^6$/m, and $8.2\times10^6$/m. For this investigation, the main effects expected on the data are related to the deflection of the wing panels from dynamic-pressure changes, the expected Reynolds-number effects on the boundary layer (corresponding to the dynamic-pressure changes) being minimal. For this reason, the dynamic pressures ($Q$) in N/m$^2$ and the corresponding unit Reynolds numbers per meter are presented on each figure. Design conditions used in the calculations from the matrix-panel method described in reference 2 correspond to having a free-stream dynamic pressure of $15\times10^3$ N/m$^2$ at a Mach number of 0.95. Calculations indicated that the spanwise distribution of section lift coefficient when the wing was deflected under load was essentially independent of angle-of-attack changes, except at very small angles of attack. No viscous effects were accounted for in the calculations and only one iteration on the loading change due to wing deflection was made; therefore, the optimum design conditions will be somewhat different from those chosen but are bracketed by the free-stream dynamic pressures above and below the design dynamic pressure. At the design conditions and at a lift coefficient of 1.0, the maximum calculated bending stress, which occurs near the wing root, is about $16.9\times10^6$ kg/m$^2$.

For the design flow conditions at a Mach number of 0.95 (dynamic pressure of $15\times10^3$ N/m$^2$ in fig. 9), it can be seen that the pitching- and rolling-moment curves are considerably more linear up to a $C_L \cong 0.6$ than for the lowest dynamic pressure, a flow condition that approximates that for the rigid wing most closely. For the lowest dynamic pressure, the fact that nonlinearities occur in the pitching- and rolling-moment curves above a $C_L \cong 0.3$ is probably related to the thinness of the airfoil section (the NACA 65A204) chosen to produce the required wing flexibility. The elliptical oblique wing previously investigated (ref. 2) had a Garabedian airfoil designed for a section lift coefficient of 1.3, was highly cambered, and had an average thickness across the span of about 10 percent chord. The latter wing did not exhibit nonlinearities in the moment curves until a $C_L \cong 0.7$ was attained. It might be reasoned, therefore, that a wing with a thicker, more highly cambered, profile could be designed with considerable flexibility to provide a more nearly uniform spanwise distribution of section lift at much higher values of $C_L$. Such a design would probably result in more linear moment curves over a much wider lift-coefficient range. The slight negative slopes of the rolling-moment and side-force curves can be reduced by a slight rearward movement of the wing pivot.

## CONCLUDING REMARKS

It was demonstrated that the asymmetric spanwise distribution of section lift coefficient associated with oblique wings can be made more uniform and the pitching- and rolling-moment curves made more linear by the proper use of designed wing flexibility. For the design Mach number of 0.95 and the design dynamic pressure of $15\times10^3$ N/m$^2$, the moment curves were considerably

more linear than at a dynamic pressure half that of the design value; thus, the wing became "self relieving" of asymmetric spanwise stalling.

Ames Research Center
National Aeronautics and Space Administration
Moffett Field, Calif. 94035, August 30, 1976

## REFERENCES

1. Hopkins, Edward J.; Meriwether, Frank D.; and Pena, Douglas F.: Experimental Aerodynamic Characteristics of Low Aspect Ratio Swept and Oblique Wings at Mach Numbers Between 0.6 and 1.4. NASA TM X-62,317, 1973.

2. Hopkins, Edward J.; and Levin, Alan D.: Study of Low Aspect Ratio Swept and Oblique Wings. AIAA J. Aircraft, vol. 12, no. 8, 1975, pp. 648–652.

3. Hopkins, Edward J.: Effects of Wing Bend on the Aerodynamic Characteristics of a Low Aspect Ratio Oblique Wing. AIAA Preprint 75-995, AIAA Aircraft Systems and Technology Meeting, Los Angeles, Calif., Aug. 4–7, 1975.

4. Hopkins, Edward J.; and Lovette, George H.: Effect of Krüger Nose Flaps on the Experimental Force and Moment Characteristics of an Oblique Wing. NASA TM X-3372, 1976.

5. Jones, Robert T.: The Spanwise Distribution of Lift for Minimum Induced Drag of Wings Having a Given Lift and a Given Bending Moment. NACA TN 2249, 1950.

TABLE 1.– MODEL GEOMETRY, REFERENCE LENGTHS, AND AREAS

| | |
|---|---|
| **Body** | |
| Radius | $r = 3.856\{1 - [1 - (2x_1/114.91)]^2\}^{3/4}$, cm |
| Length | |
| Closed | 114.91 cm |
| Cutoff | 91.44 cm |
| Maximum diameter | 7.71 cm |
| **Wing** | |
| Span ($\Lambda = 0$) | 104.08 cm |
| Span (reference), $b$ | 74.80 cm |
| Area (reference), $S$ | 1365.09 $cm^2$ |
| Mean aerodynamic chord (reference), $\bar{c}$ | 21.62 cm |
| Aspect ratio ($\Lambda = 6$) | 7.9 |
| Aspect ratio ($\Lambda = 45°$) | 4.1 |
| Root chord | 22.51 cm |
| Tip chord (projected) | 3.81 cm |
| Taper ratio | 0.169 |
| Profile perpendicular to the 0.25$c$ line | NACA 65A204 (see table 2 and fig. 2(c)) |

TABLE 2.– COORDINATES FOR THE NACA 65A204 PROFILE

| *X/C* | *Z/C* | *X/C* | *Z/C* |
|---|---|---|---|
| 0 | 0 | 0 | 0 |
| .00040 | .00111 | .00060 | −.00096 |
| .00086 | .00160 | .00114 | −.00132 |
| .00133 | .00198 | .00167 | −.00158 |
| .00180 | .00231 | .00220 | −.00180 |
| .00228 | .00211 | .00272 | −.00199 |
| .00276 | .00287 | .00324 | −.00215 |
| .00324 | .00312 | .00376 | −.00229 |
| .00421 | .00356 | .00479 | −.00253 |
| .00519 | .00395 | .00581 | −.00273 |
| .00617 | .00431 | .00683 | −.00291 |
| .00716 | .00464 | .00784 | −.00306 |
| .00815 | .00496 | .00885 | −.00320 |
| .00914 | .00525 | .00986 | −.00333 |
| .01013 | .00554 | .01087 | −.00345 |
| .01112 | .00581 | .01188 | −.00356 |
| .01212 | .00607 | .01288 | −.00366 |
| .01958 | .00776 | .02042 | −.00423 |
| .02456 | .00871 | .02544 | −.00449 |
| .02955 | .00956 | .03045 | −.00469 |
| .03454 | .01033 | .03546 | −.00484 |
| .03953 | .01106 | .04047 | −.00497 |
| .04453 | .01174 | .04547 | −.00508 |
| .04952 | .01241 | .05048 | −.00519 |
| .05452 | .01305 | .05548 | −.00531 |
| .05951 | .01369 | .06049 | −.00542 |
| .06451 | .01431 | .06549 | −.00554 |
| .06951 | .01491 | .07049 | −.00566 |
| .07450 | .01549 | .07550 | −.00577 |
| .07950 | .01606 | .08050 | −.00587 |
| .08450 | .01660 | .08550 | −.00597 |
| .08950 | .01713 | .09050 | −.00605 |
| .09450 | .01764 | .09550 | −.00614 |
| .09950 | .01814 | .10050 | −.00622 |
| .14952 | .02243 | .15048 | −.00682 |
| .19956 | .02579 | .20044 | −.00719 |
| .24961 | .02841 | .25039 | −.00738 |
| .29968 | .03041 | .30033 | −.00744 |
| .34975 | .03185 | .35026 | −.00737 |
| .39982 | .03275 | .40018 | −.00717 |
| .44990 | .03309 | .45010 | −.00680 |
| .49998 | .03282 | .50002 | −.00622 |
| .55005 | .03193 | .54995 | −.00541 |
| .60012 | .03043 | .59988 | −.00440 |
| .65019 | .02839 | .64981 | −.00329 |
| .70024 | .02583 | .69976 | −.00217 |
| .75029 | .02273 | .75971 | −.00113 |
| .80035 | .01903 | .79965 | −.00034 |
| .85034 | .01453 | .84966 | −.00010 |
| .90024 | .00983 | .89976 | −.00002 |
| .95012 | .00491 | .94988 | −.00001 |
| 1.00000 | .00000 | 1.00000 | .00000 |

TABLE 3.– INDEX OF DATA FIGURES

| Figure | Mach number, $M$ | Sweep, $\Lambda$, deg |
|---|---|---|
| 4 | 0.25 | 45 |
| 5 | .4 | |
| 6 | .6 | |
| 7 | .8 | |
| 8 | .9 | |
| 9 | .95 | |
| 10 | 1.1 | |
| 11 | 1.2 | |
| 12 | 1.6 | |
| 13 | 2.0 | |
| 14 | .25 | 50 |
| 15 | .4 | |
| 16 | .6 | |
| 17 | .8 | |
| 18 | .9 | |
| 19 | .95 | |
| 20 | 1.1 | |
| 21 | 1.2 | |
| 22 | 1.6 | |
| 23 | 2.0 | |
| 24 | .4 | 55 |
| 25 | .6 | |
| 26 | .8 | |
| 27 | .9 | |
| 28 | .95 | |
| 29 | 1.1 | |
| 30 | 1.2 | |
| 31 | 1.6 | |
| 32 | 2.0 | |
| 33 | .25 | 60 |
| 34 | .4 | |
| 35 | .6 | |
| 36 | .8 | |
| 37 | .9 | |
| 38 | .95 | |
| 39 | 1.1 | |
| 40 | 1.2 | |
| 41 | 1.6 | |
| 42 | 2.0 | |
| 43 | 0.25–0.95 | 0 |

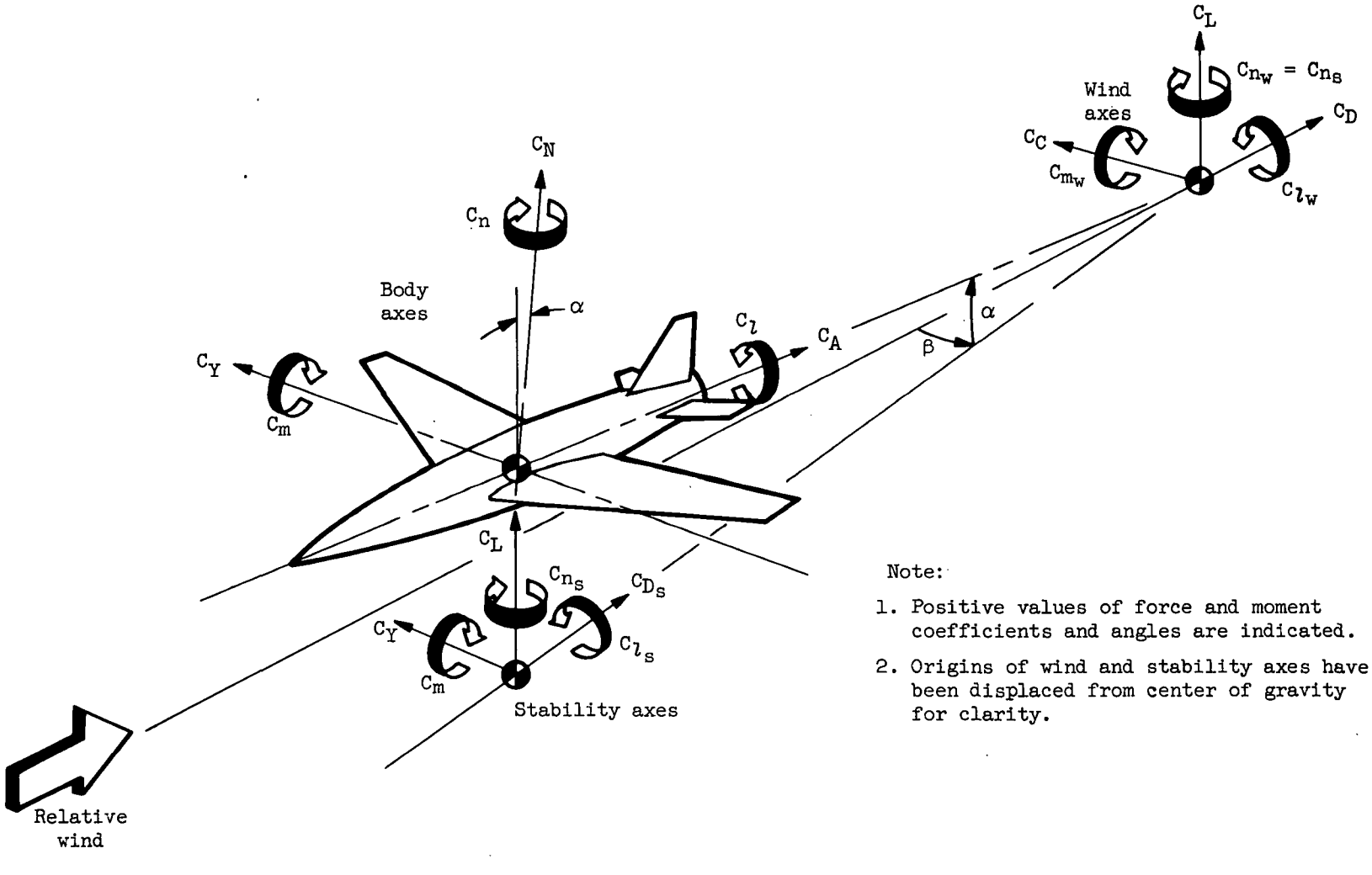


Figure 1.– Axes systems.

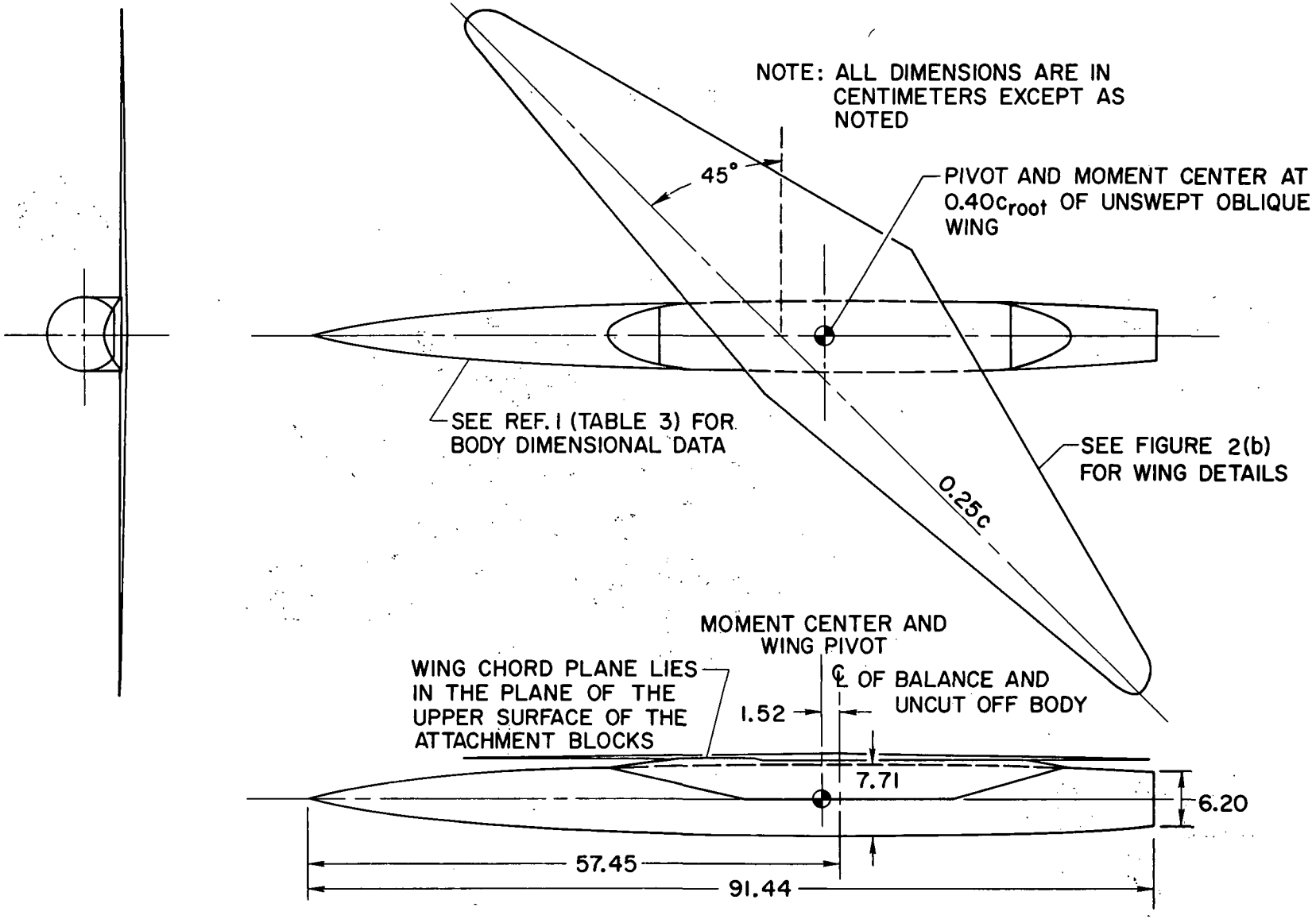


(a) Wing mounted on top of body.

Figure 2.– Trapezoidal oblique wing and body details.

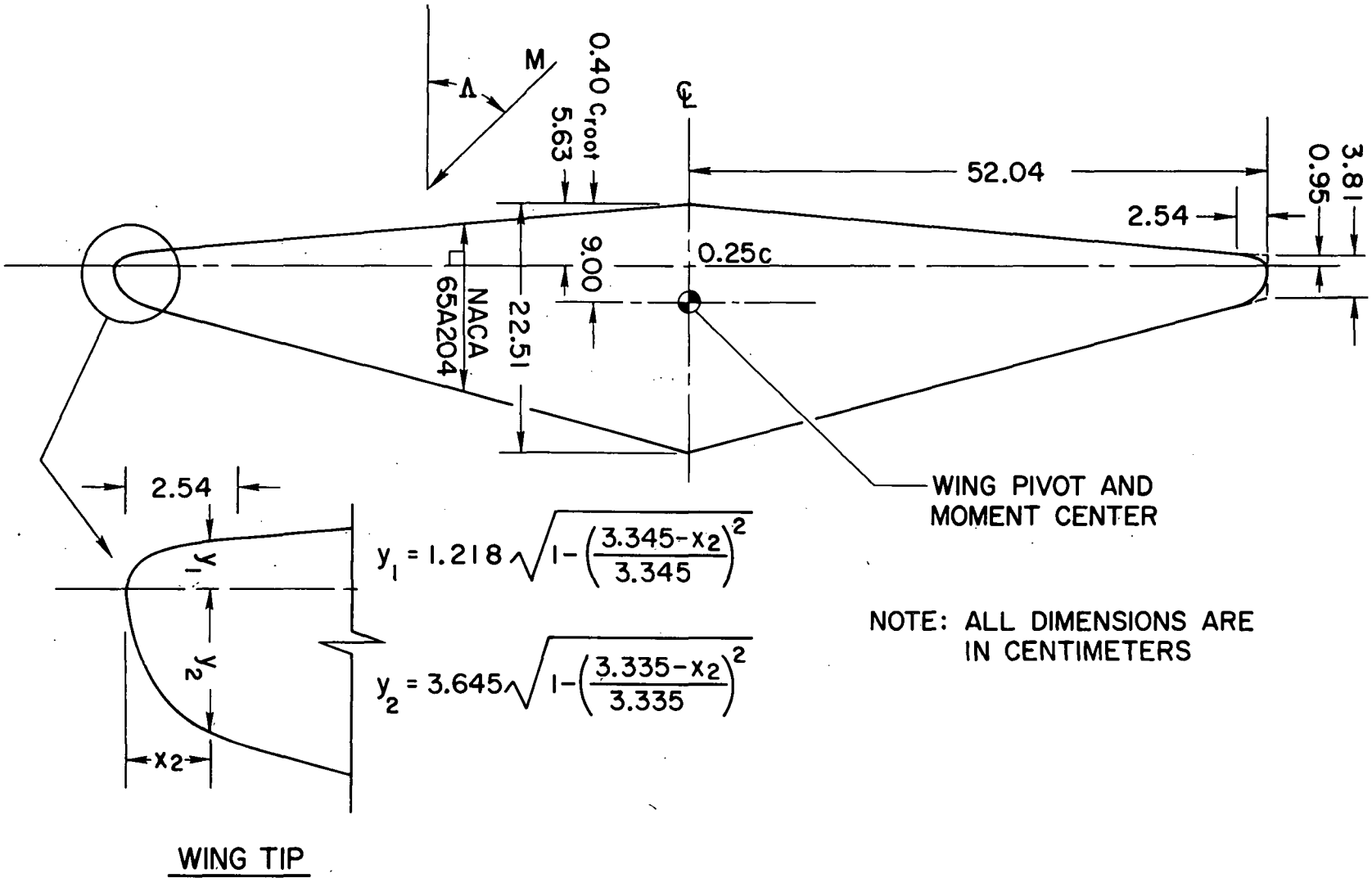


(b) Wing planform.

Figure 2.– Continued.

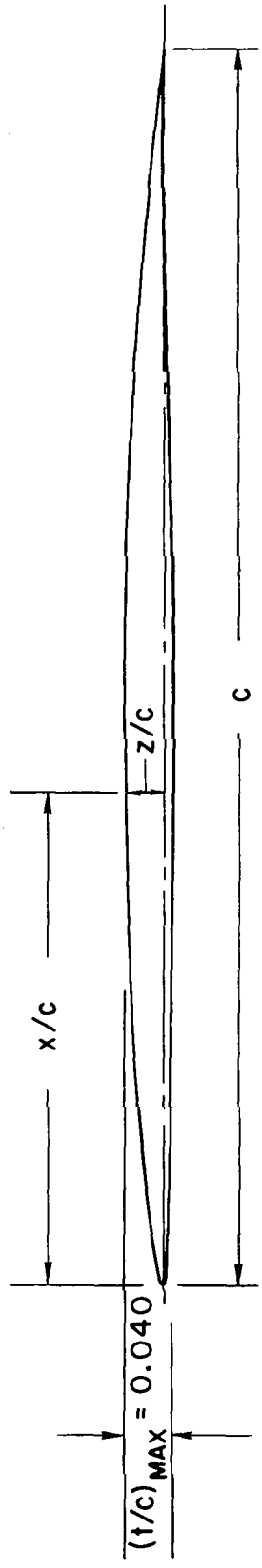


(c) NACA 65204 profile.

Figure 2.– Continued.

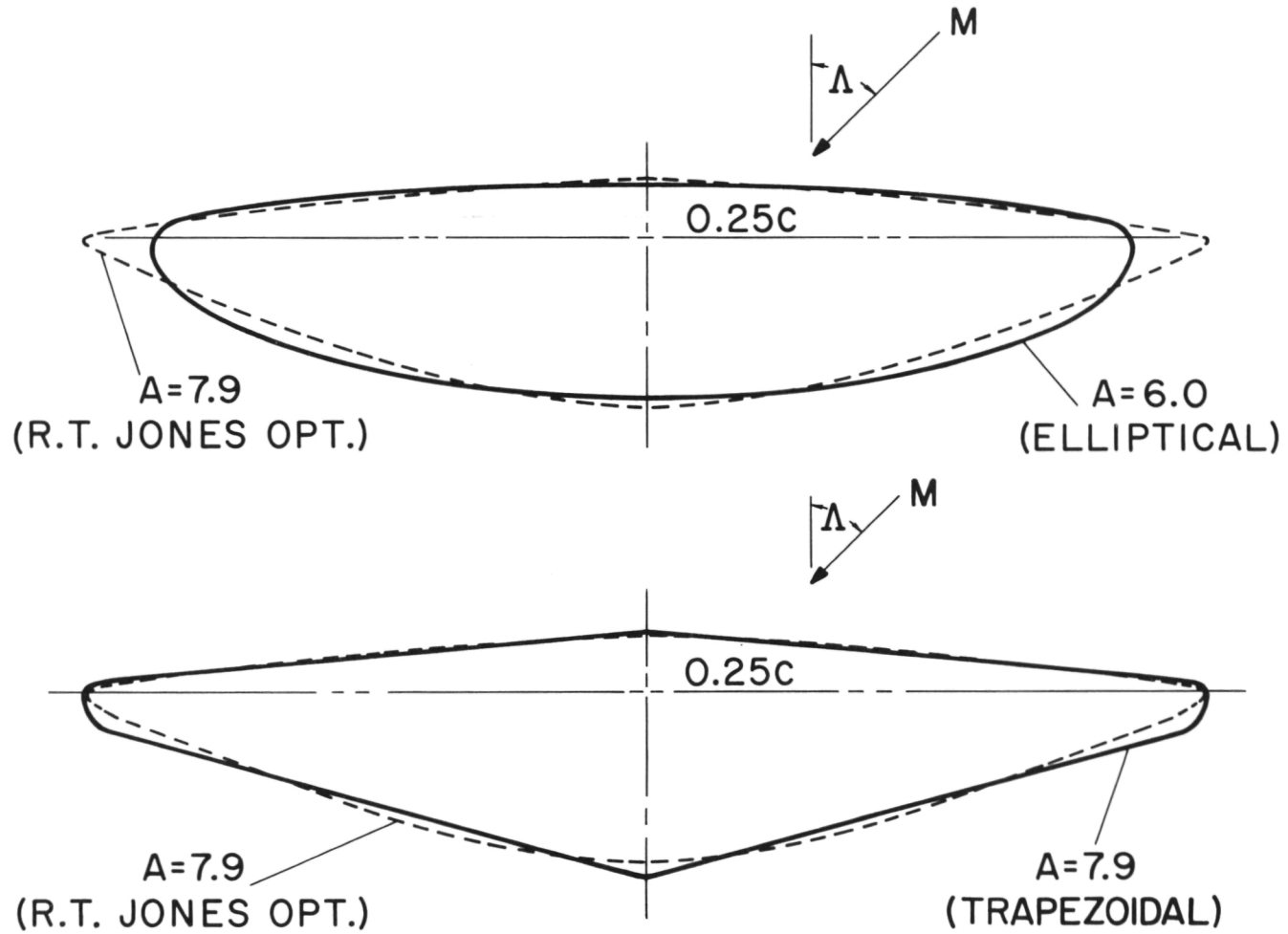


(d) Planform comparison.

Figure 2.– Concluded.

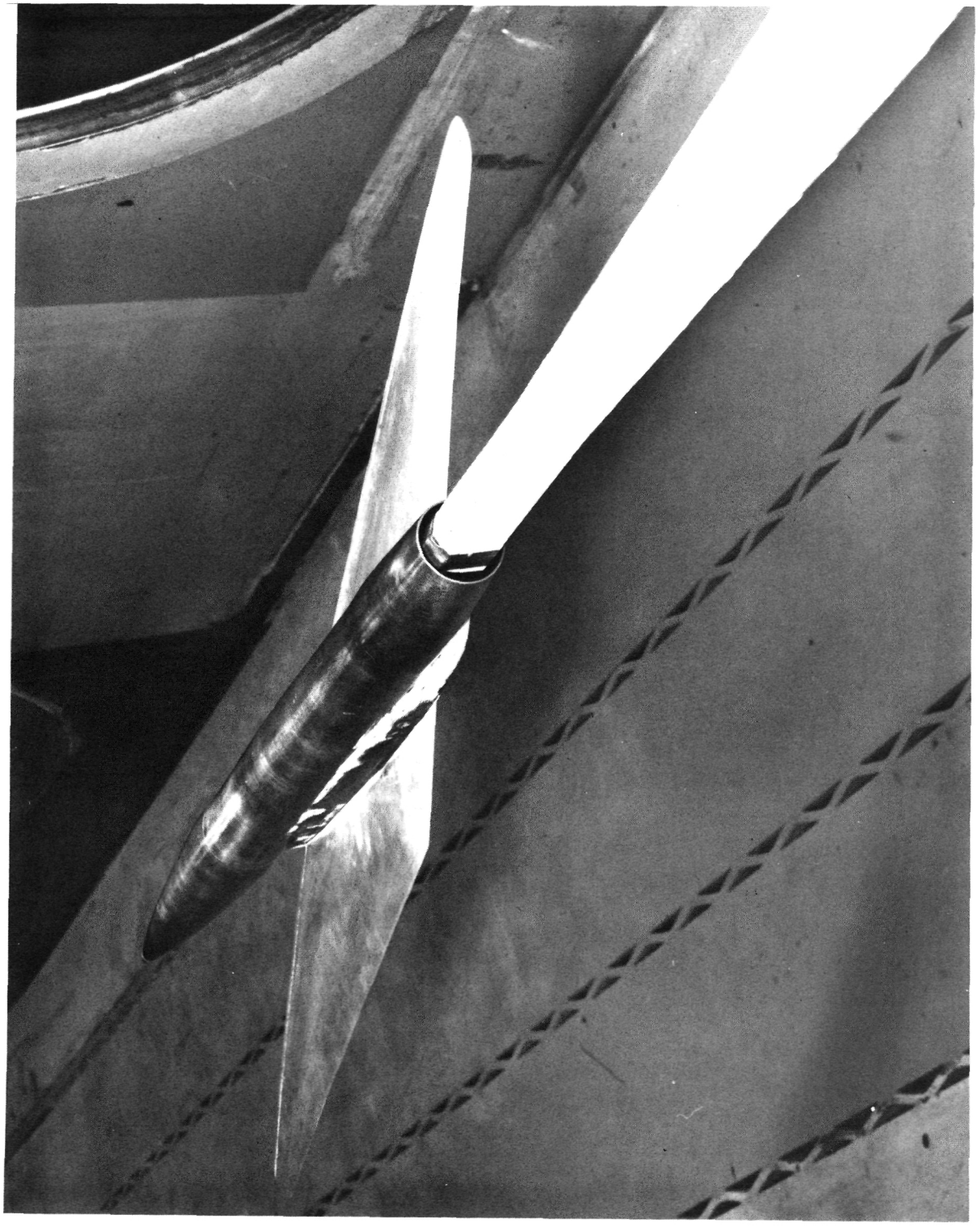

Figure 3.– Trapezoidal oblique wing mounted in the Ames 6- by 6-Foot Wind Tunnel.

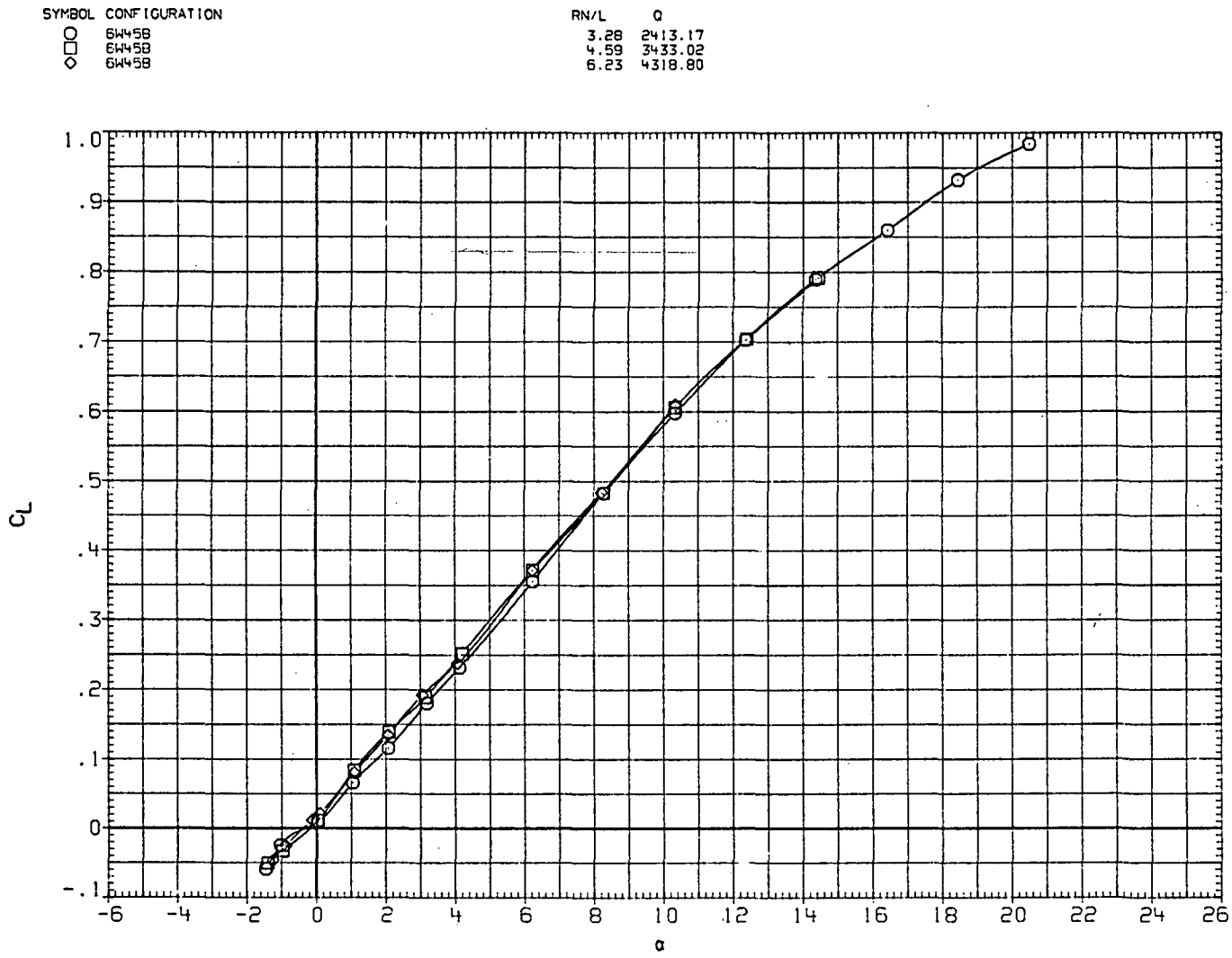


(a) $C_L$ vs $\alpha$

Figure 4.– Flexibility effects due to dynamic-pressure changes on the aerodynamic characteristics of the trapezoidal oblique wing: $\Lambda = 45°, M = 0.25$.

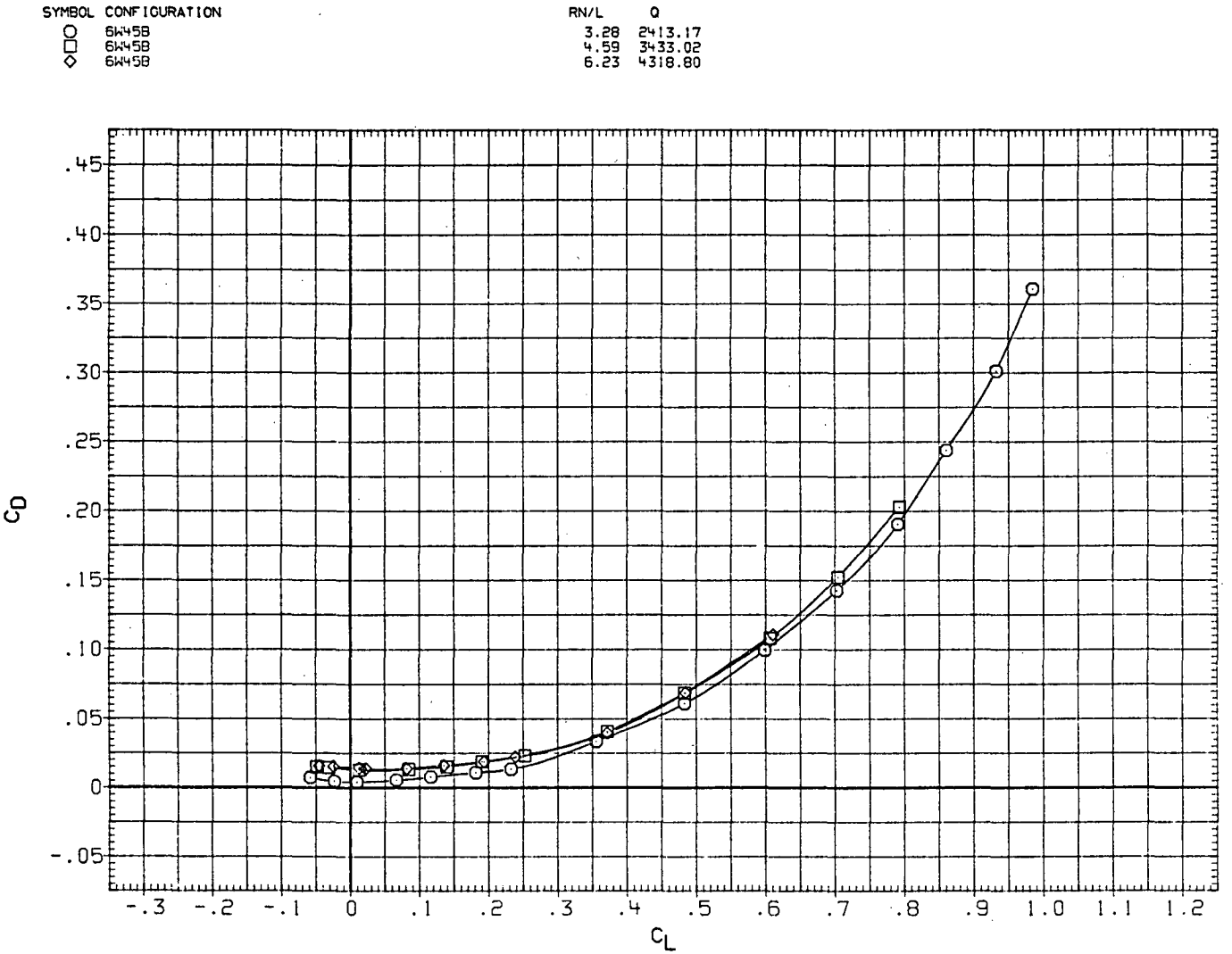


(b) $C_D$ vs $C_L$

Figure 4.– Continued.

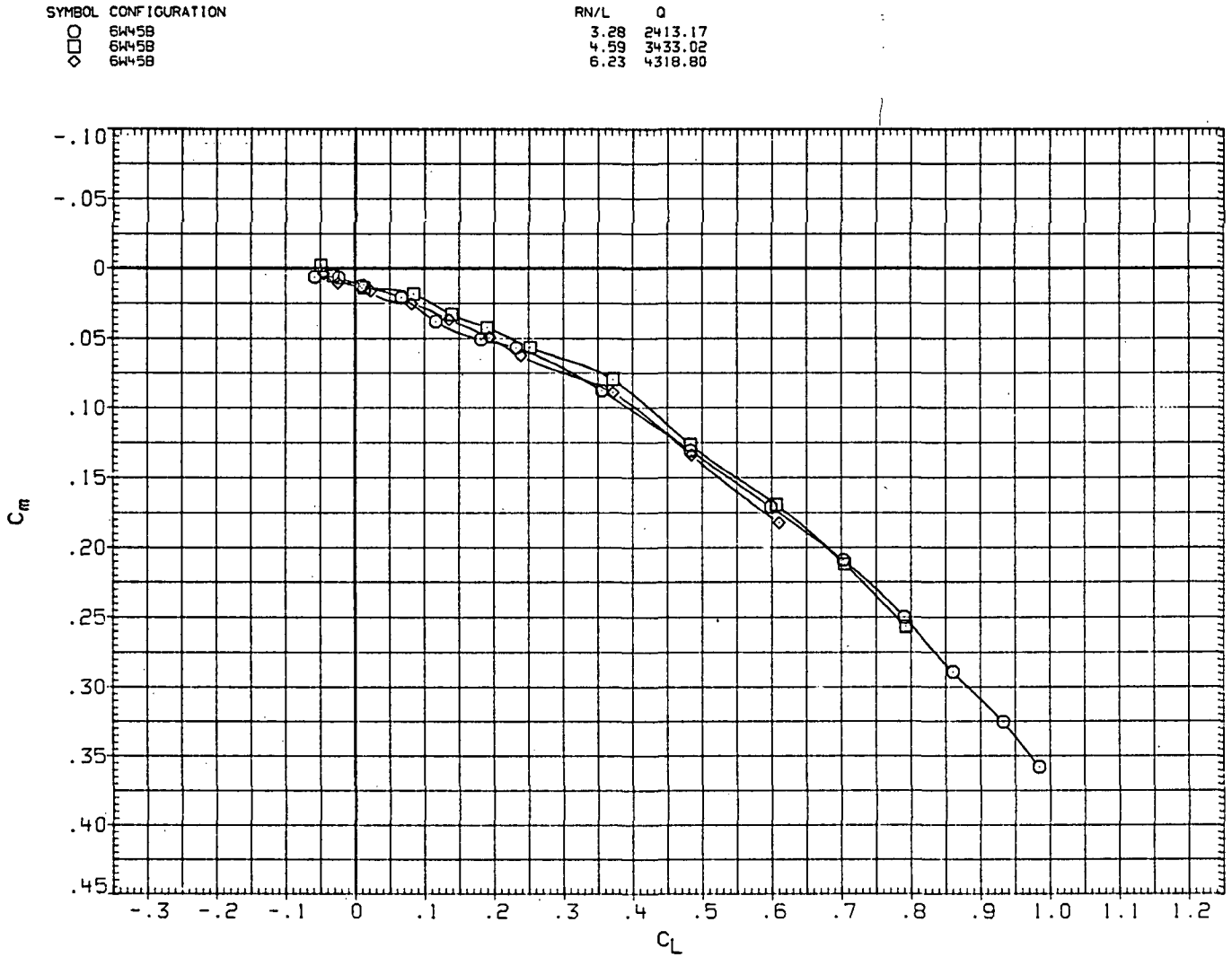


(c) $C_m$ vs $C_L$

Figure 4.– Continued.


(d) $L/D$ vs $C_L$

Figure 4.– Continued.

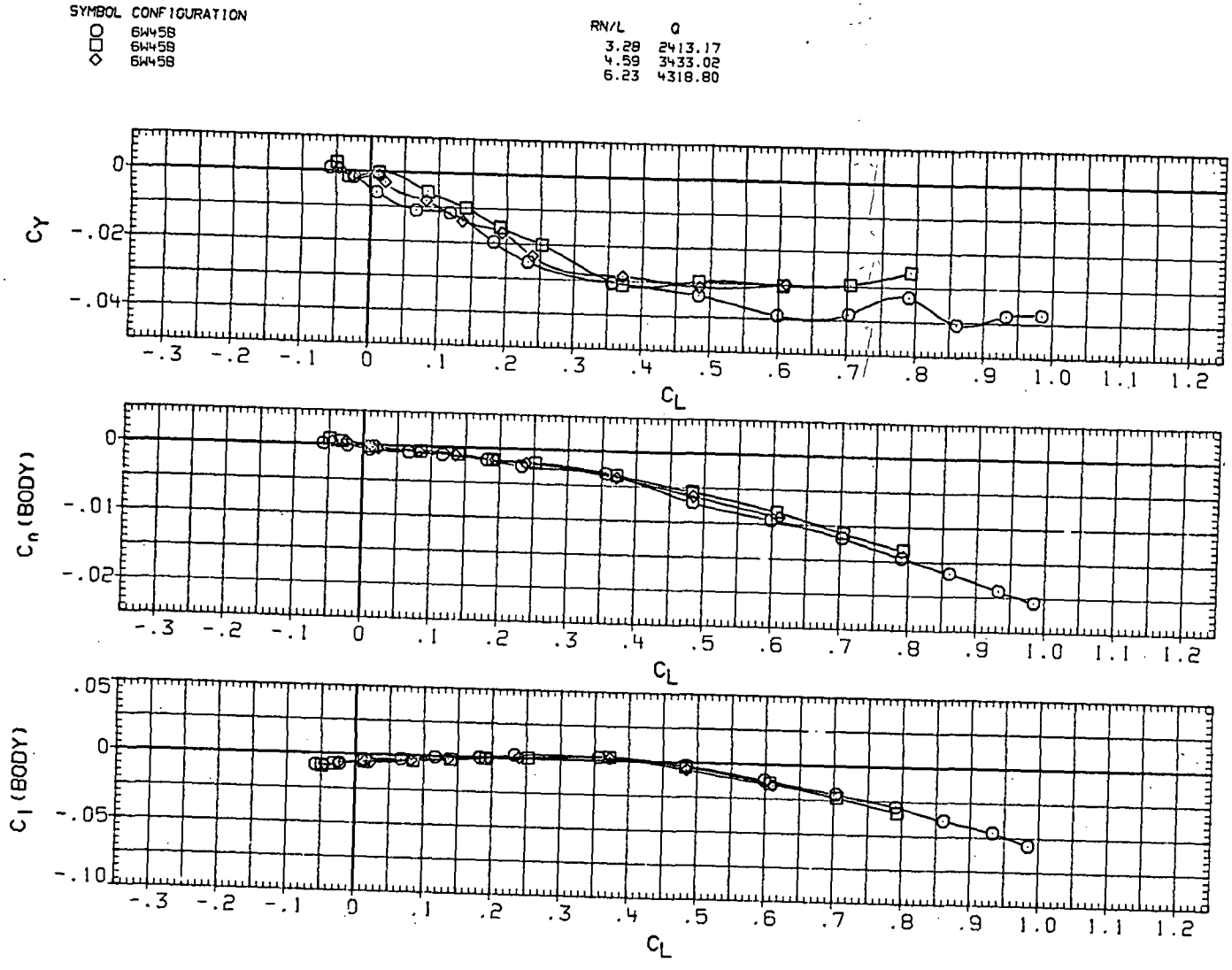


(e) $C_Y$, $C_n$, and $C_l$ vs $C_L$

Figure 4.– Concluded.

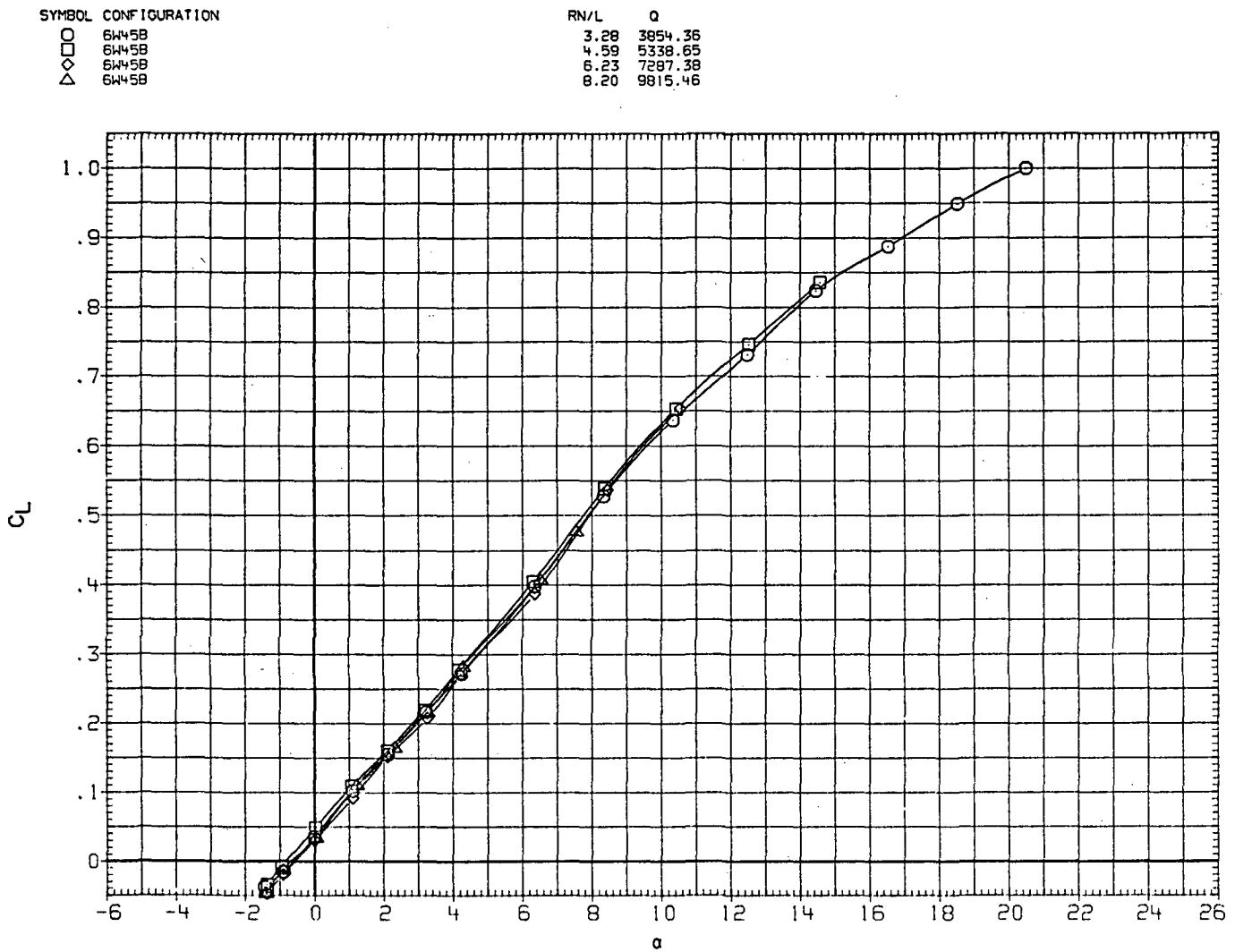


(a) $C_L$ vs $\alpha$

Figure 5.– Flexibility effects due to dynamic-pressure changes on the aerodynamic characteristics of the trapezoidal oblique wing: $\Lambda = 45°, M = 0.4$.

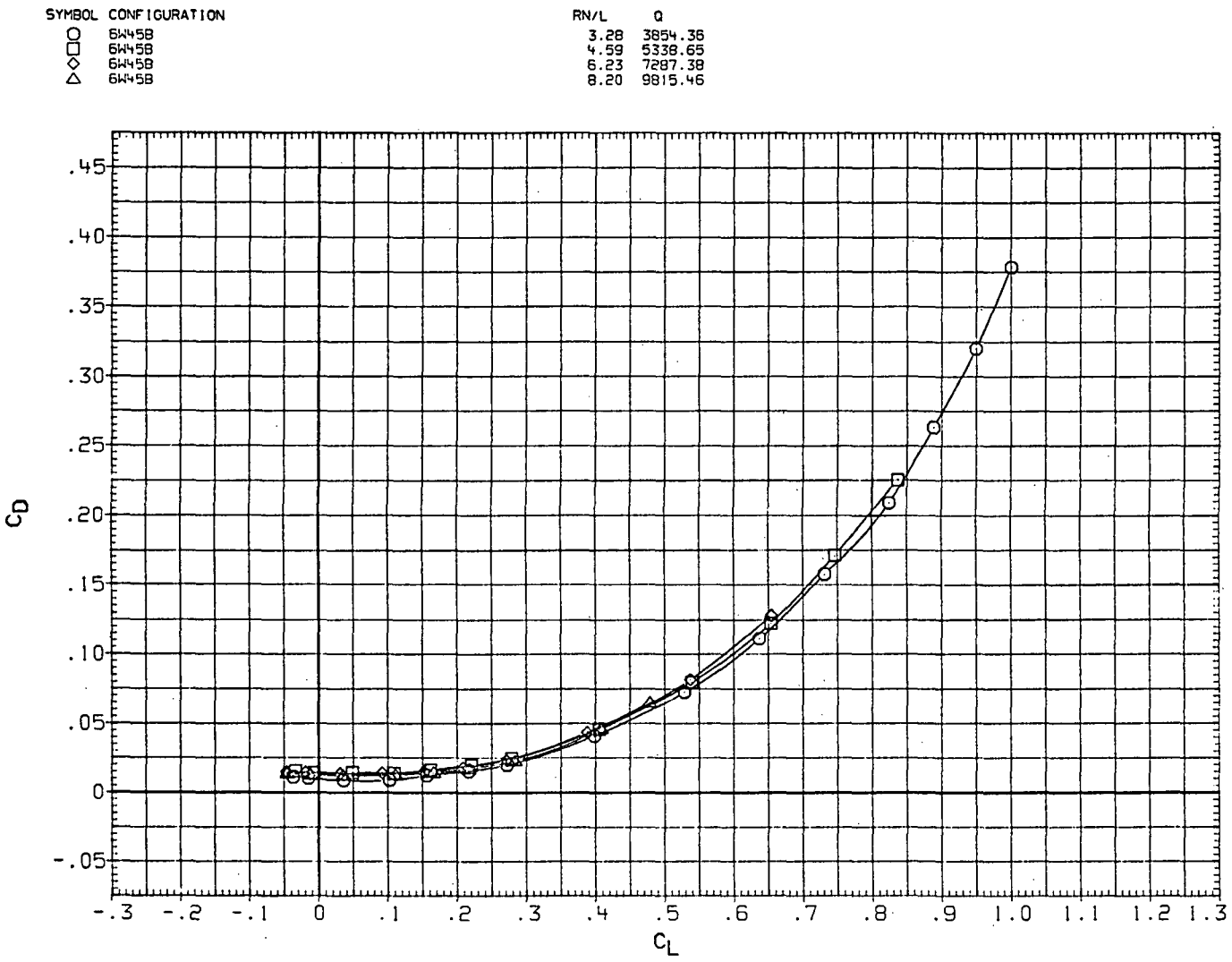


(b) $C_D$ vs $C_L$

Figure 5.– Continued.

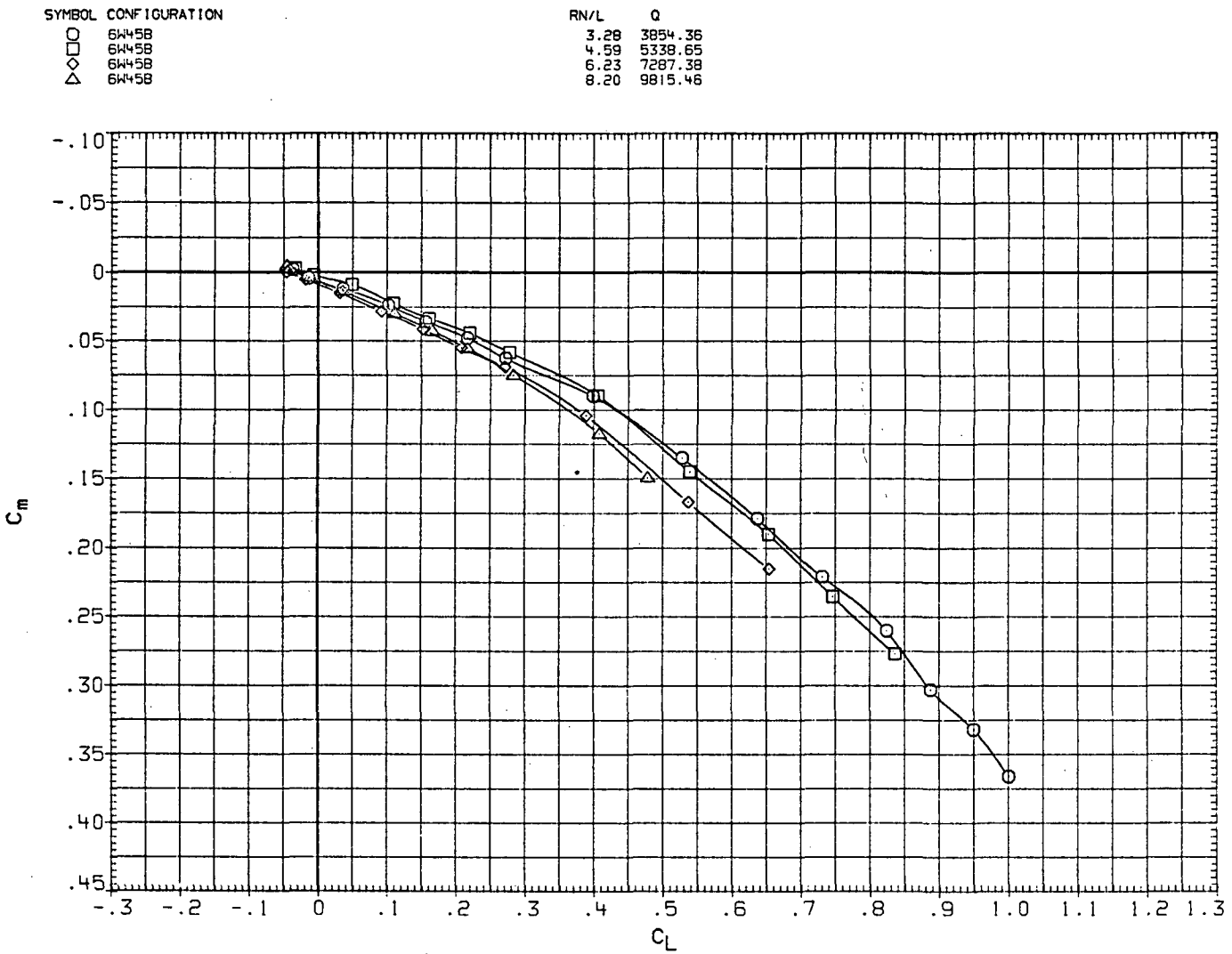


(c) $C_m$ vs $C_L$

Figure 5.– Continued.

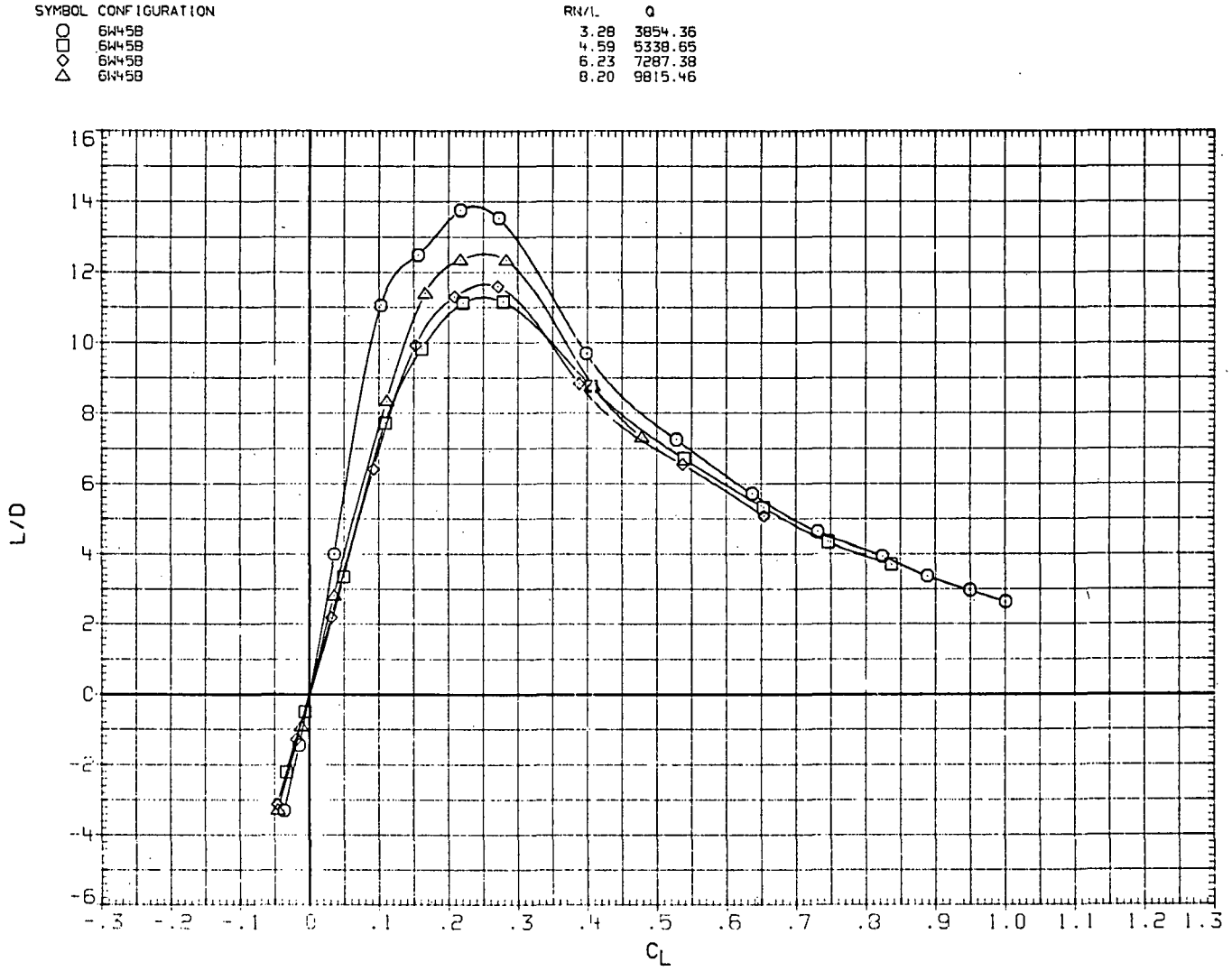


(d) $L/D$ vs $C_L$

Figure 5.– Continued.

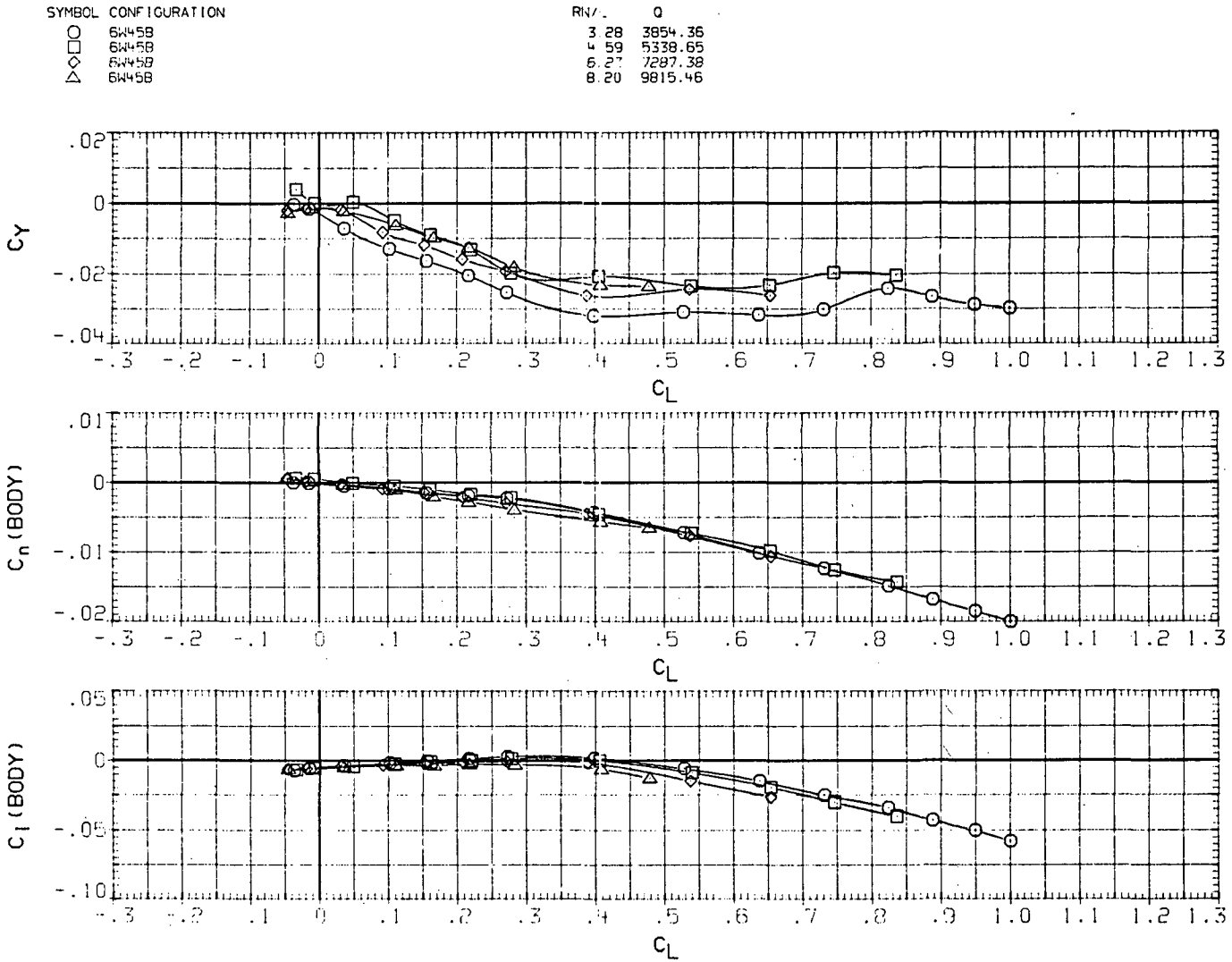


(e) $C_Y$, $C_n$, and $C_l$ vs $C_L$

Figure 5.– Concluded.

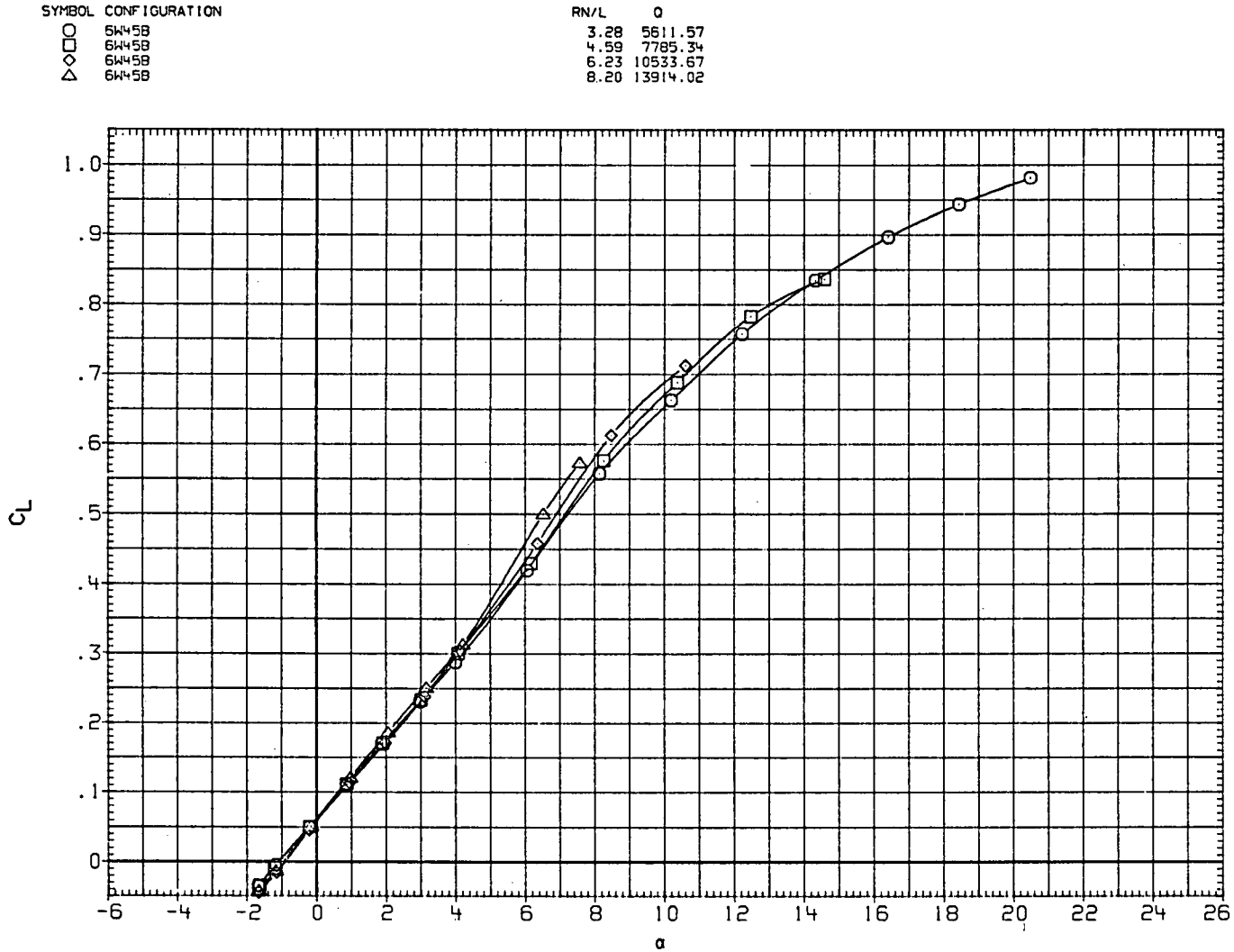


(a) $C_L$ vs $\alpha$

Figure 6.– Flexibility effects due to dynamic-pressure changes on the aerodynamic characteristics of the trapezoidal oblique wing: $\Lambda = 45°, M = 0.6$.

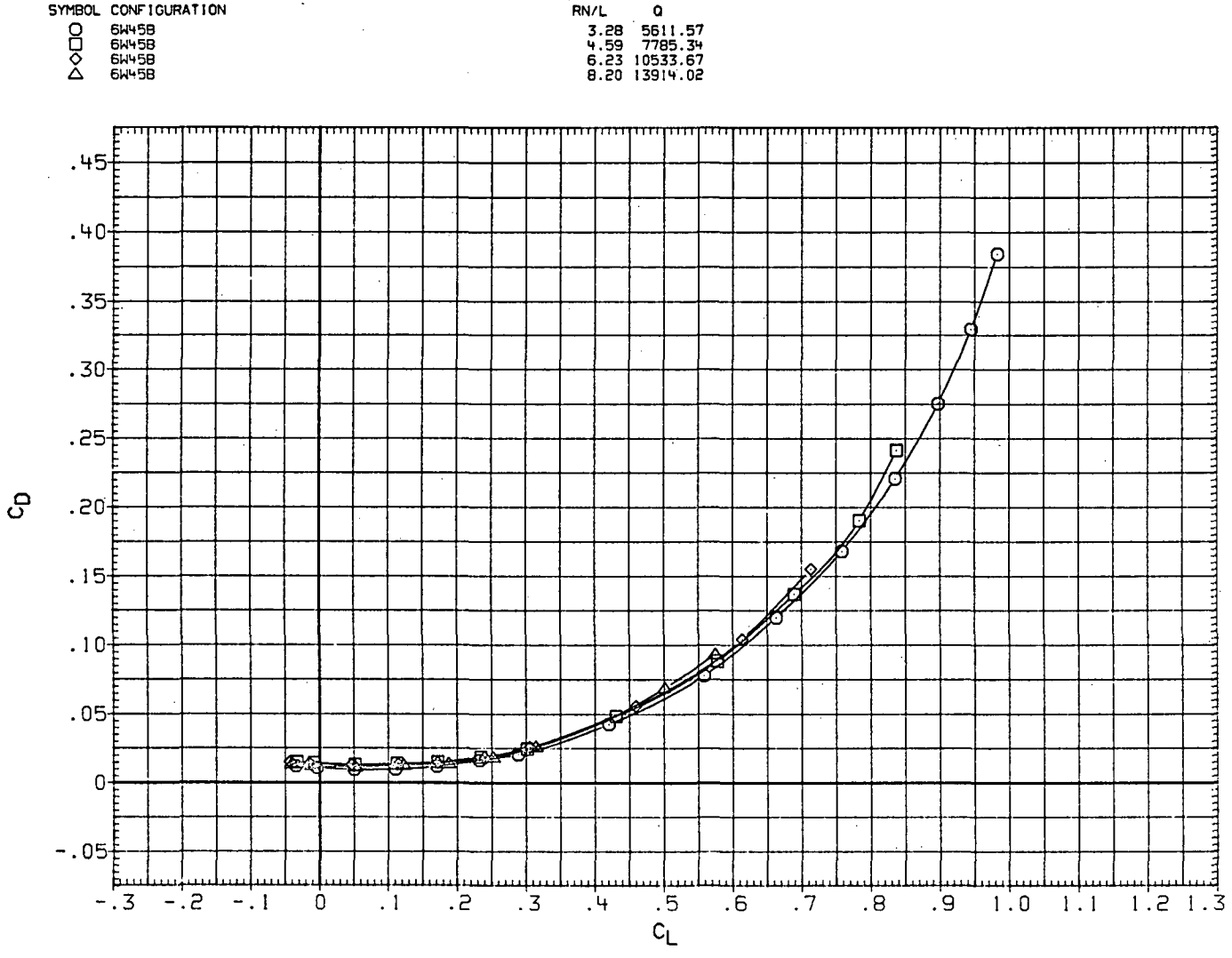


(b) $C_D$ vs $C_L$

Figure 6.– Continued.

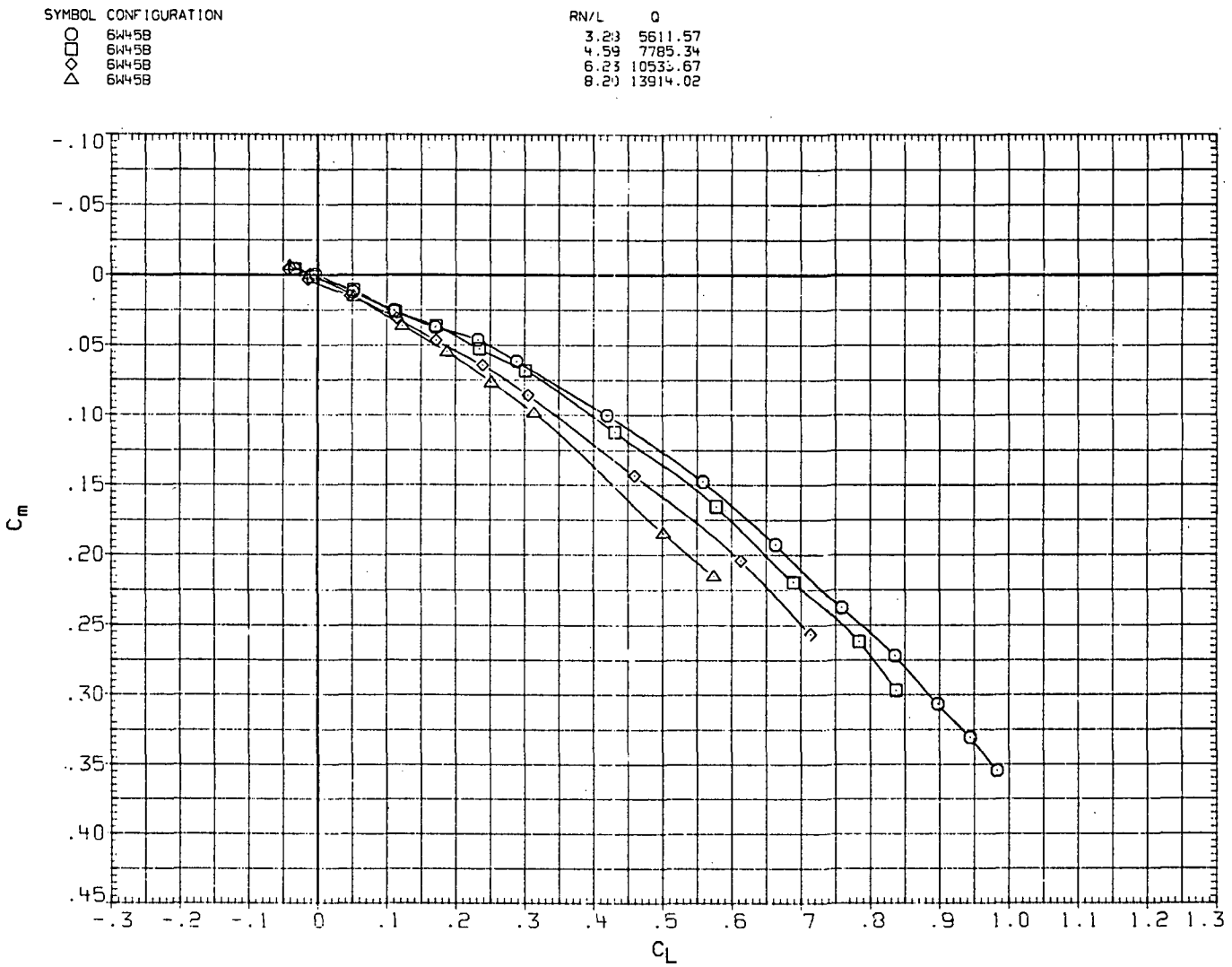


(c) $C_m$ vs $C_L$

Figure 6.– Continued.

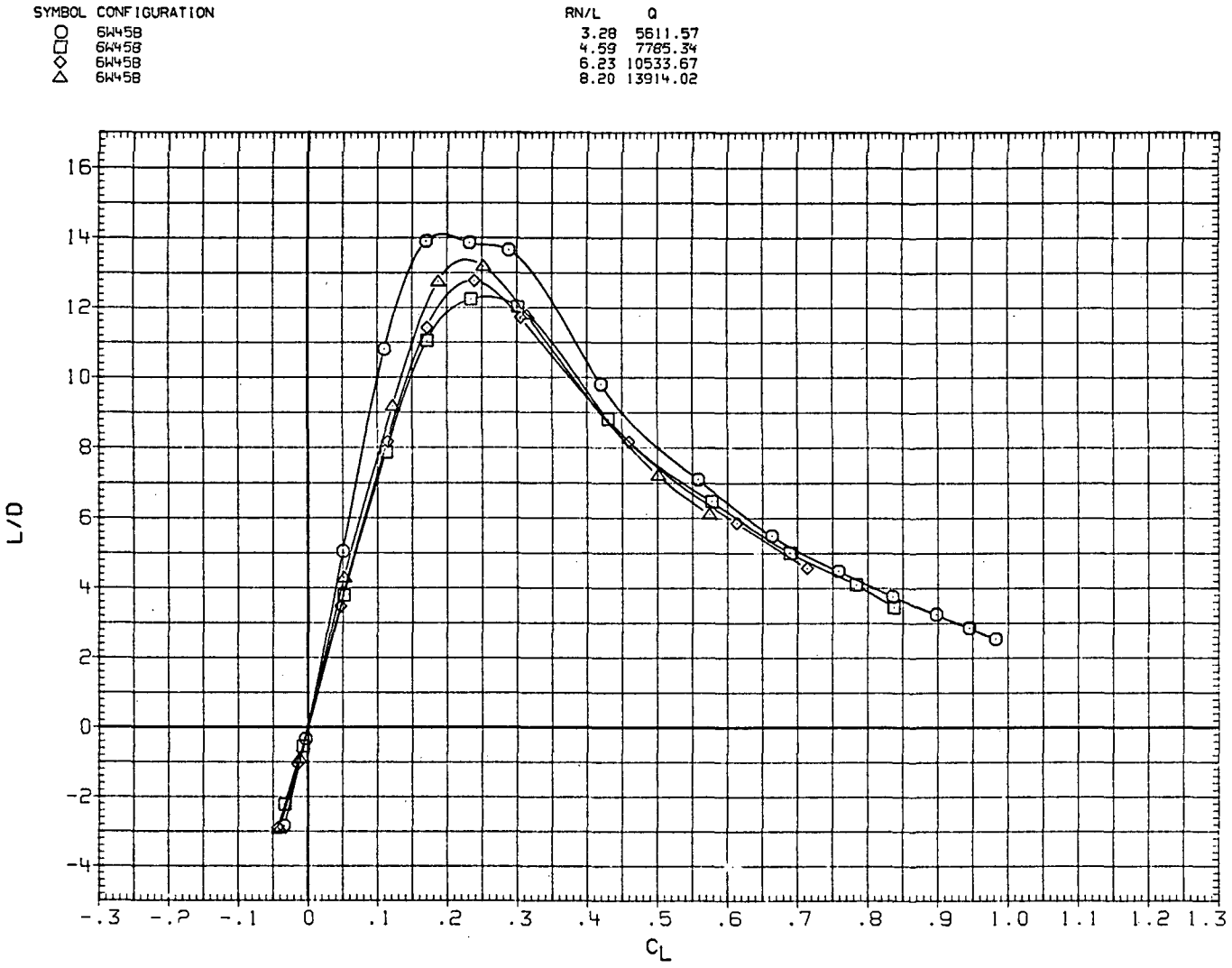


(d) $L/D$ vs $C_L$

Figure 6.– Continued.

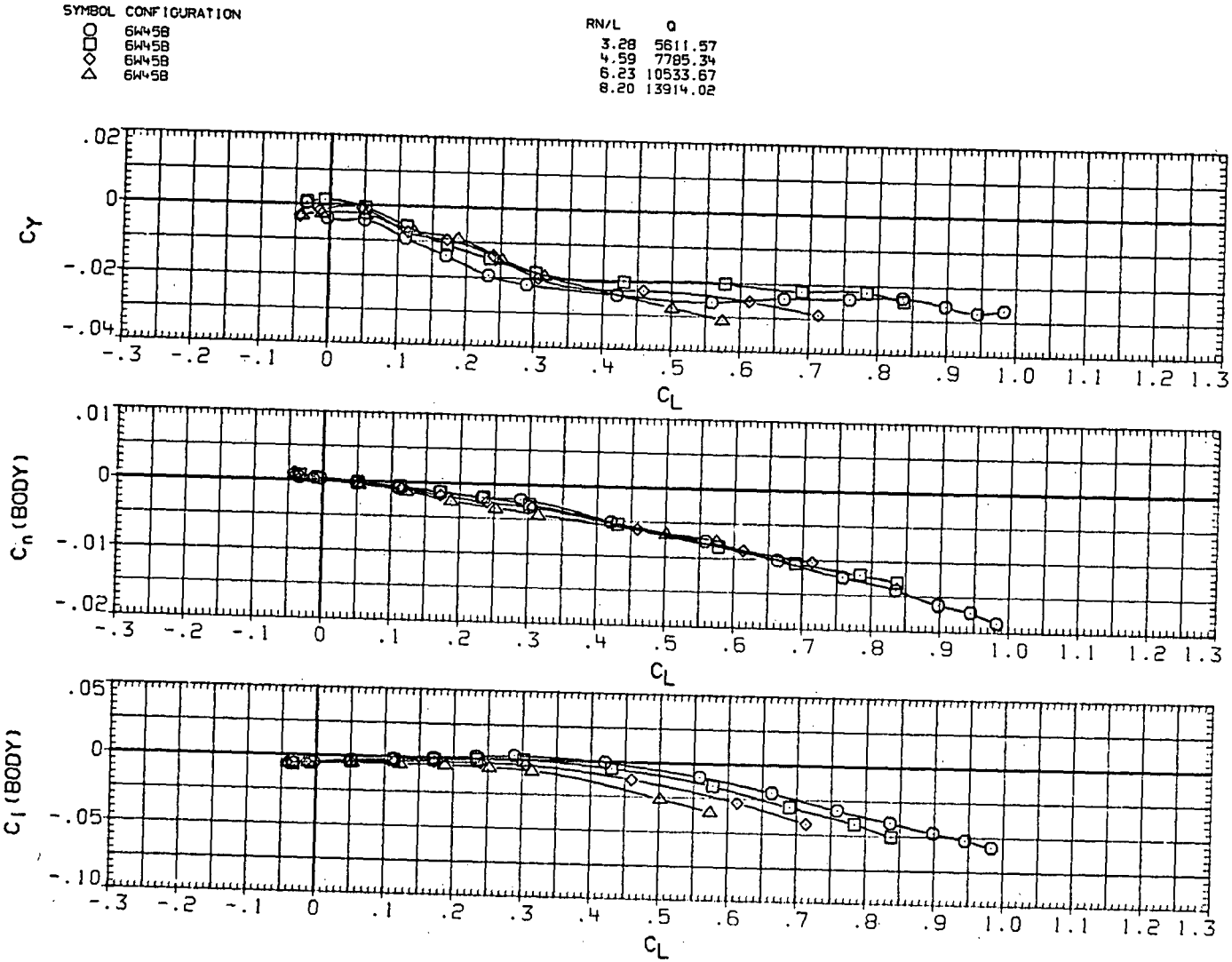


(e) $C_Y$, $C_n$, and $C_l$ vs $C_L$

Figure 6.– Concluded.


(a) $C_L$ vs $\alpha$

Figure 7.— Flexibility effects due to dynamic-pressure changes on the aerodynamic characteristics of the trapezoidal oblique wing: $\Lambda = 45°, M = 0.8$.

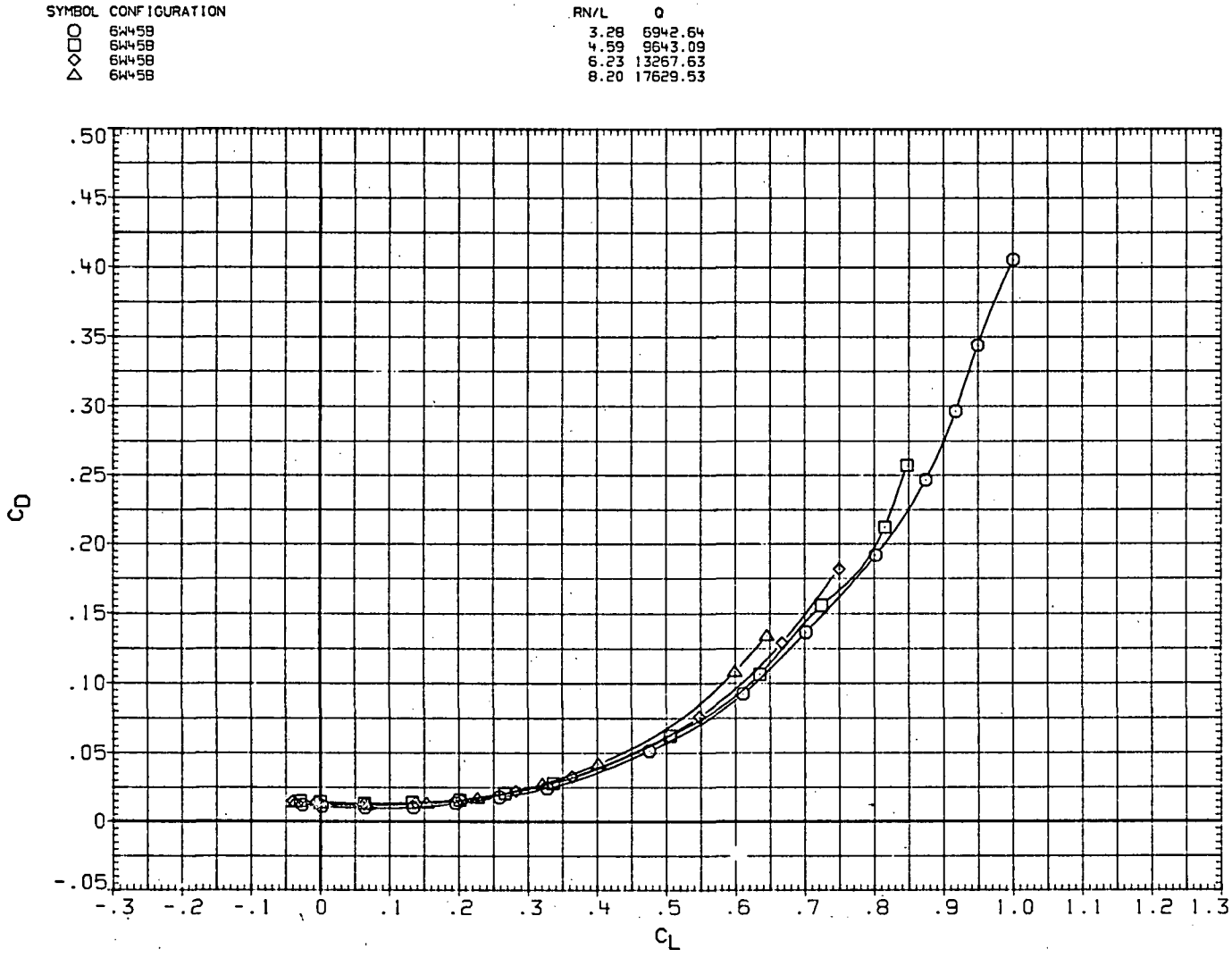


(b) $C_D$ vs $C_L$

Figure 7.– Continued.

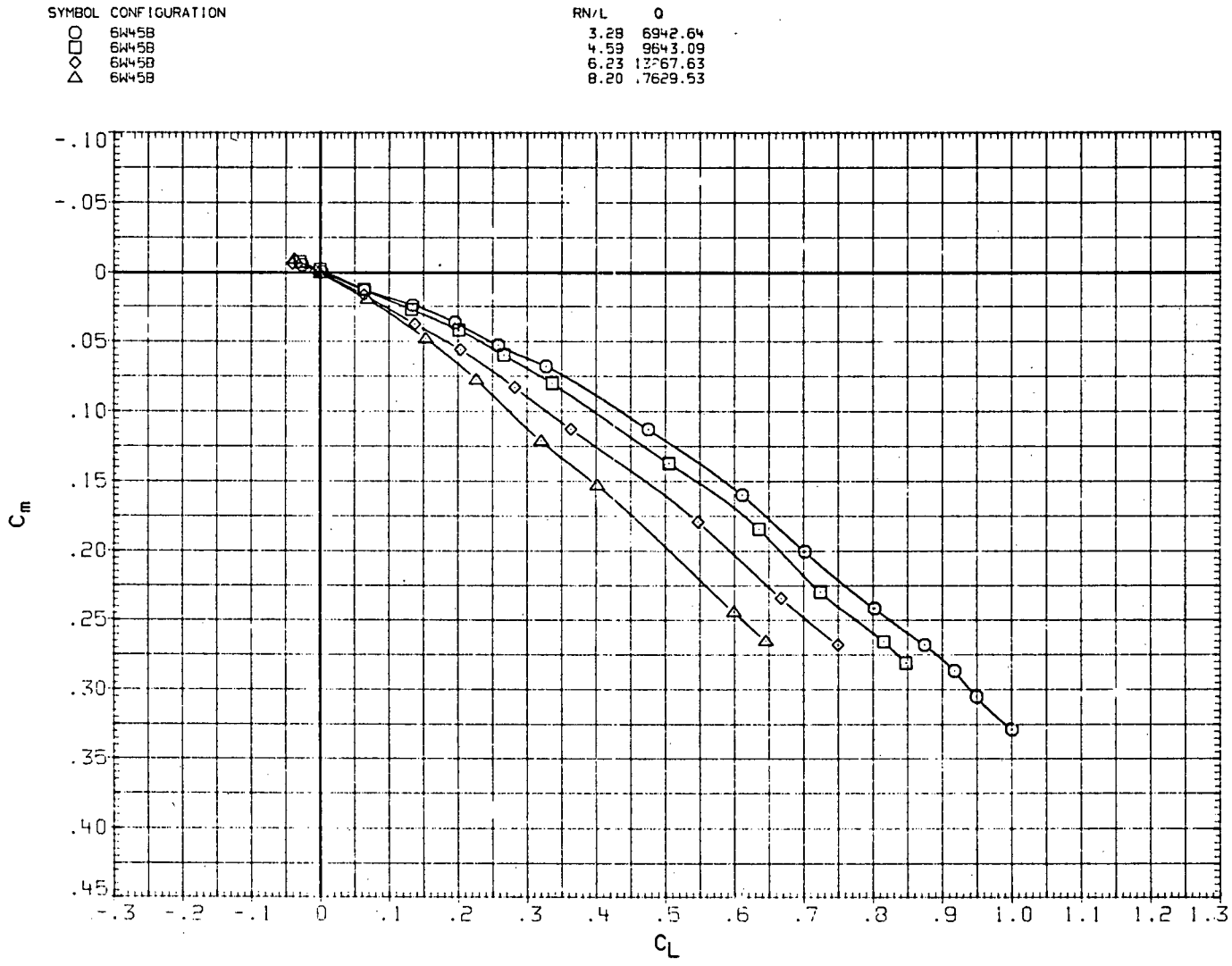


(c) $C_m$ vs $C_L$

Figure 7.– Continued.

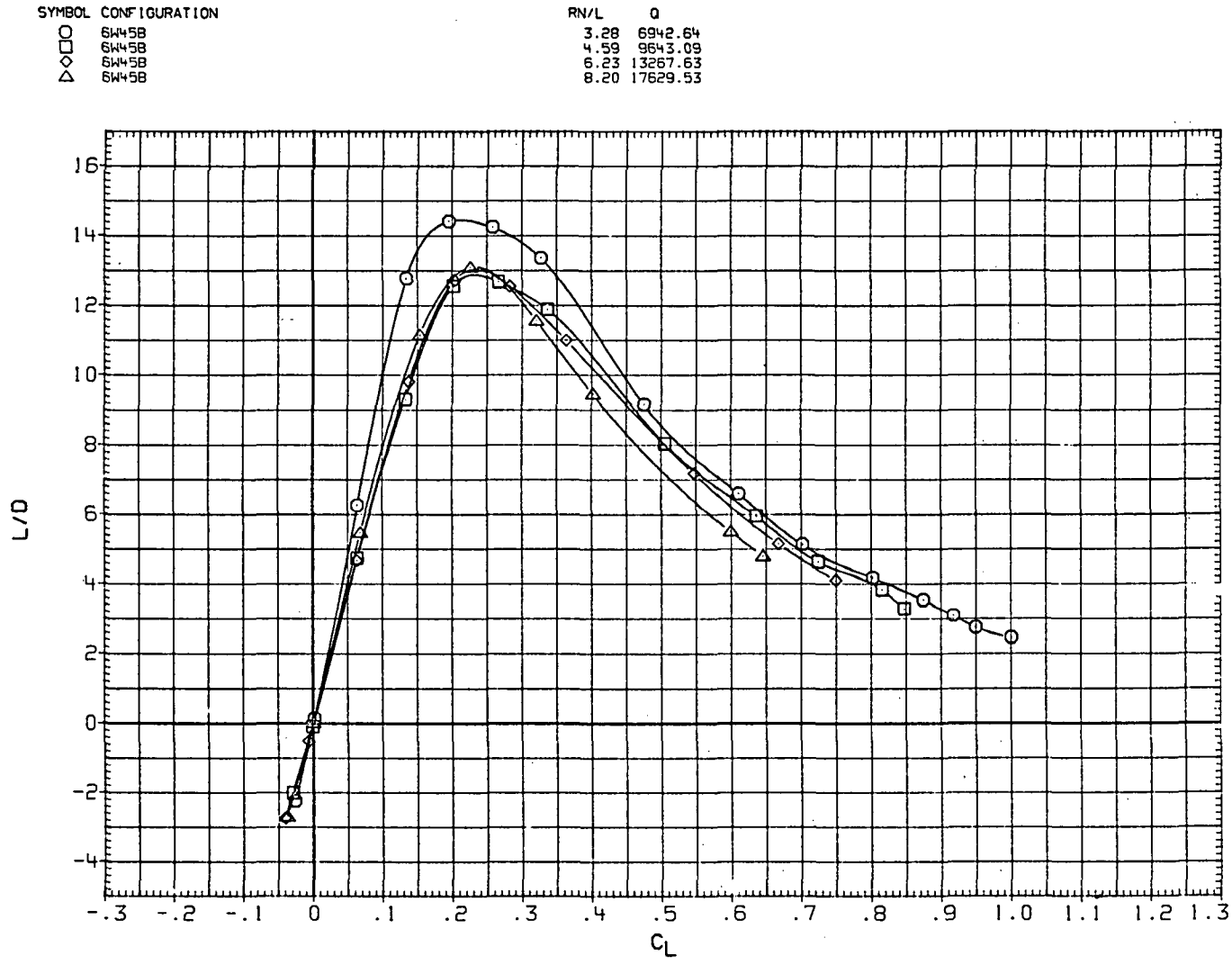


(d) $L/D$ vs $C_L$

Figure 7.– Continued.

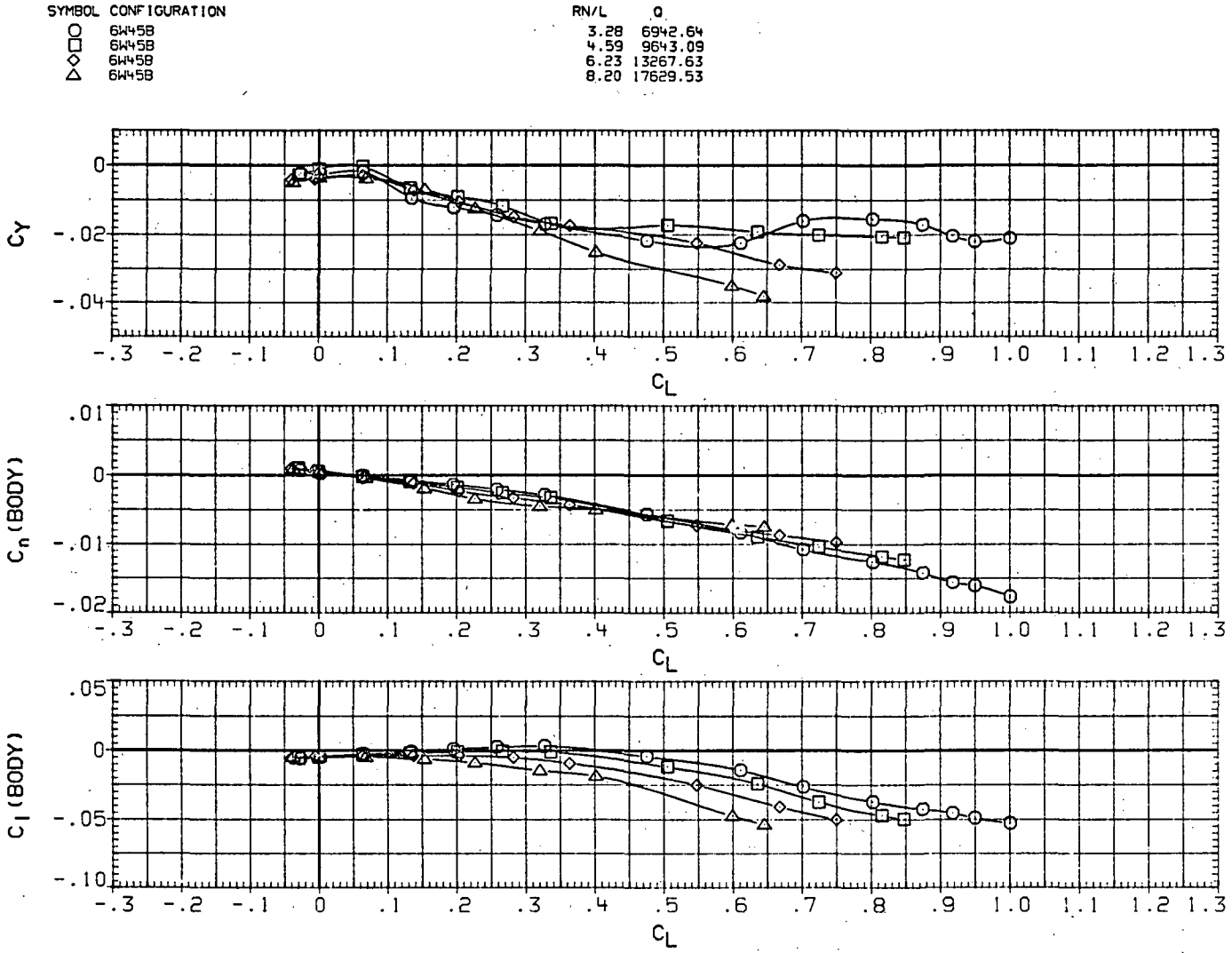


(e) $C_Y$, $C_n$, and $C_l$ vs $C_L$

Figure 7.– Concluded.

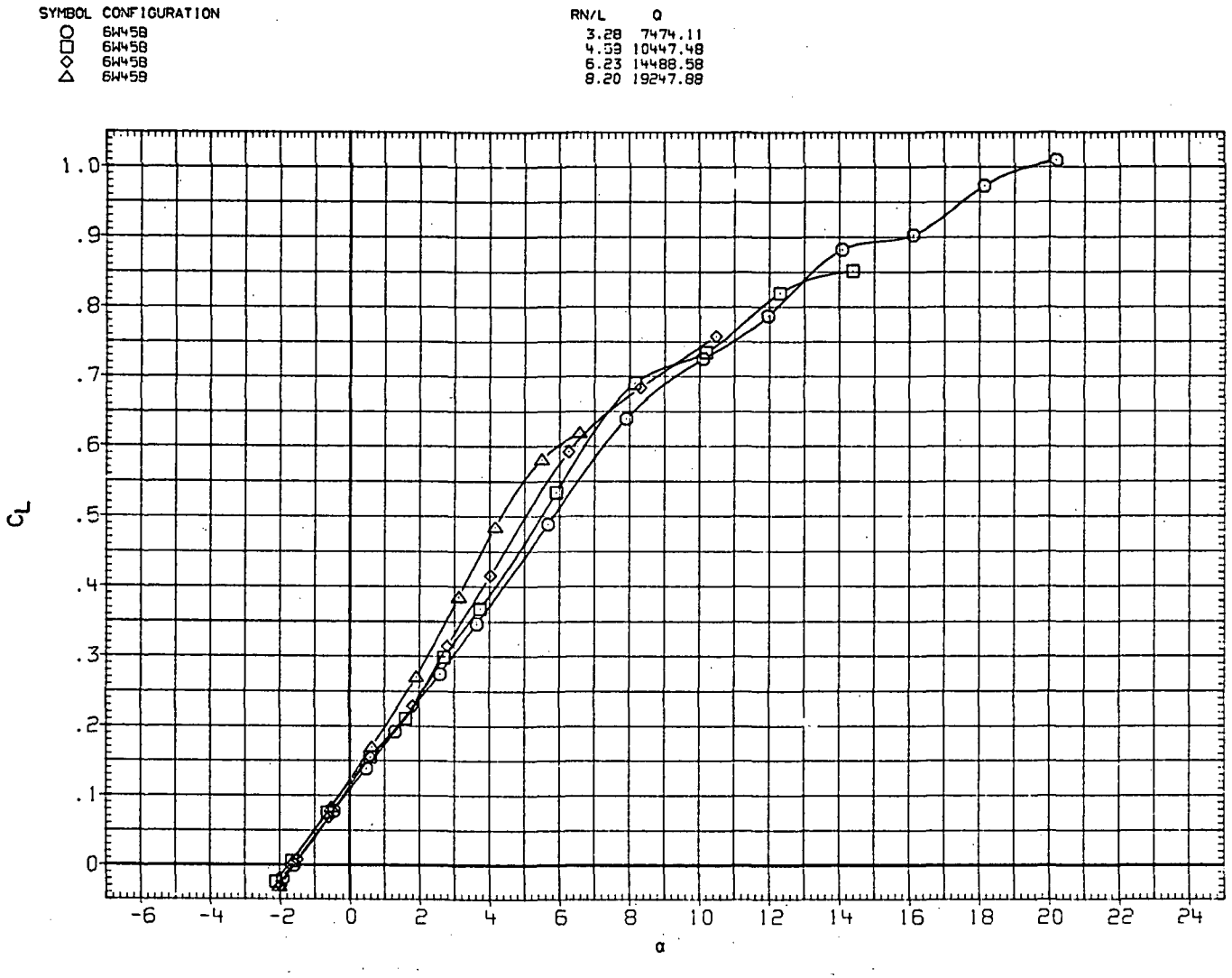


(a) $C_L$ vs $\alpha$

Figure 8.– Flexibility effects due to dynamic-pressure changes on the aerodynamic characteristics of the trapezoidal oblique wing: $\Lambda = 45°, M = 0.9$.

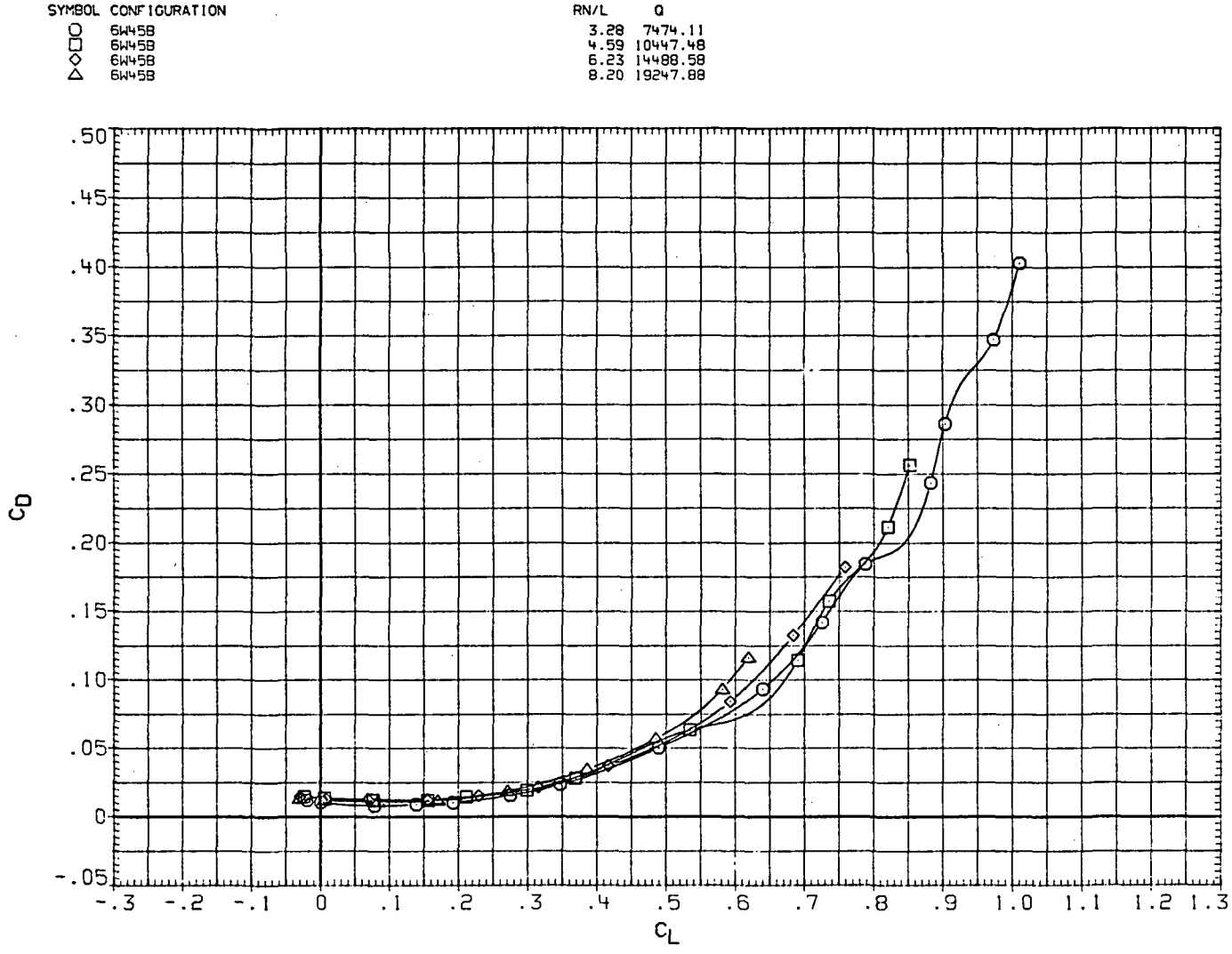


(b) $C_D$ vs $C_L$

Figure 8.– Continued.

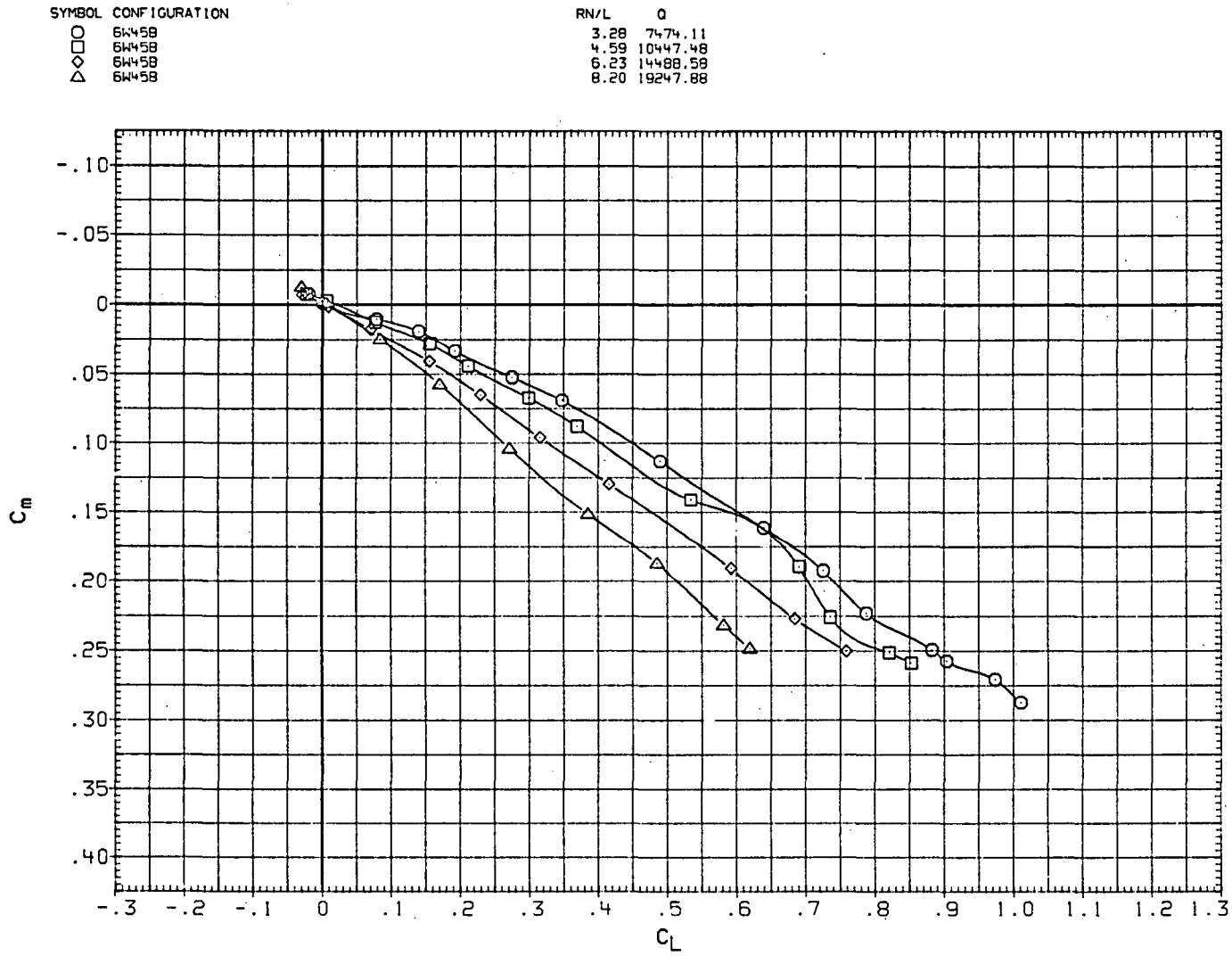


(c) $C_m$ vs $C_L$

Figure 8.– Continued.

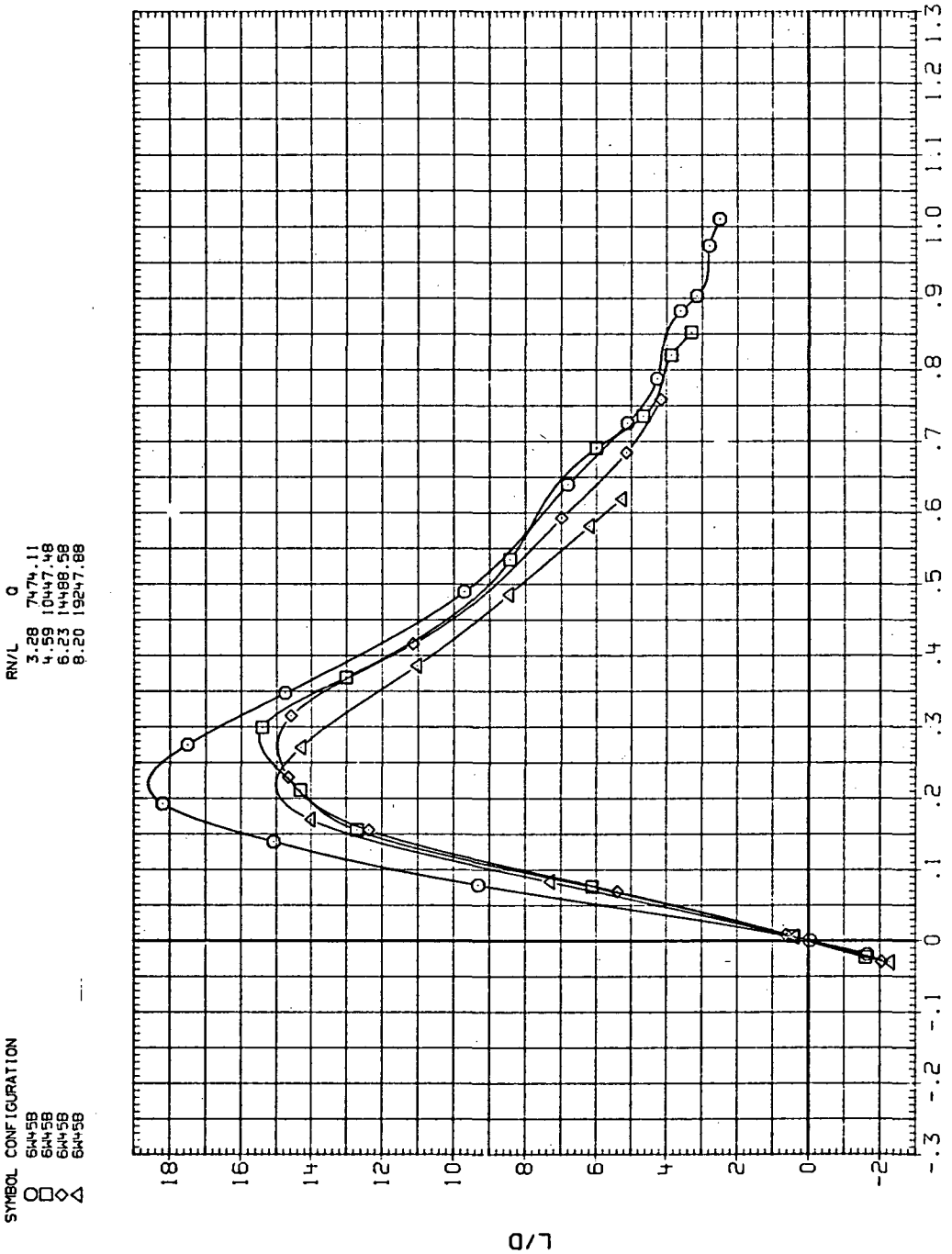


(d) $L/D$ vs $C_L$

Figure 8.– Continued.

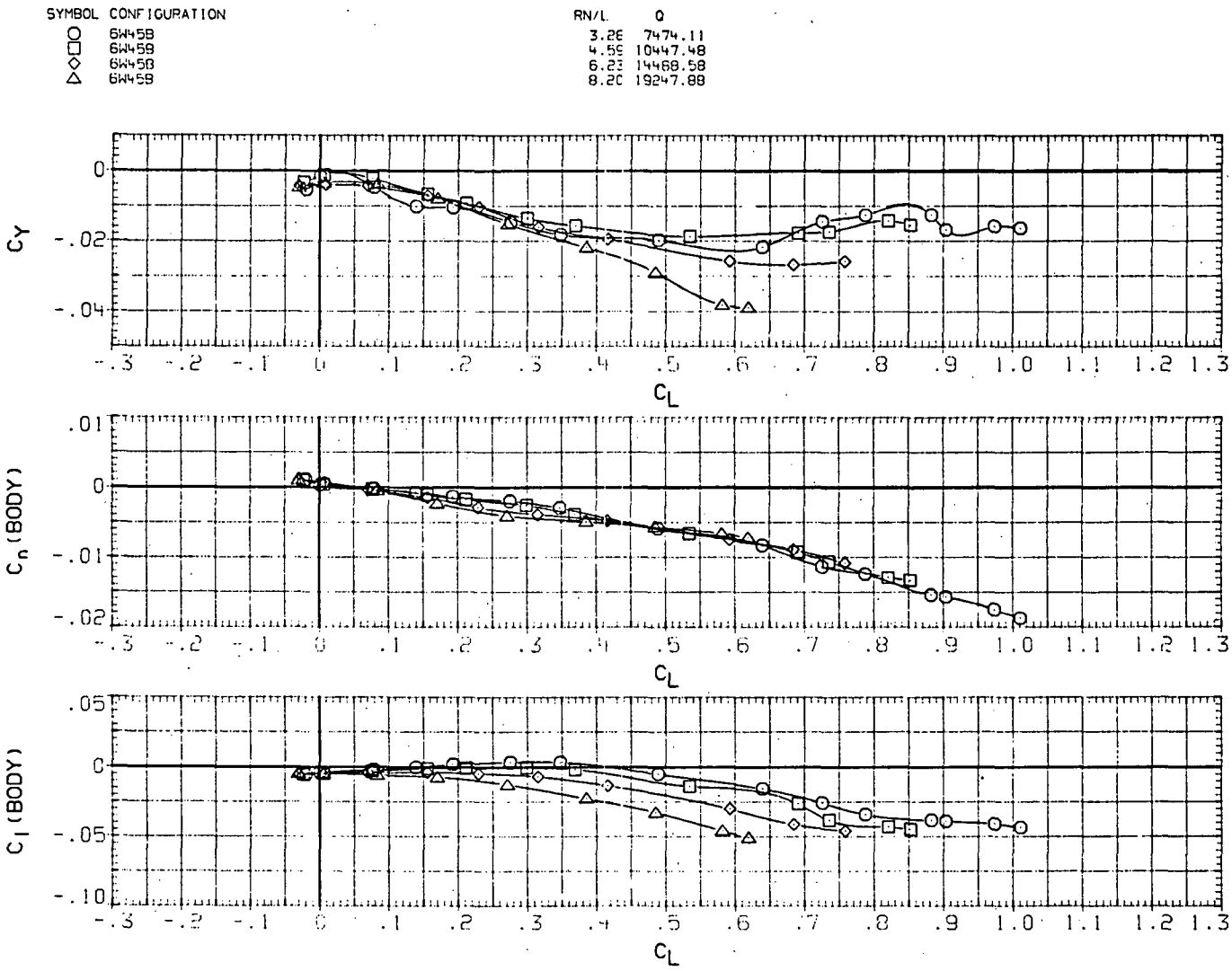


(e) $C_Y$, $C_n$, and $C_l$ vs $C_L$

Figure 8.– Concluded.

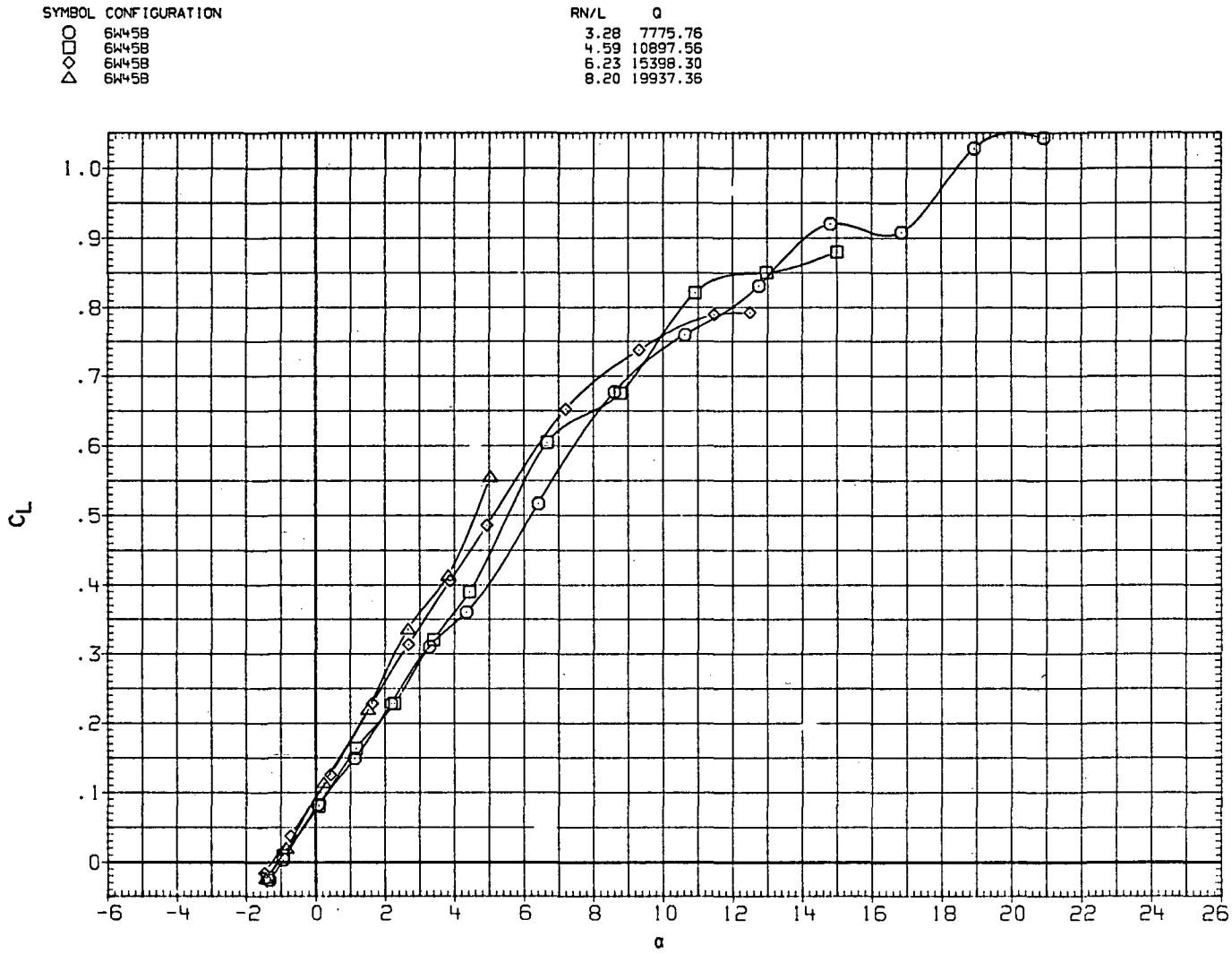


(a) $C_L$ vs $\alpha$

Figure 9.– Flexibility effects due to dynamic-pressure changes on the aerodynamic characteristics of the trapezoidal oblique wing: $\Lambda = 45°, M = 0.95$.

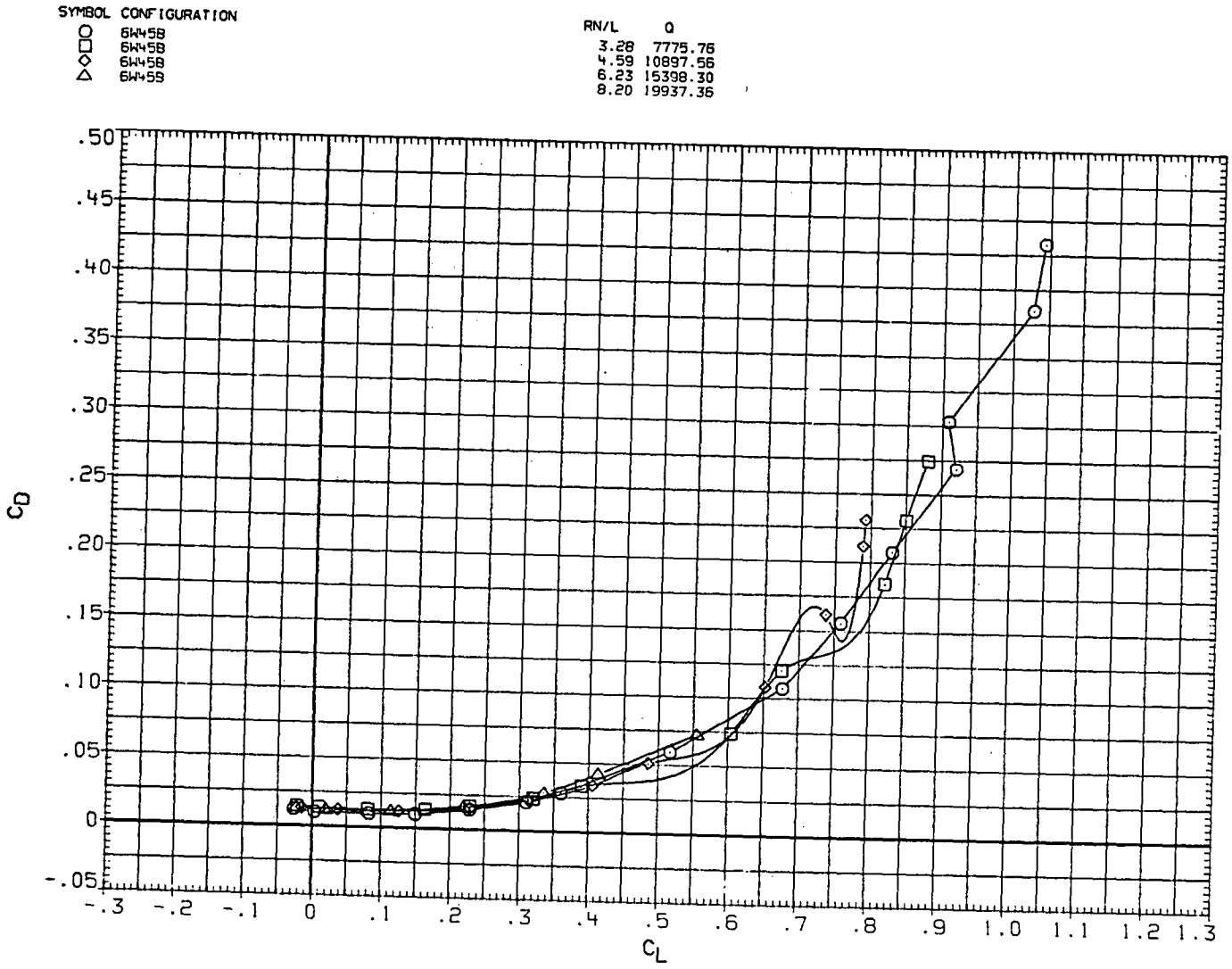


(b) $C_D$ vs $C_L$

Figure 9.– Continued.

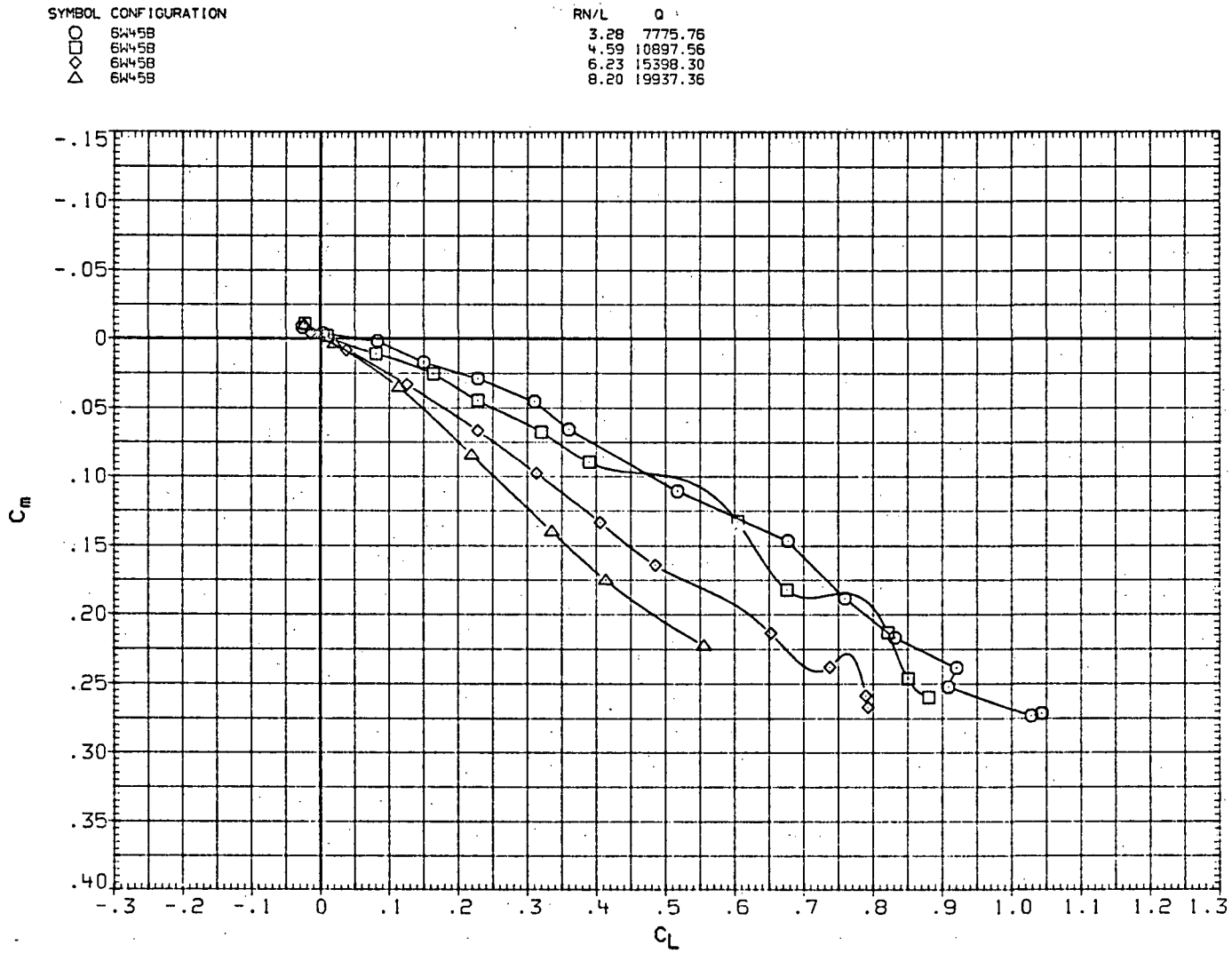


(c) $C_m$ vs $C_L$

Figure 9.– Continued.

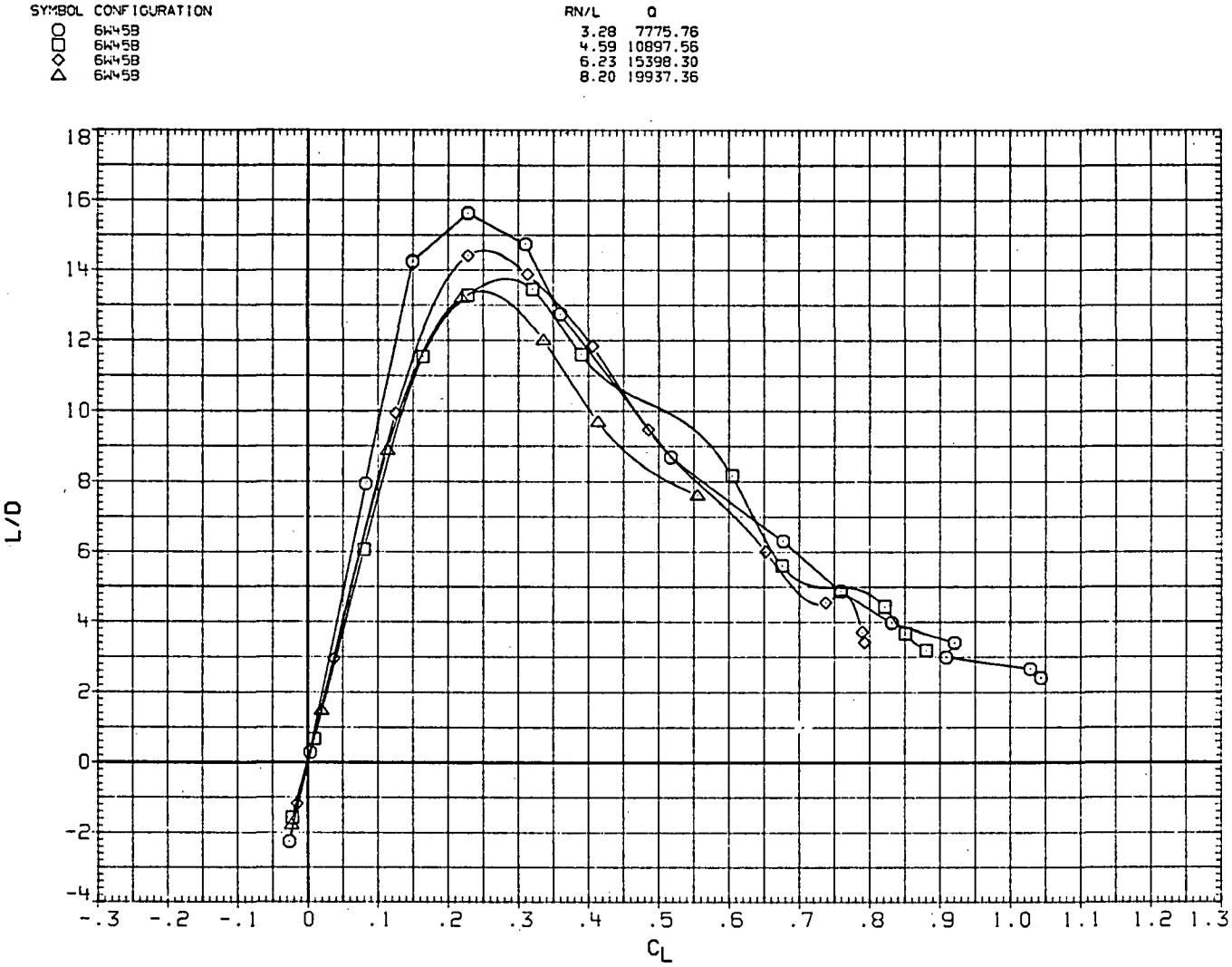


(d) $L/D$ vs $C_L$

Figure 9.– Continued.

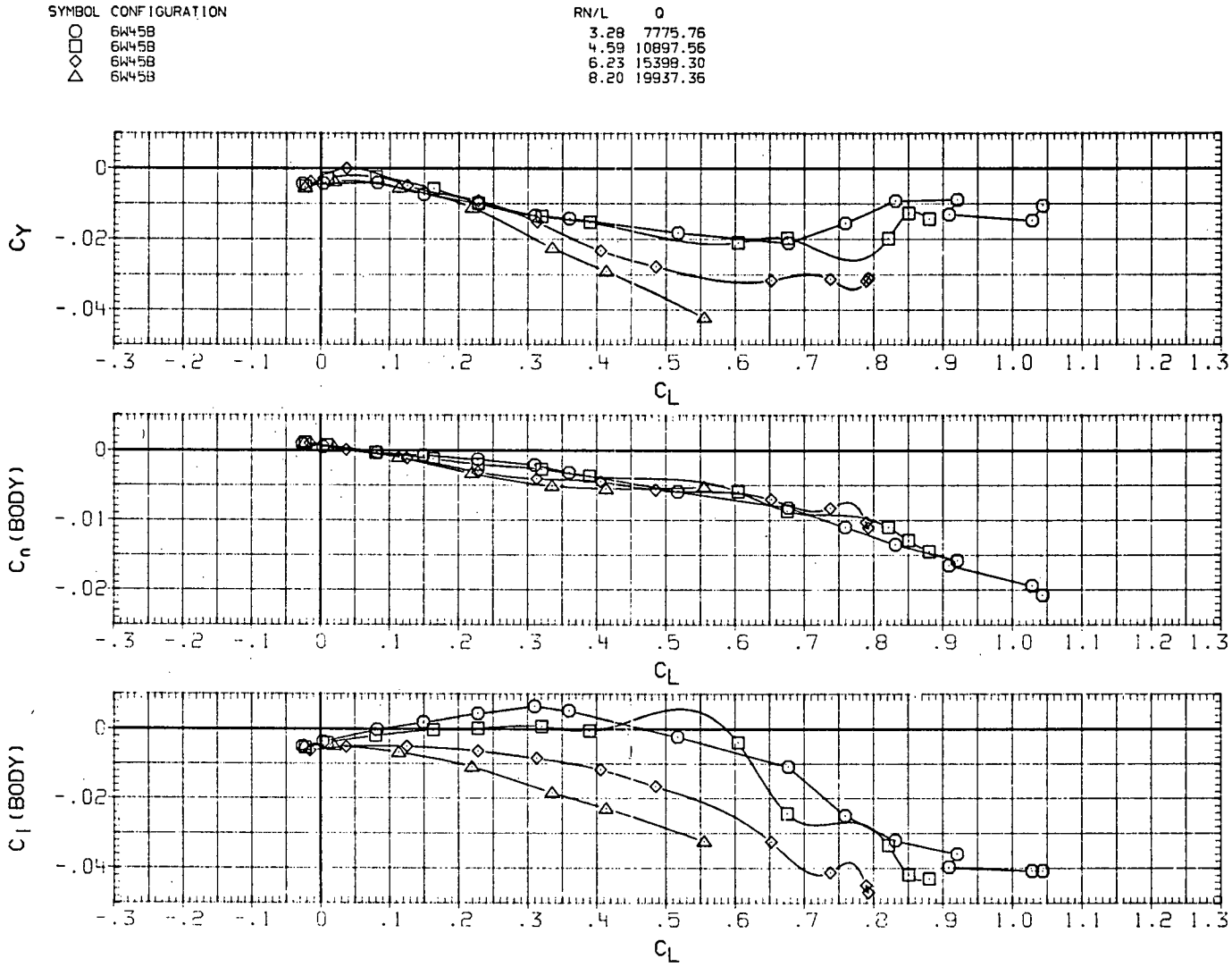


(e) $C_Y$, $C_n$, and $C_l$ vs $C_L$

Figure 9.– Concluded.

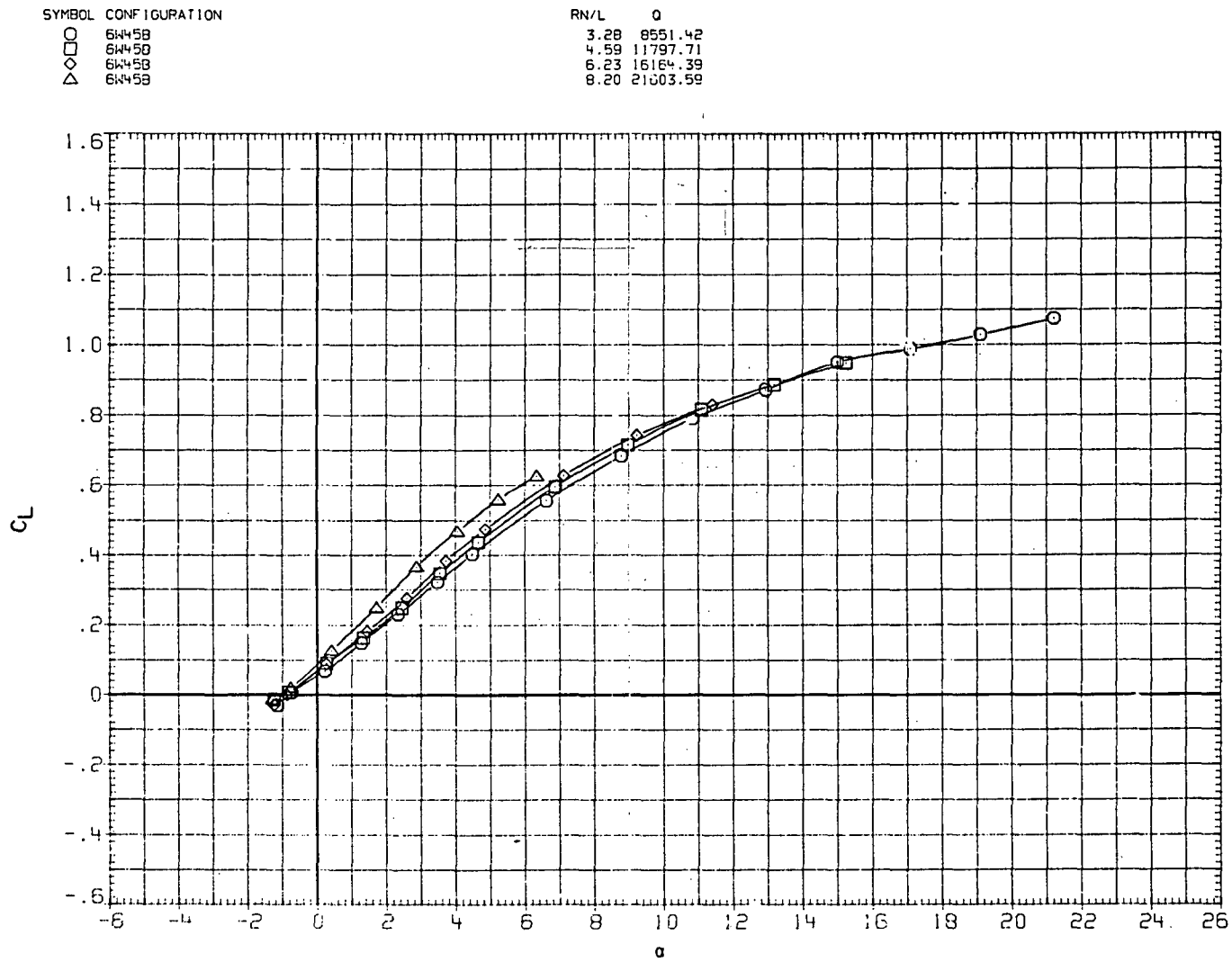


(a) $C_L$ vs $\alpha$

Figure 10.– Flexibility effects due to dynamic-pressure changes on the aerodynamic characteristics of the trapezoidal oblique wing: $\Lambda = 45°, M = 1.1$.

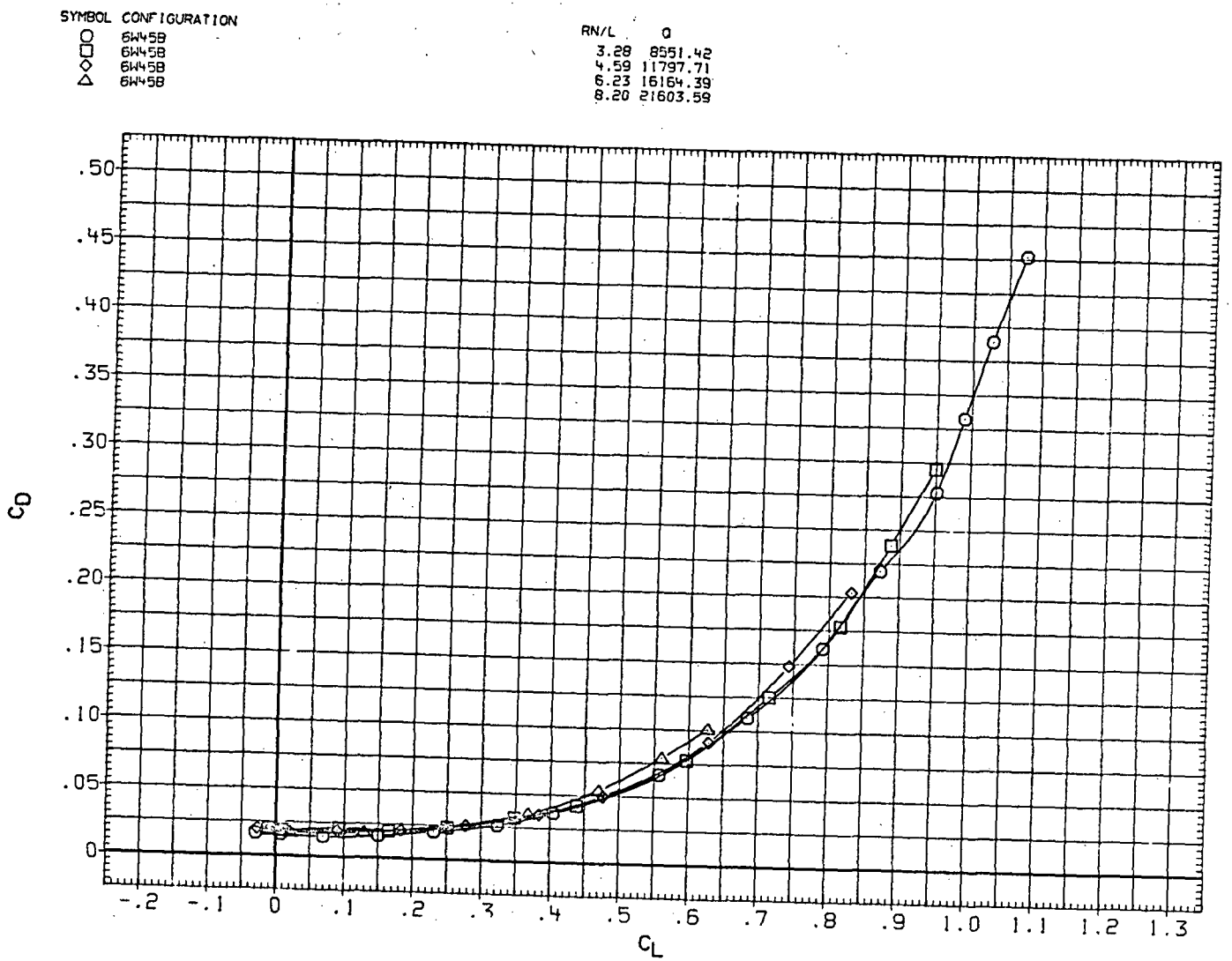


(b) $C_D$ vs $C_L$

Figure 10.– Continued.

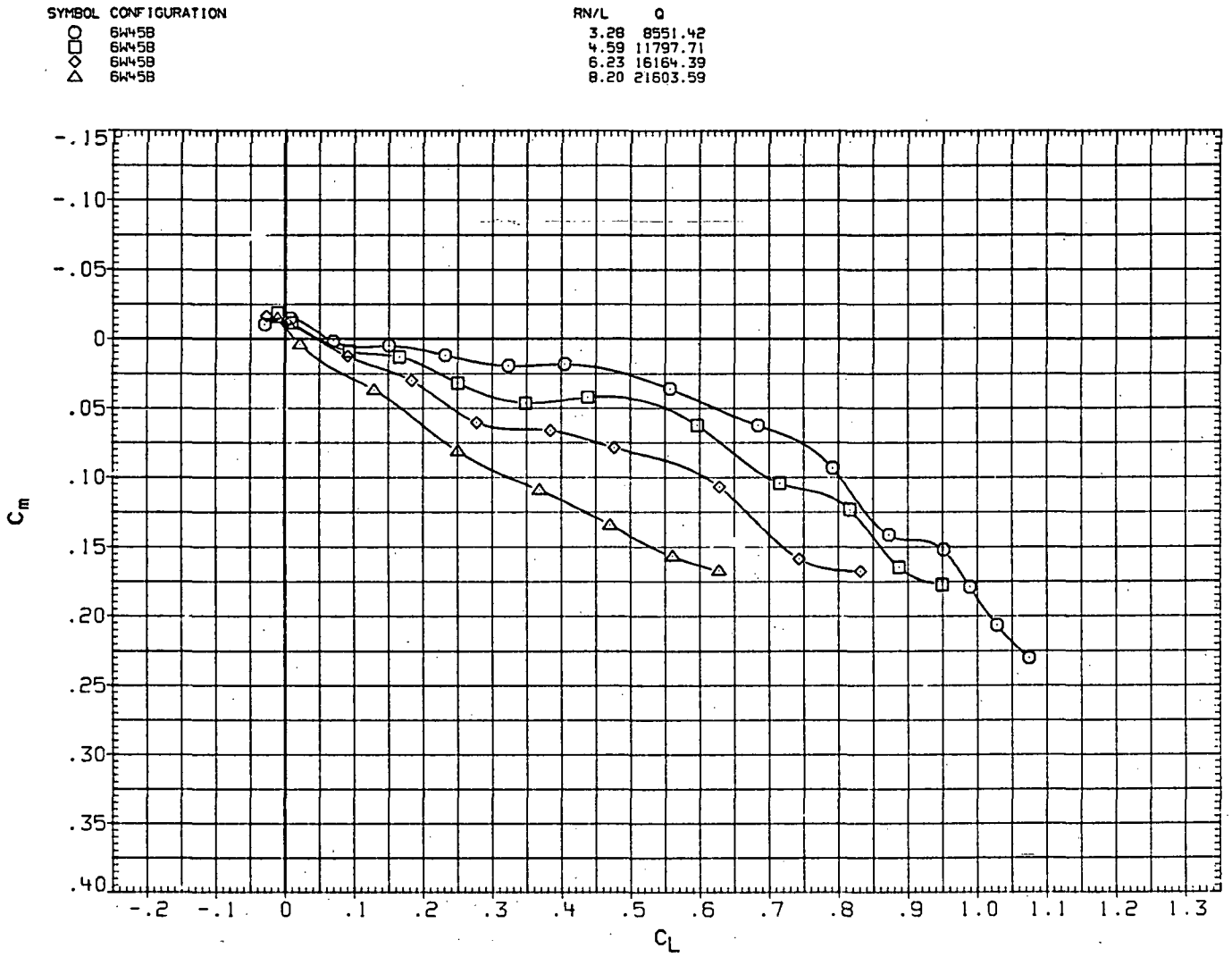


(c) $C_m$ vs $C_L$

Figure 10.– Continued.


(d) $L/D$ vs $C_L$

Figure 10.– Continued.

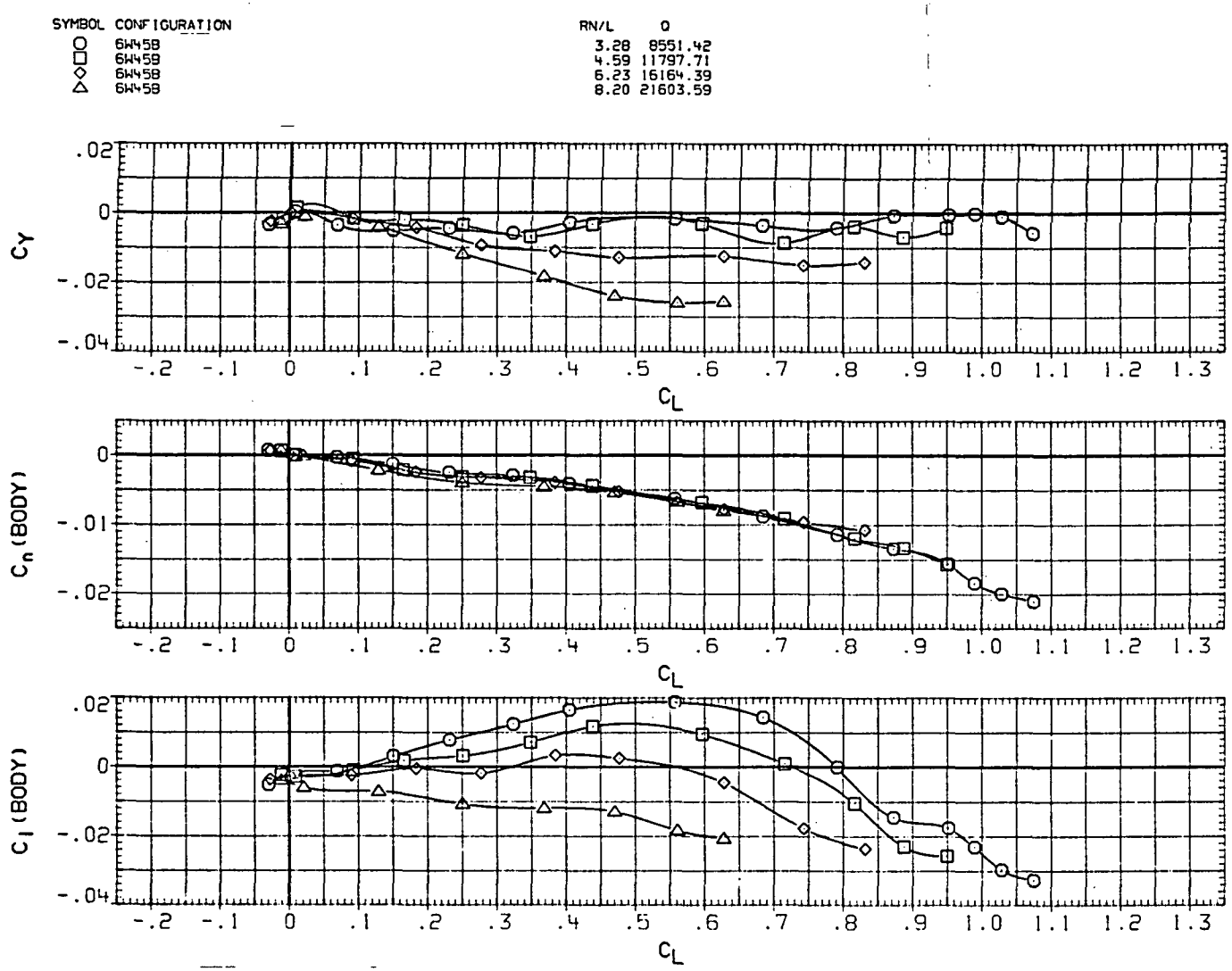


(e) $C_Y$, $C_n$, and $C_l$ vs $C_L$

Figure 10.– Concluded.

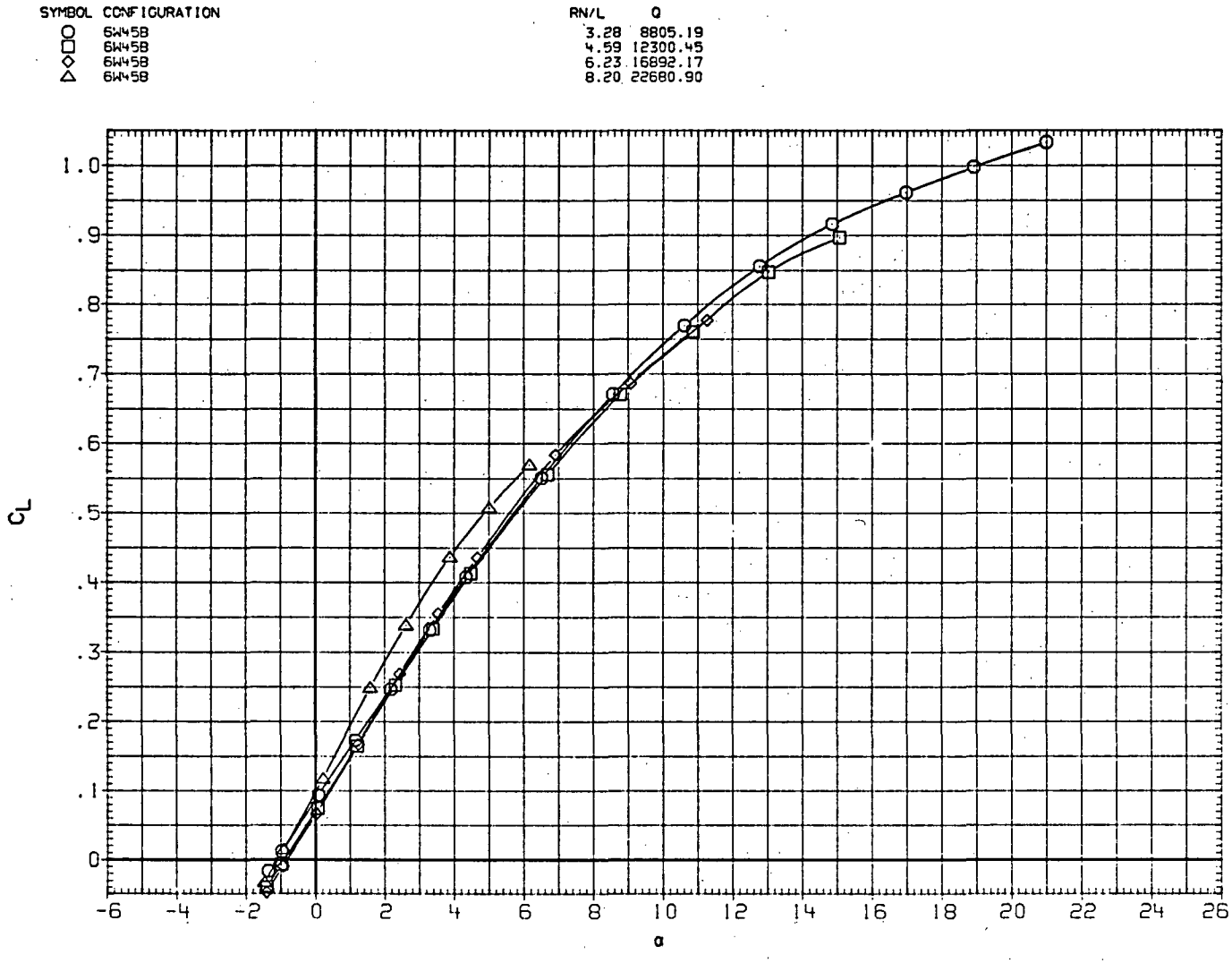


(a) $C_L$ vs $\alpha$

Figure 11.– Flexibility effects due to dynamic-pressure changes on the aerodynamic characteristics of the trapezoidal oblique wing: $\Lambda = 45°, M = 1.2$.

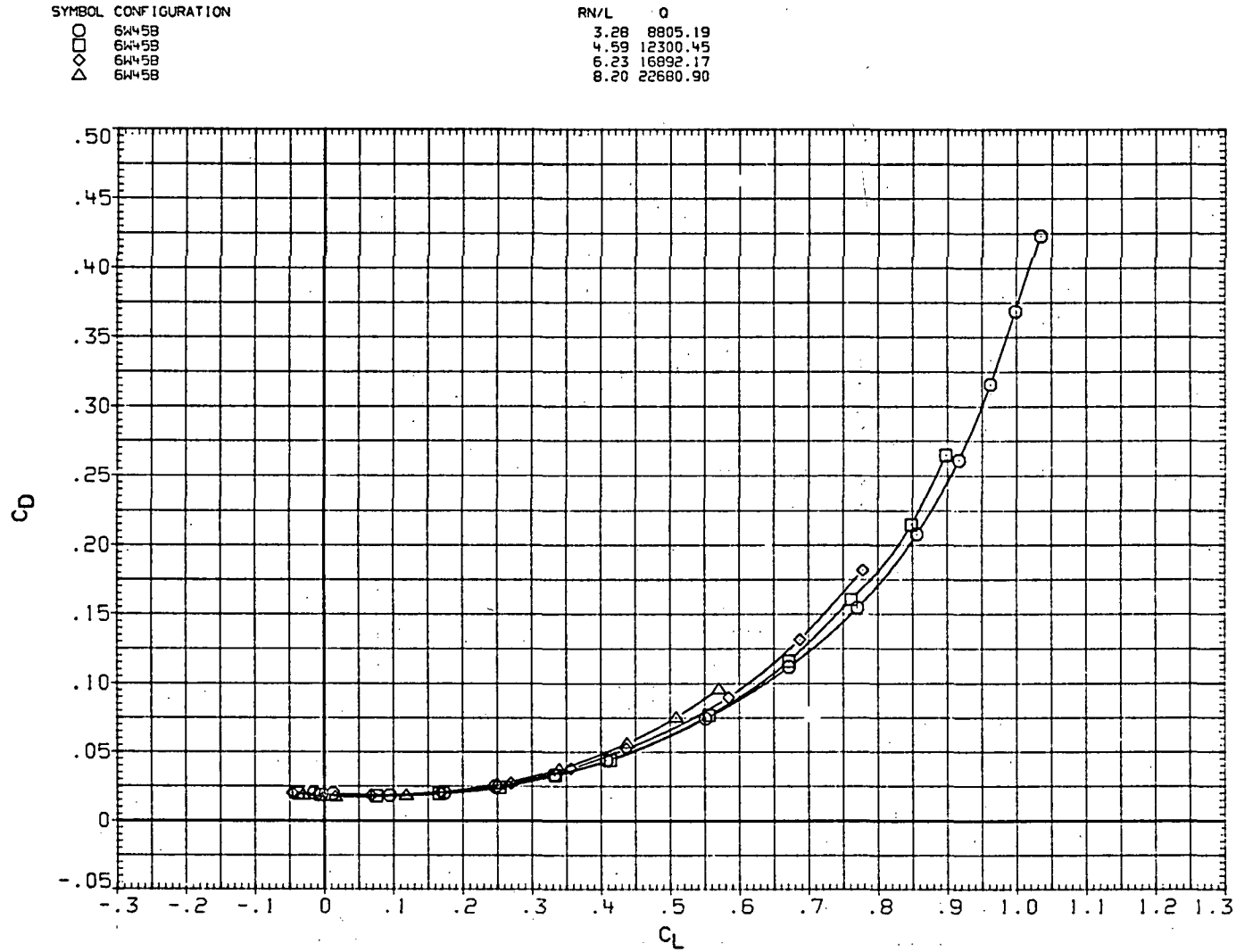


(b) $C_D$ vs $C_L$

Figure 11.– Continued.

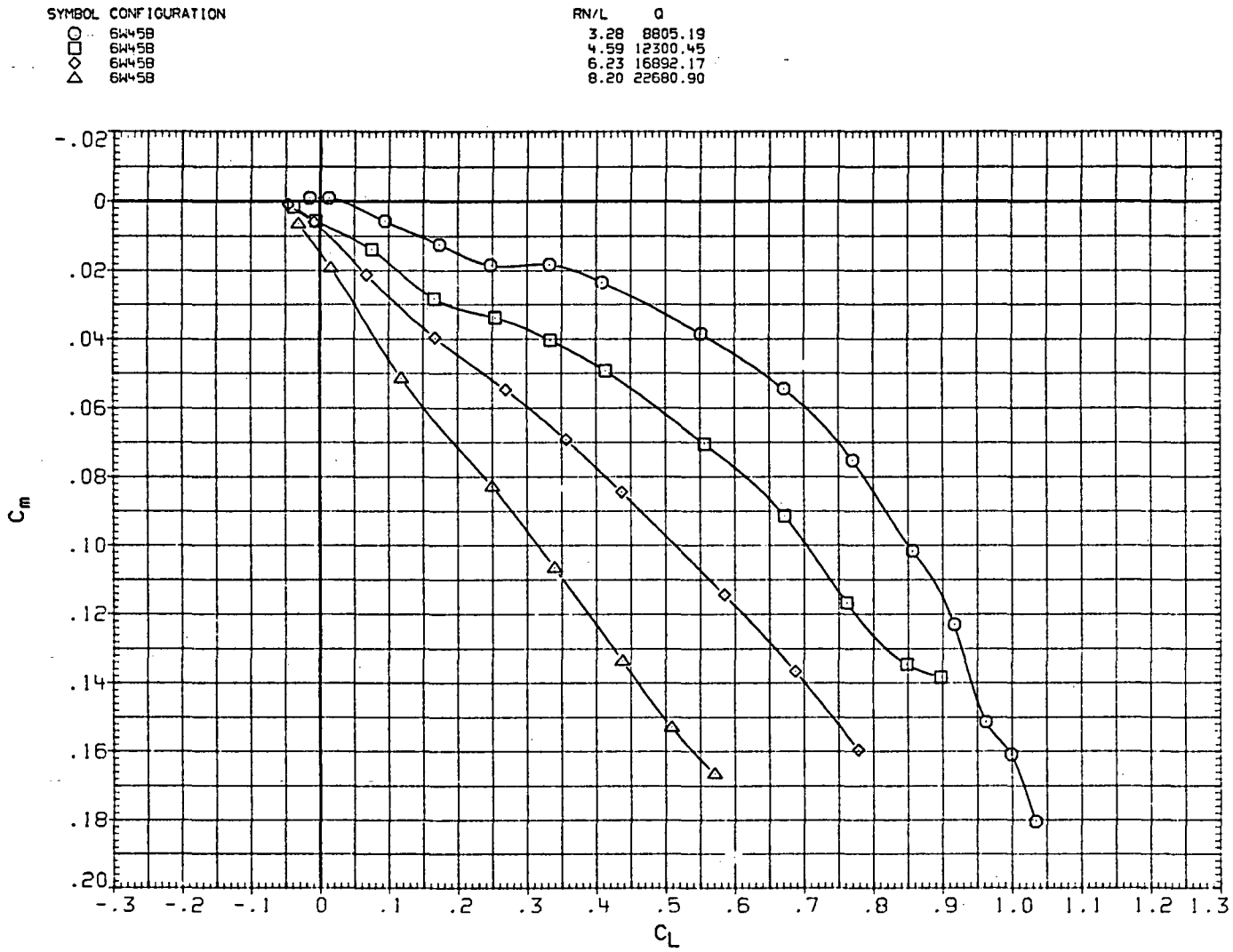


(c) $C_m$ vs $C_L$

Figure 11.– Continued.

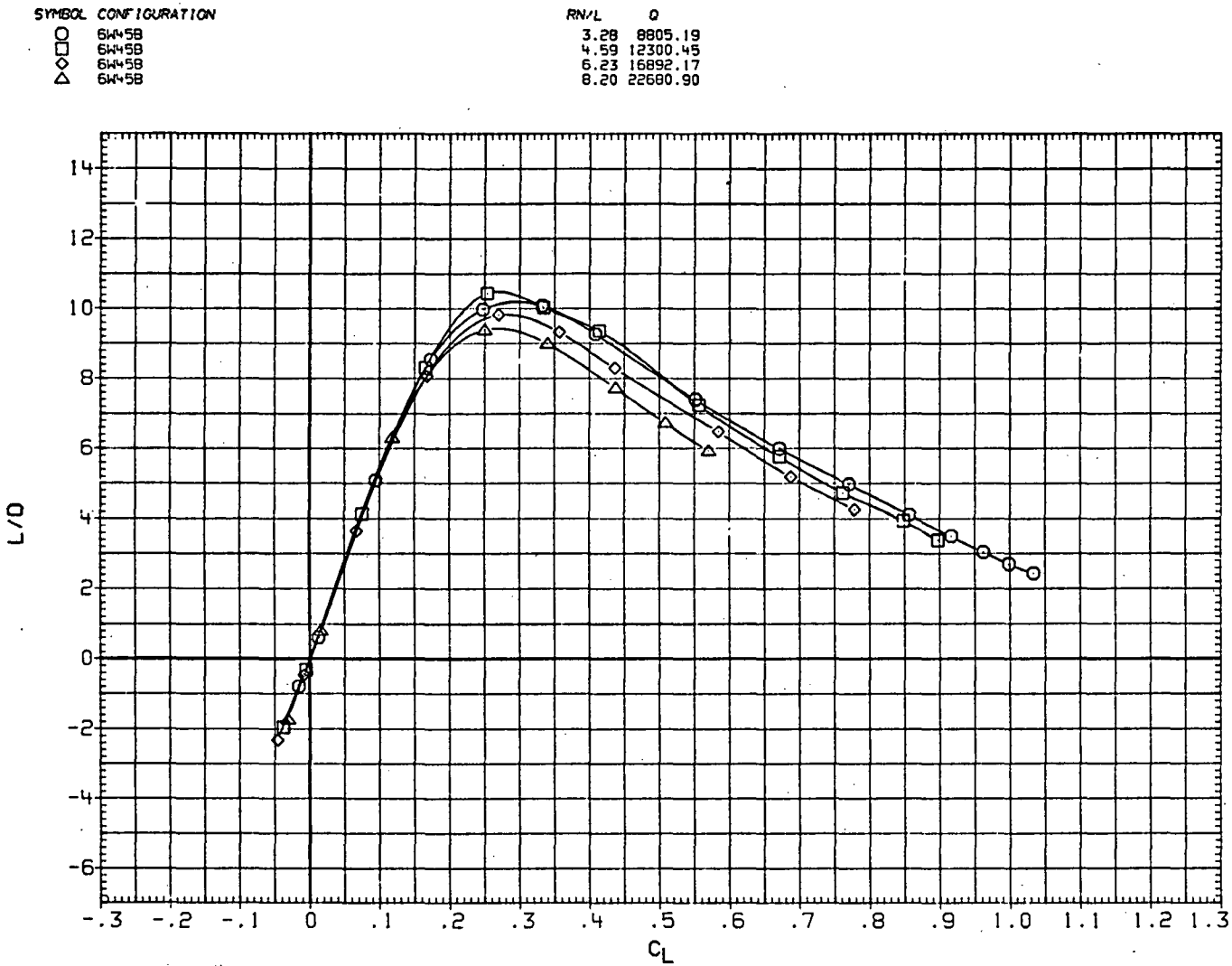


(d) $L/D$ vs $C_L$

Figure 11.– Continued.

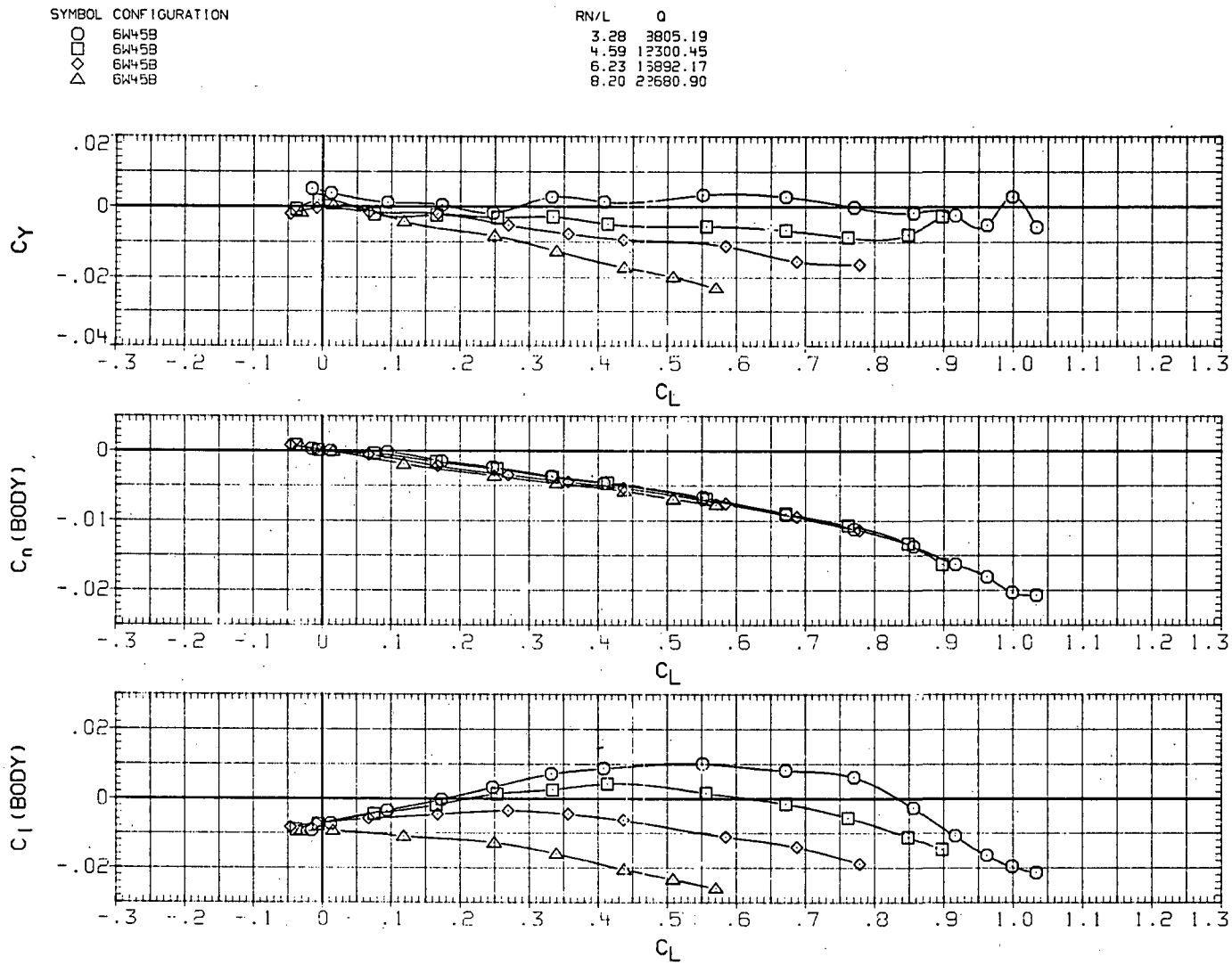


(e) $C_Y$, $C_n$, and $C_l$ vs $C_L$

Figure 11.– Concluded.

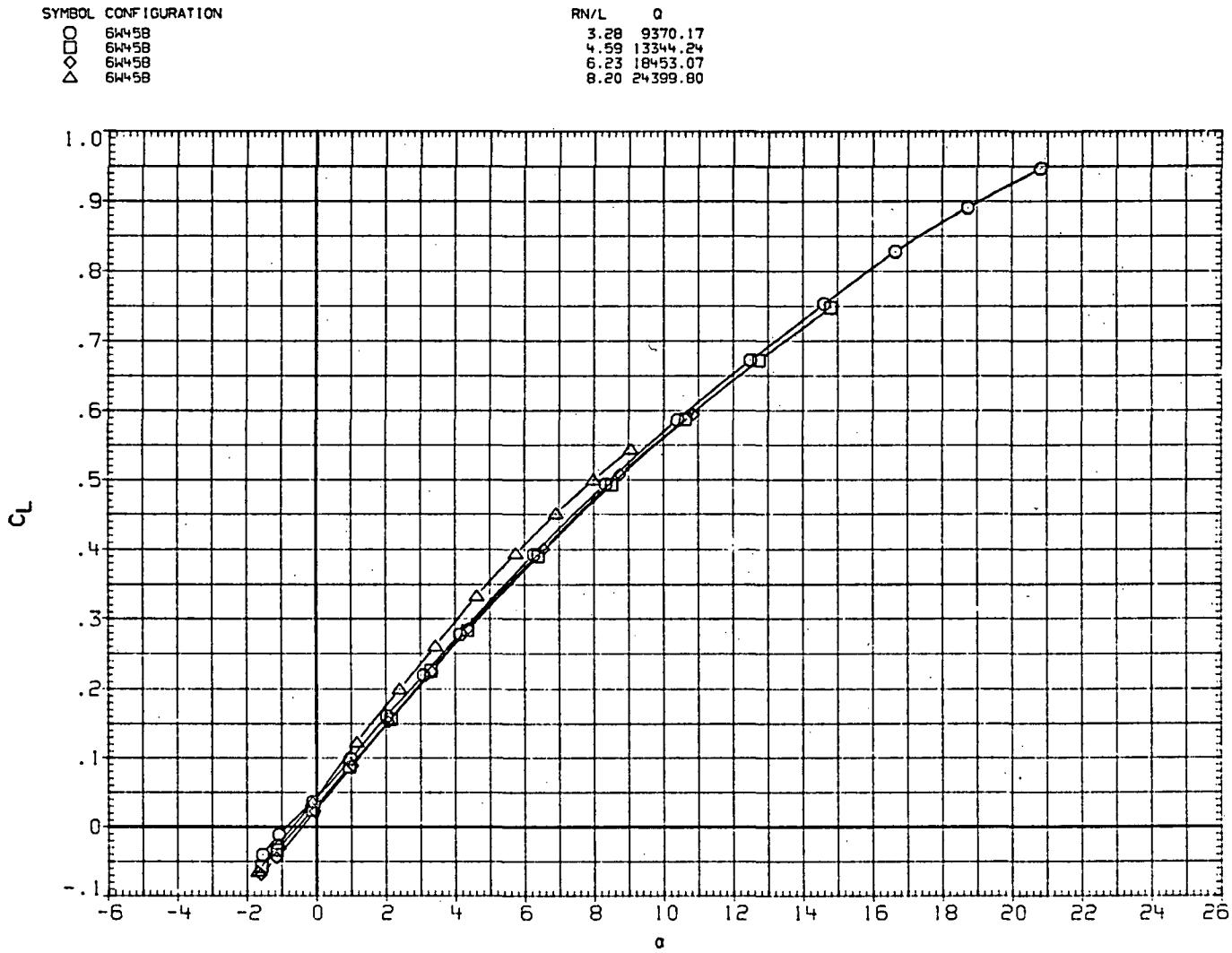


(a) $C_L$ vs $\alpha$

Figure 12.– Flexibility effects due to dynamic-pressure changes on the aerodynamic characteristics of the trapezoidal oblique wing: $\Lambda = 45°, M = 1.6$.

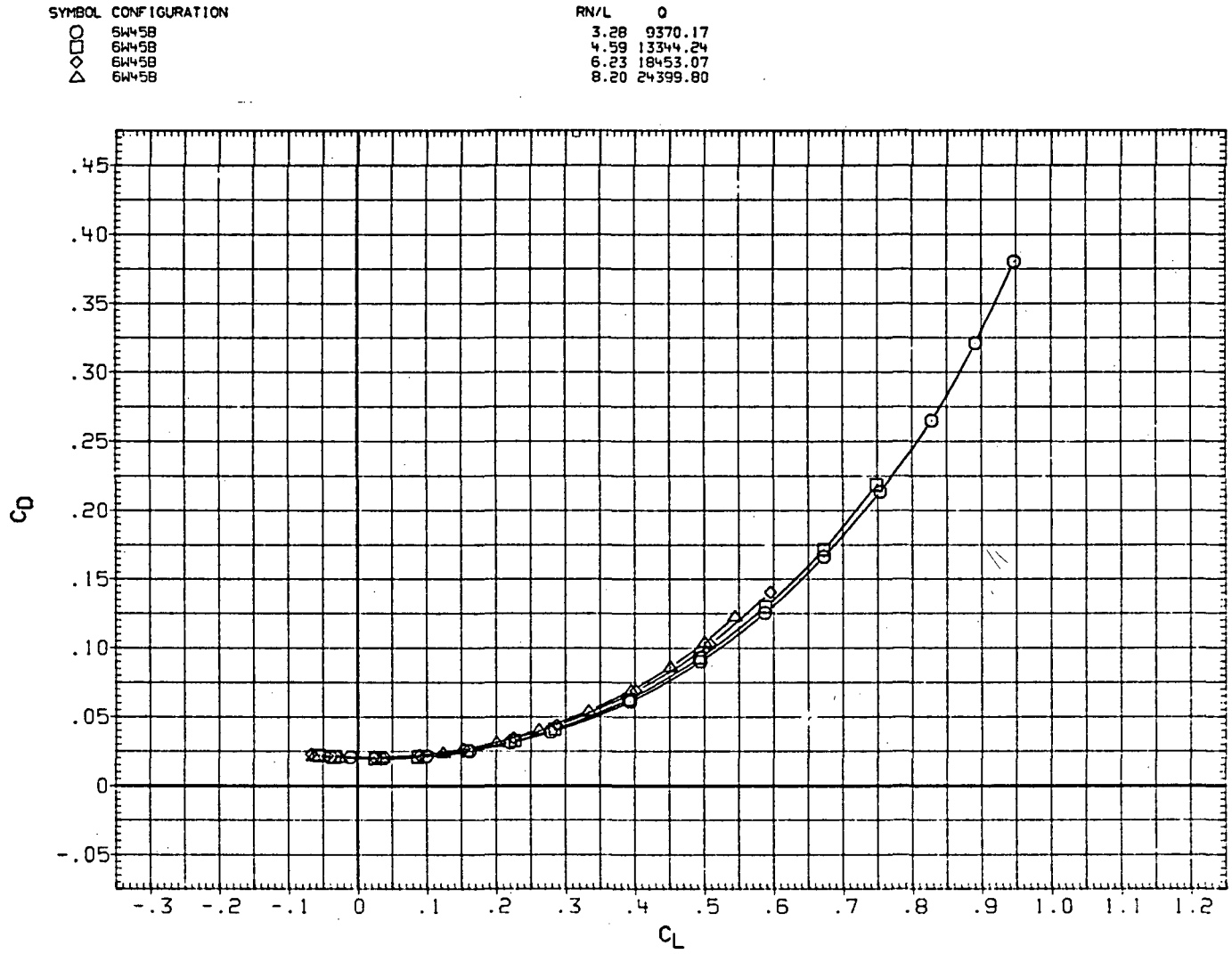


(b) $C_D$ vs $C_L$

Figure 12.– Continued.

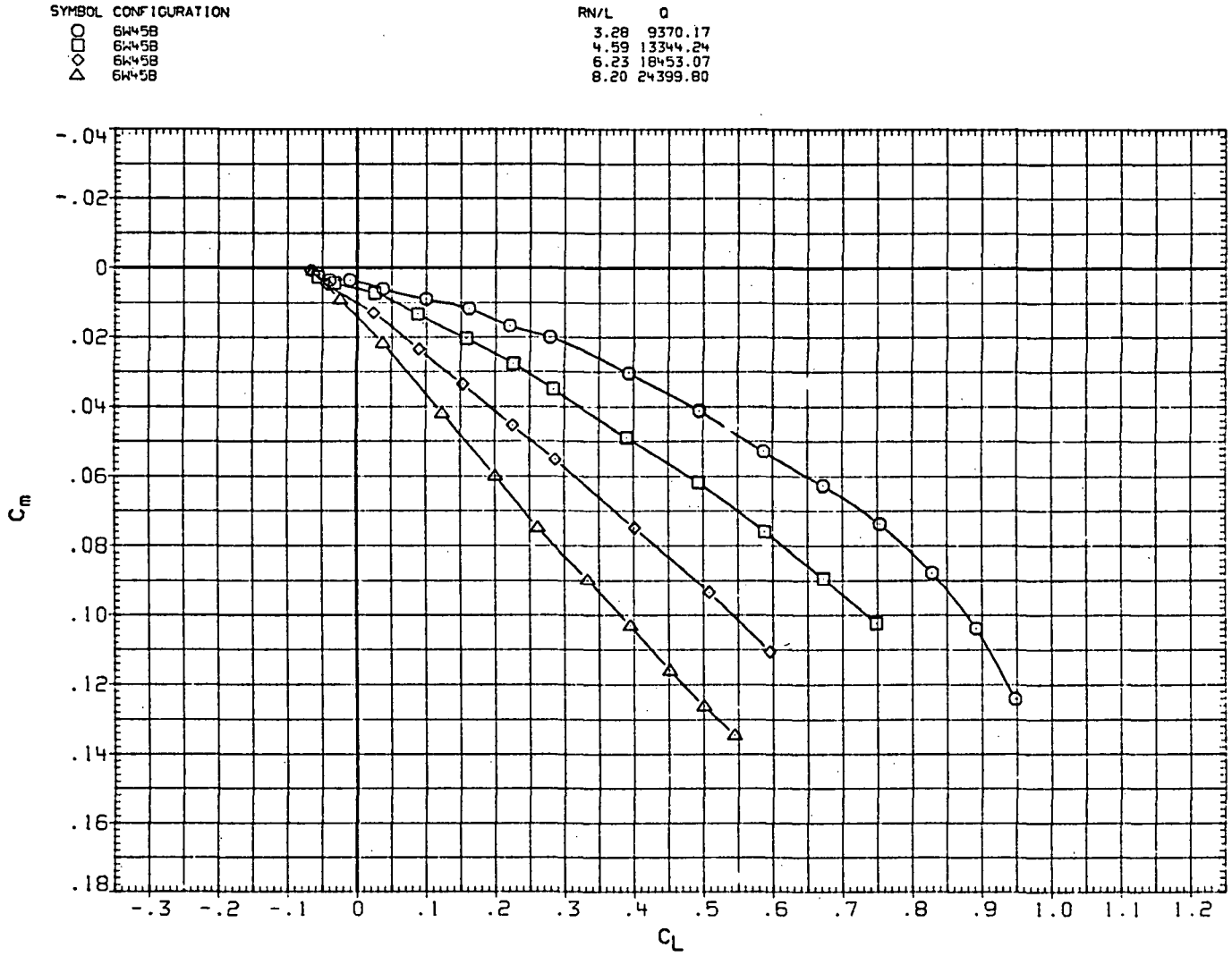


(c) $C_m$ vs $C_L$

Figure 12.– Continued.


(d) $L/D$ vs $C_L$

Figure 12.– Continued.

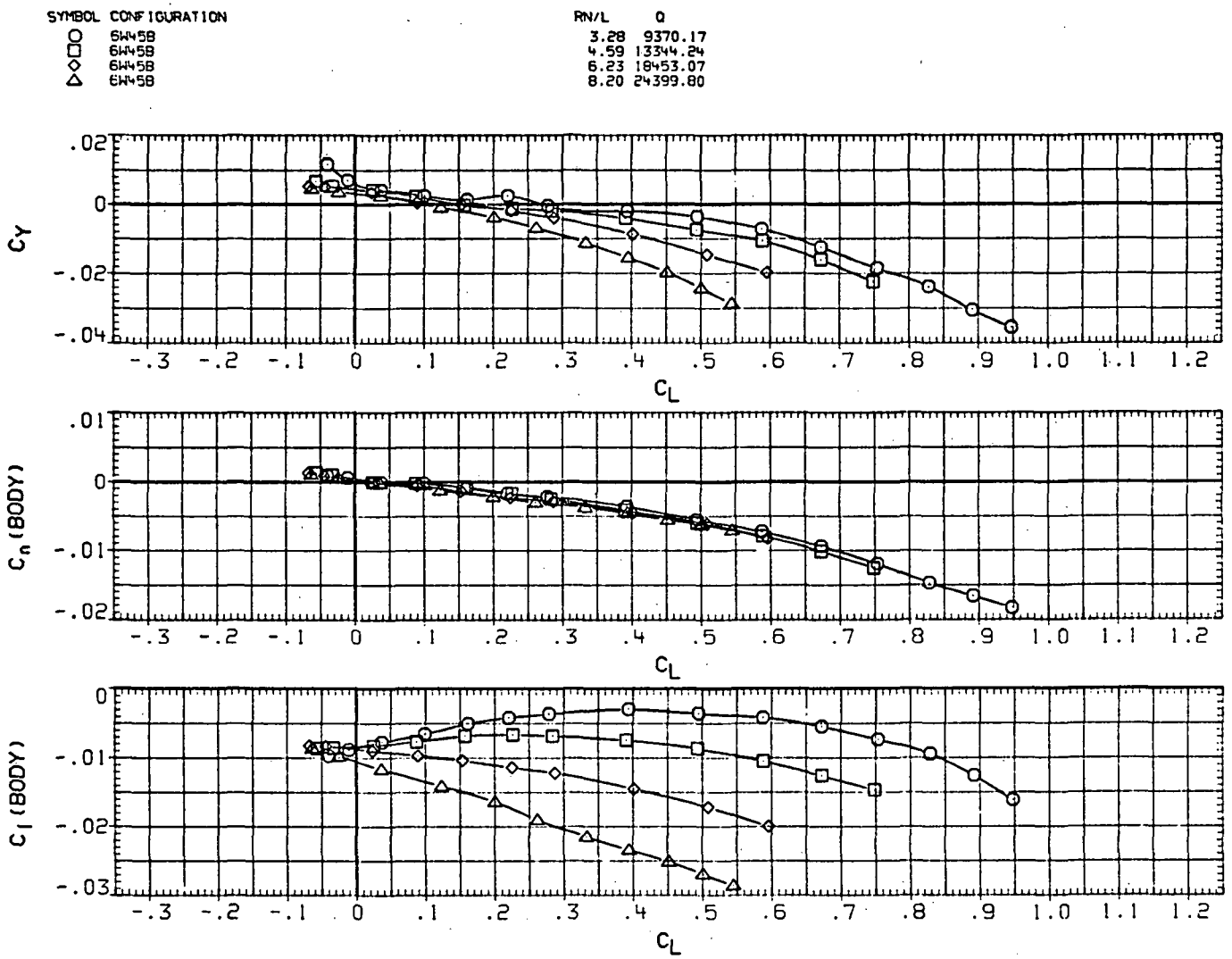


(e) $C_Y$, $C_n$, and $C_l$ vs $C_L$

Figure 12.– Concluded.

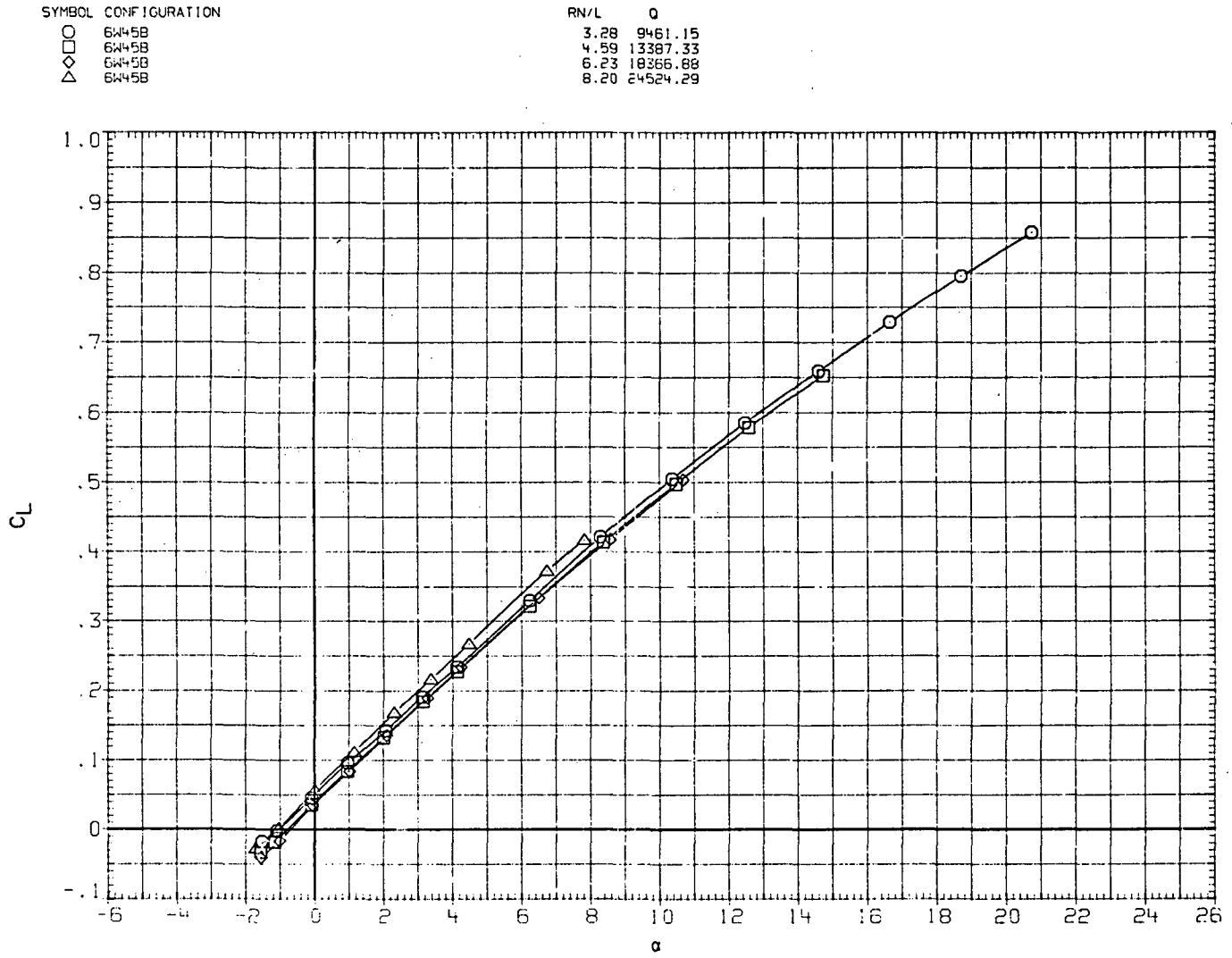


(a) $C_L$ vs $\alpha$

Figure 13.– Flexibility effects due to dynamic-pressure changes on the aerodynamic characteristics of the trapezoidal oblique wing: $\Lambda = 45°, M = 2.0$.

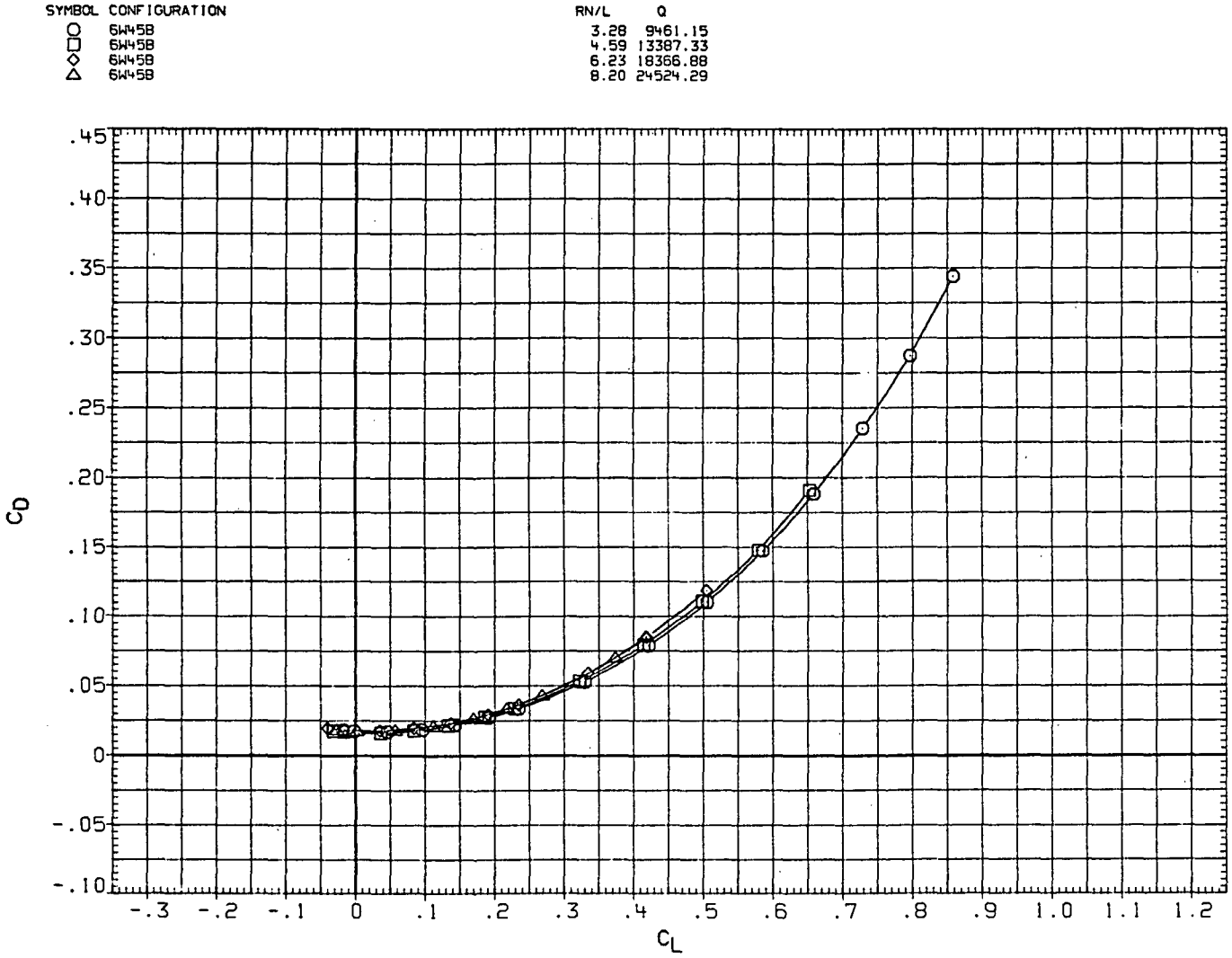


(b) $C_D$ vs $C_L$

Figure 13.– Continued.

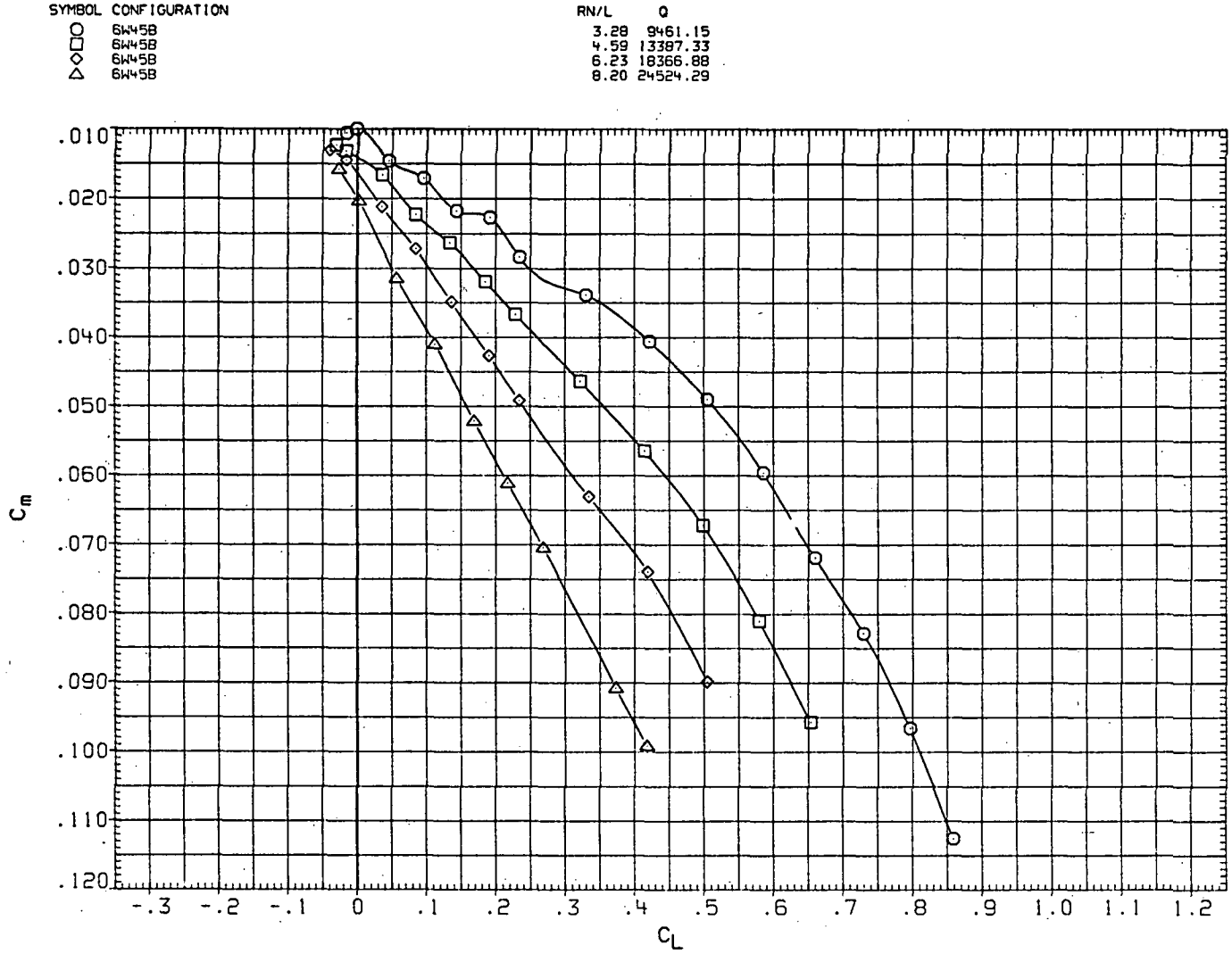


(c) $C_m$ vs $C_L$

Figure 13.– Continued.


(d) $L/D$ vs $C_L$

Figure 13.– Continued.

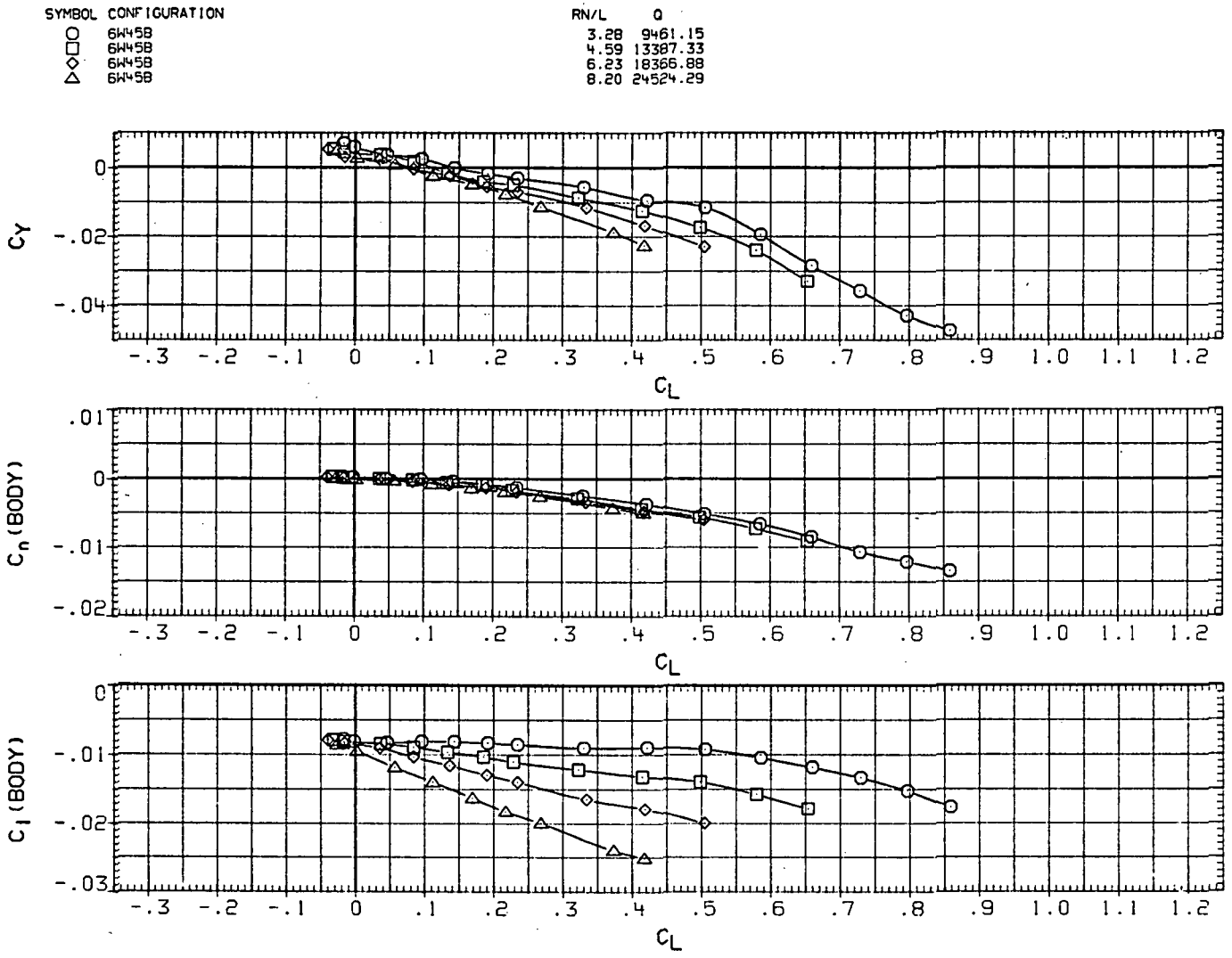


(e) $C_Y$, $C_n$ and $C_l$ vs $C_L$

Figure 13.– Concluded.

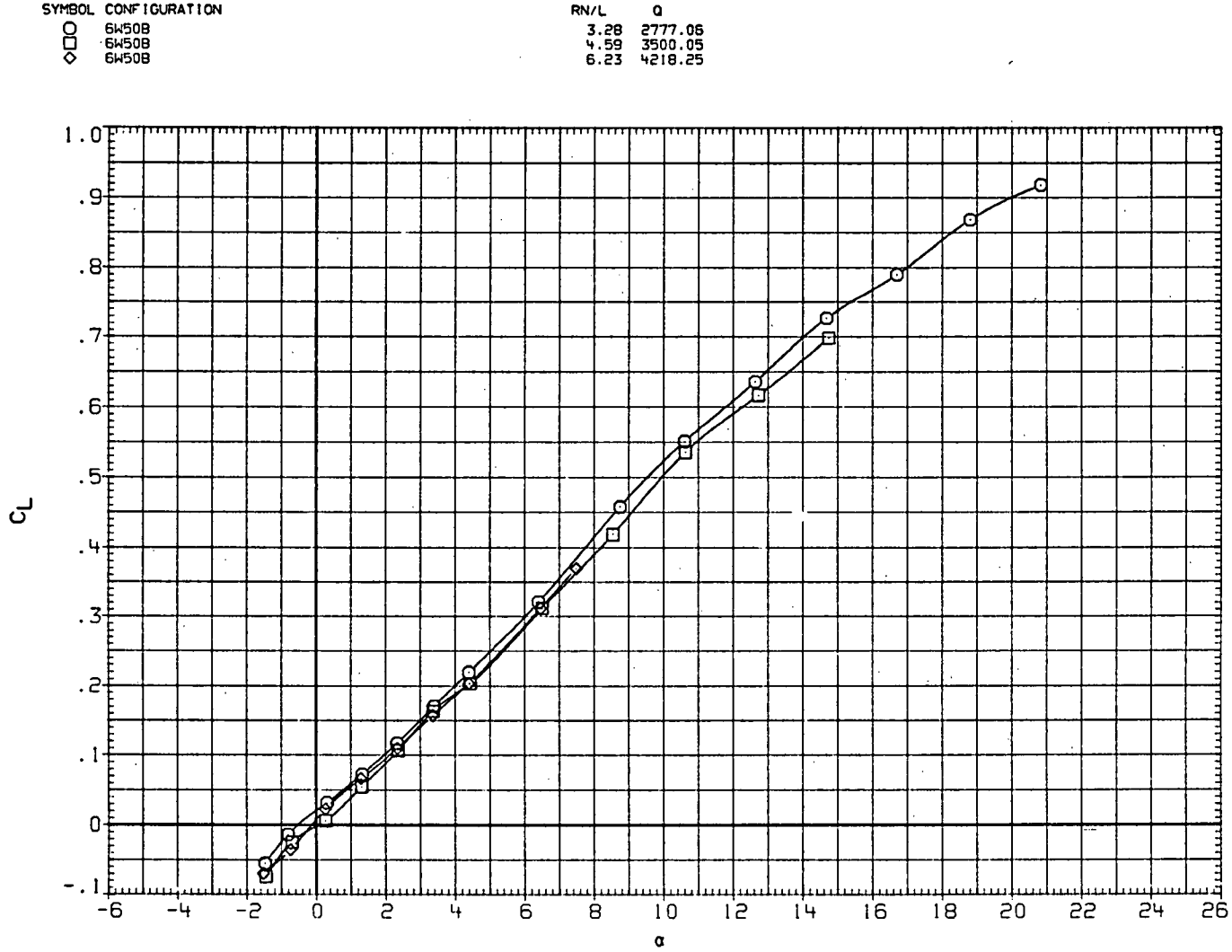


(a) $C_L$ vs $\alpha$

Figure 14.– Flexibility effects due to dynamic-pressure changes on the aerodynamic characteristics of the trapezoidal oblique wing: $\Lambda = 50°, M = 0.25$.

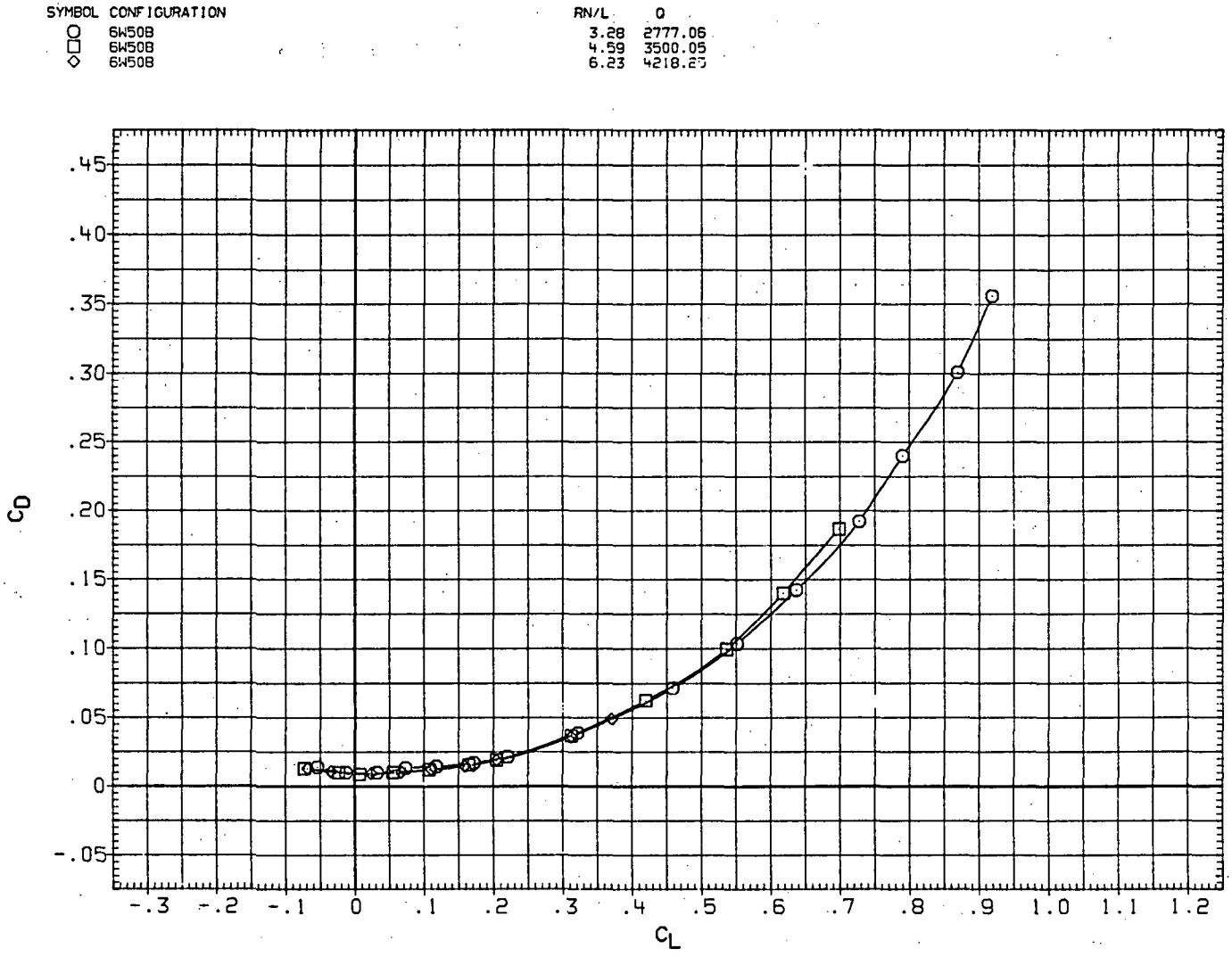


(b) $C_D$ vs $C_L$

Figure 14.– Continued.

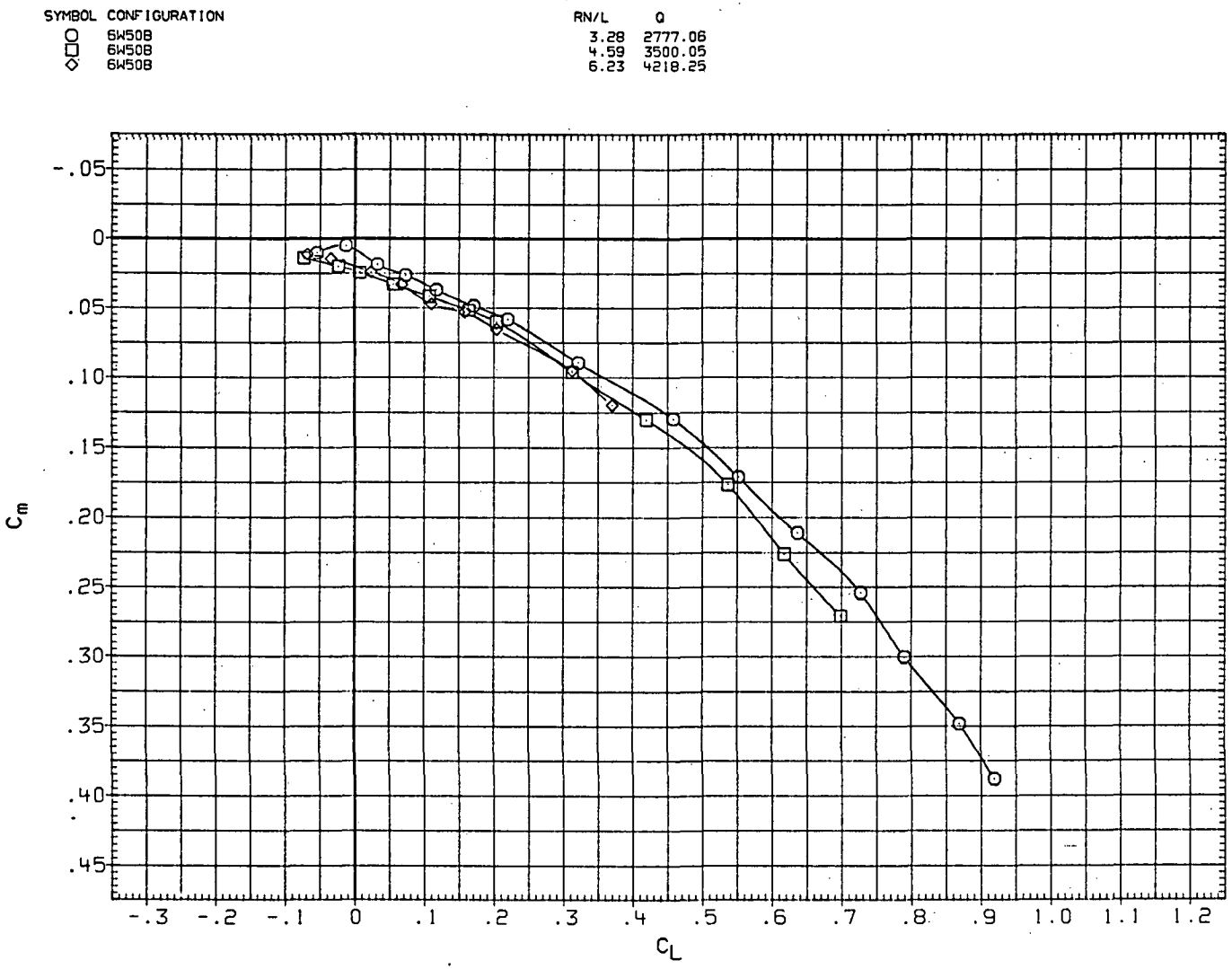


(c) $C_m$ vs $C_L$

Figure 14.– Continued.

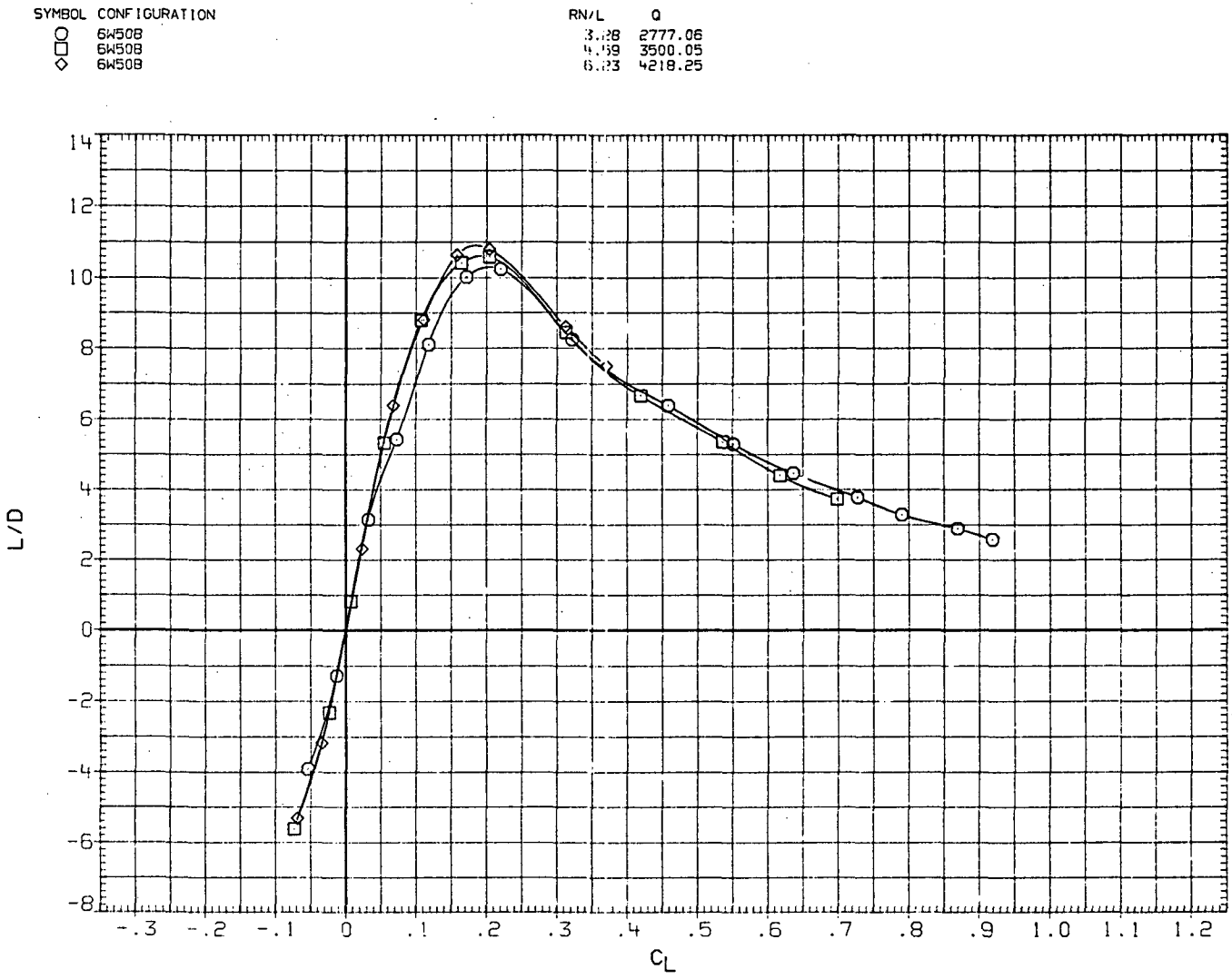


(d) $L/D$ vs $C_L$

Figure 14.– Continued.

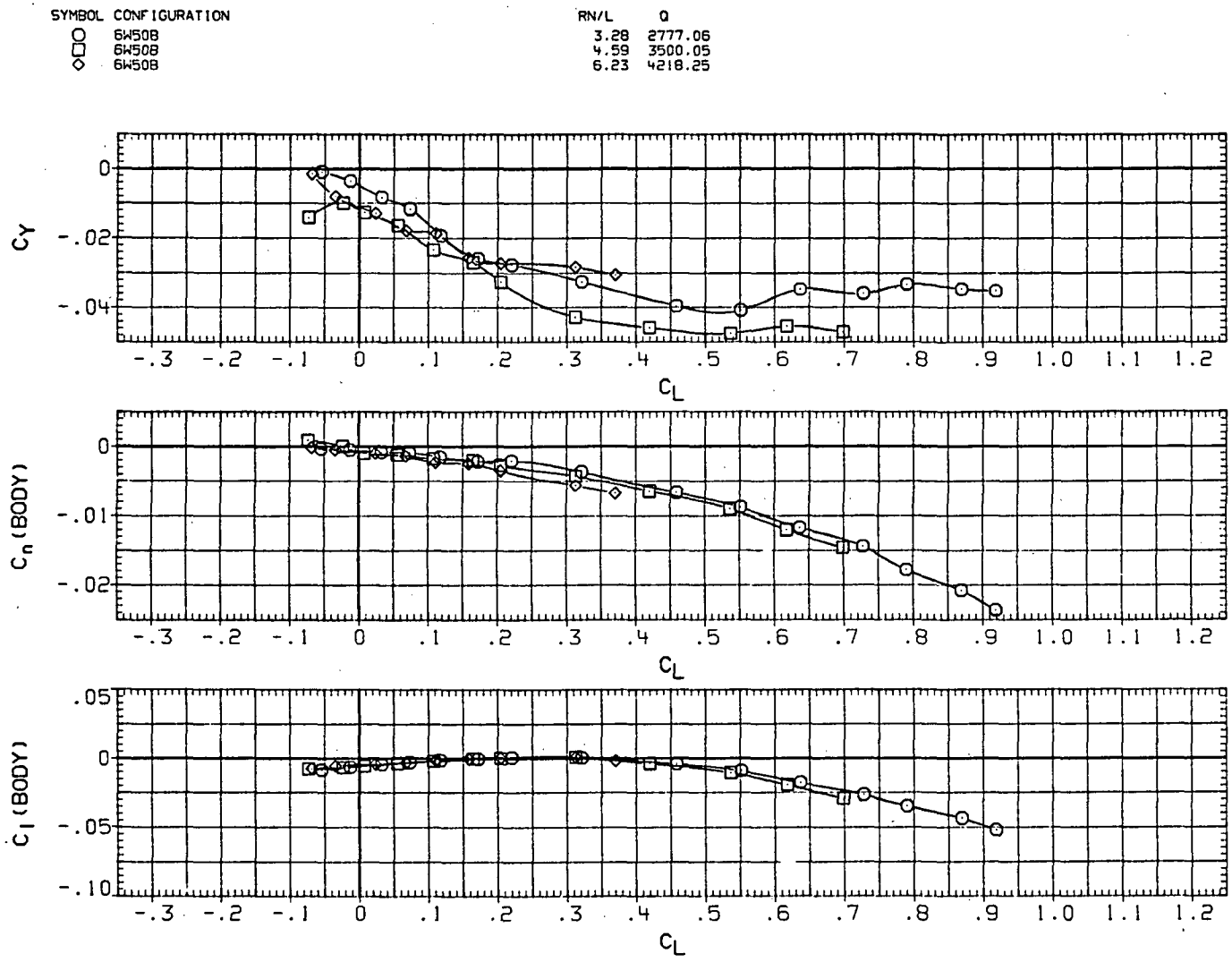


(e) $C_Y$, $C_n$, and $C_l$ vs $C_L$

Figure 14.– Concluded.

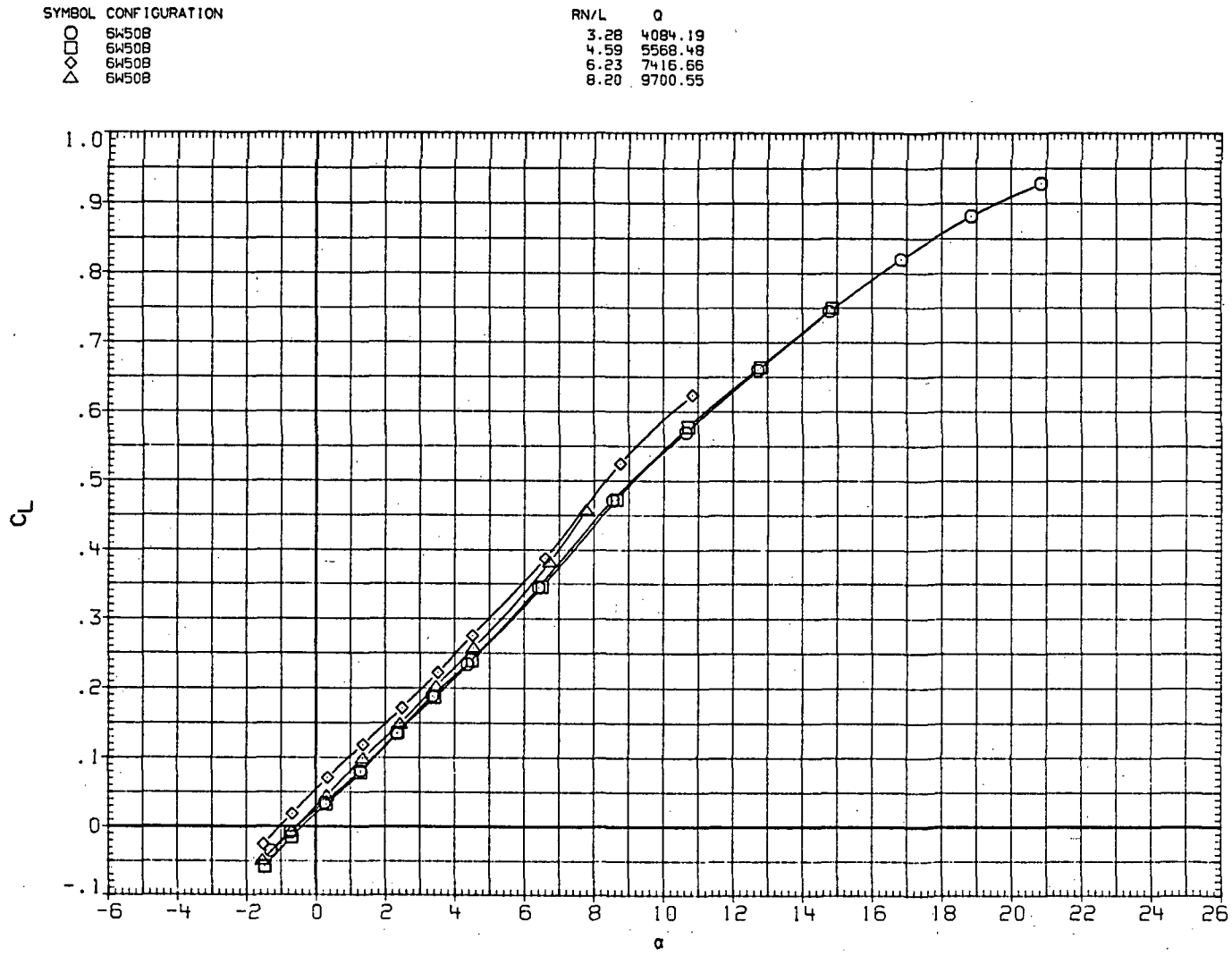


(a) $C_L$ vs $\alpha$

Figure 15.– Flexibility effects due to dynamic-pressure changes on the aerodynamic characteristics of the trapezoidal oblique wing: $\Lambda = 50°, M = 0.4$.

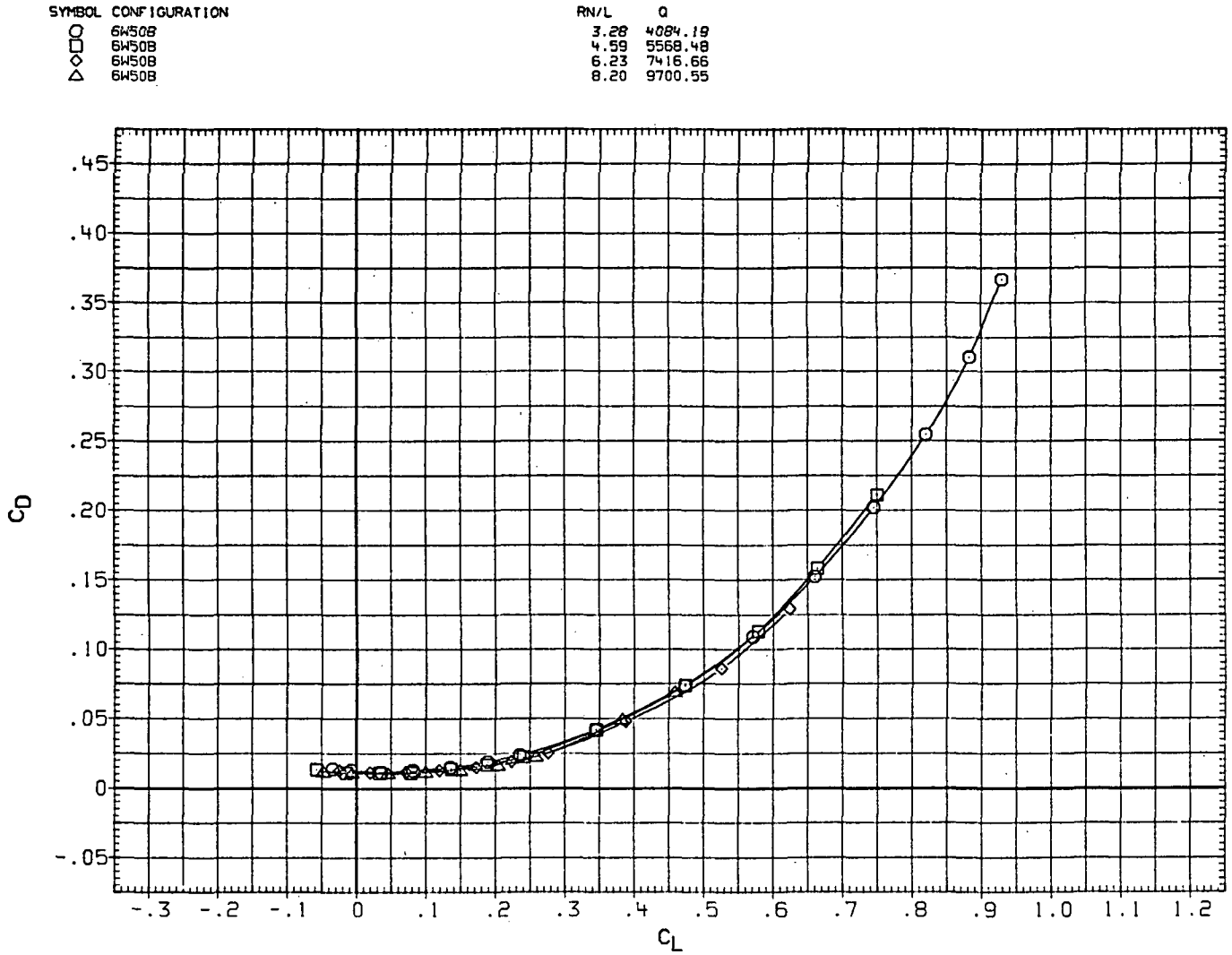


(b) $C_D$ vs $C_L$

Figure 15.– Continued.


(c) $C_m$ vs $C_L$

Figure 15.– Continued.

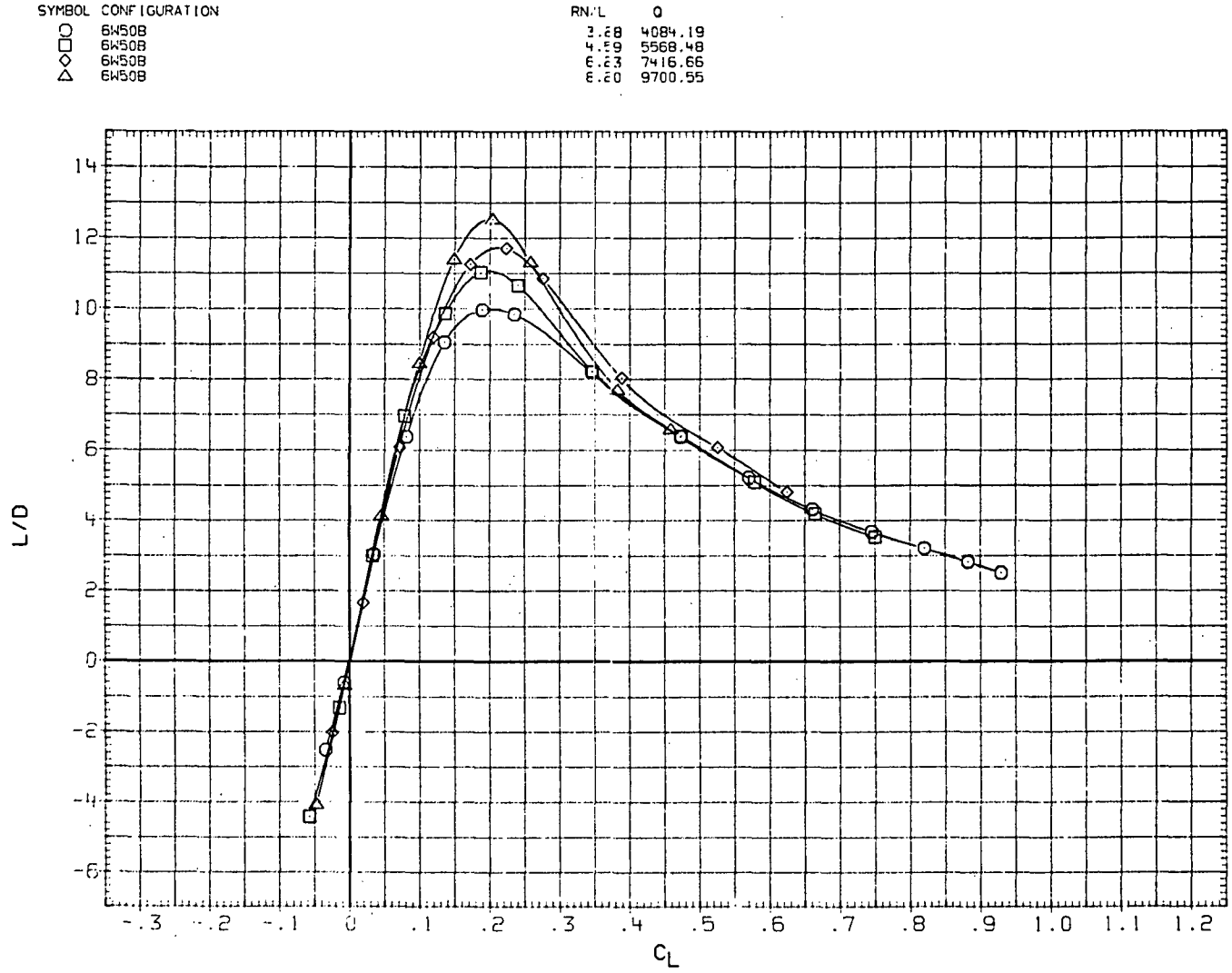


(d) $L/D$ vs $C_L$

Figure 15.– Continued.

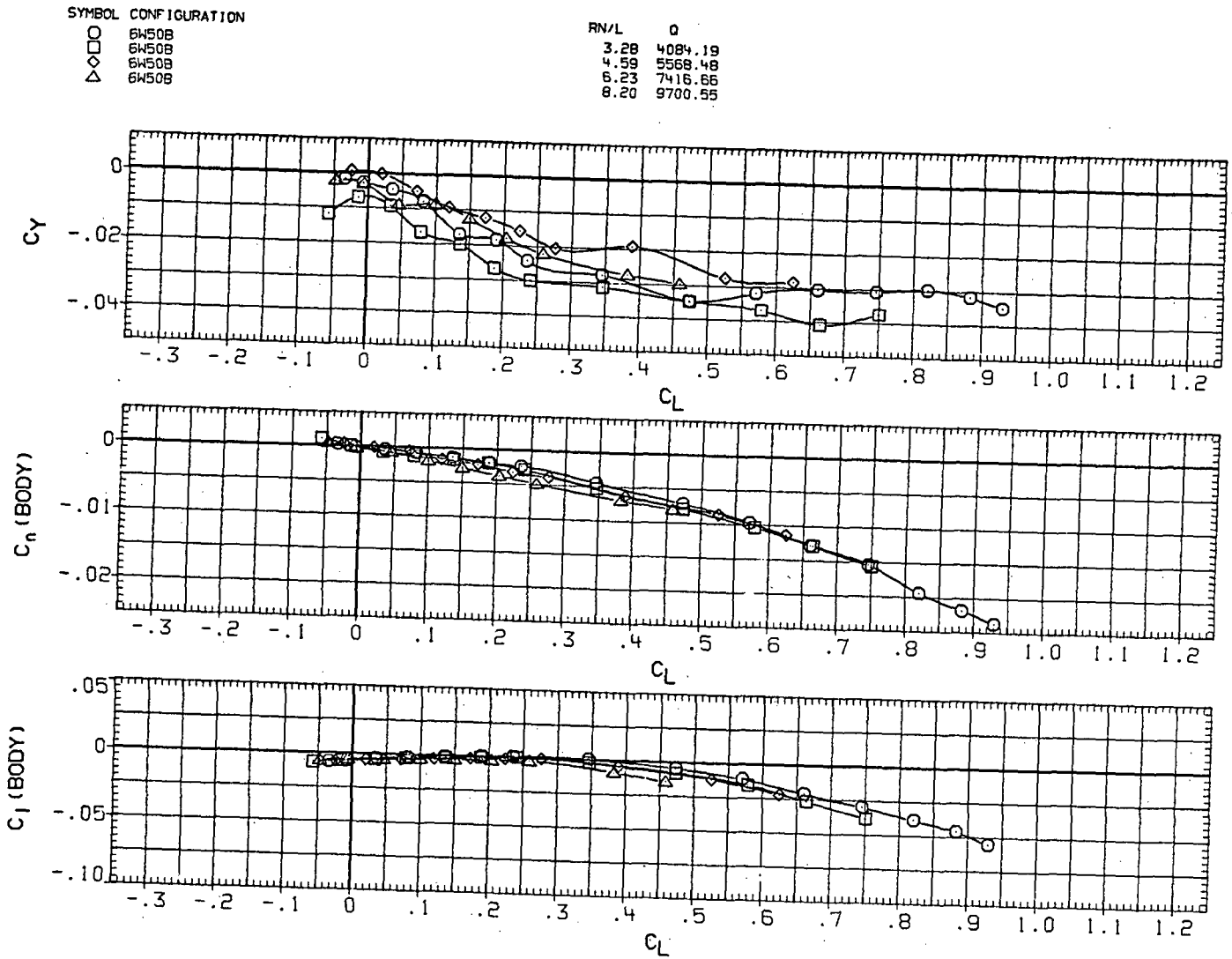


(e) $C_Y$, $C_n$, and $C_l$ vs $C_L$

Figure 15.– Concluded.

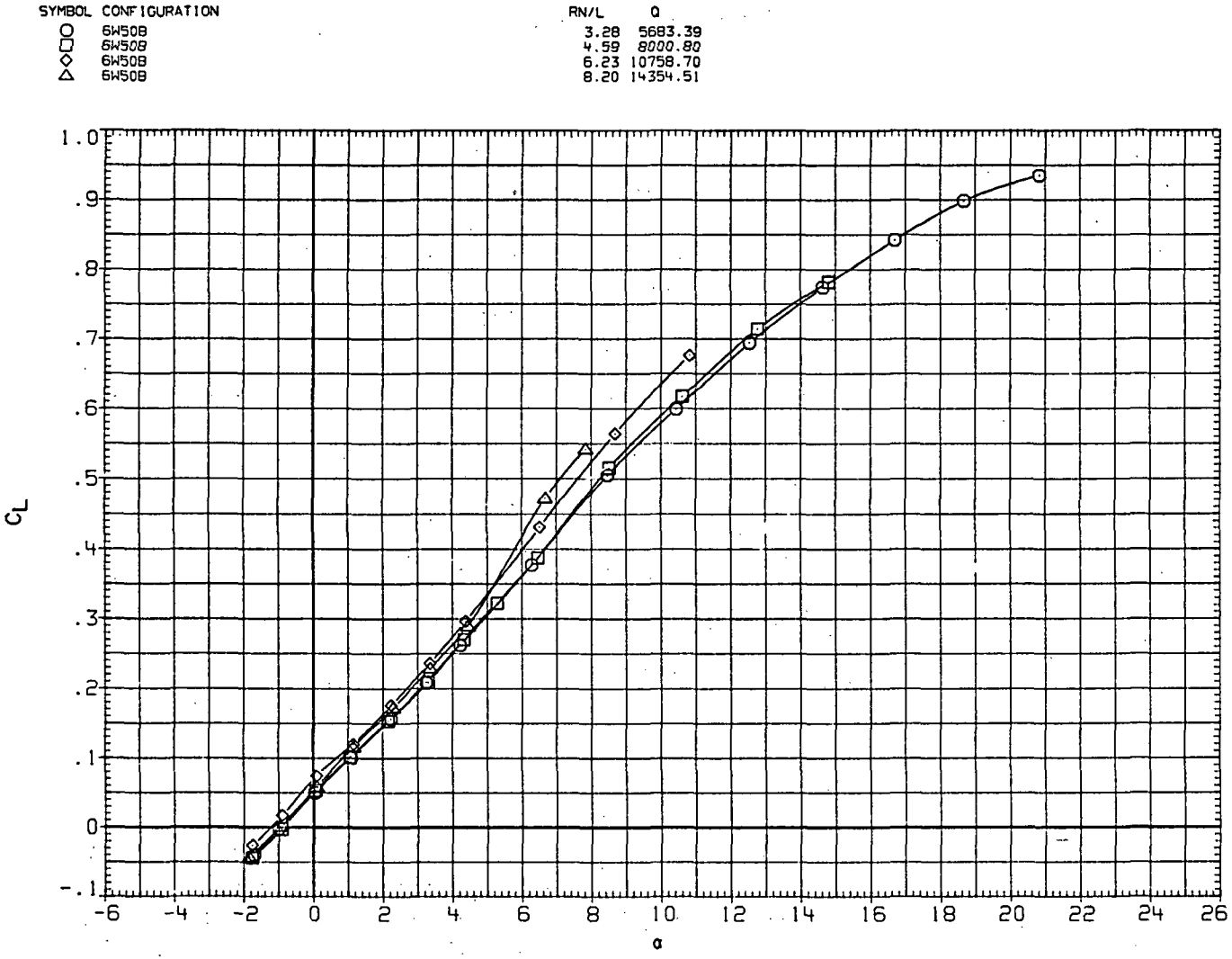


(a) $C_L$ vs $\alpha$

Figure 16.– Flexibility effects due to dynamic-pressure changes on the aerodynamic characteristics of the trapezoidal oblique wing: $\Lambda = 50°, M = 0.6$.

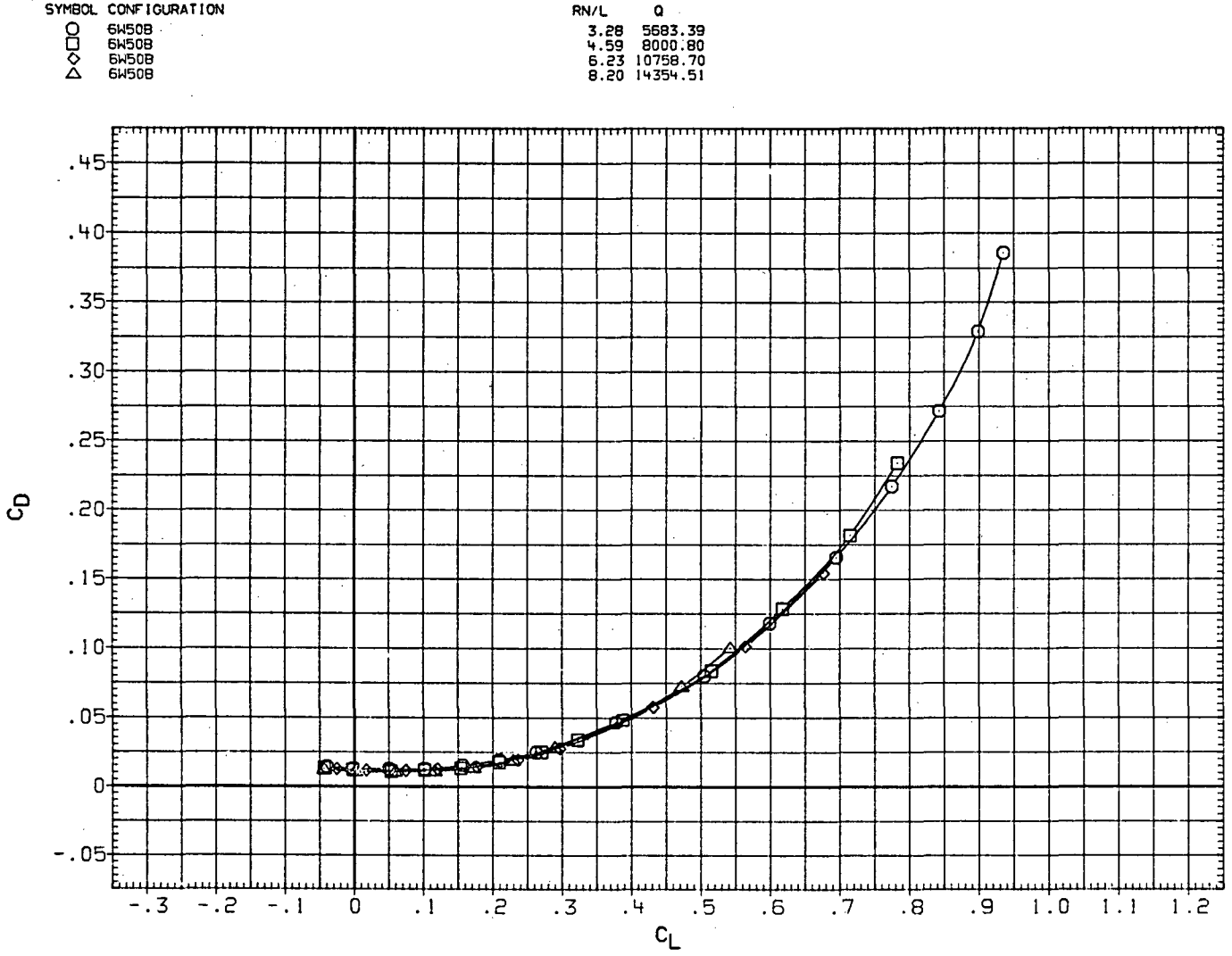


(b) $C_D$ vs $C_L$

Figure 16.– Continued.

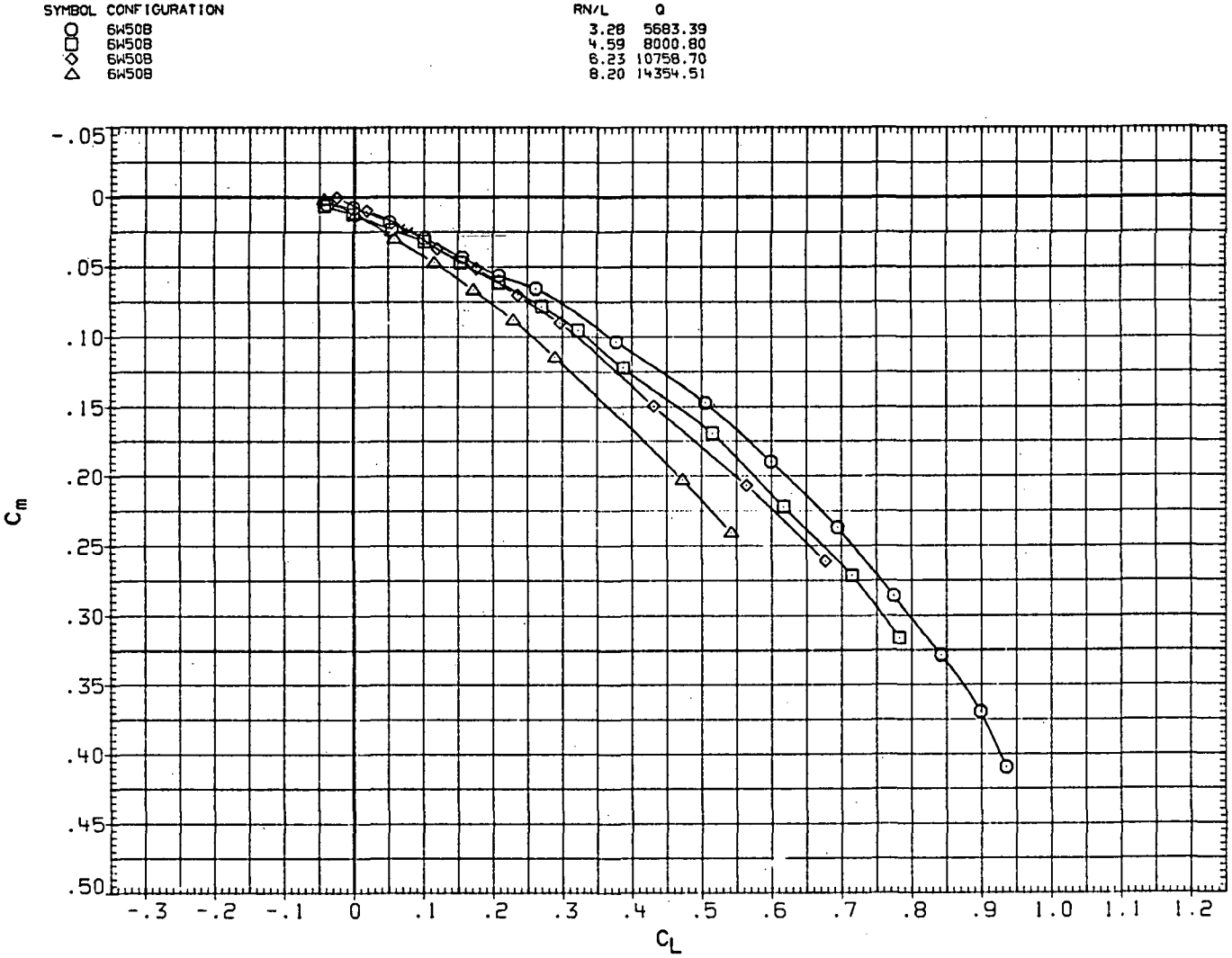


(c) $C_m$ vs $C_L$

Figure 16.– Continued.

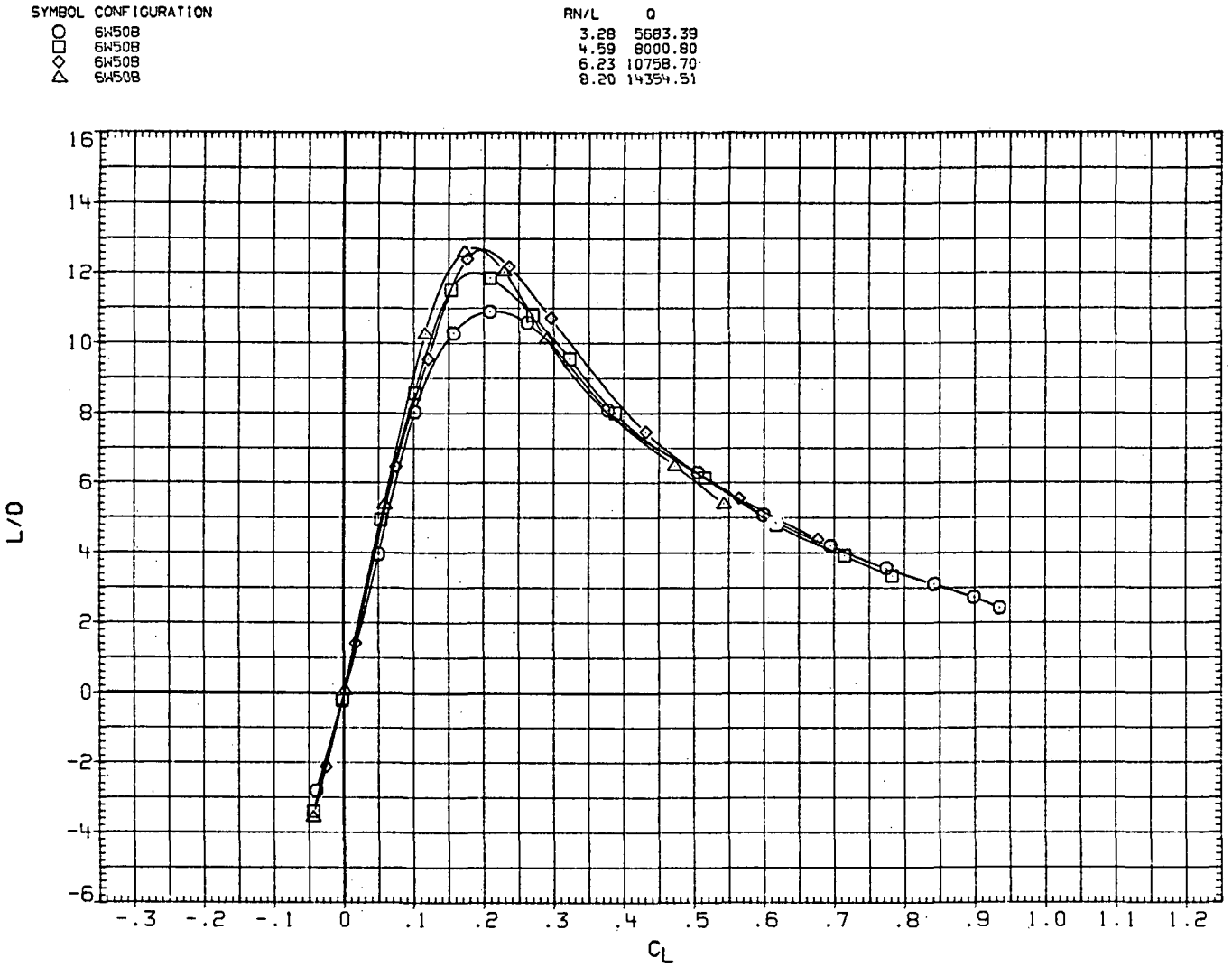


(d) $L/D$ vs $C_L$

Figure 16.– Continued.

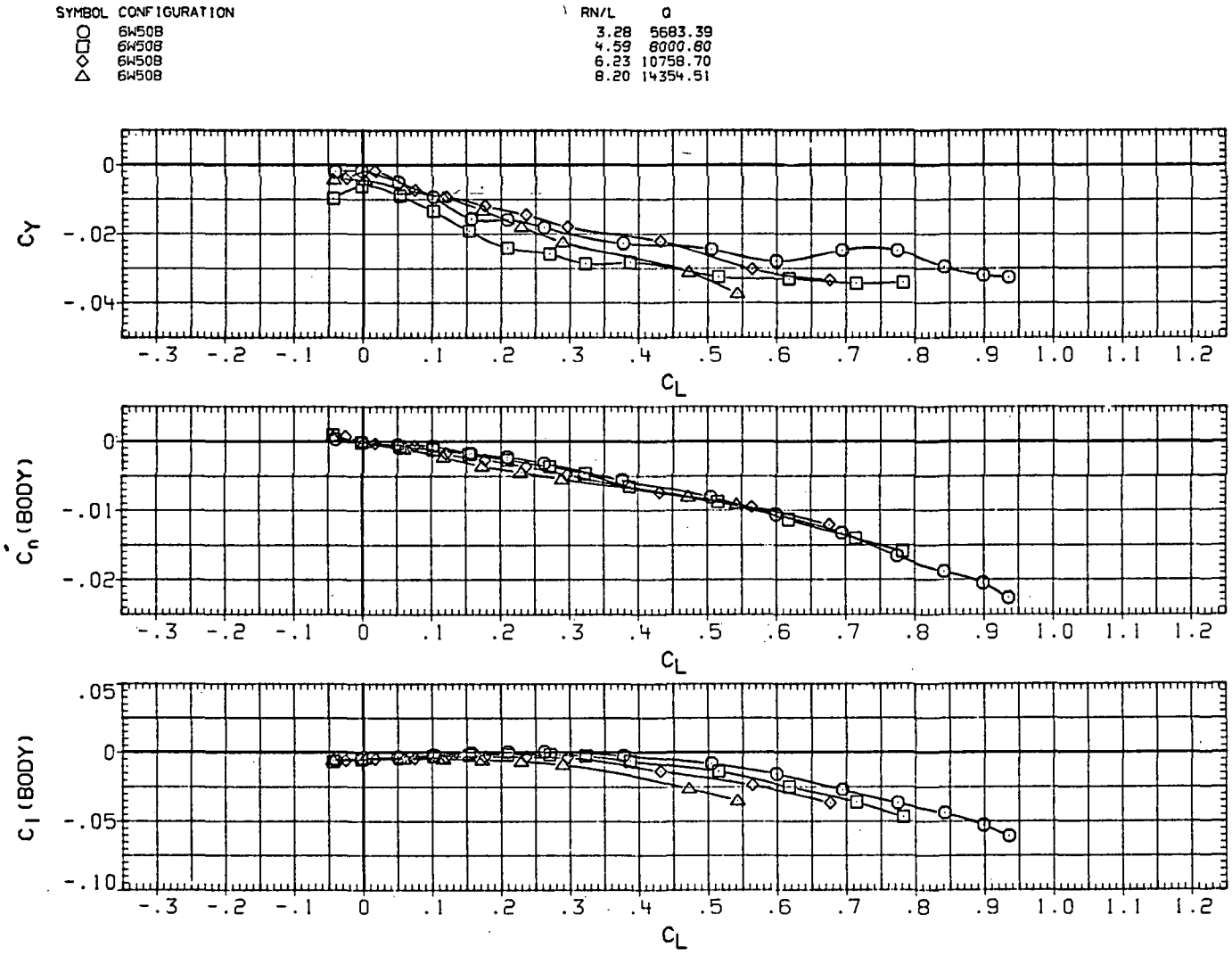


(e) $C_Y$, $C_n$, and $C_l$ vs $C_L$

Figure 16.– Concluded.

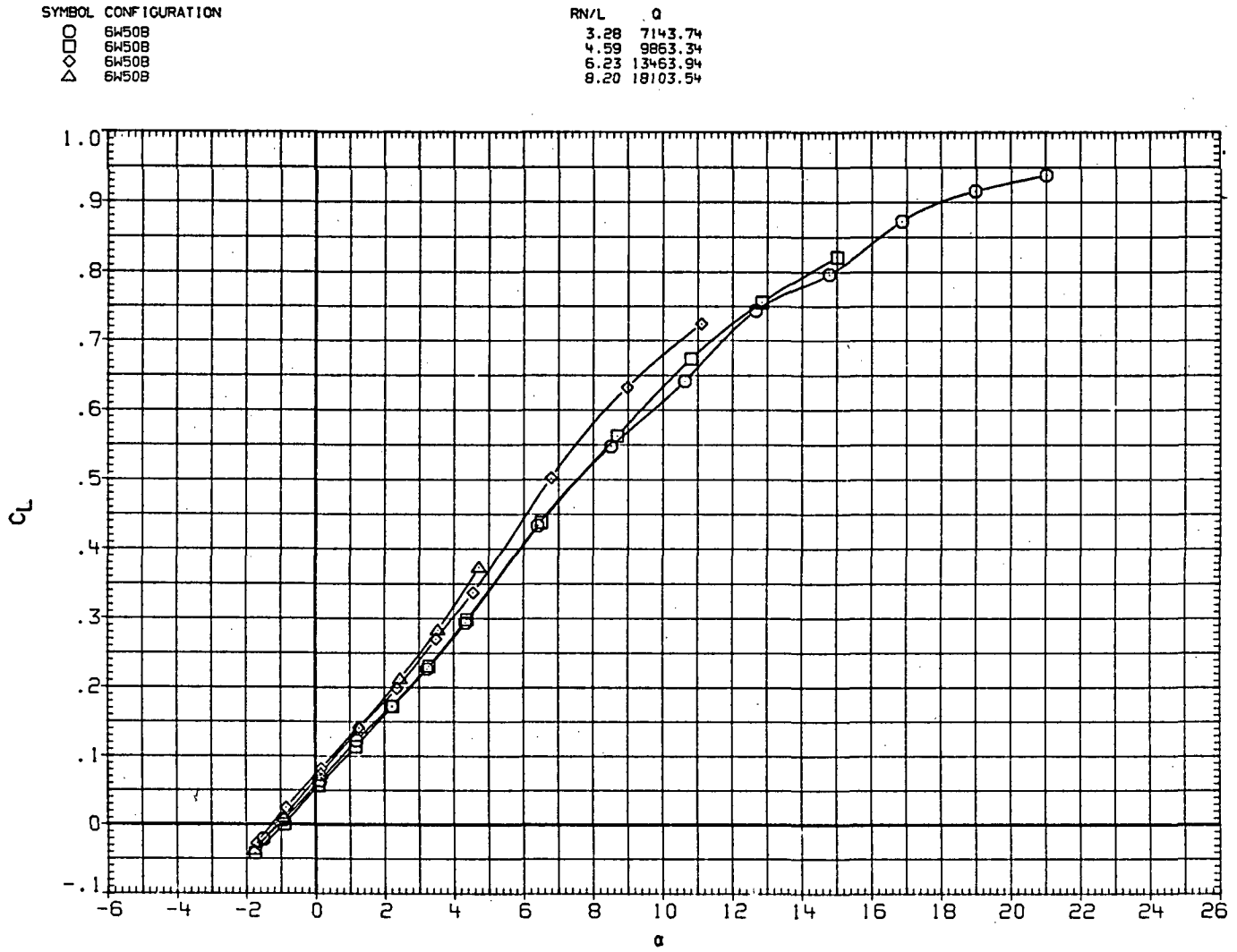


(a) $C_L$ vs $\alpha$

Figure 17.– Flexibility effects due to dynamic-pressure changes on the aerodynamic characteristics of the trapezoidal oblique wing: $\Lambda = 50°, M = 0.8$.

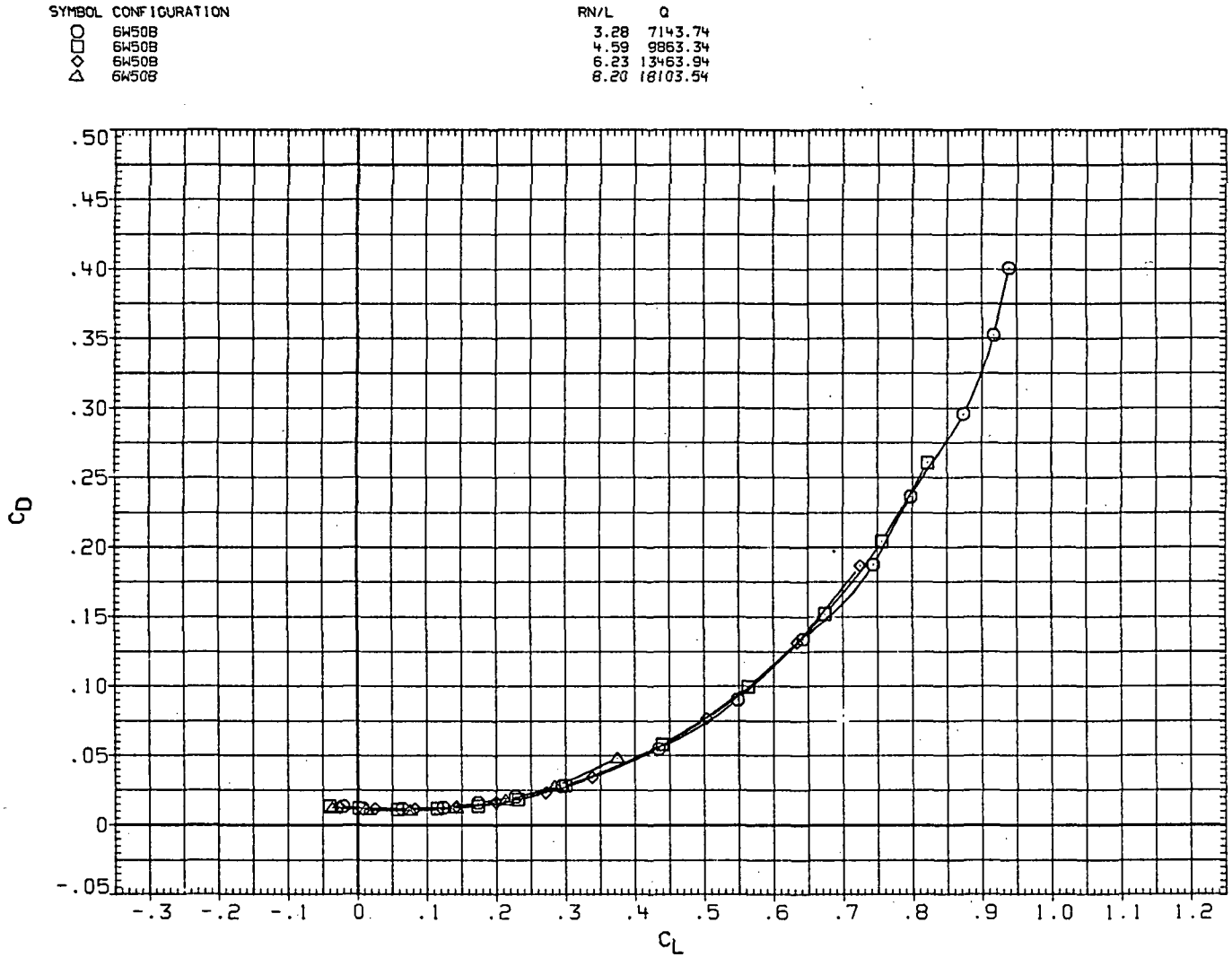


(b) $C_D$ vs $C_L$

Figure 17.– Continued.


(c) $C_m$ vs $C_L$

Figure 17.– Continued.

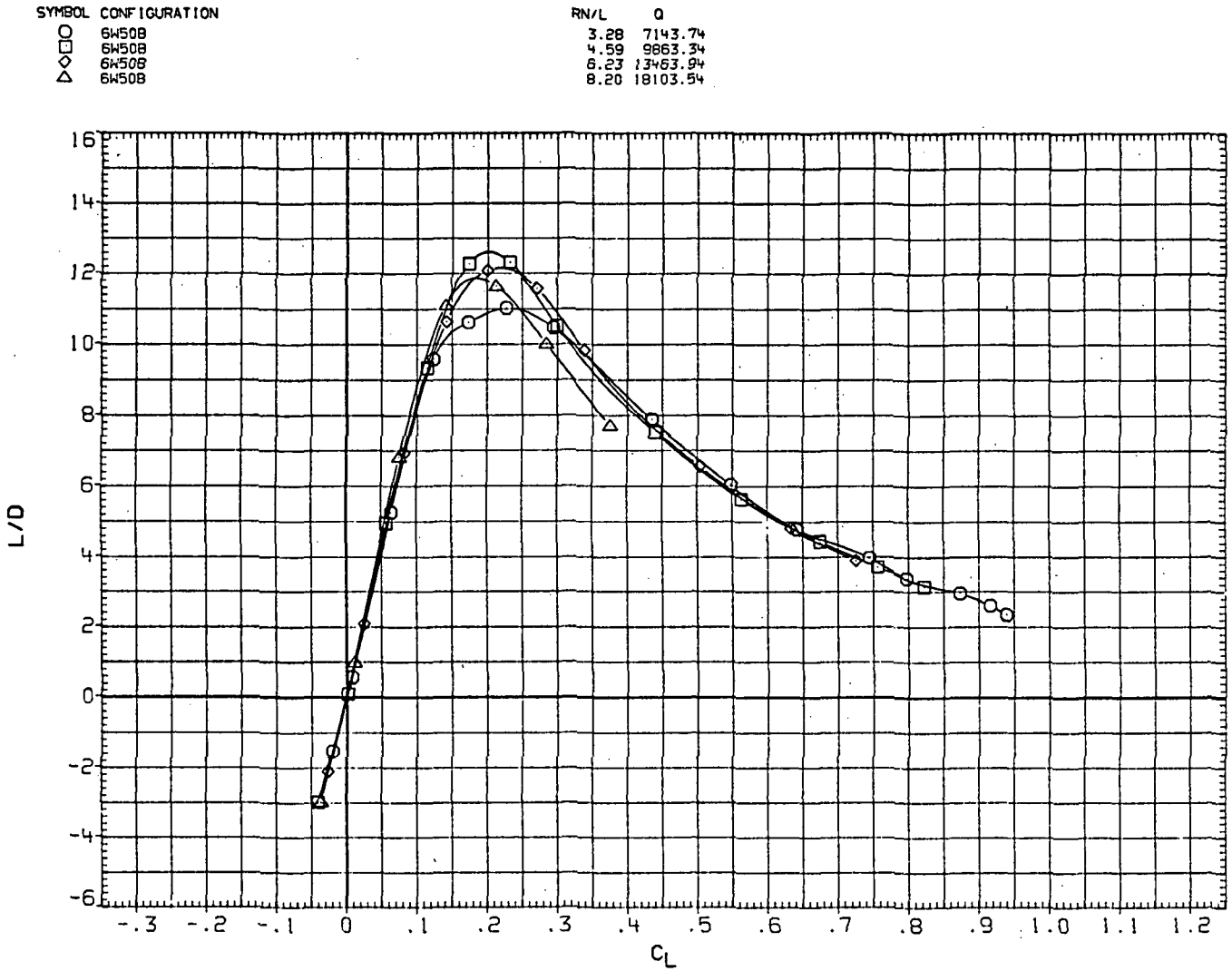


(d) $L/D$ vs $C_L$

Figure 17.– Continued.

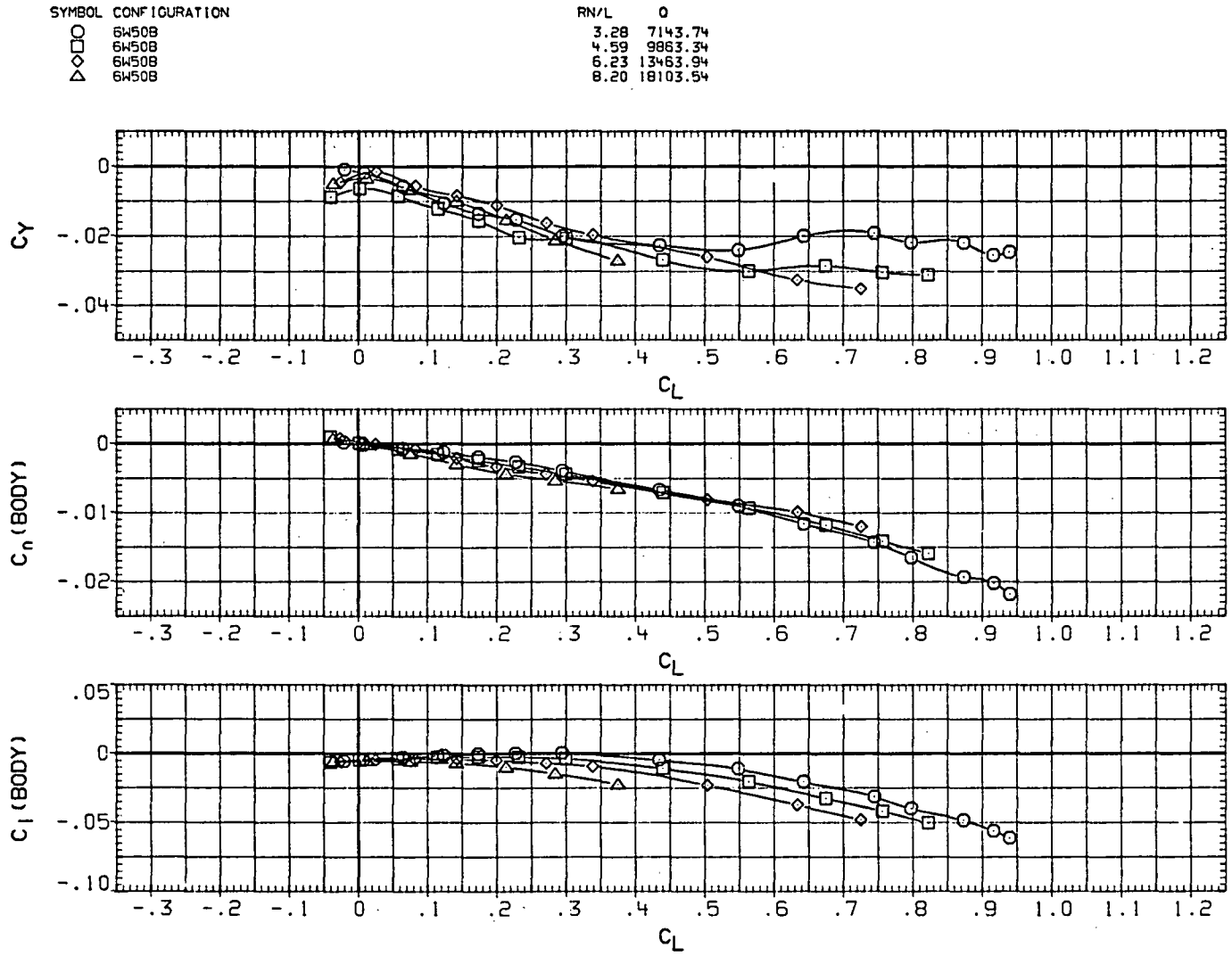


(e) $C_Y$, $C_n$, and $C_l$ vs $C_L$

Figure 17.– Concluded.

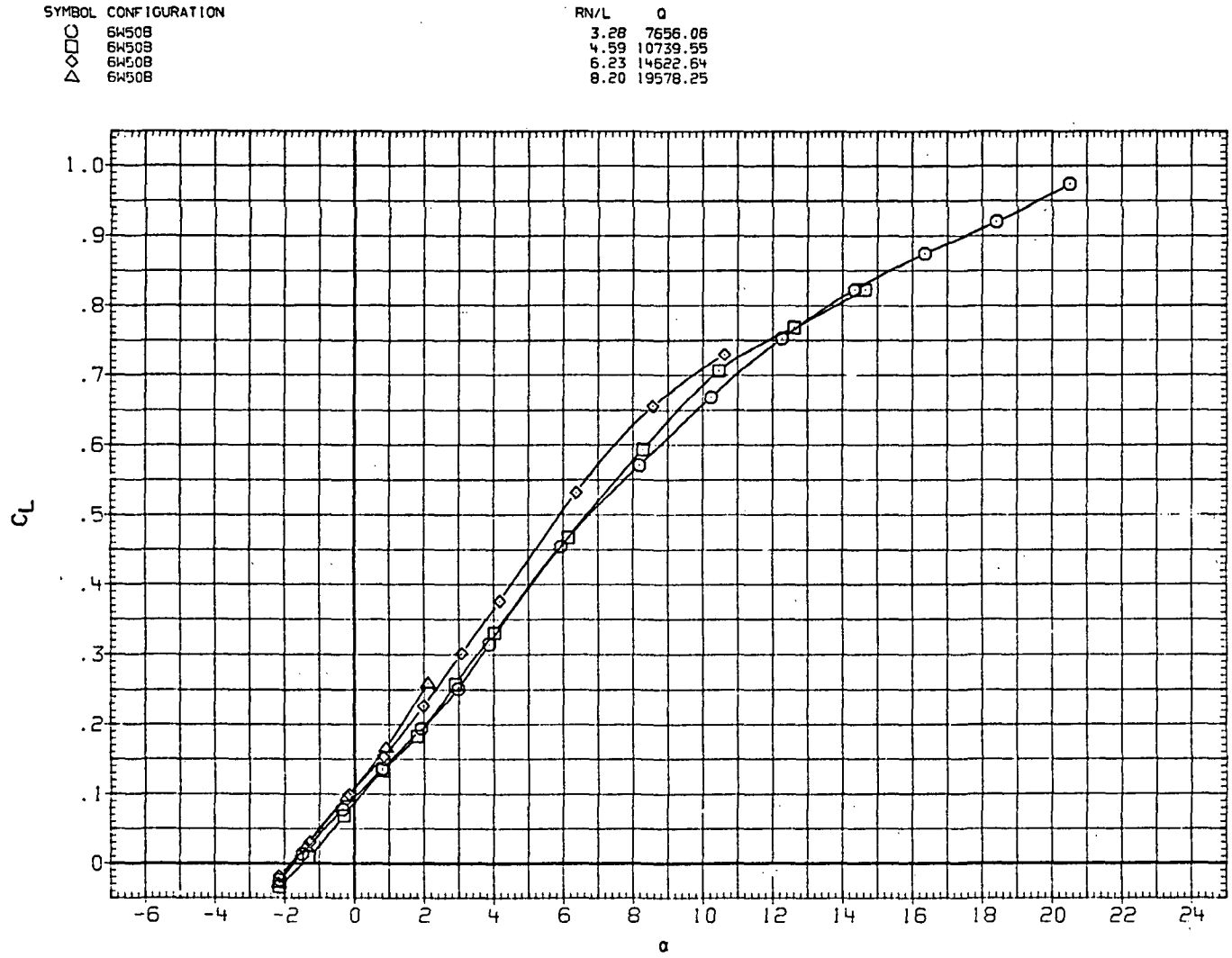


(a) $C_L$ vs $\alpha$

Figure 18.– Flexibility effects due to dynamic-pressure changes on the aerodynamic characteristics of the trapezoidal oblique wing: $\Lambda = 50°, M = 0.9$.

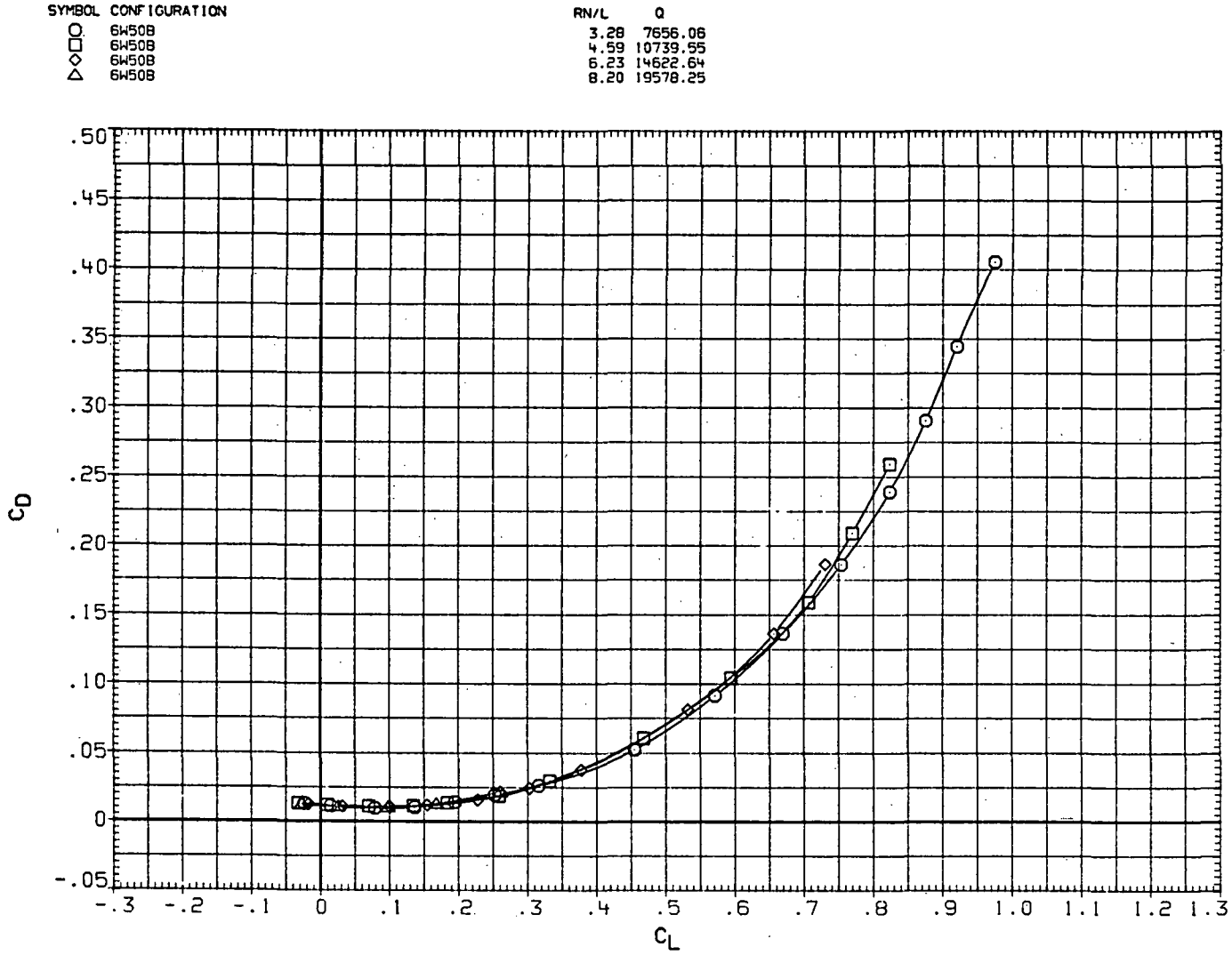


(b) $C_D$ vs $C_L$

Figure 18.– Continued.

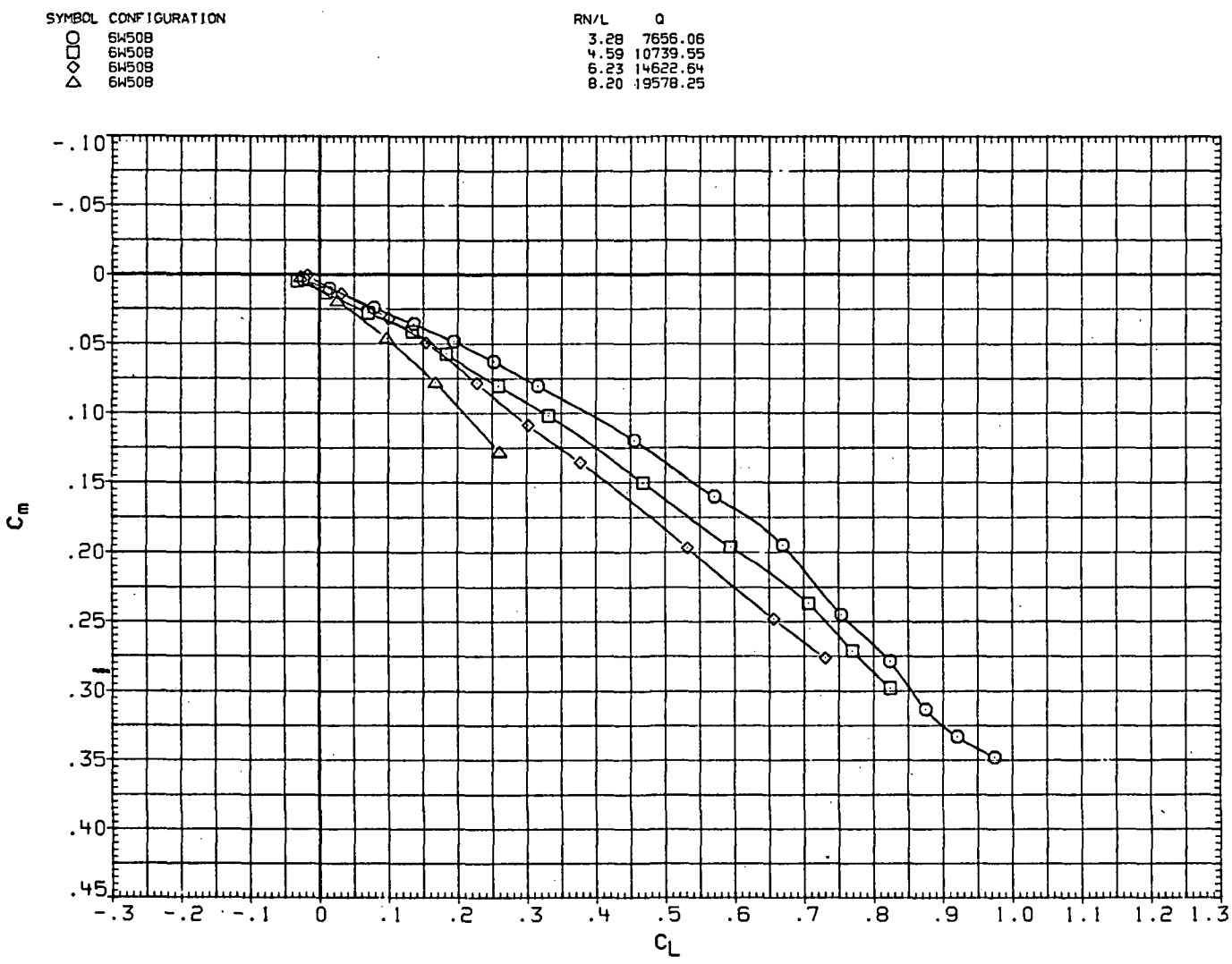


(c) $C_m$ vs $C_L$

Figure 18.– Continued.

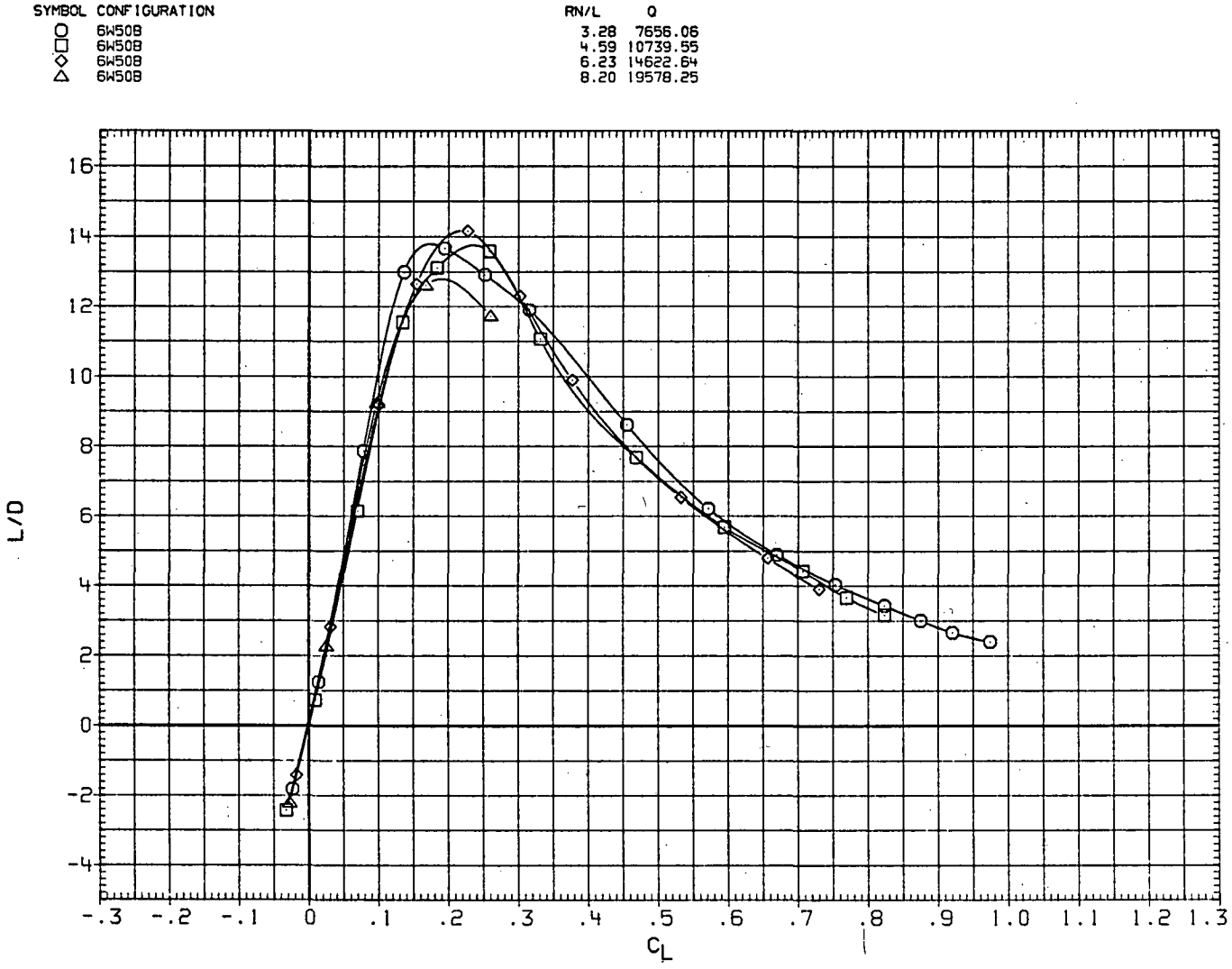


(d) $L/D$ vs $C_L$

Figure 18.– Continued.

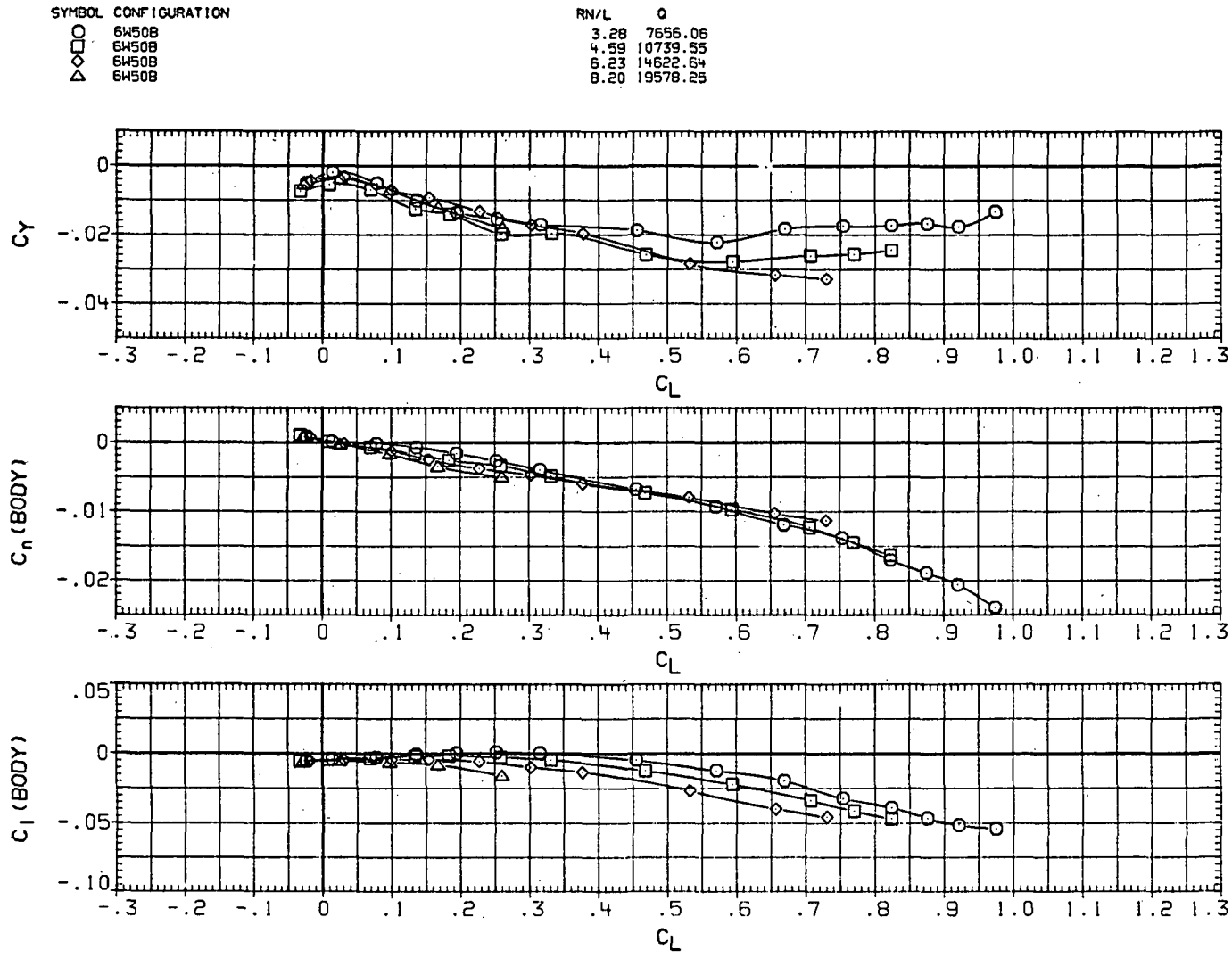


(e) $C_Y$, $C_n$, and $C_l$ vs $C_L$

Figure 18.– Concluded.

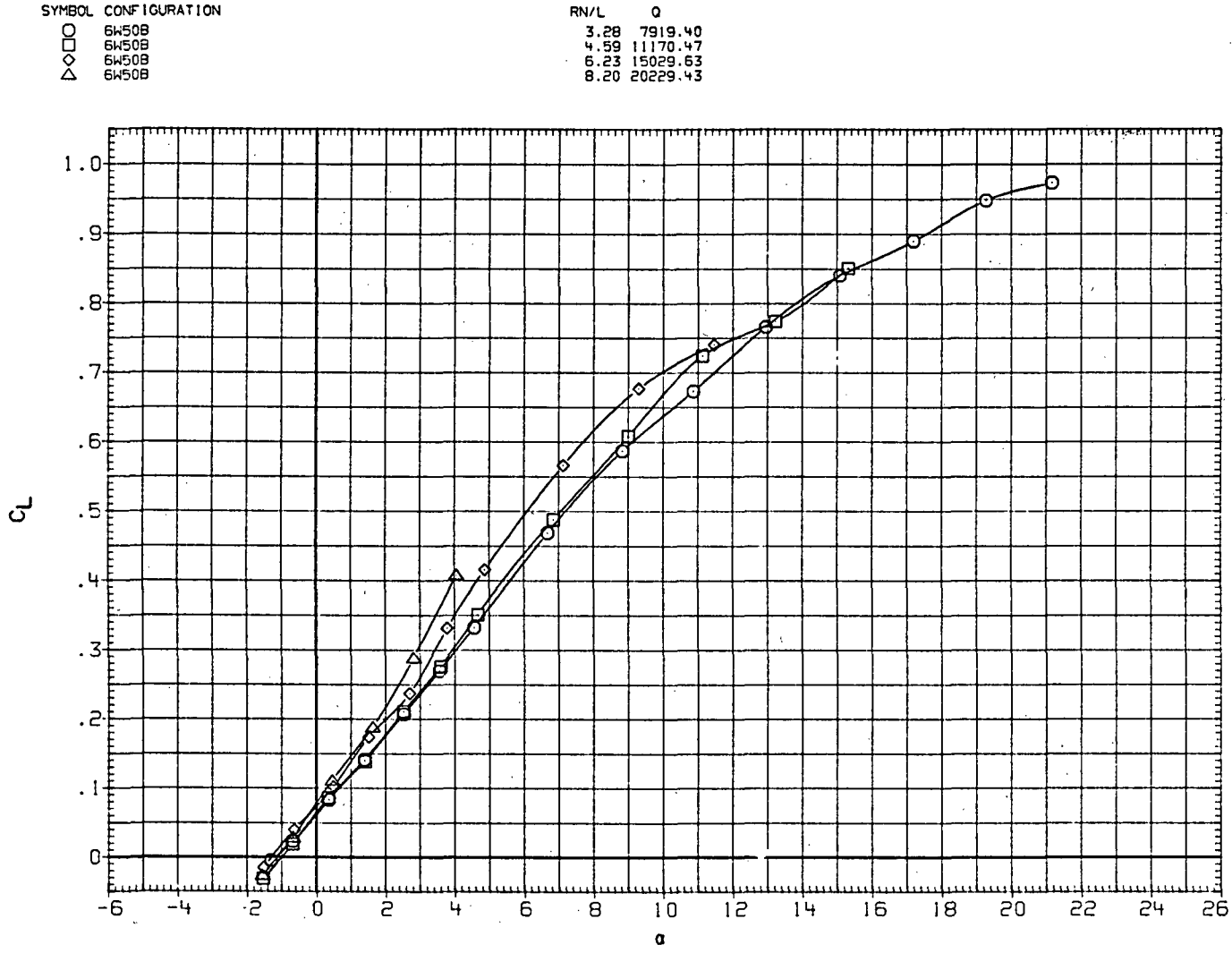


(a) $C_L$ vs $\alpha$

Figure 19.– Flexibility effects due to dynamic-pressure changes on the aerodynamic characteristics of the trapezoidal oblique wing: $\Lambda = 50°, M = 0.95$.

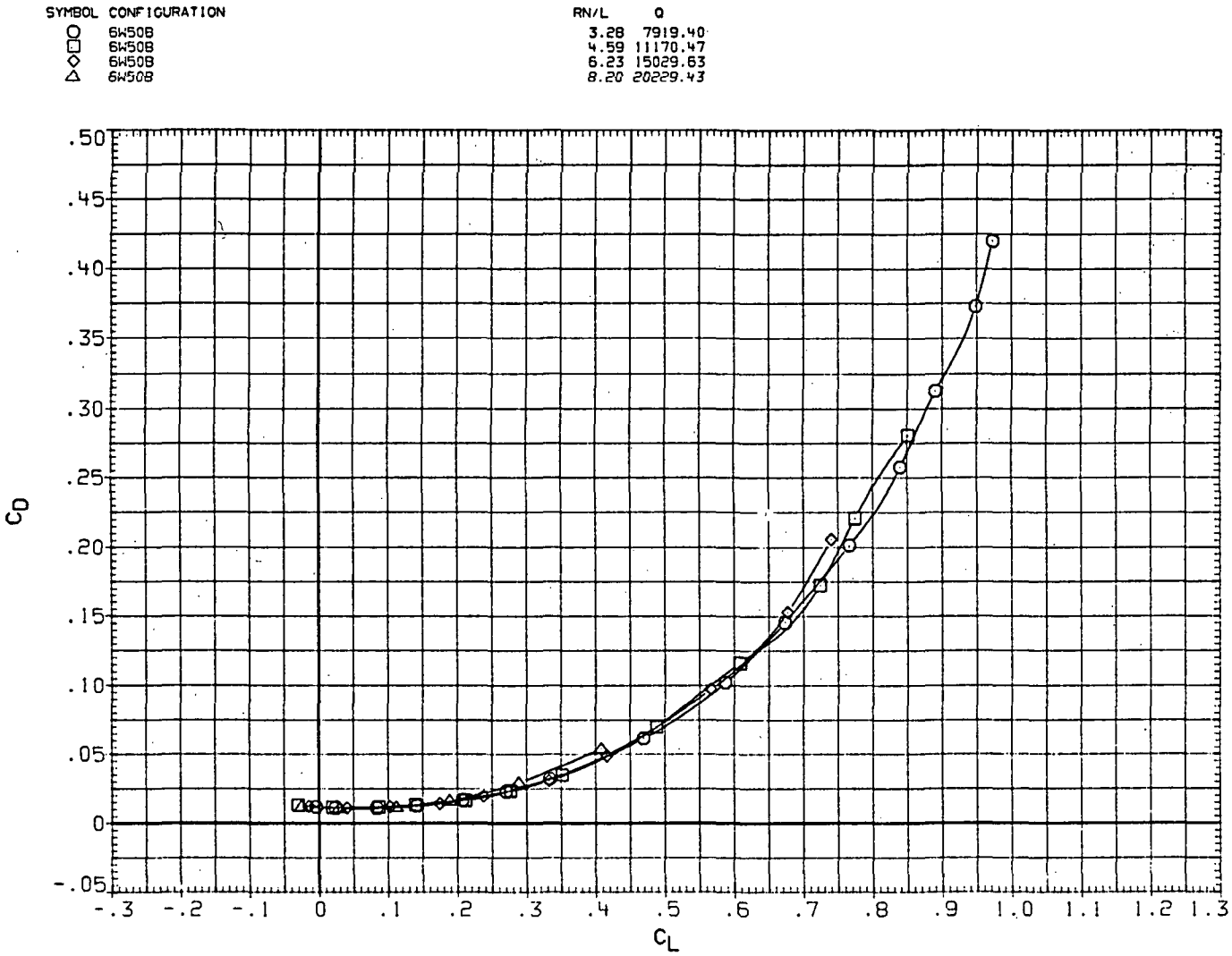


(b) $C_D$ vs $C_L$

Figure 19.– Continued.

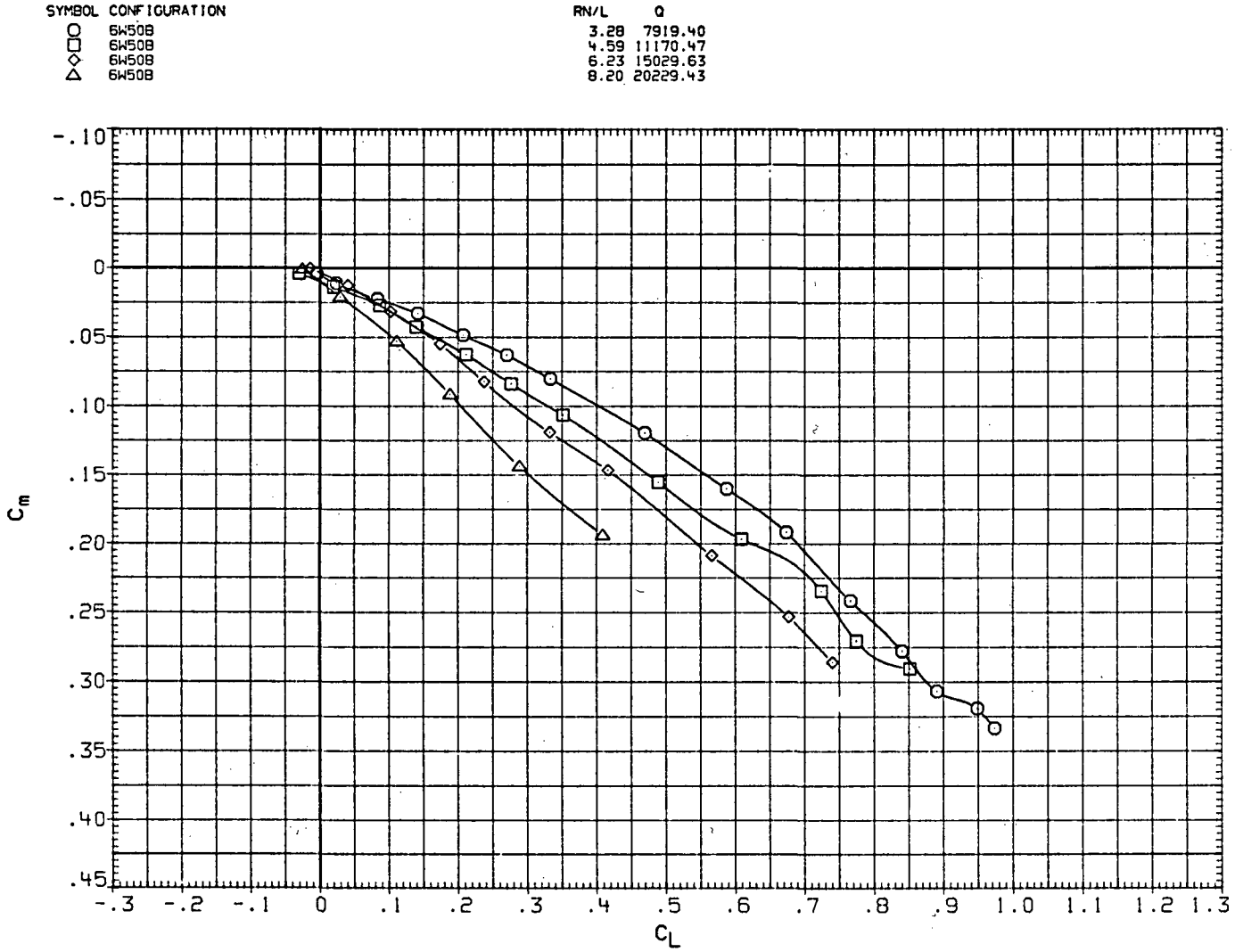


(c) $C_m$ vs $C_L$

Figure 19.– Continued.

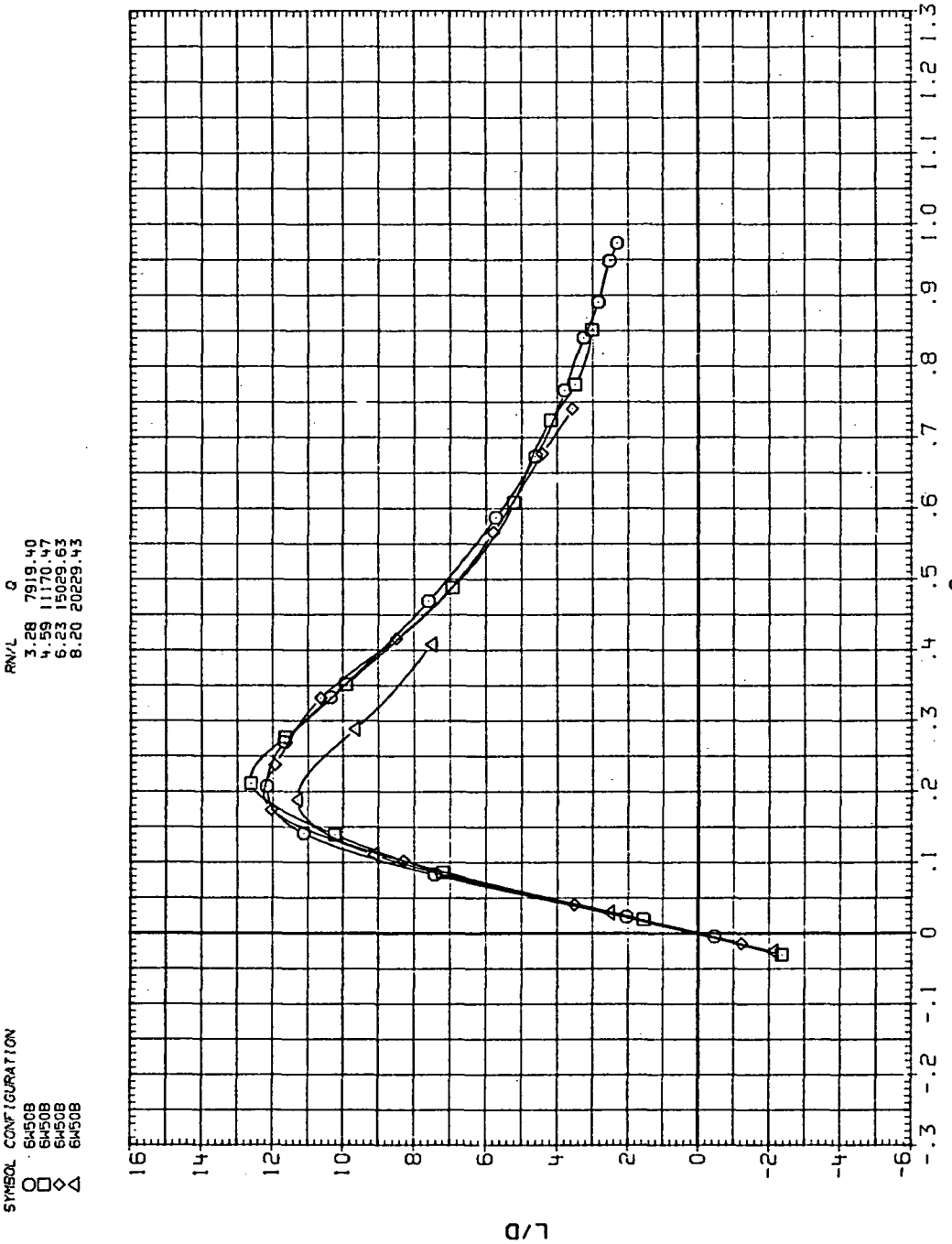


(d) $L/D$ vs $C_L$

Figure 19.– Continued.

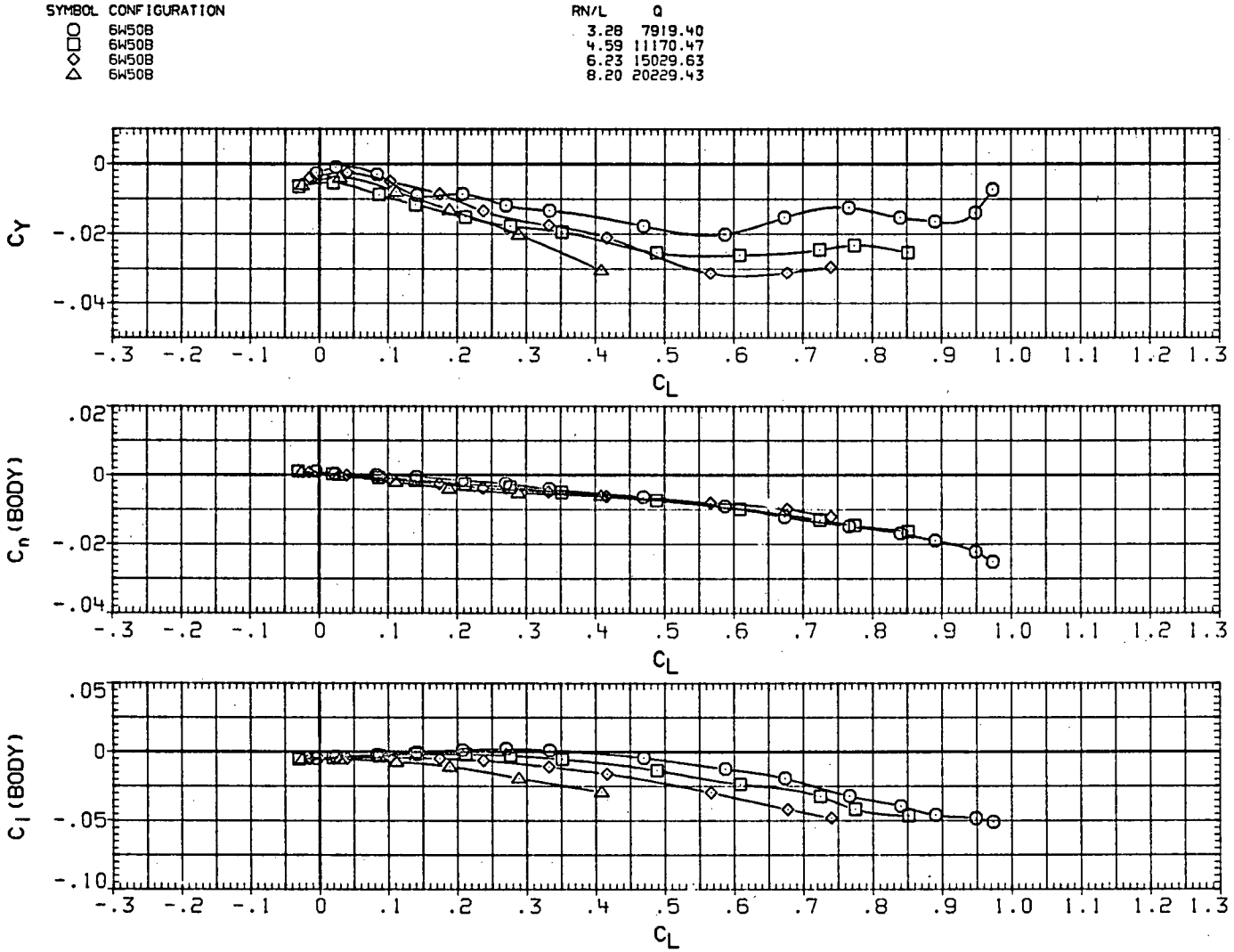


(e) $C_Y$, $C_n$, and $C_l$ vs $C_L$

Figure 19.– Concluded.

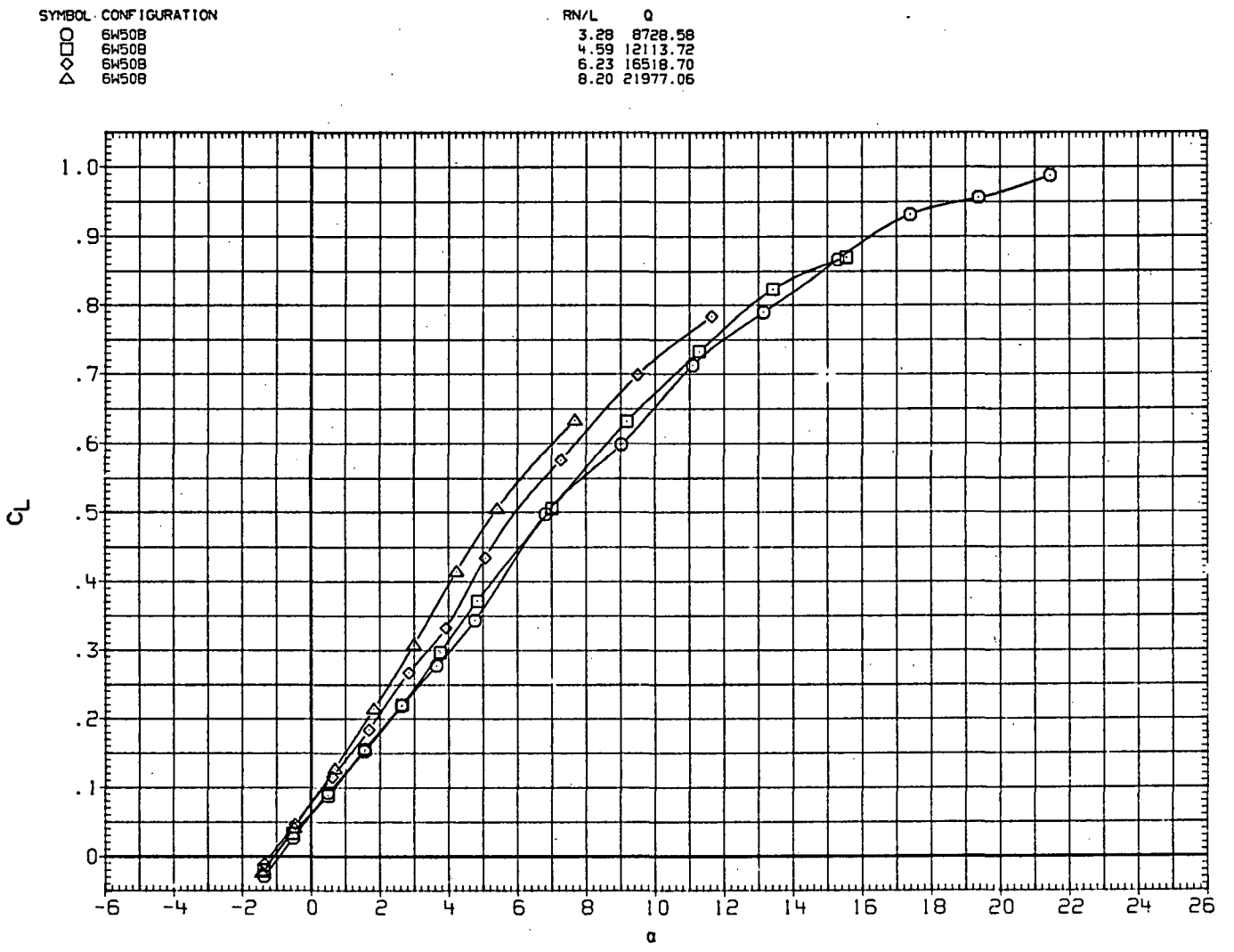


(a) $C_L$ vs $\alpha$

Figure 20.– Flexibility effects due to dynamic-pressure changes on the aerodynamic characteristics of the trapezoidal oblique wing: $\Lambda = 50°, M = 1.1$.

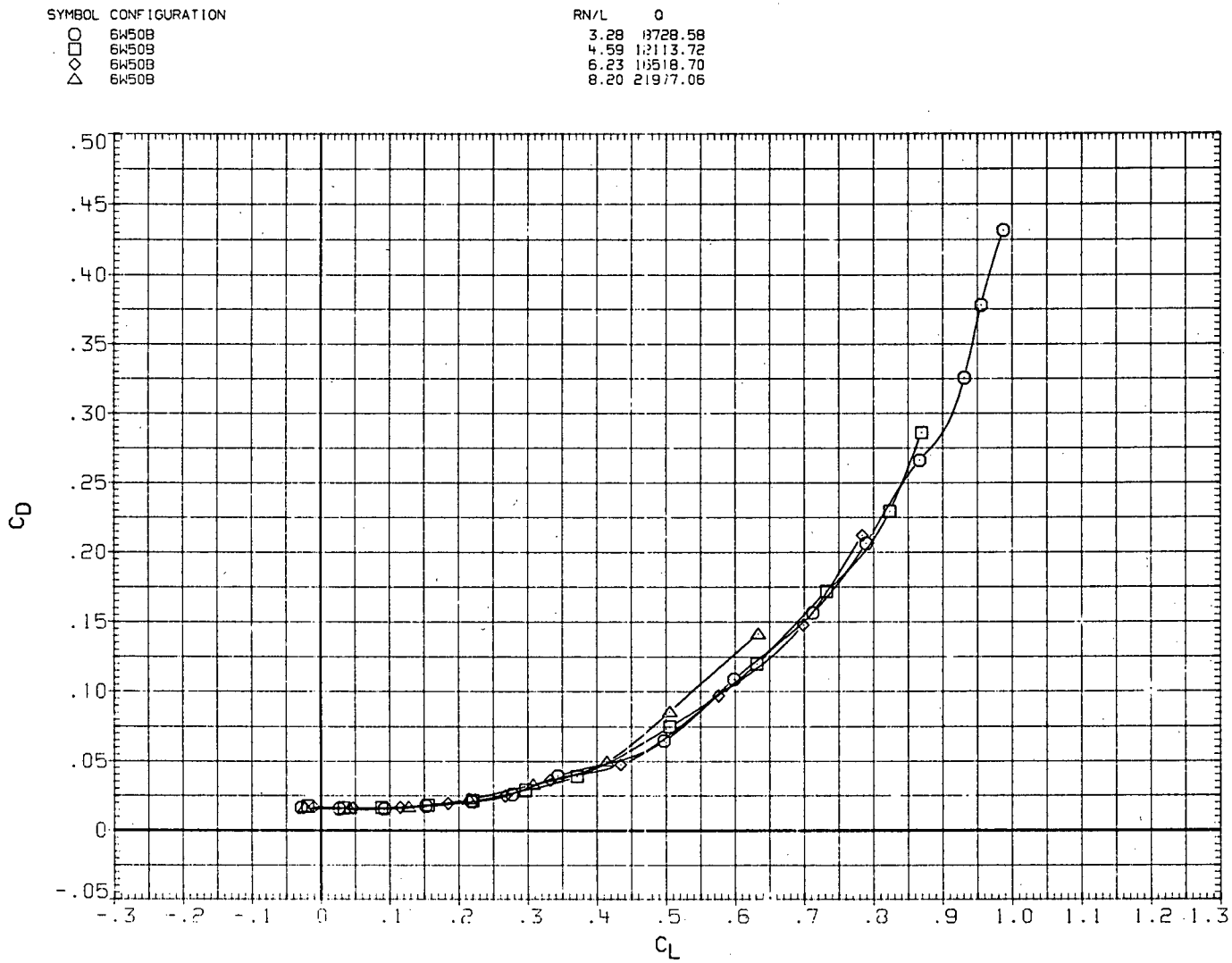


(b) $C_D$ vs $C_L$

Figure 20.– Continued.

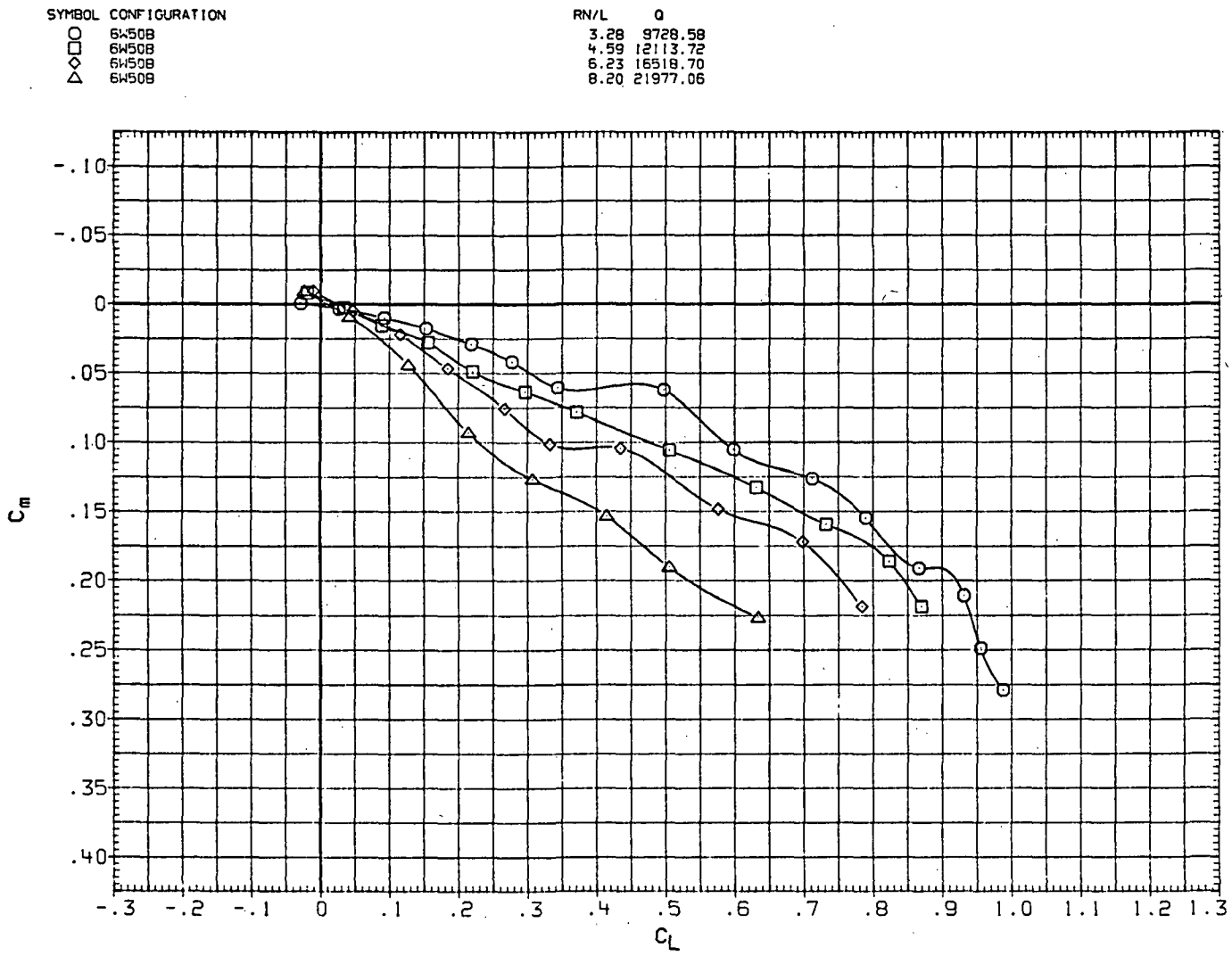


(c) $C_m$ vs $C_L$

Figure 20.– Continued.

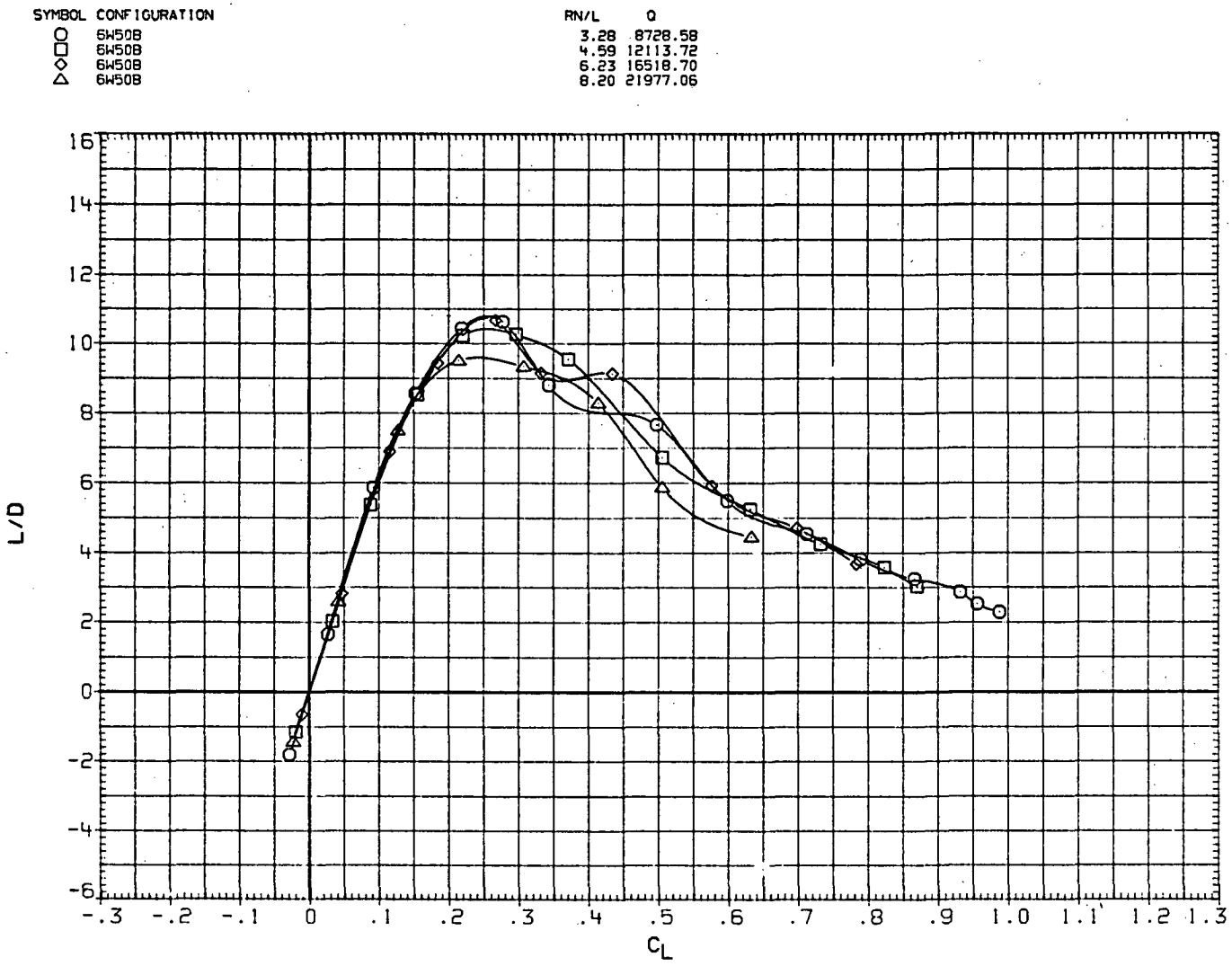


(d) $L/D$ vs $C_L$

Figure 20.– Continued.

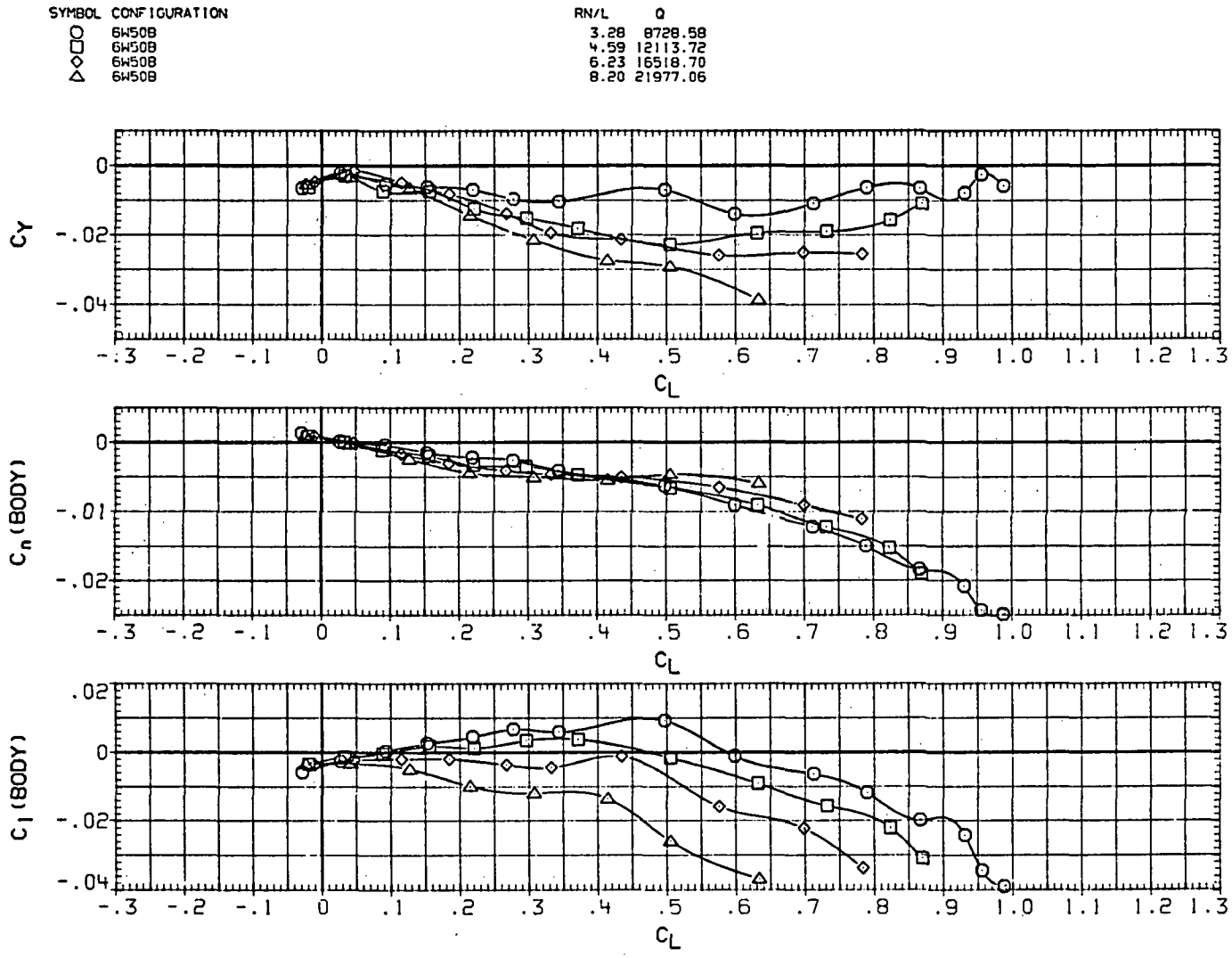


(e) $C_Y$, $C_n$, and $C_l$ vs $C_L$

Figure 20.– Concluded.

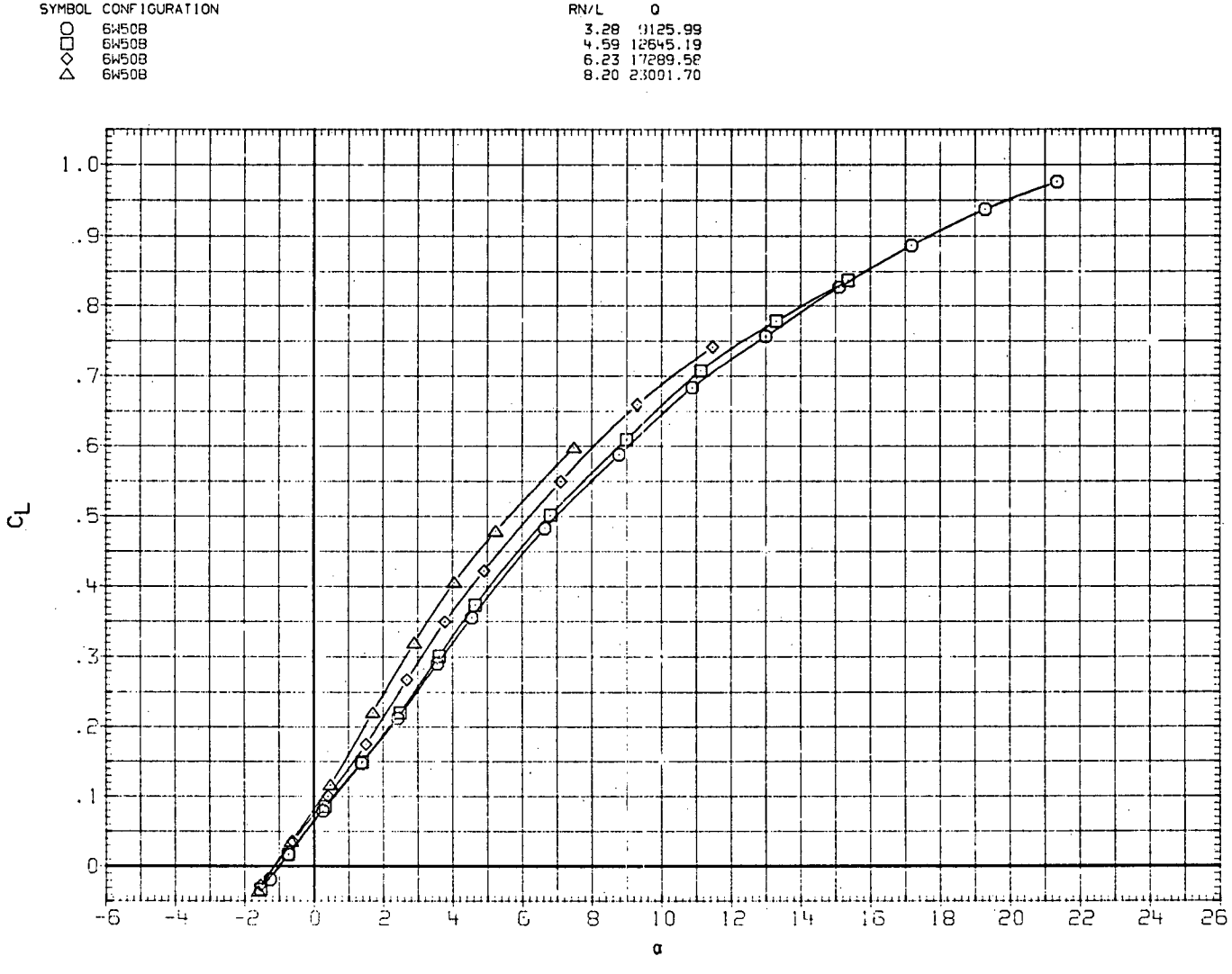


(a) $C_L$ vs $\alpha$

Figure 21.– Flexibility effects due to dynamic-pressure changes on the aerodynamic characteristics of the trapezoidal oblique wing: $\Lambda = 50°, M = 1.2$.

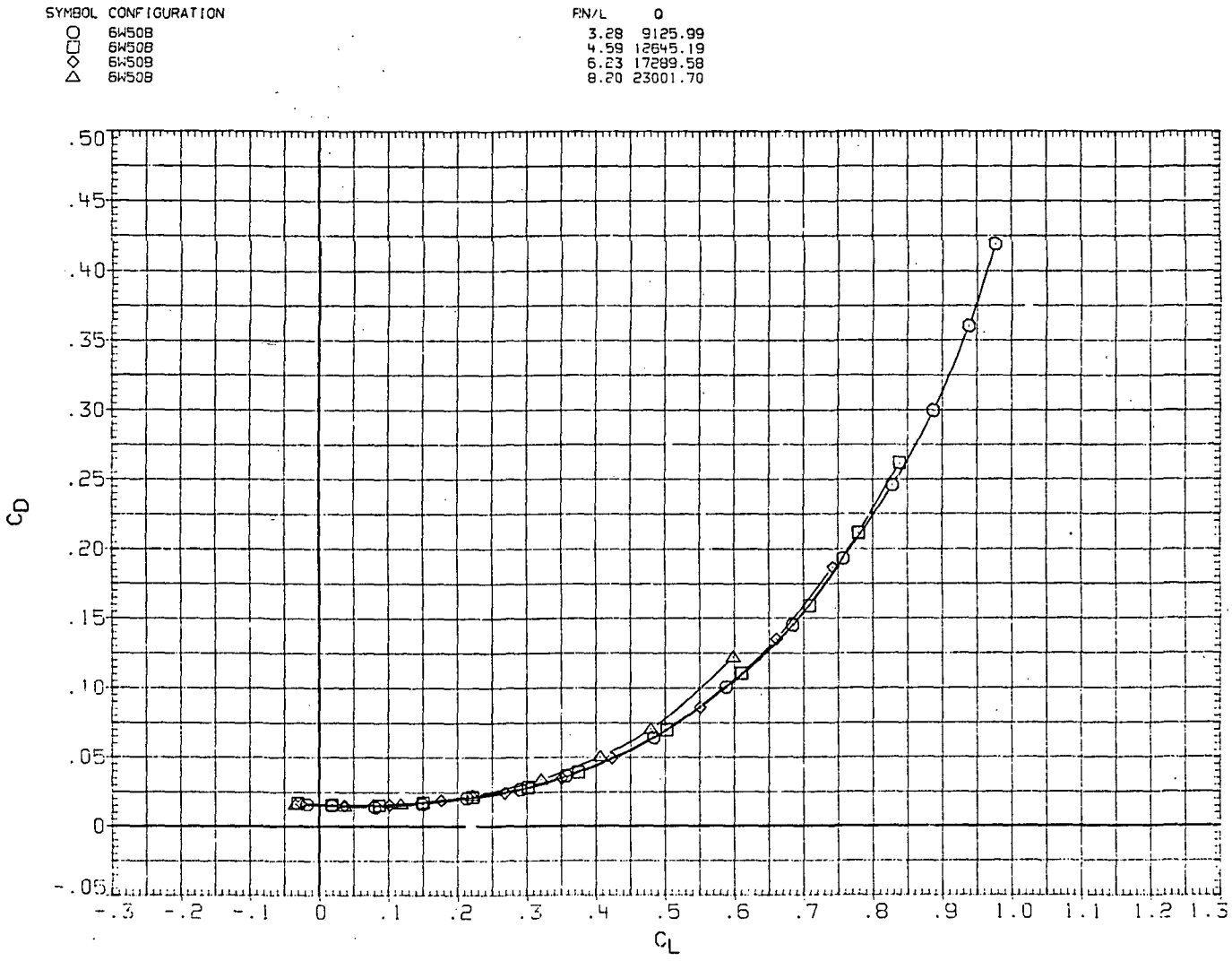


(b) $C_D$ vs $C_L$

Figure 21.– Continued.

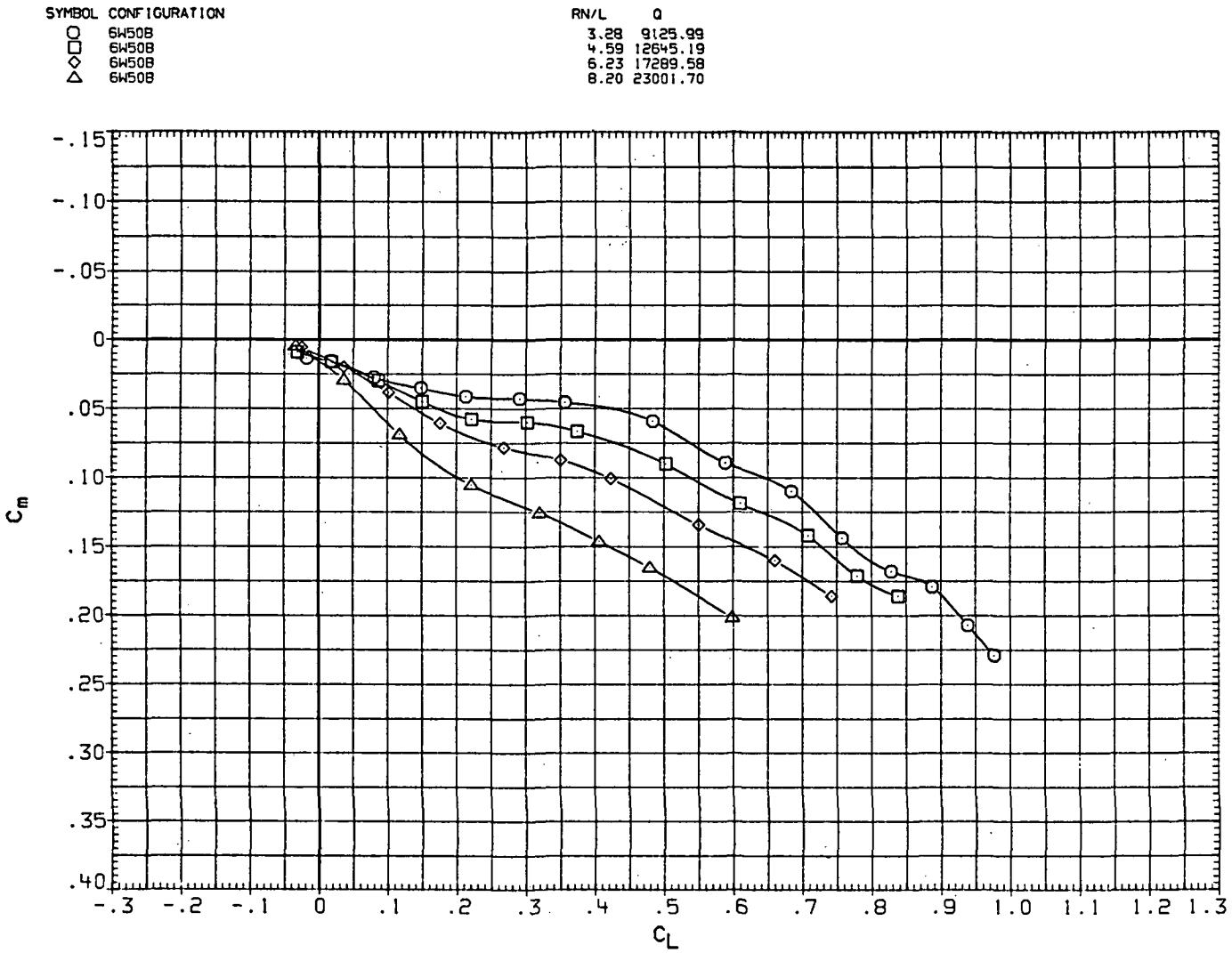


(c) $C_m$ vs $C_L$

Figure 21.– Continued.


(d) $L/D$ vs $C_L$

Figure 21.– Continued.

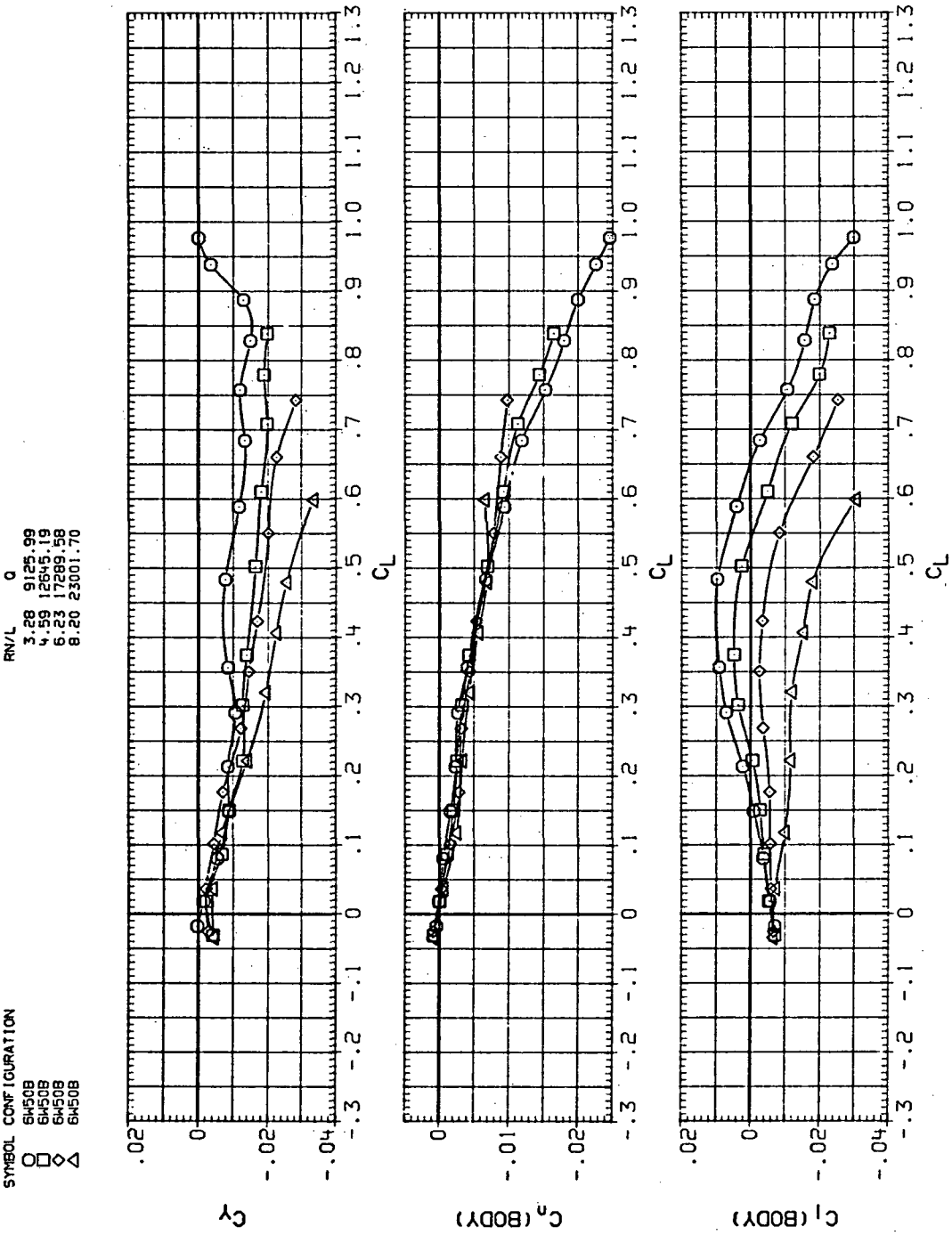


(e) $C_Y$, $C_n$, and $C_l$ vs $C_L$

Figure 21.– Concluded.

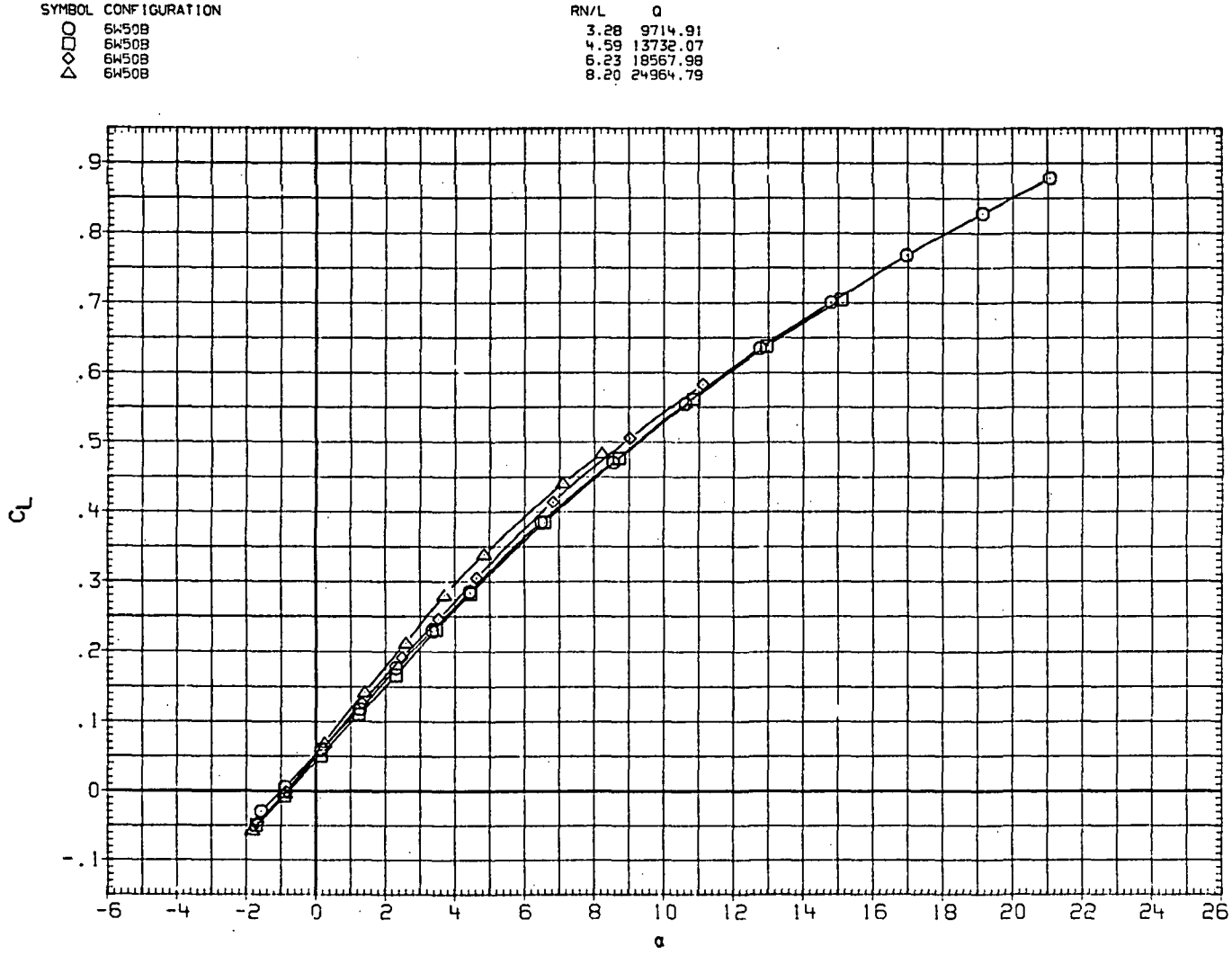


(a) $C_L$ vs $\alpha$

Figure 22.– Flexibility effects due to dynamic-pressure changes on the aerodynamic characteristics of the trapezoidal oblique wing: $\Lambda = 50°, M = 1.6$.

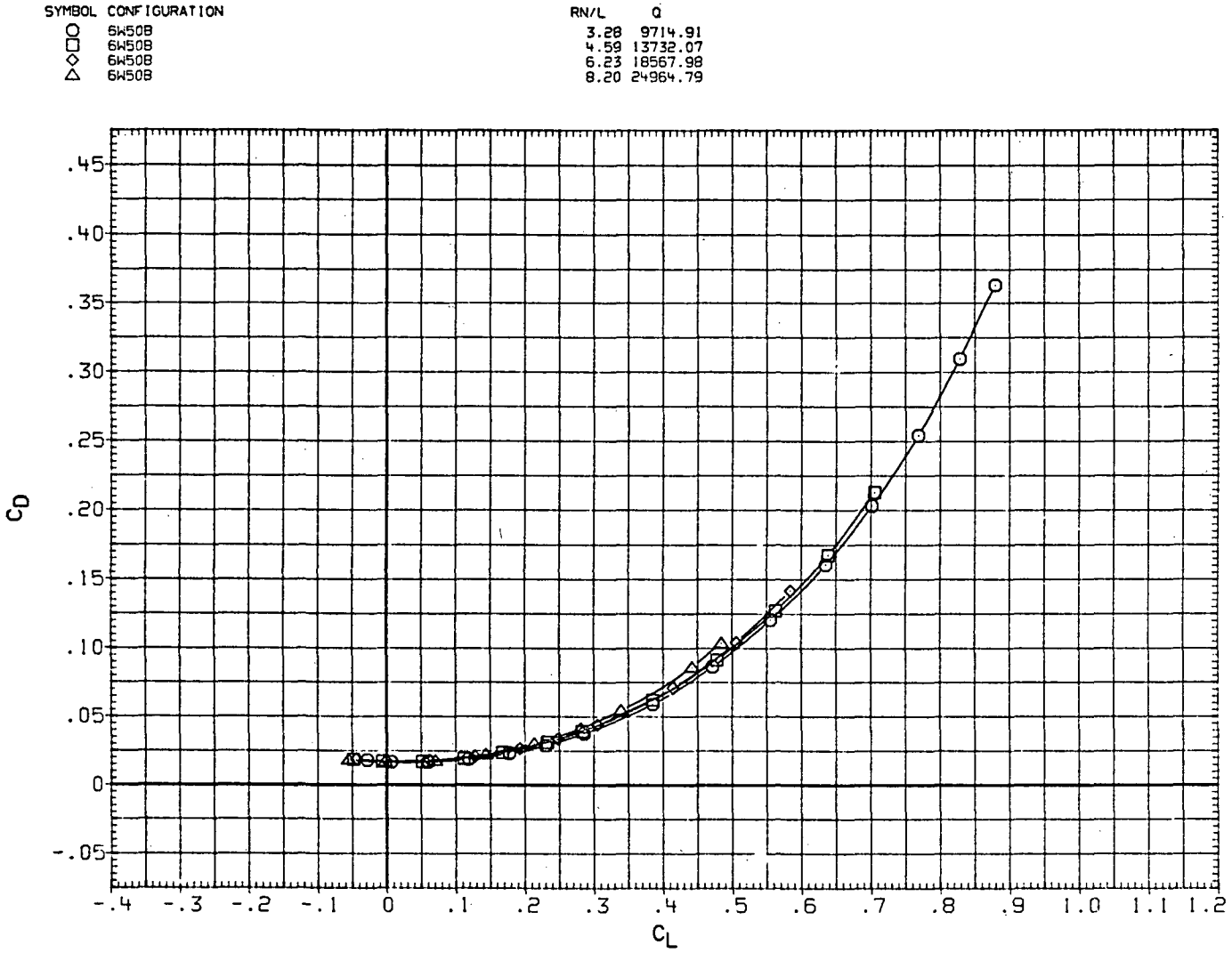


(b) $C_D$ vs $C_L$

Figure 22.– Continued.

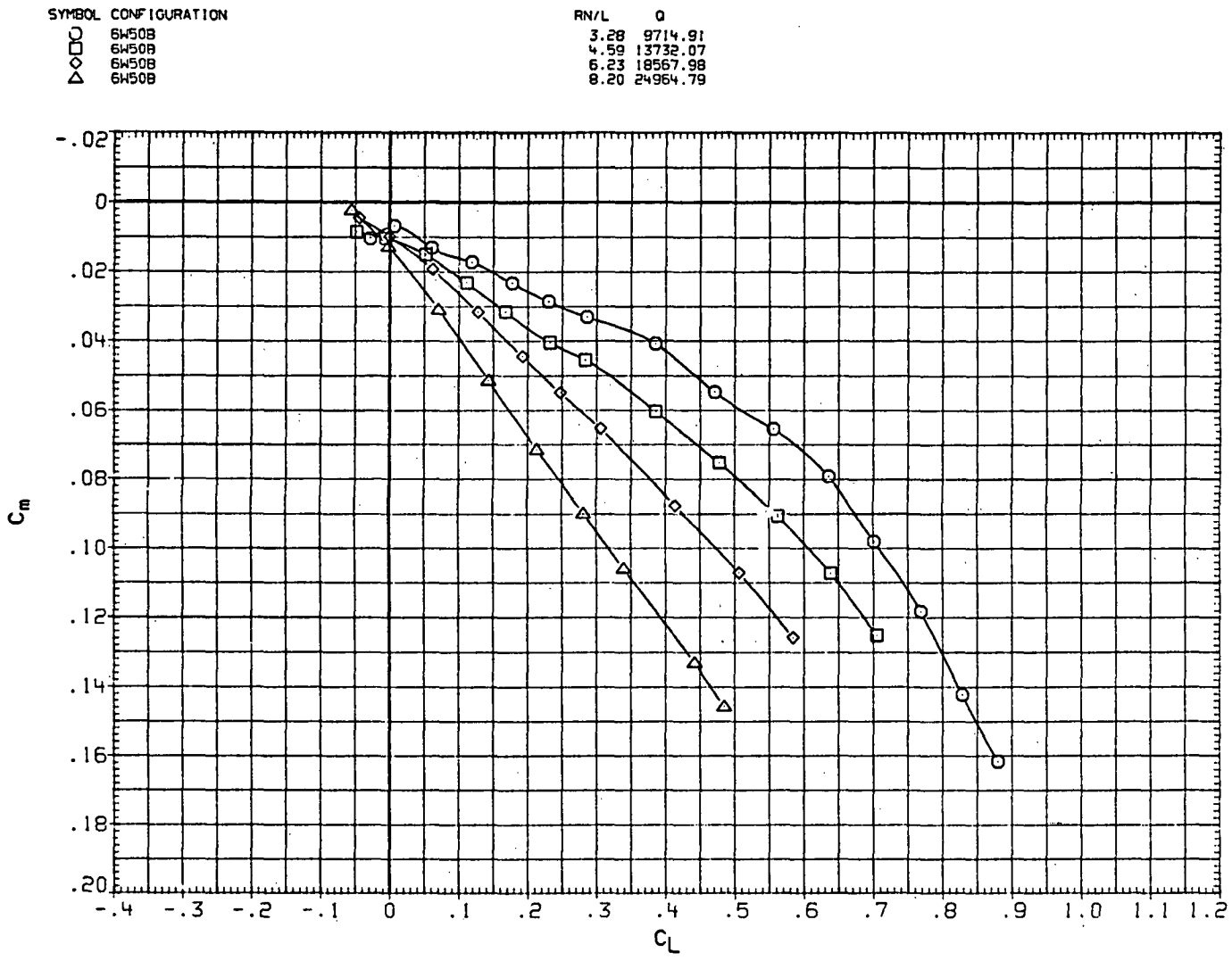


(c) $C_m$ vs $C_L$

Figure 22.– Continued.

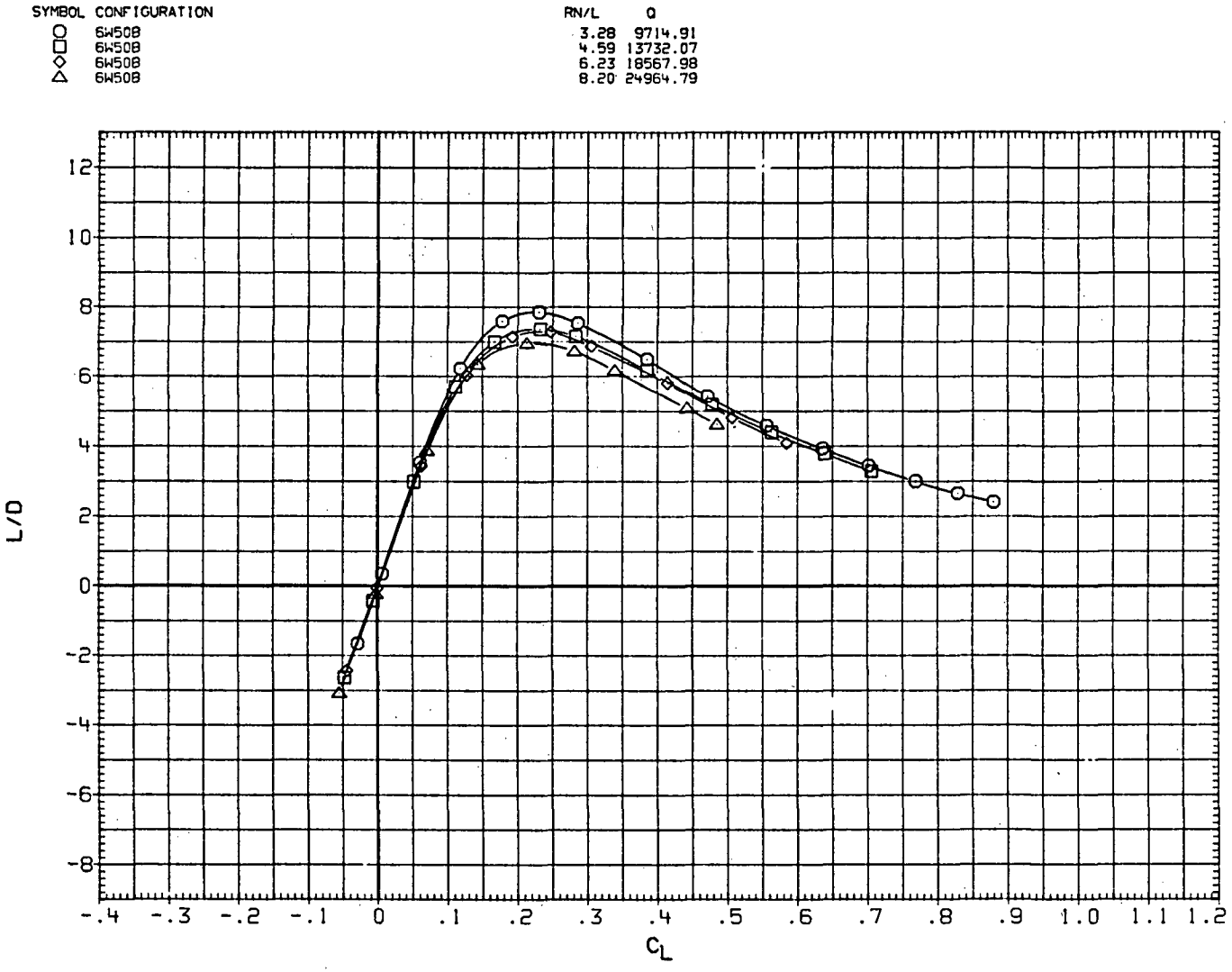


(d) $L/D$ vs $C_L$

Figure 22.– Continued.

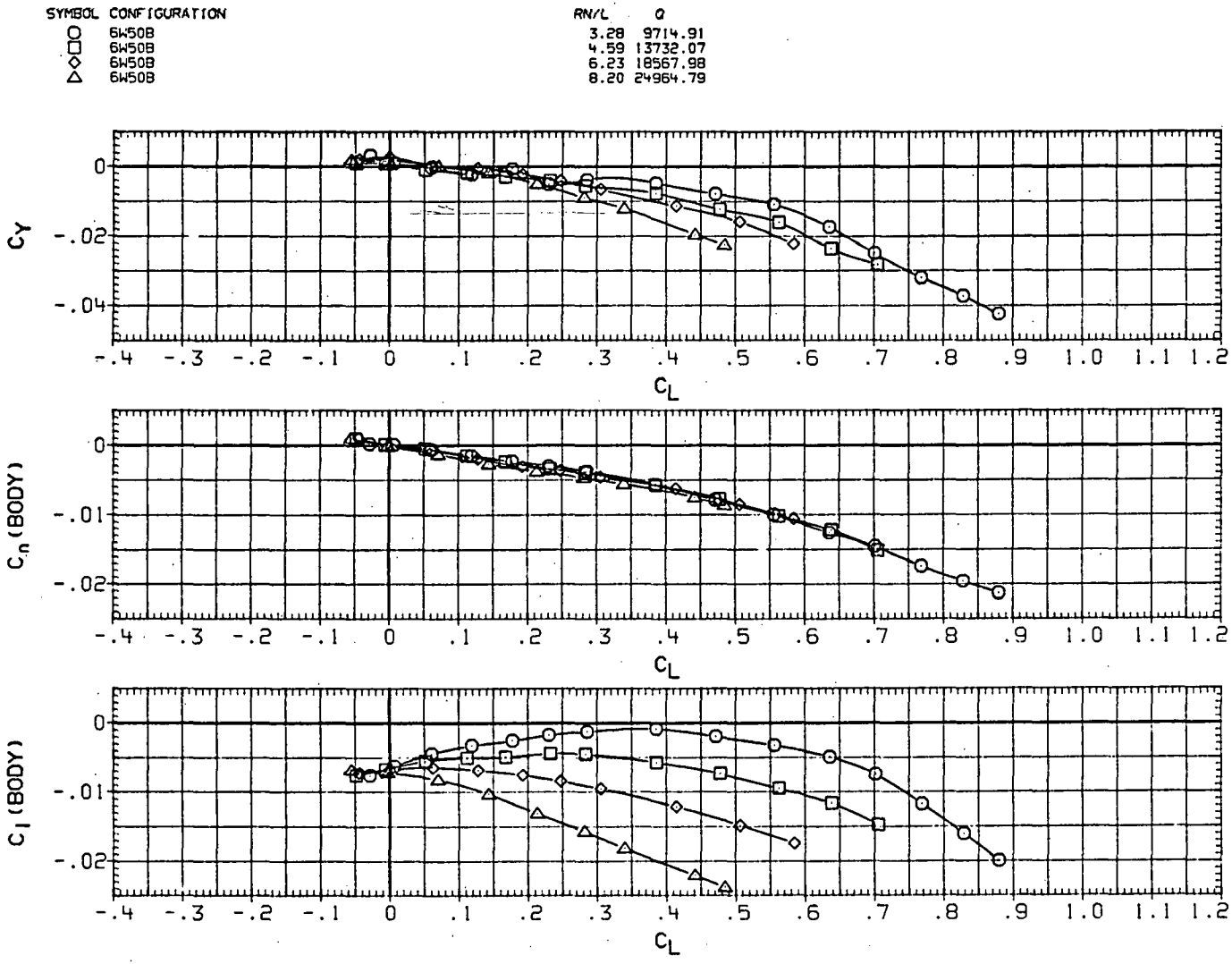


(e) $C_Y$, $C_n$, and $C_l$ vs $C_L$

Figure 22.– Concluded.

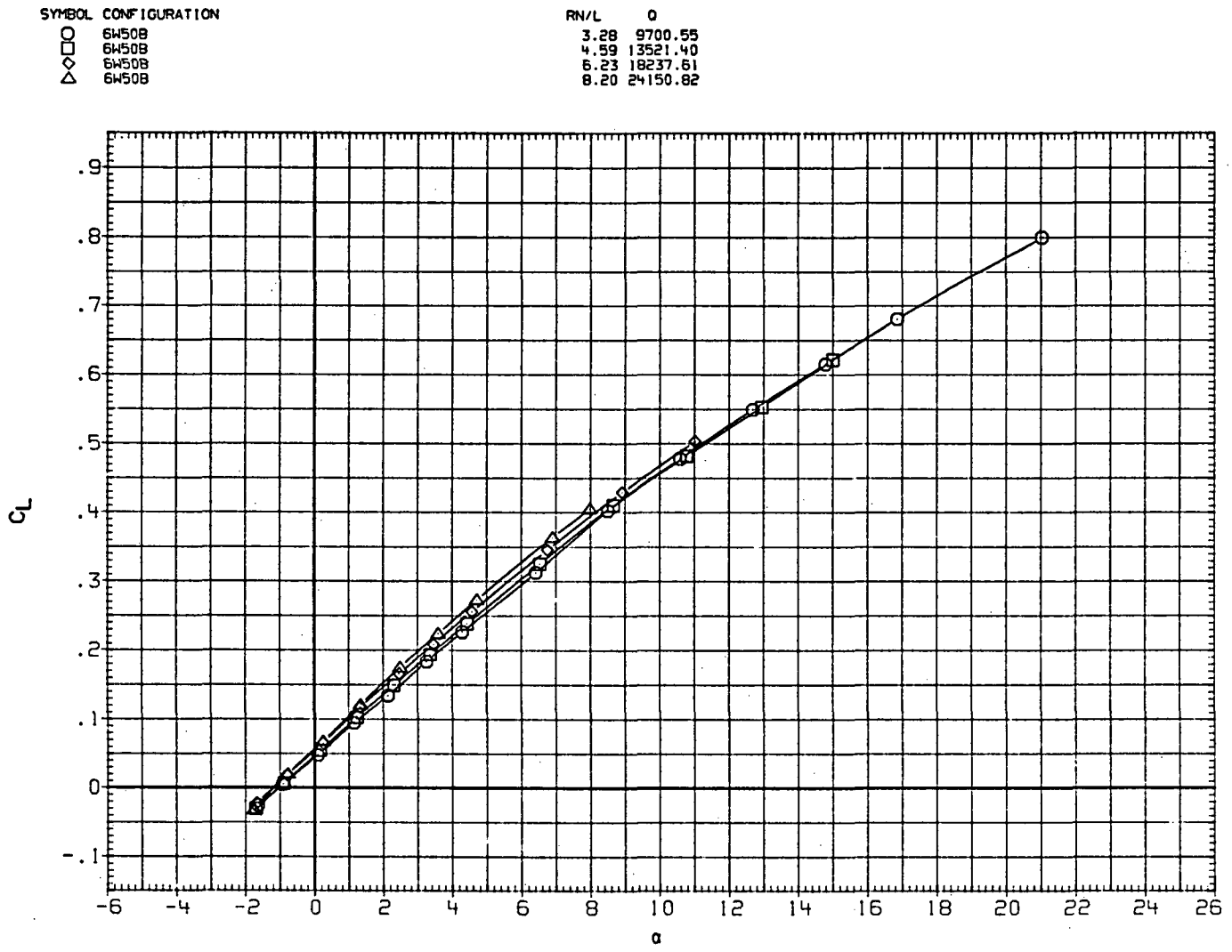


(a) $C_L$ vs $\alpha$

Figure 23.– Flexibility effects due to dynamic-pressure changes on the aerodynamic characteristics of the trapezoidal oblique wing: $\Lambda = 50°, M = 2.0$.

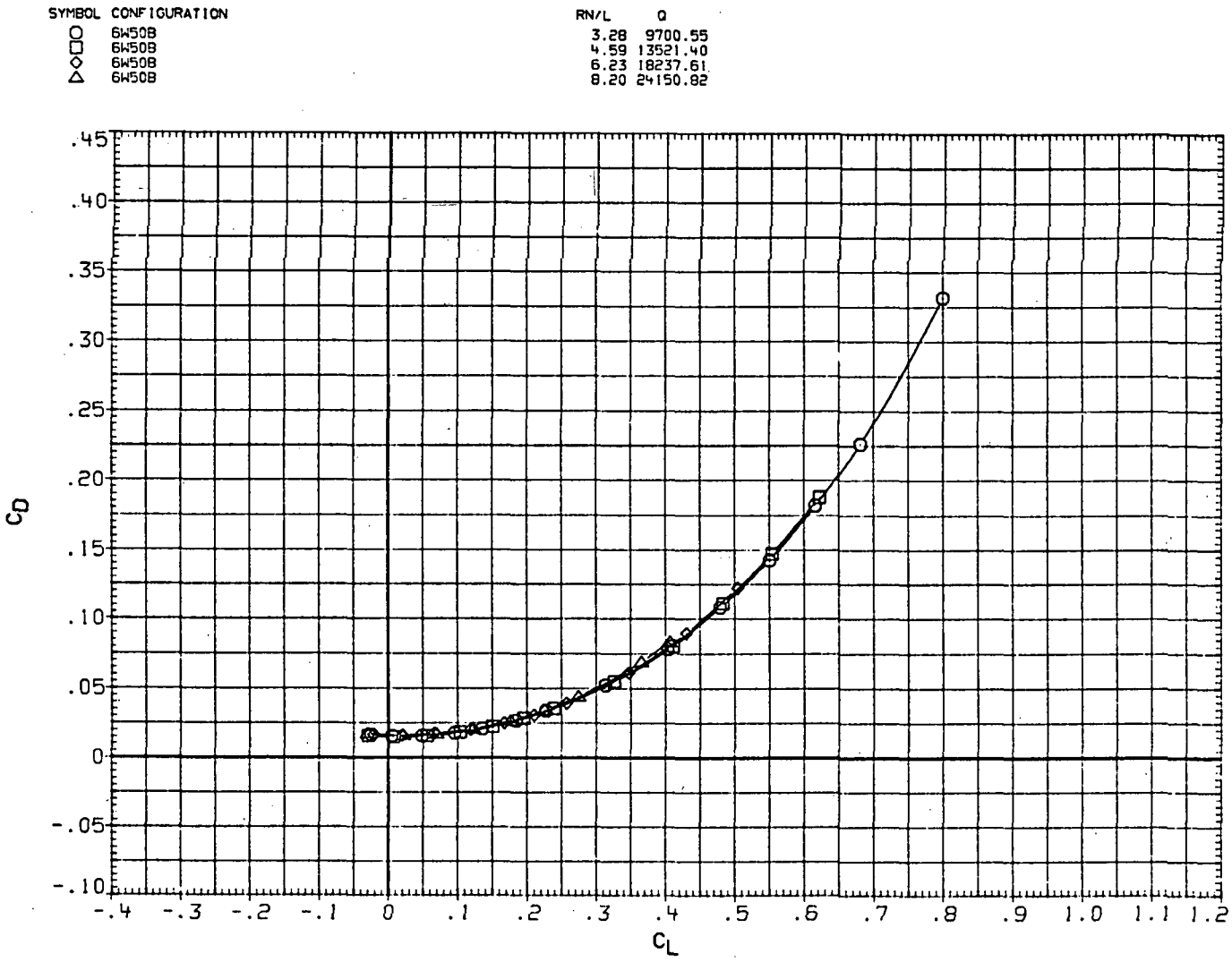


(b) $C_D$ vs $C_L$

Figure 23.– Continued.


(c) $C_m$ vs $C_L$

Figure 23.– Continued.


(d) $L/D$ vs $C_L$

Figure 23.– Continued.

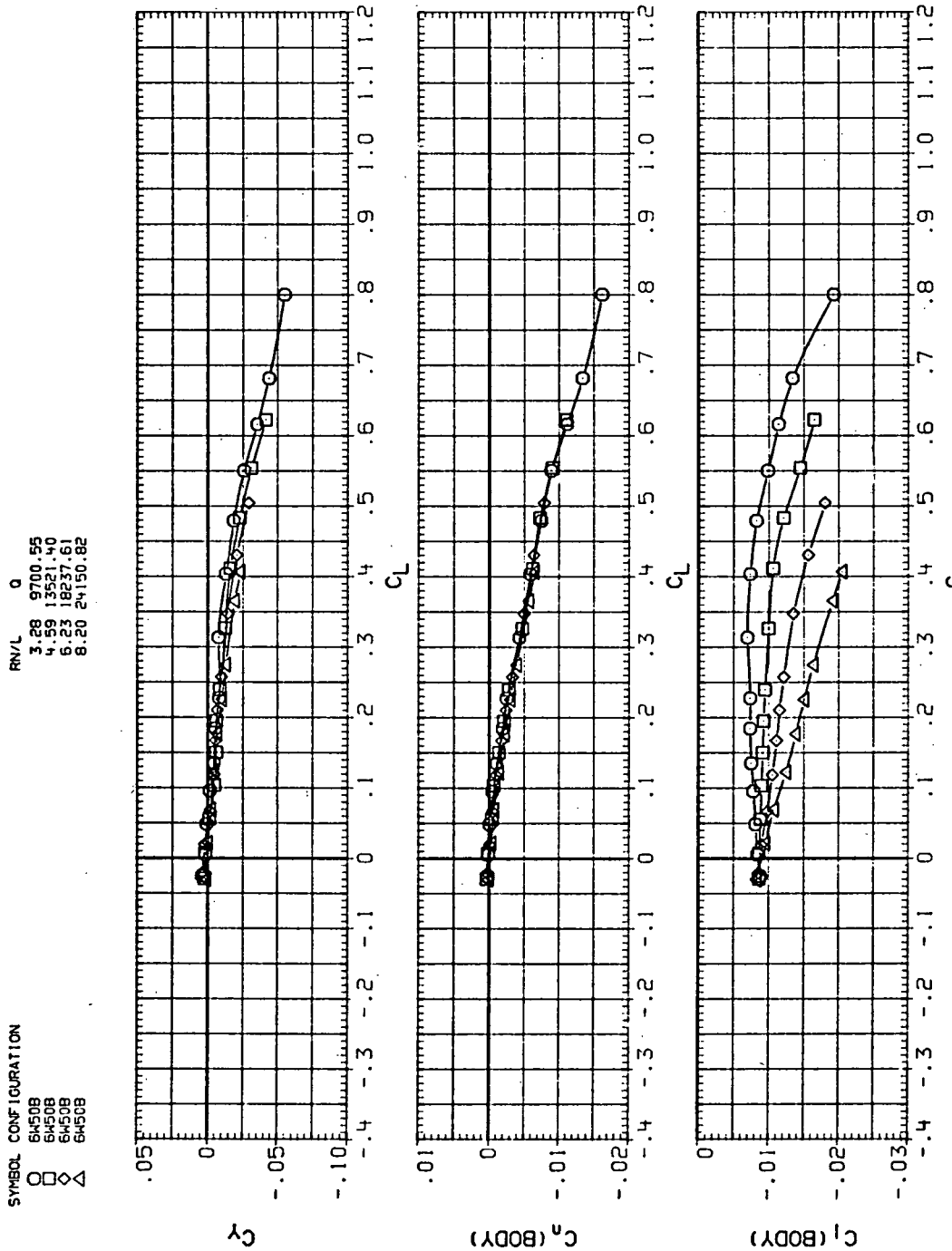


(e) $C_Y$, $C_n$, and $C_l$ vs $C_L$

Figure 23.– Concluded.

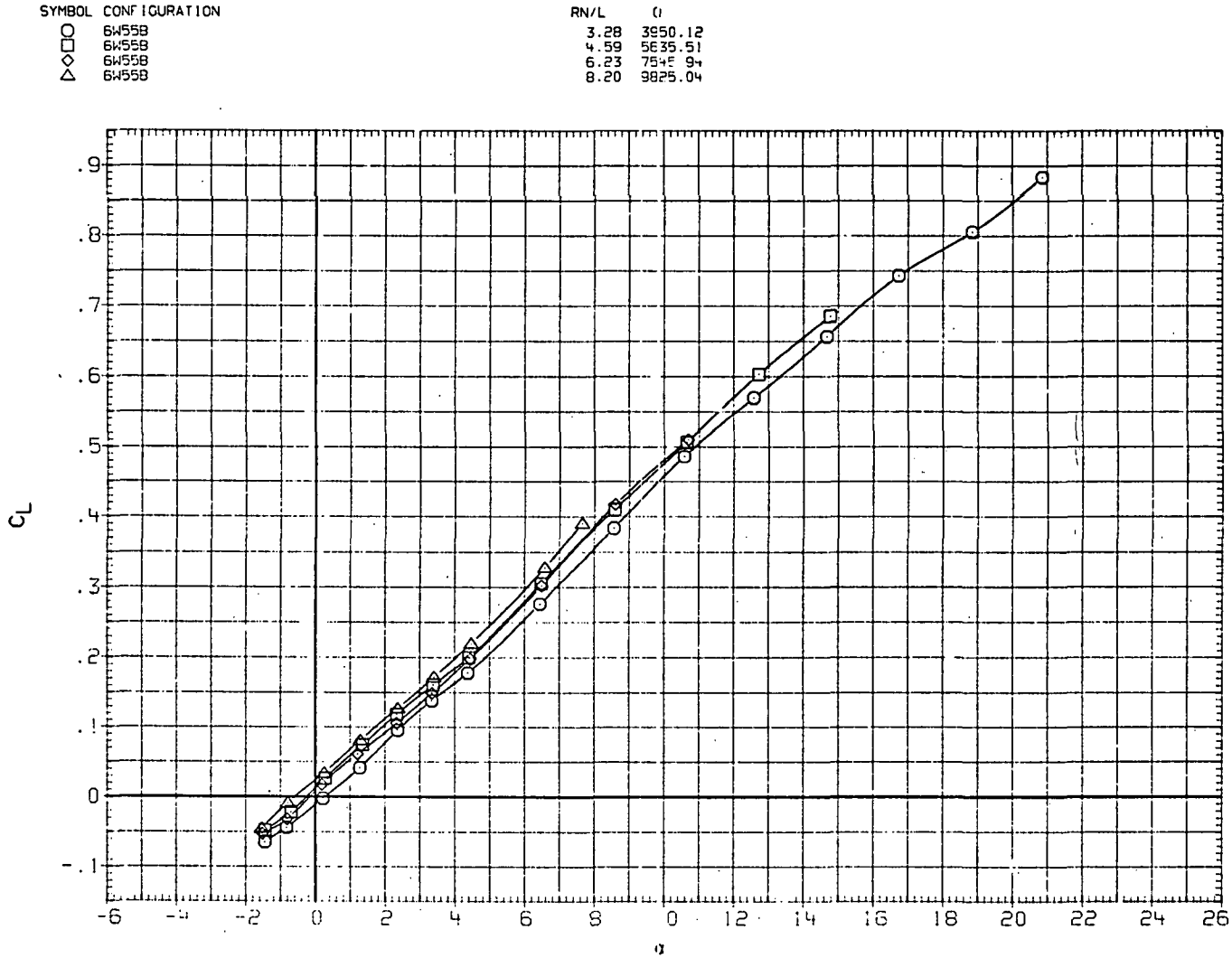


(a) $C_L$ vs $\alpha$

Figure 24.– Flexibility effects due to dynamic-pressure changes on the aerodynamic characteristics of the trapezoidal oblique wing: $\Lambda = 55°, M = 0.4$.

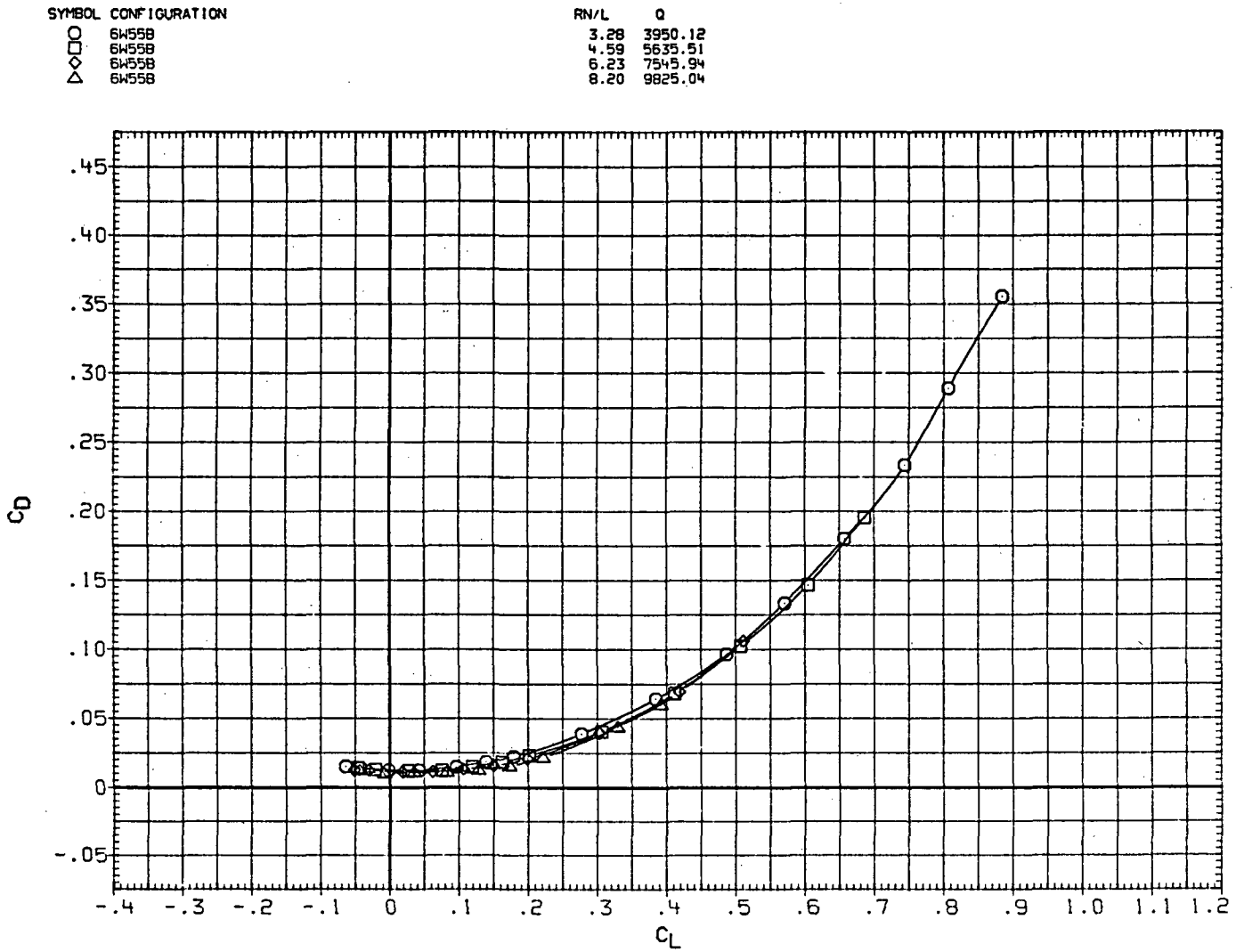


(b) $C_D$ vs $C_L$

Figure 24.– Continued.

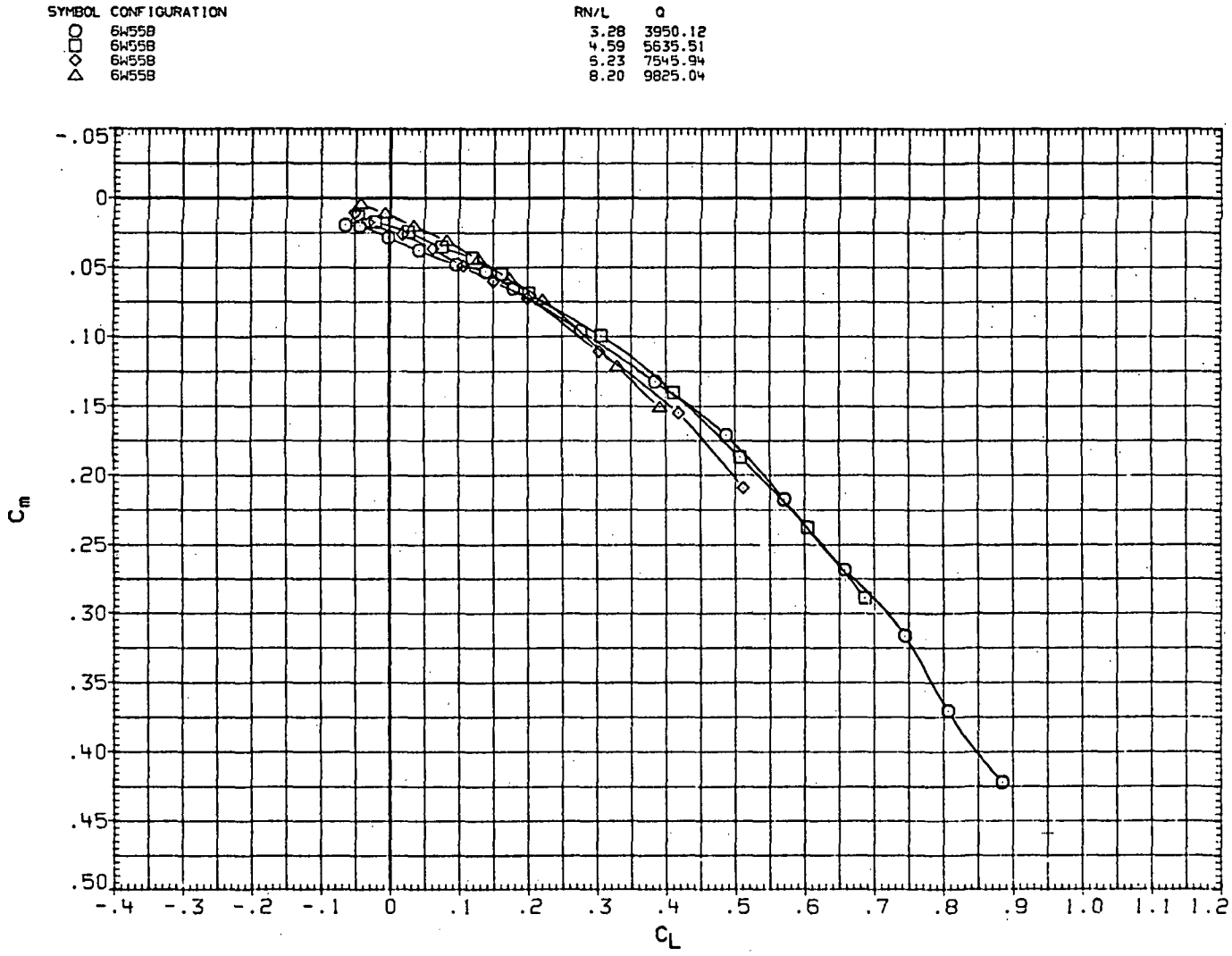


(c) $C_m$ vs $C_L$

Figure 24.– Continued.

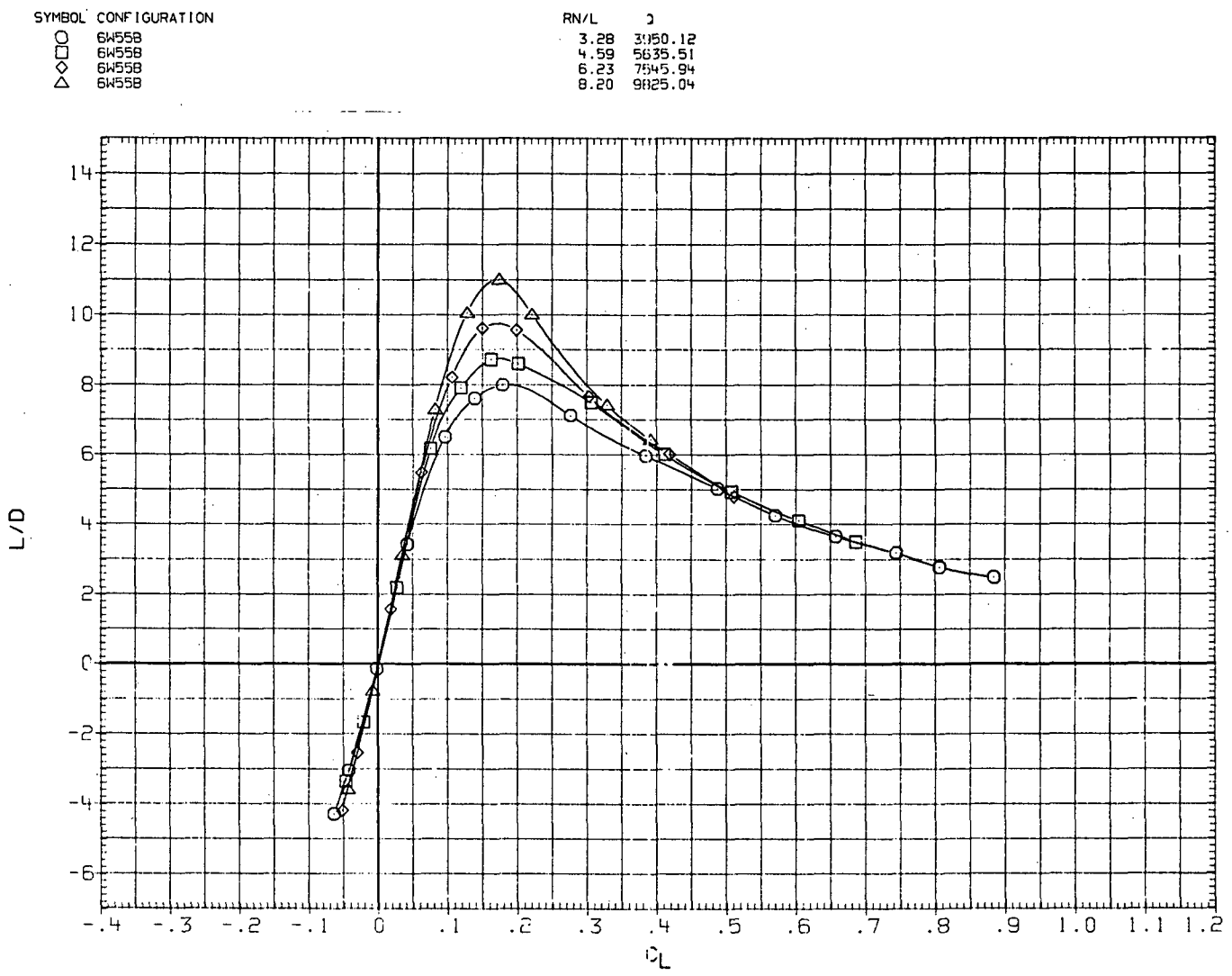


(d) $L/D$ vs $C_L$

Figure 24.– Continued.

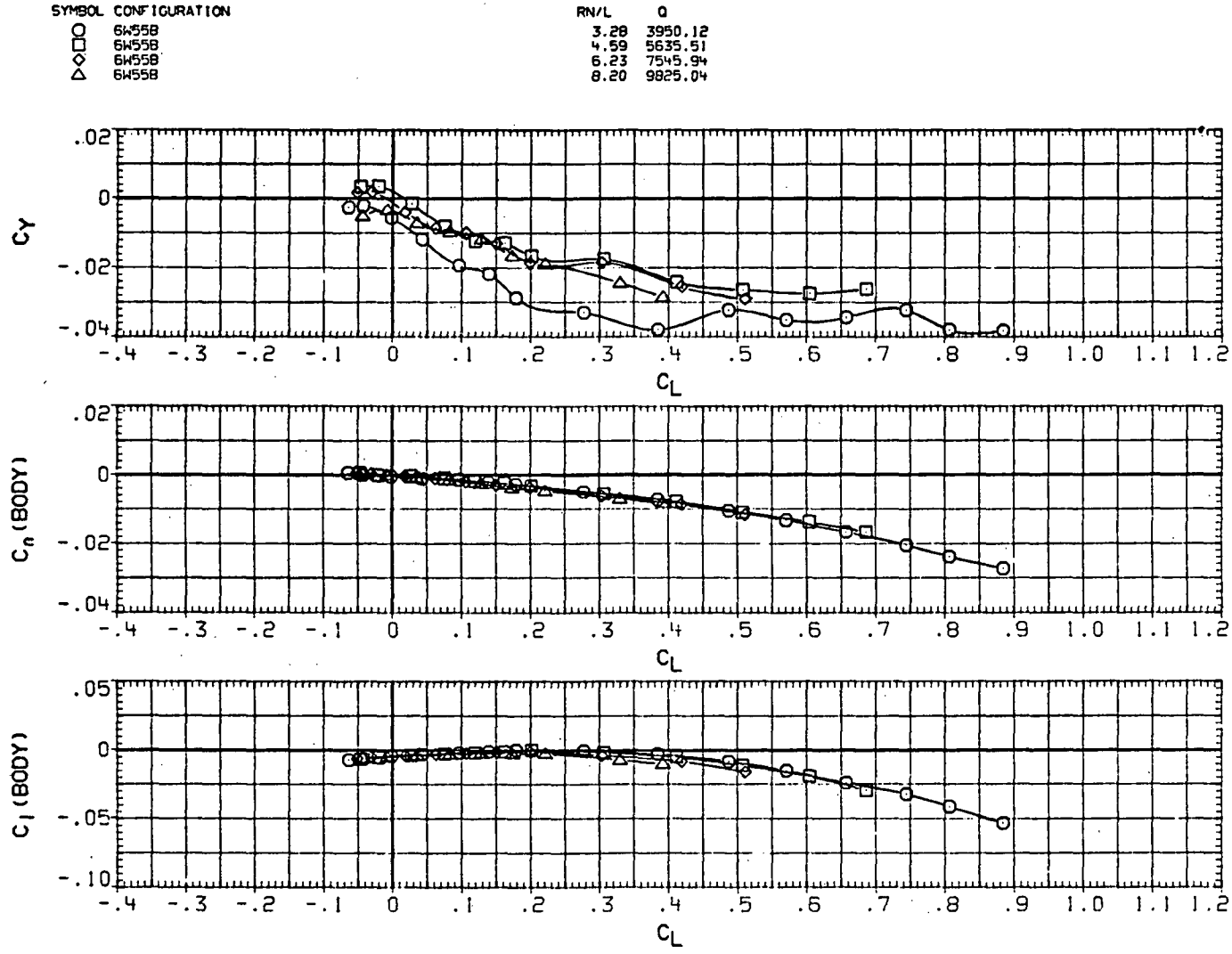


(e) $C_Y$, $C_n$, and $C_l$ vs $C_L$

Figure 24.– Concluded.

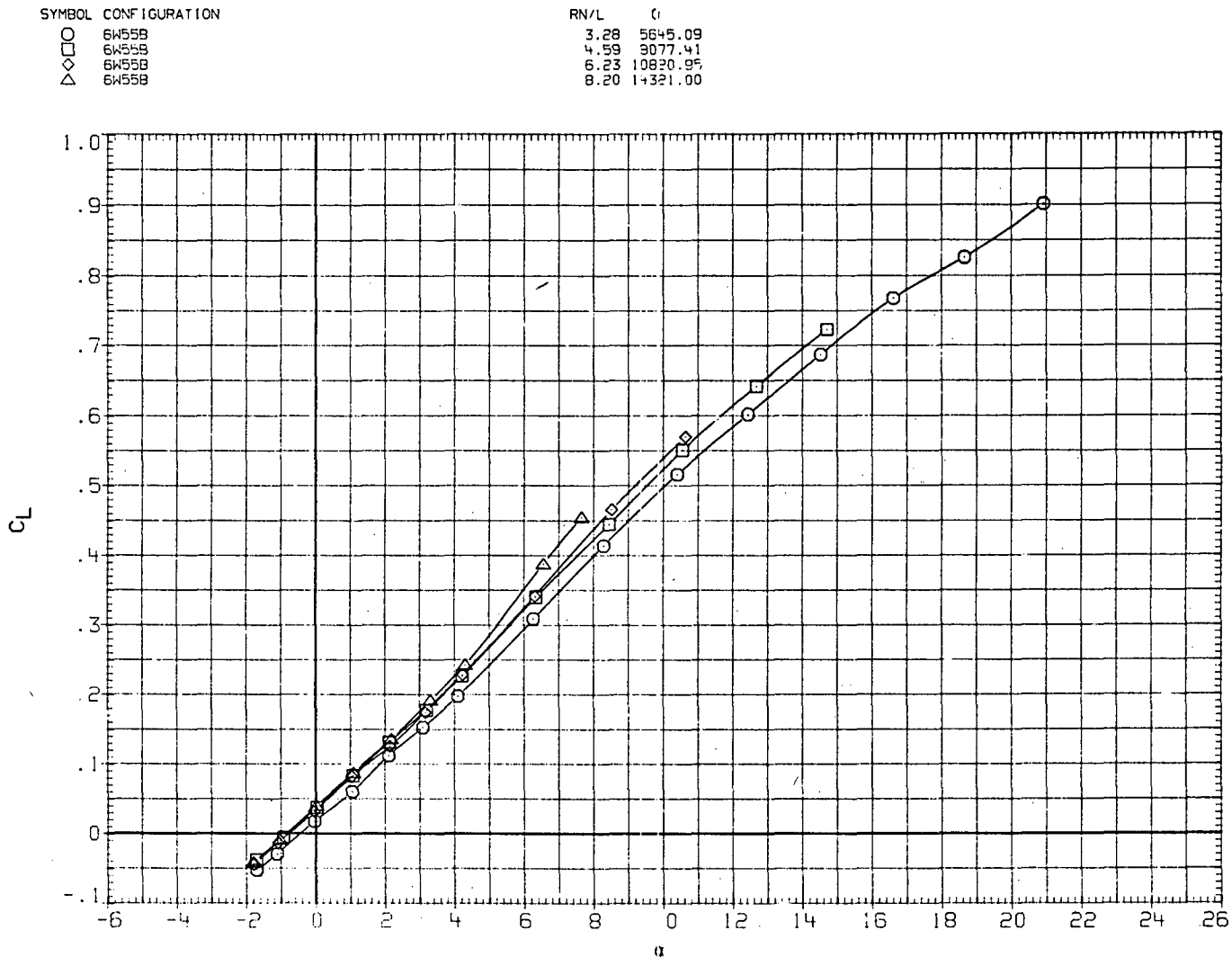


(a) $C_L$ vs $\alpha$

Figure 25.– Flexibility effects due to dynamic-pressure changes on the aerodynamic characteristics of the trapezoidal oblique wing: $\Lambda = 55°, M = 0.6$.

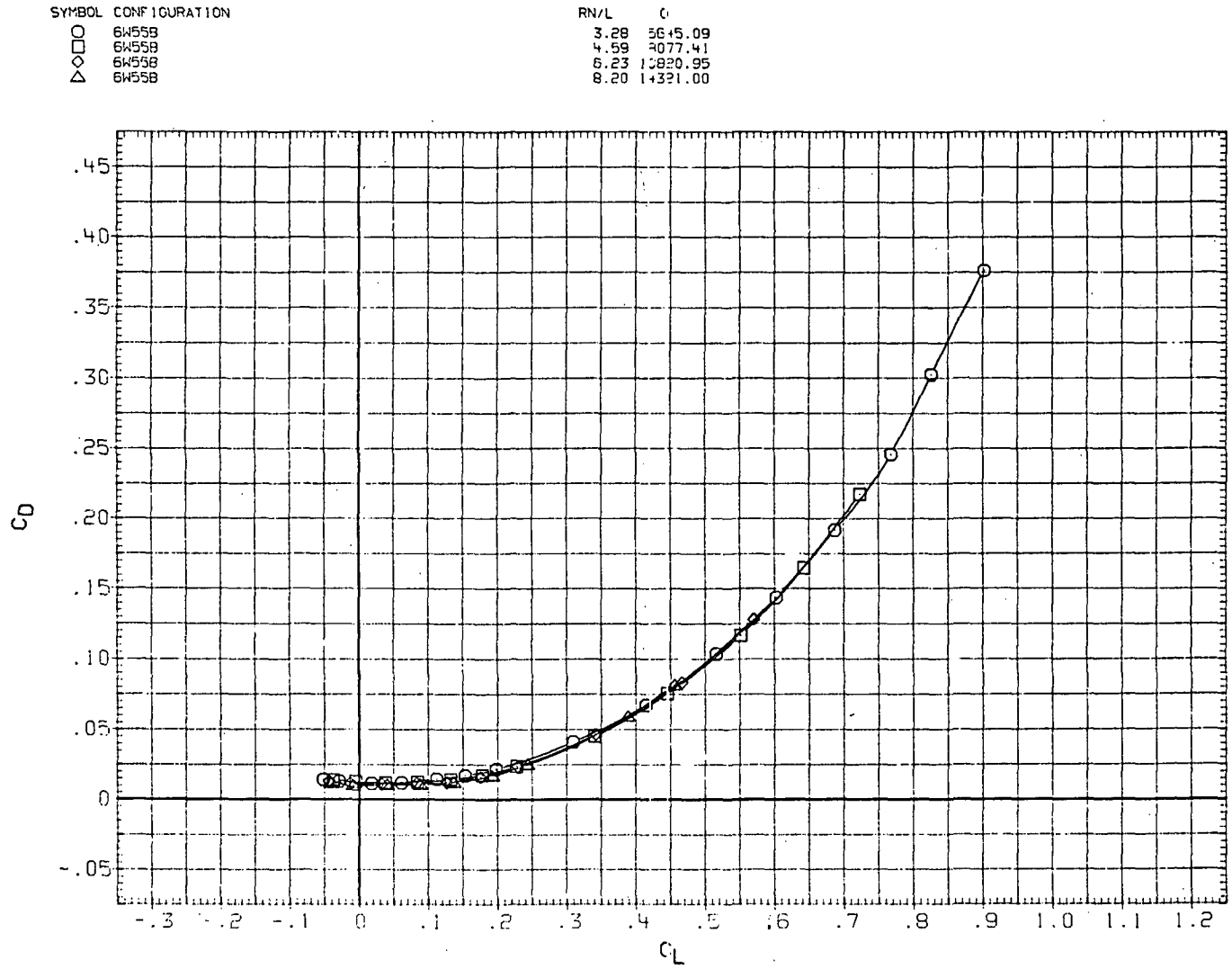


(b) $C_D$ vs $C_L$

Figure 25.– Continued.

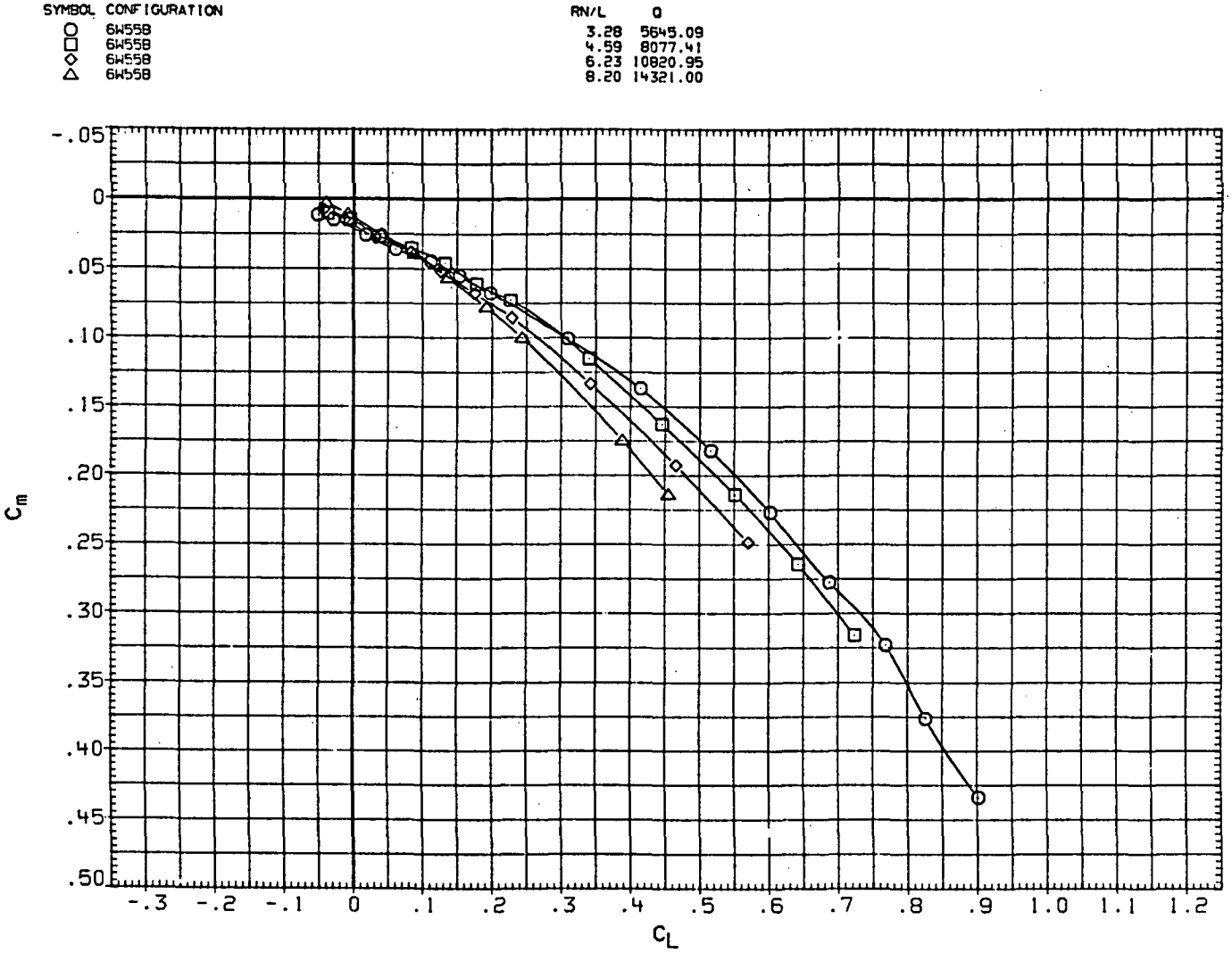


(c) $C_m$ vs $C_L$

Figure 25.– Continued.


(d) $L/D$ vs $C_L$

Figure 25.– Continued.

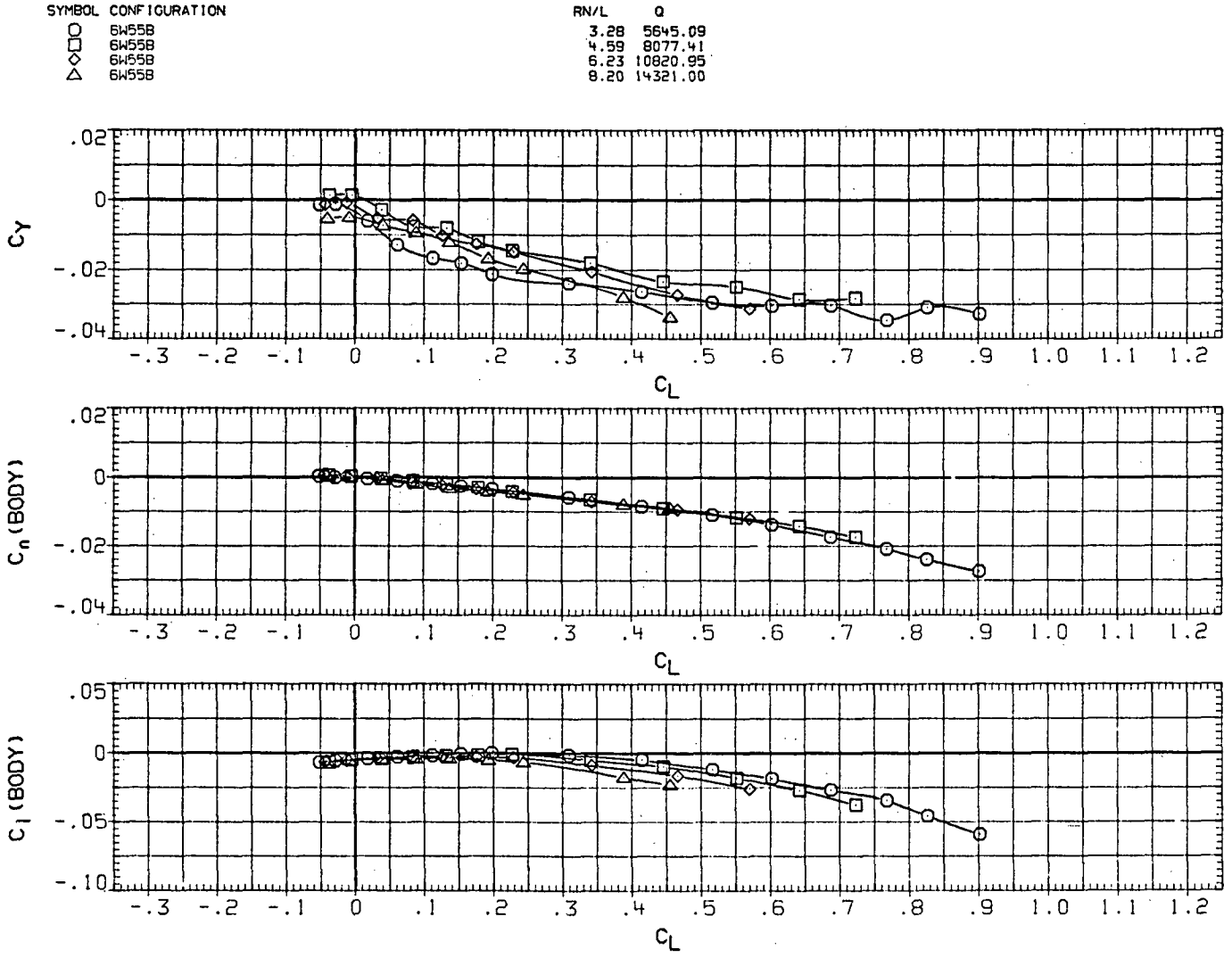


(e) $C_Y$, $C_n$, and $C_l$ vs $C_L$

Figure 25.– Concluded.

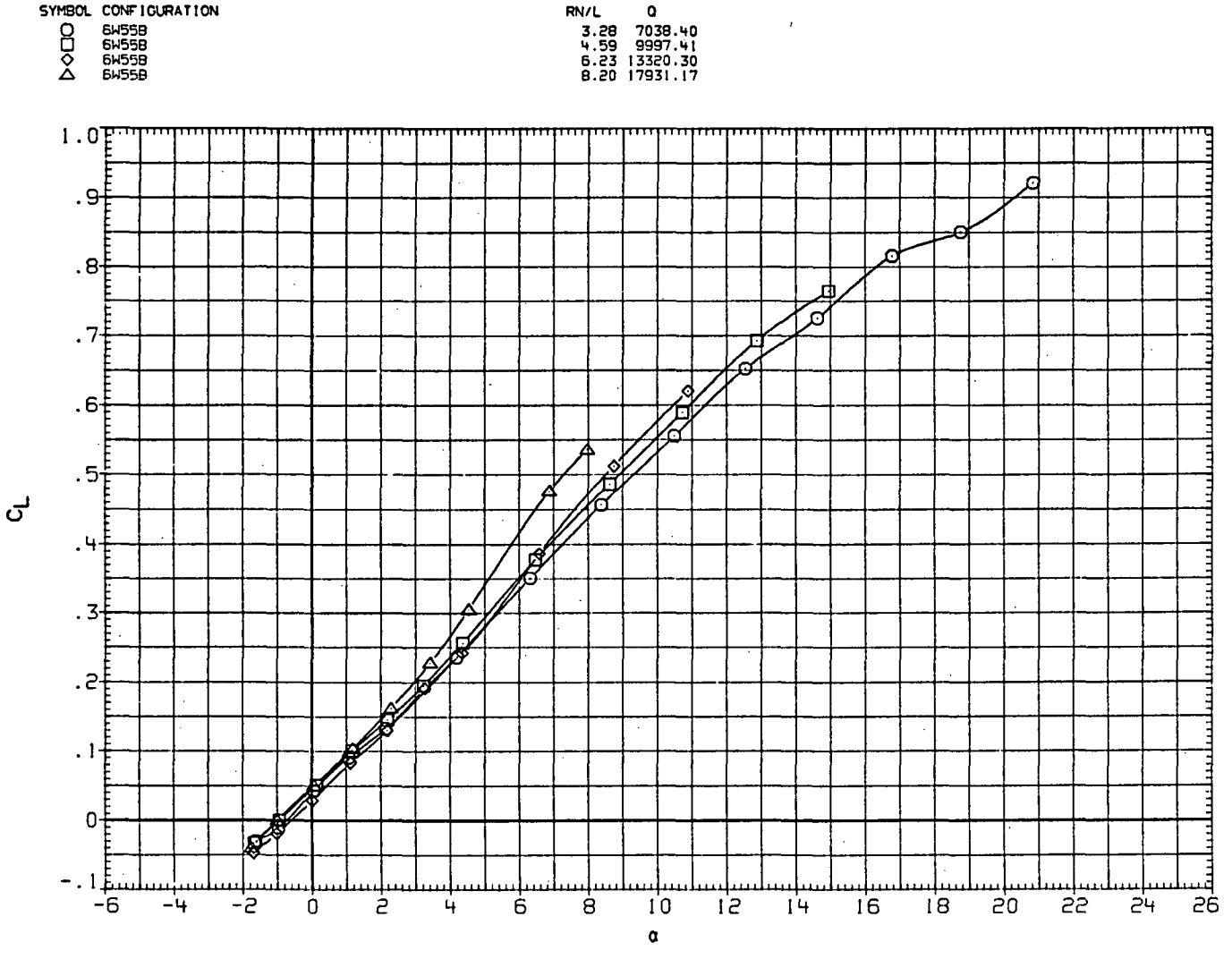


(a) $C_L$ vs $\alpha$

Figure 26.– Flexibility effects due to dynamic-pressure changes on the aerodynamic characteristics of the trapezoidal oblique wing: $\Lambda = 55°, M = 0.8$.

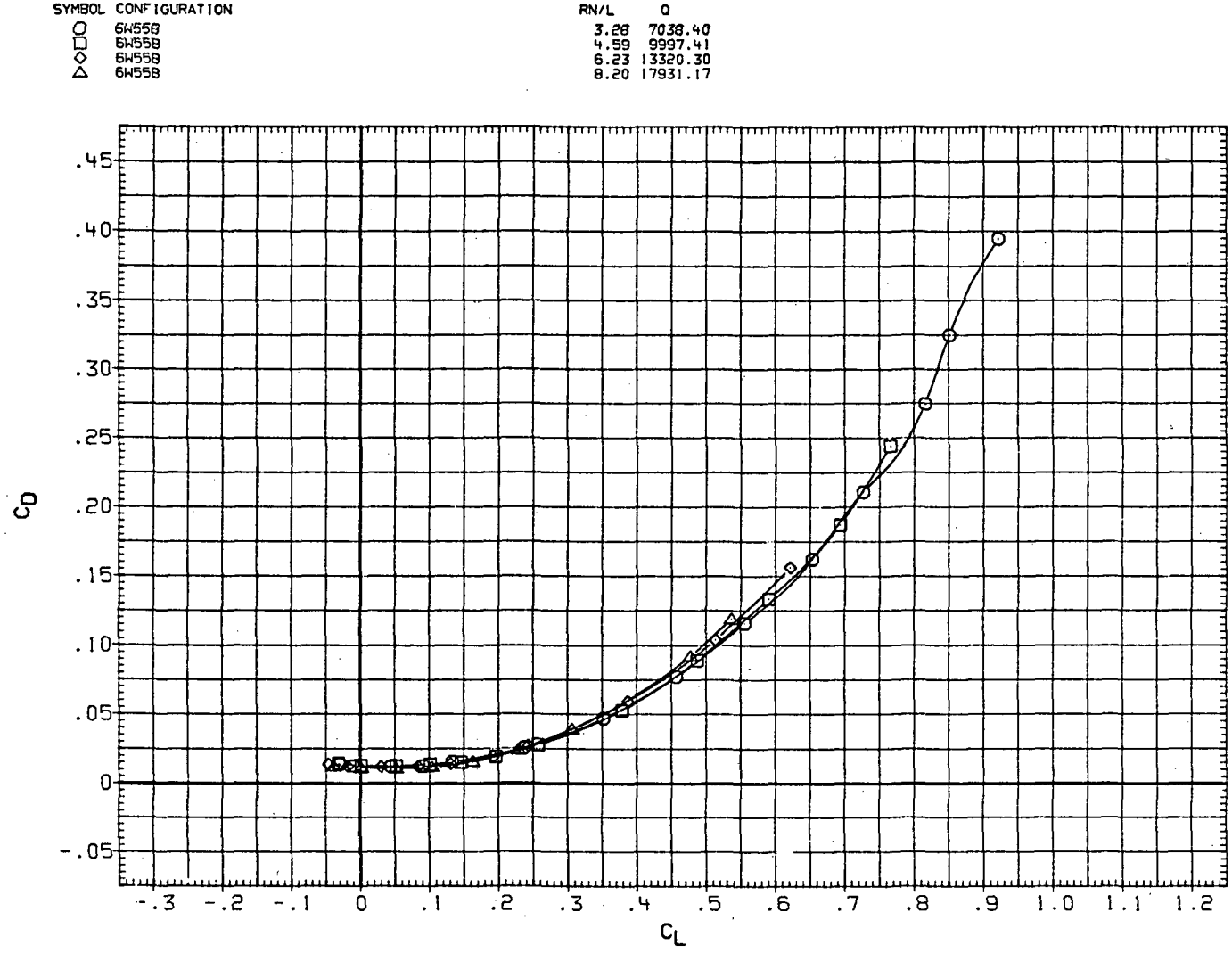


(b) $C_D$ vs $C_L$

Figure 26.– Continued.

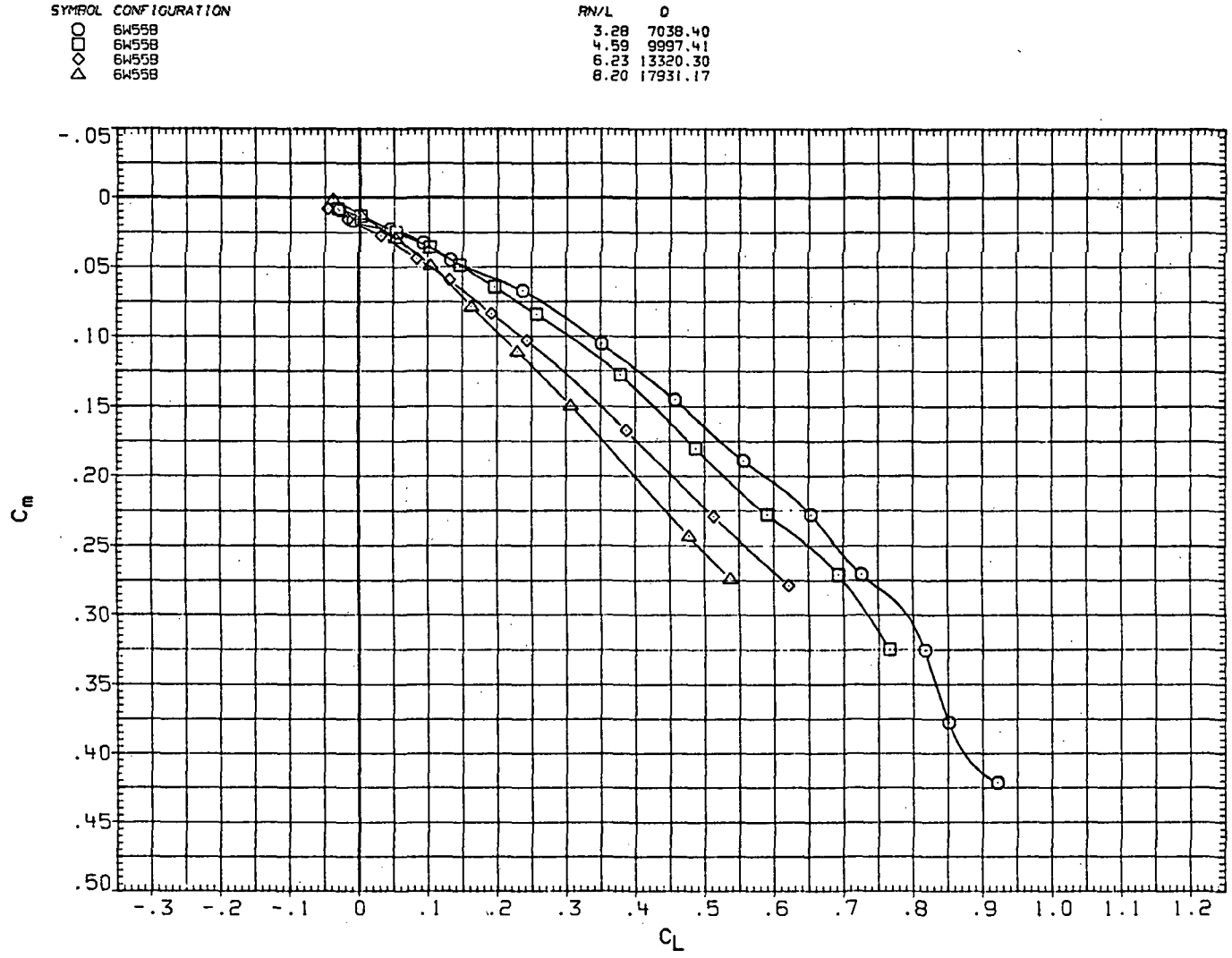


(c) $C_m$ vs $C_L$

Figure 26.– Continued.

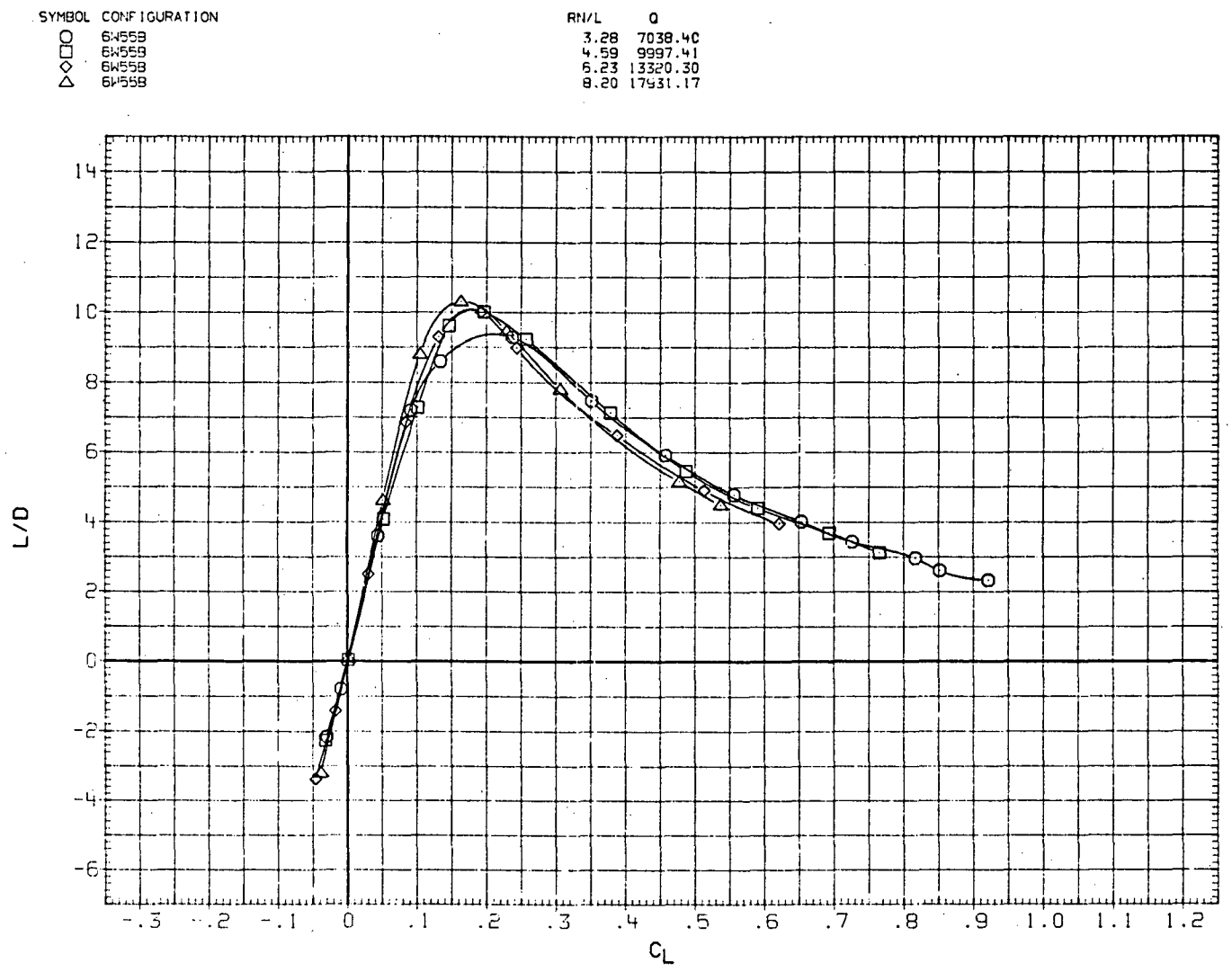


(d) $L/D$ vs $C_L$

Figure 26.– Continued.

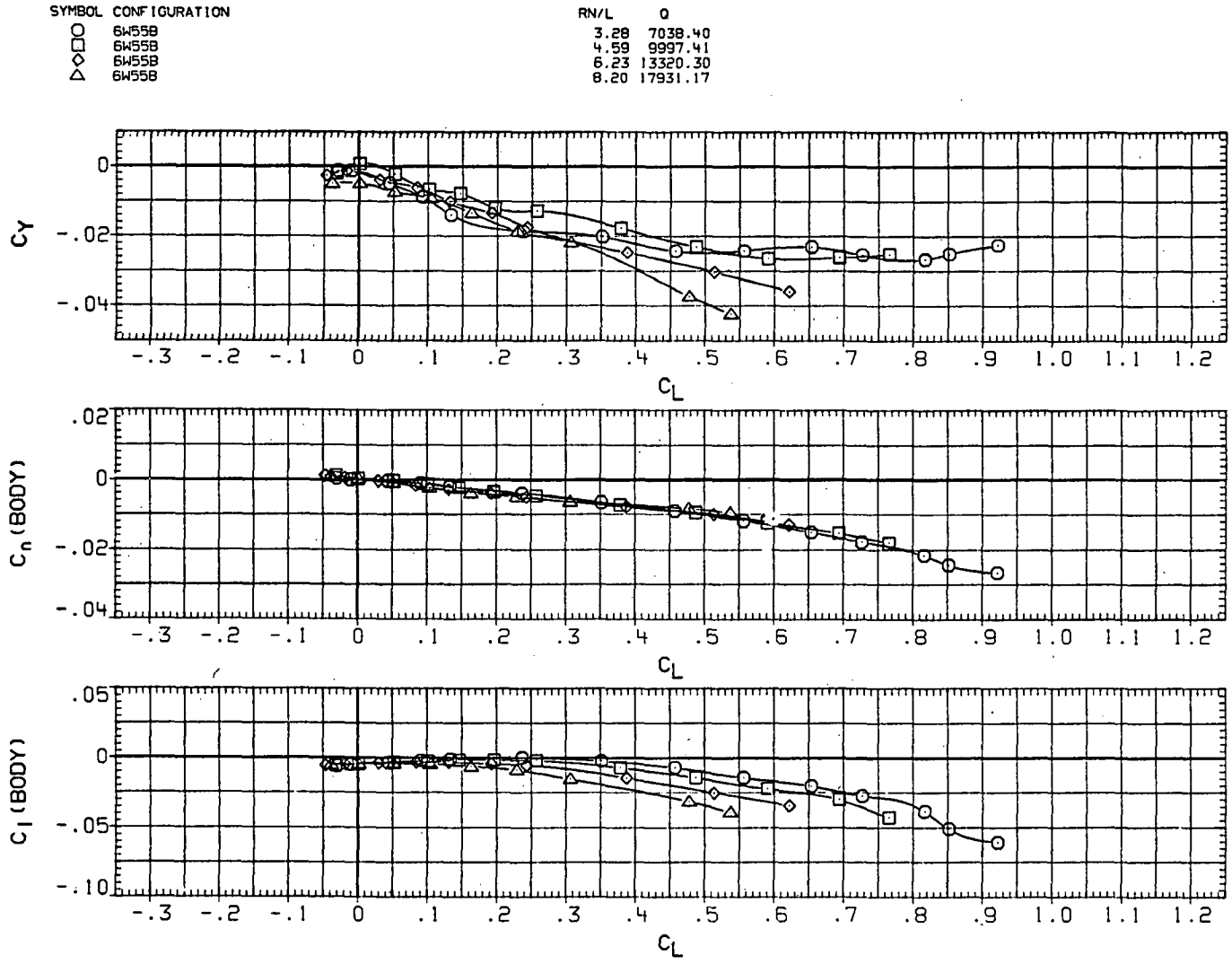


(e) $C_Y$, $C_n$, and $C_l$ vs $C_L$

Figure 26.– Concluded.

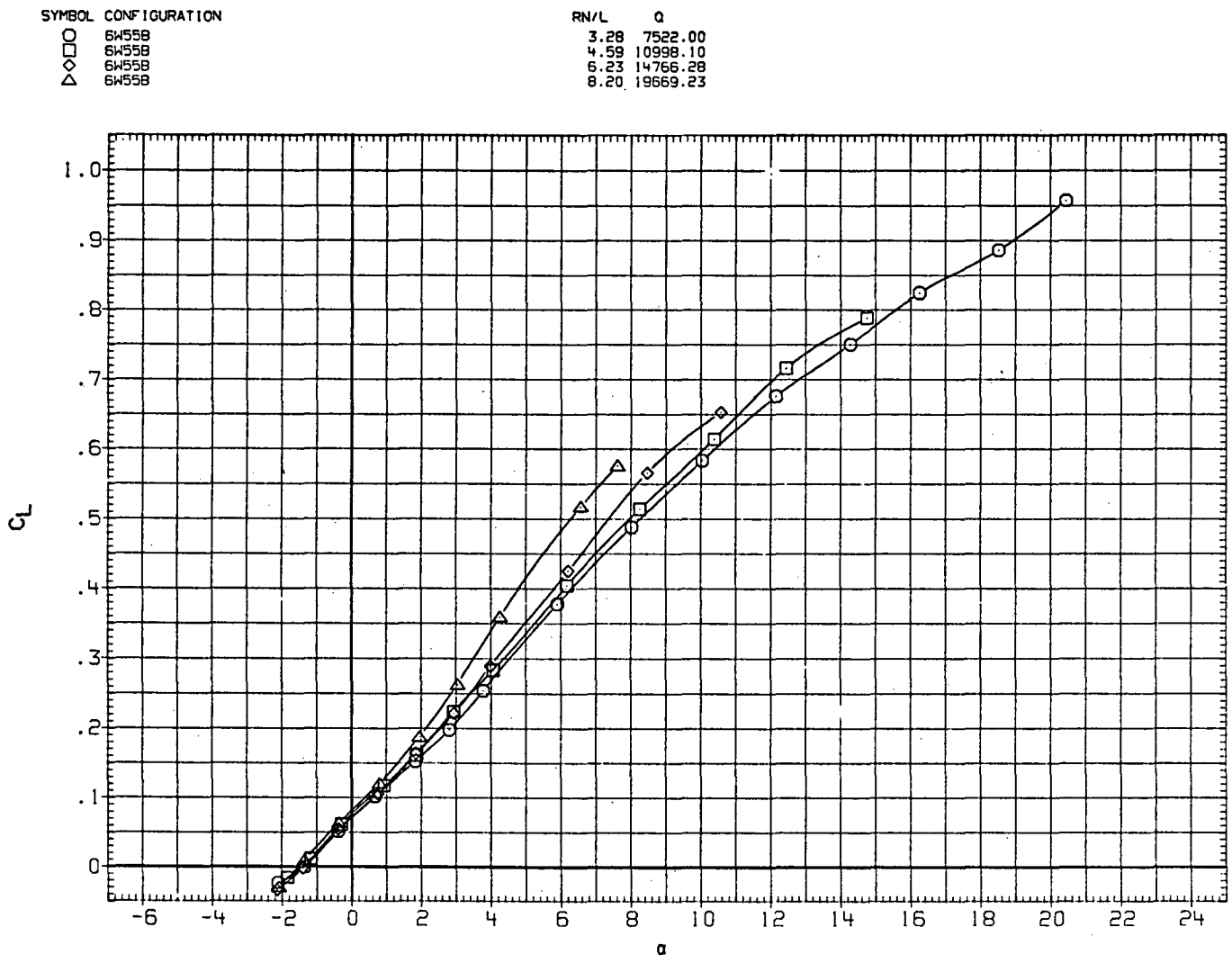


(a) $C_L$ vs $\alpha$

Figure 27.– Flexibility effects due to dynamic-pressure changes on the aerodynamic characteristics of the trapezoidal oblique wing: $\Lambda = 55°, M = 0.9$.

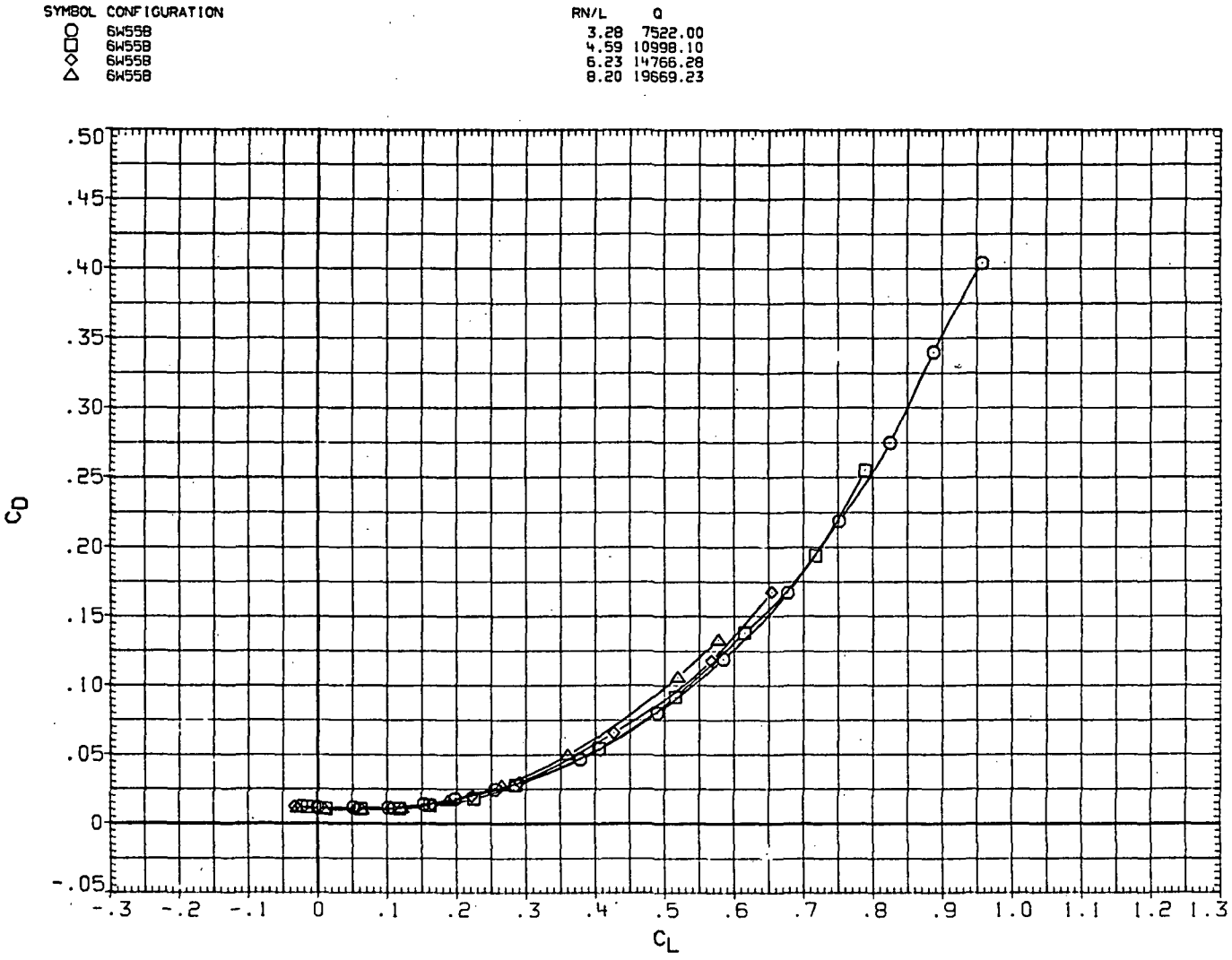


(b) $C_D$ vs $C_L$

Figure 27.– Continued.

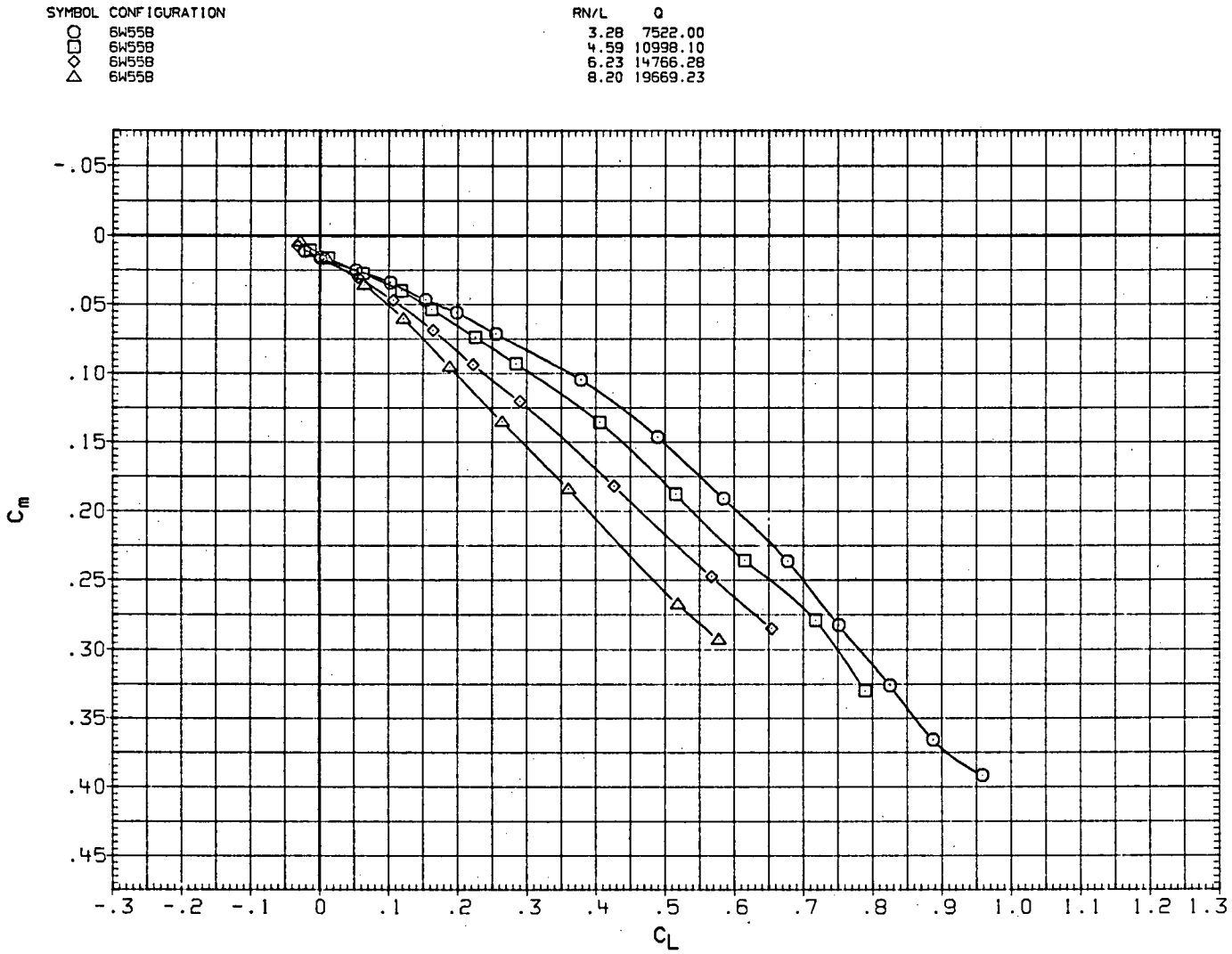


(c) $C_m$ vs $C_L$

Figure 27.– Continued.

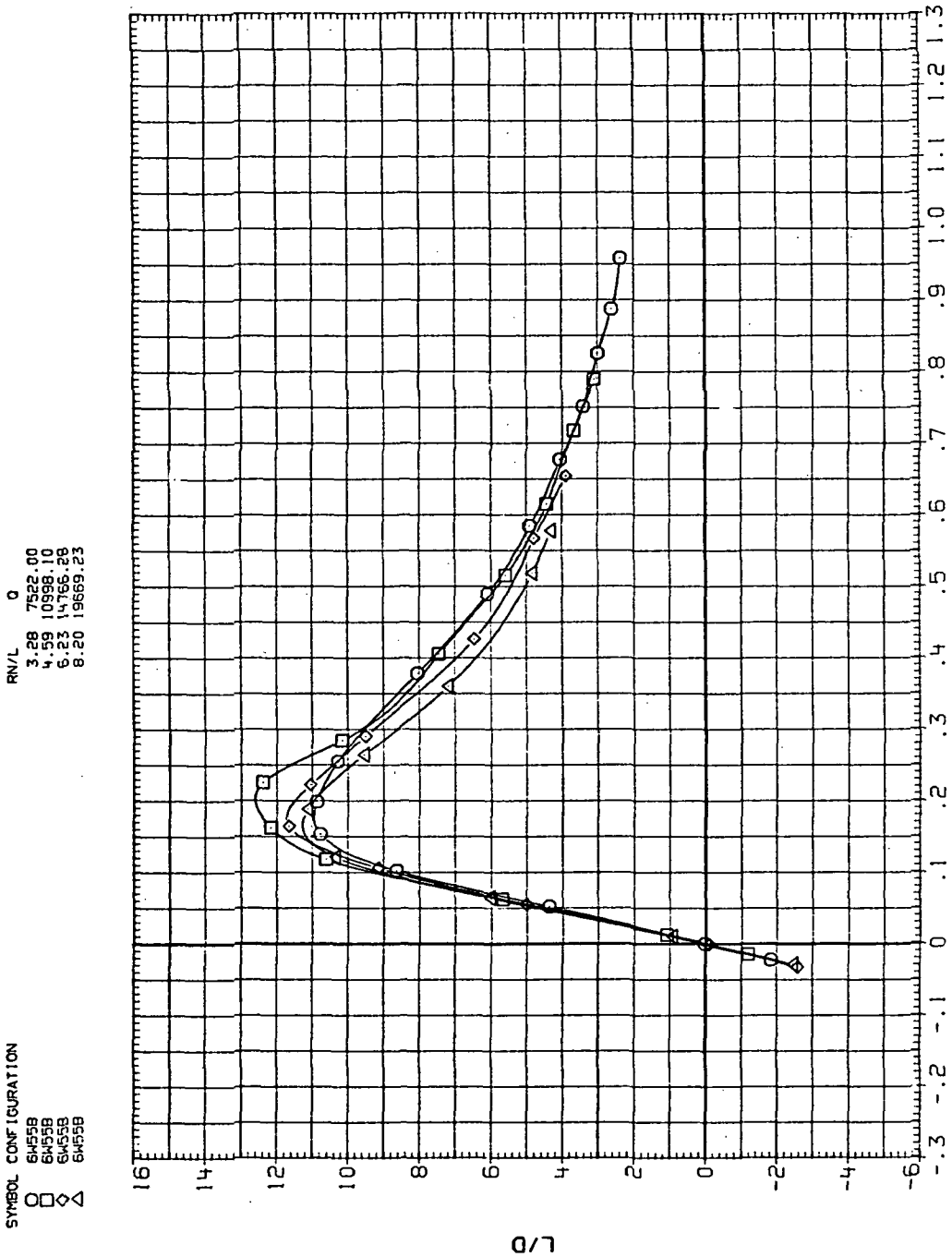


(d) $L/D$ vs $C_L$

Figure 27.– Continued.

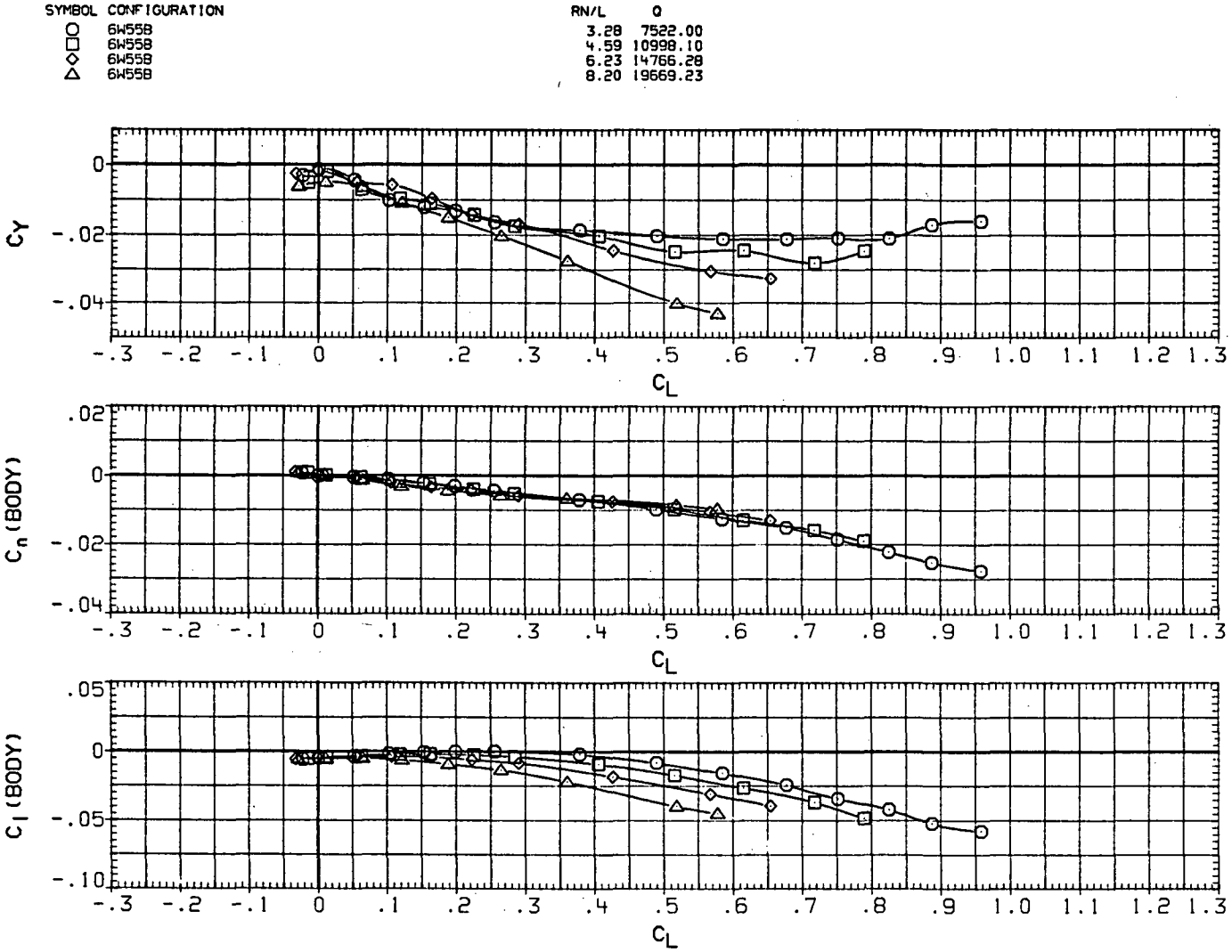


(e) $C_Y$, $C_n$, and $C_l$ vs $C_L$

Figure 27.– Concluded.

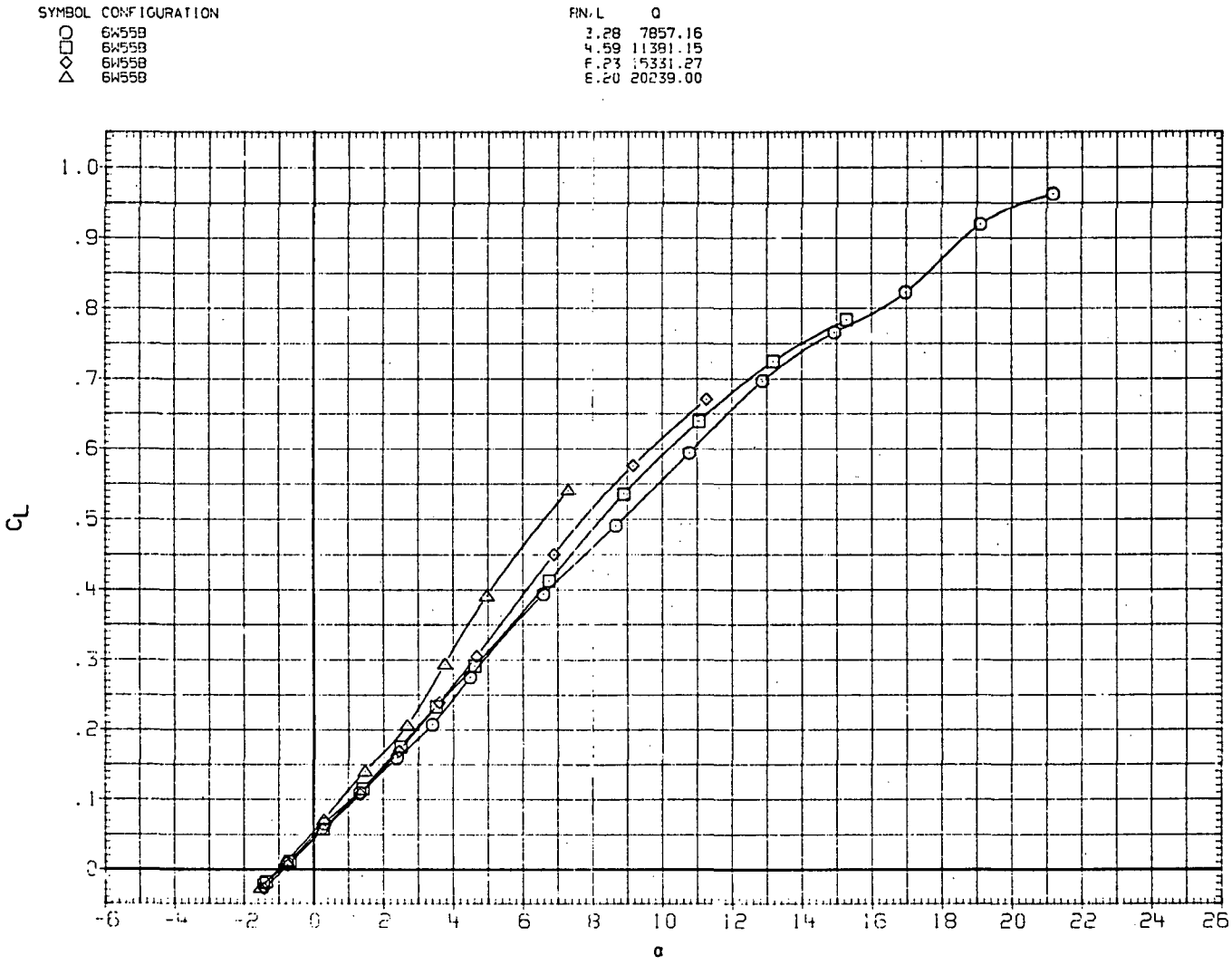


(a) $C_L$ vs $\alpha$

Figure 28.– Flexibility effects due to dynamic-pressure changes on the aerodynamic characteristics of the trapezoidal oblique wing: $\Lambda = 55°, M = 0.95$.

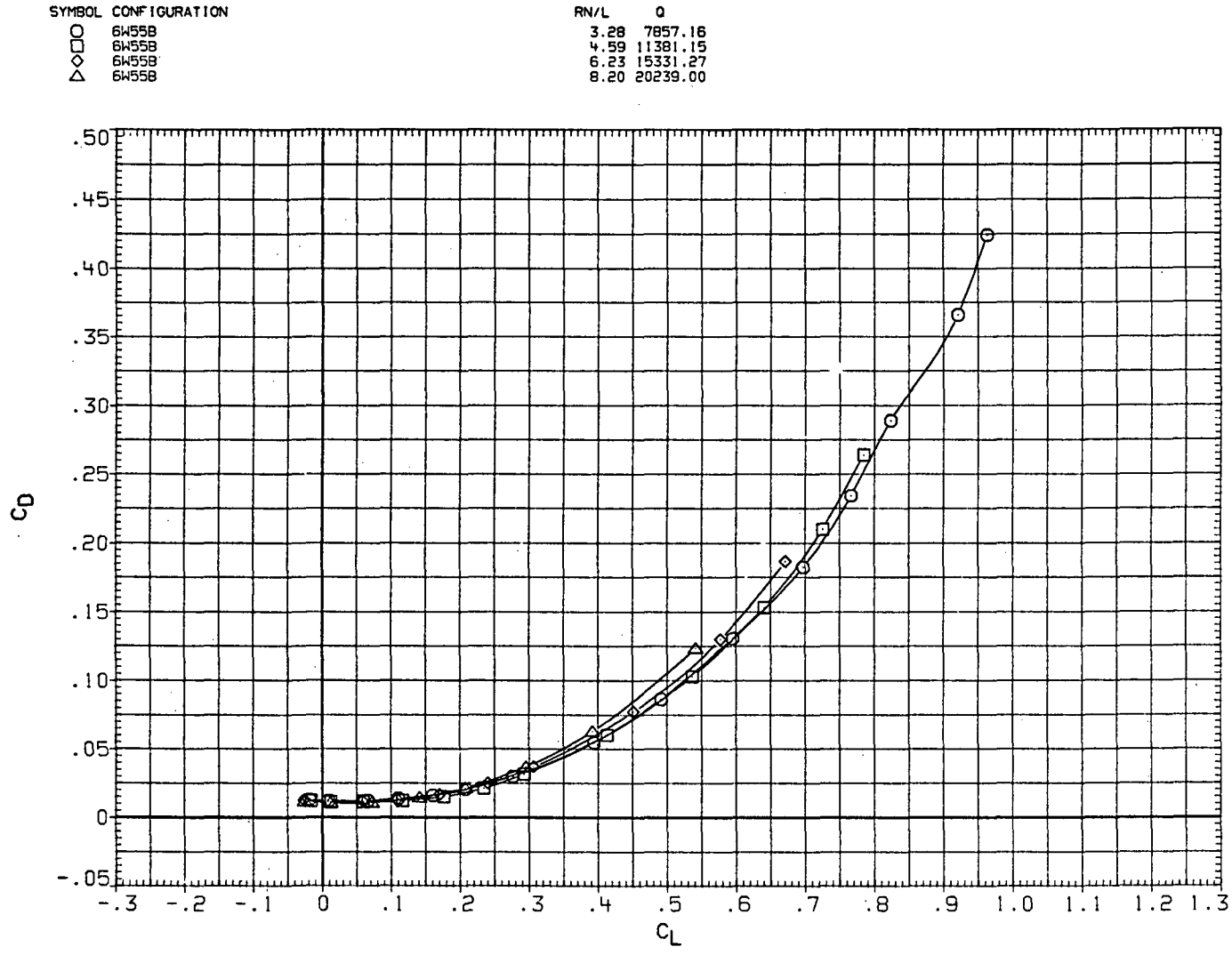


(b) $C_D$ vs $C_L$

Figure 28.– Continued.

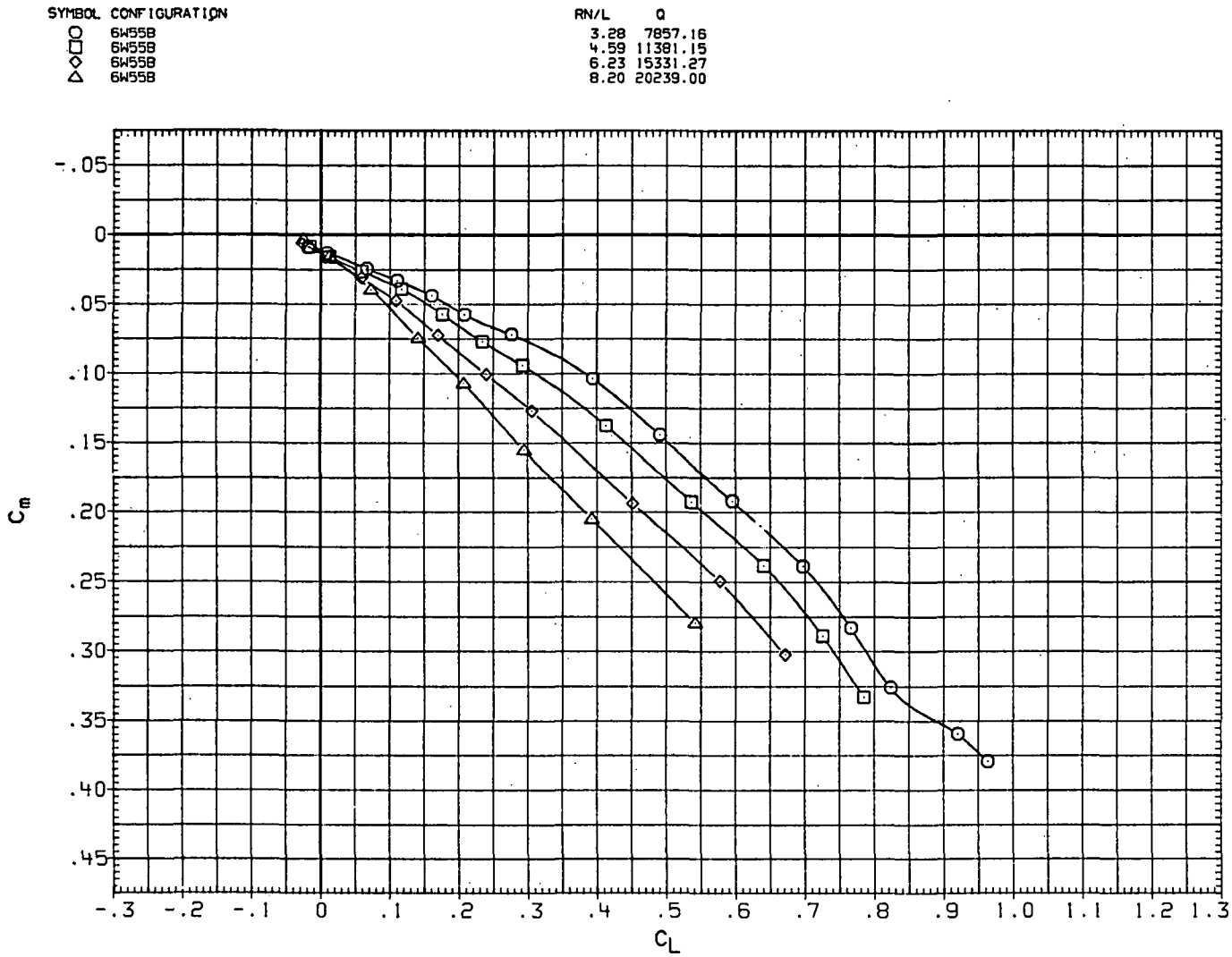


(c) $C_m$ vs $C_L$

Figure 28.– Continued.

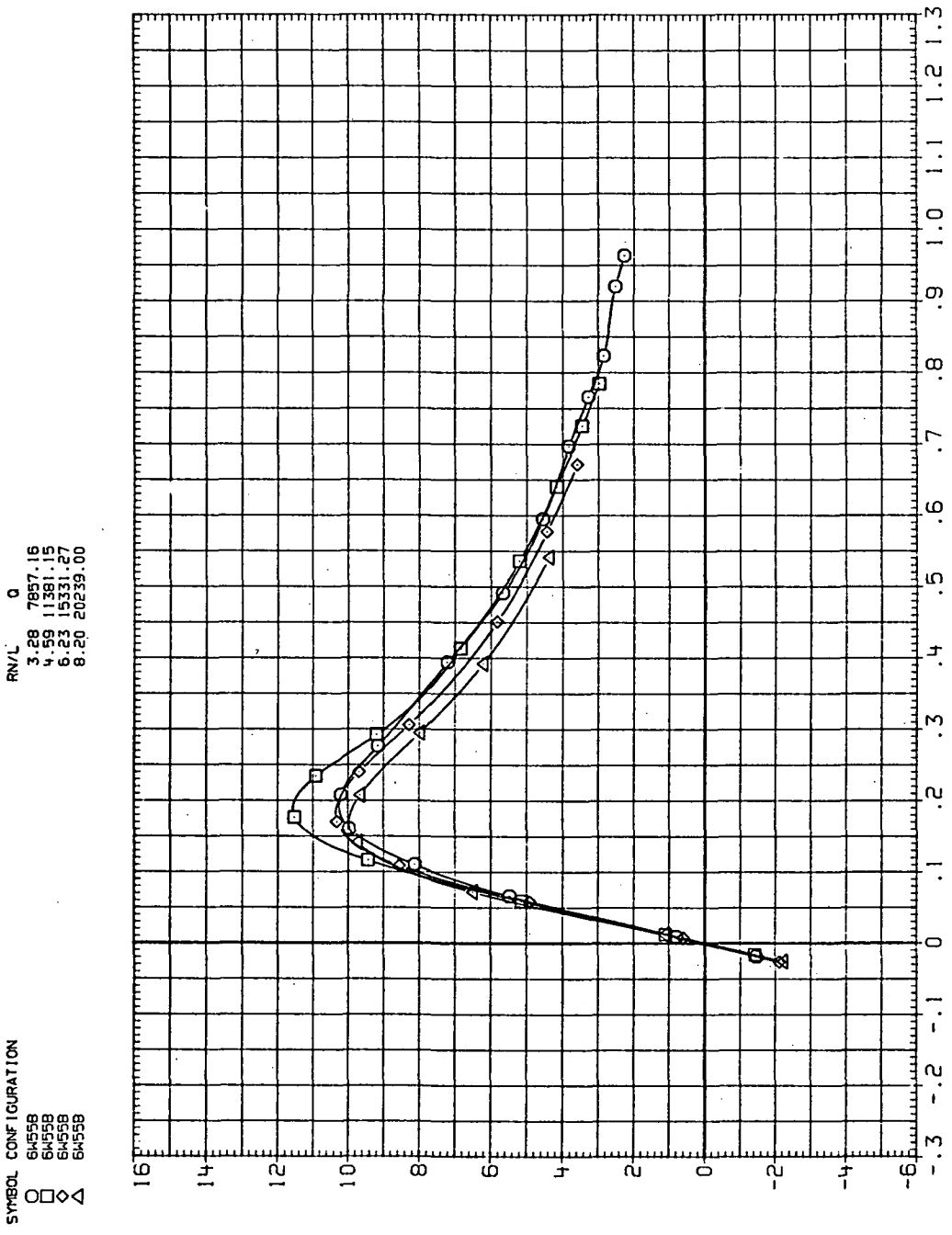


(d) $L/D$ vs $C_L$

Figure 28.– Continued.

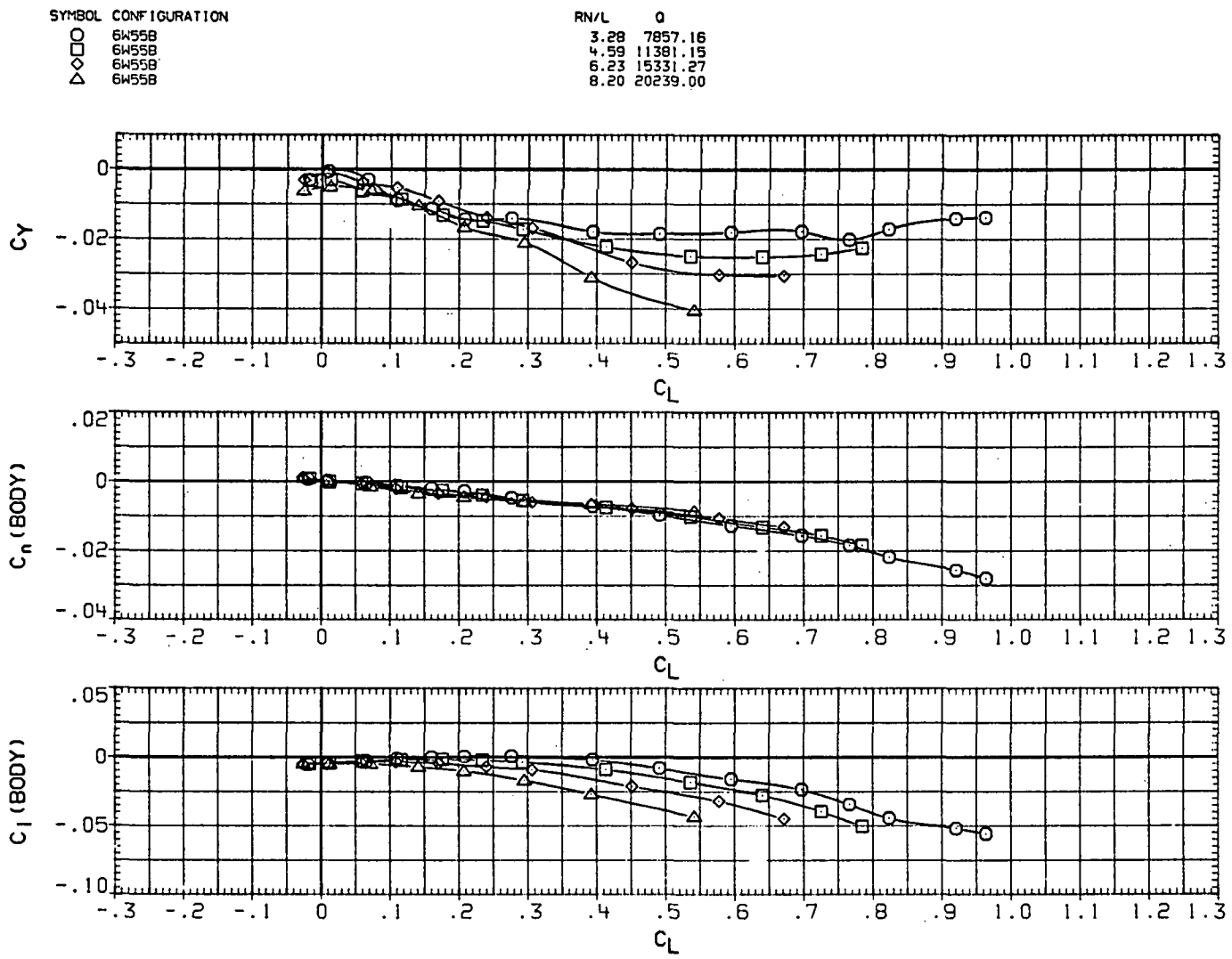


(e) $C_Y$, $C_n$, and $C_l$ vs $C_L$

Figure 28.– Concluded.

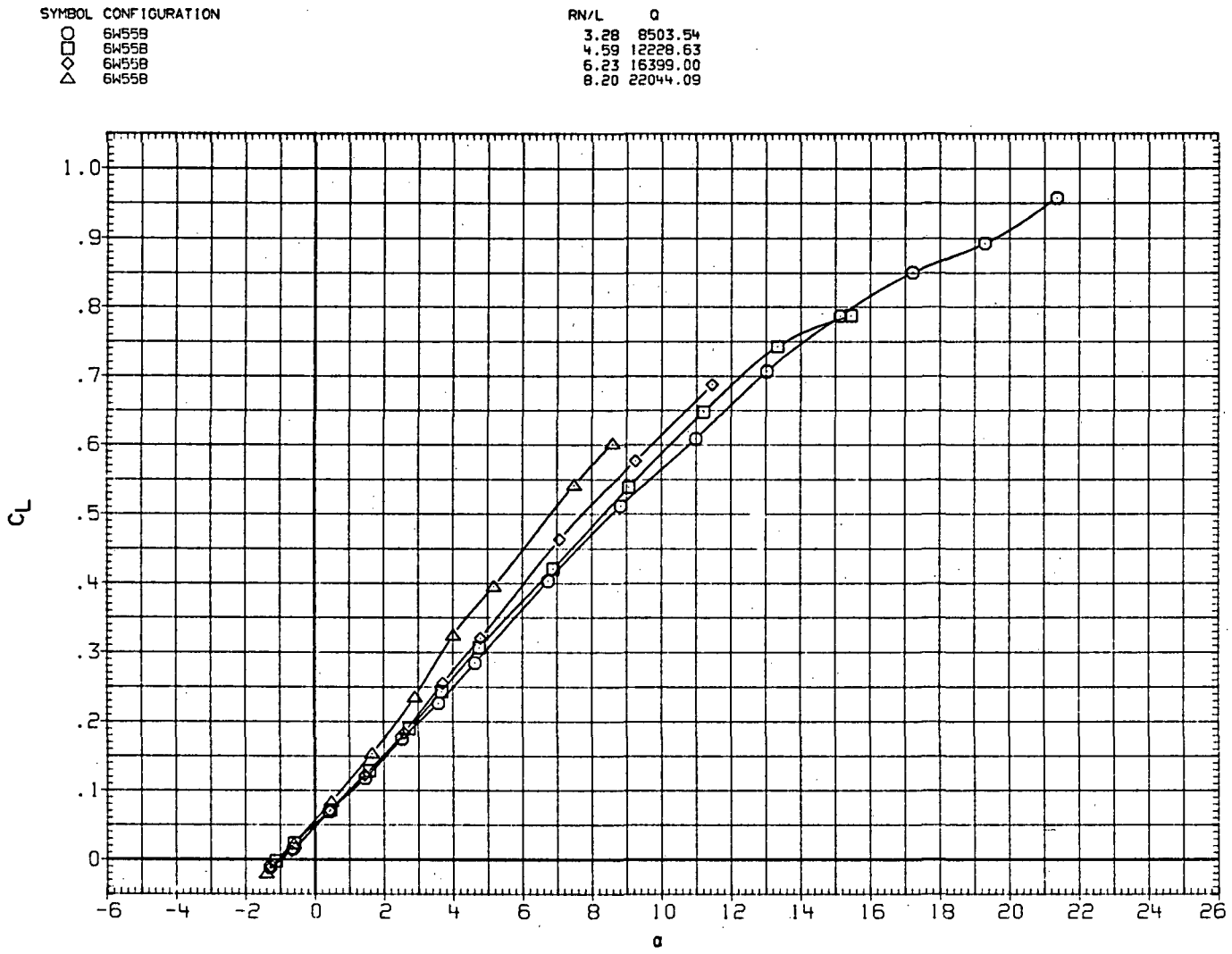


(a) $C_L$ vs $\alpha$

Figure 29.– Flexibility effects due to dynamic-pressure changes on the aerodynamic characteristics of the trapezoidal oblique wing: $\Lambda = 55°, M = 1.1$.

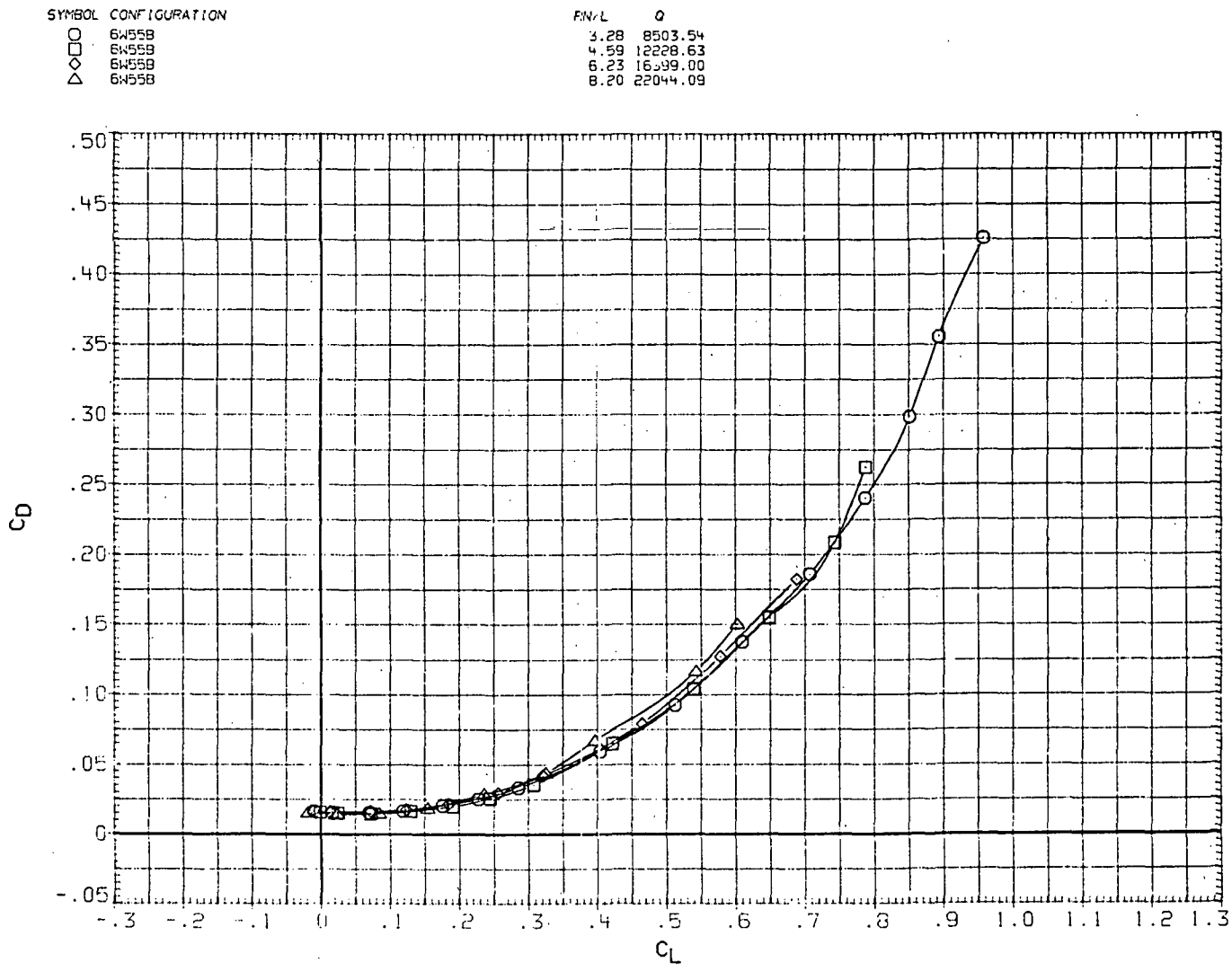


(b) $C_D$ vs $C_L$

Figure 29.– Continued.

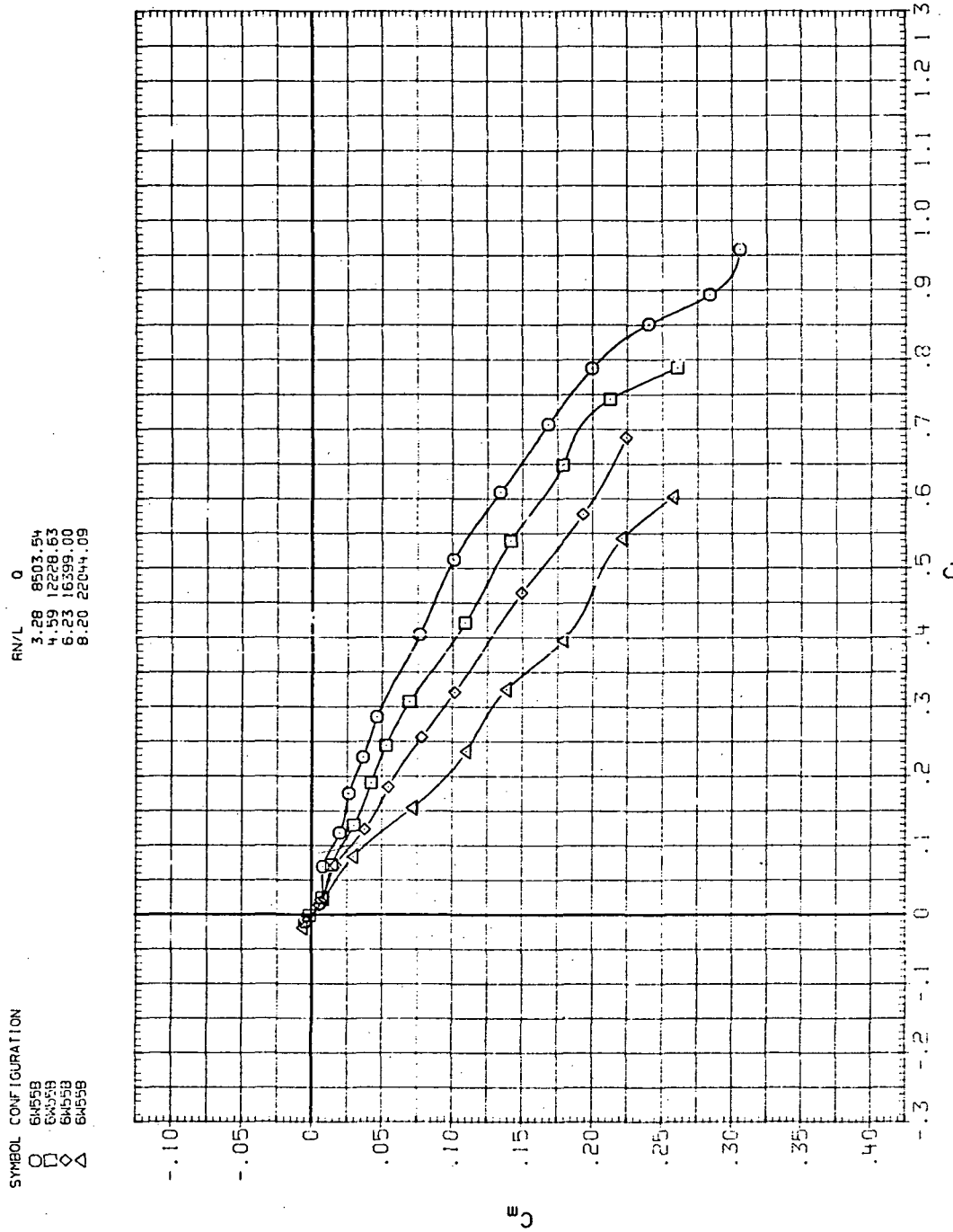


(c) $C_m$ vs $C_L$

Figure 29.– Continued.


(d) $L/D$ vs $C_L$

Figure 29.– Continued.

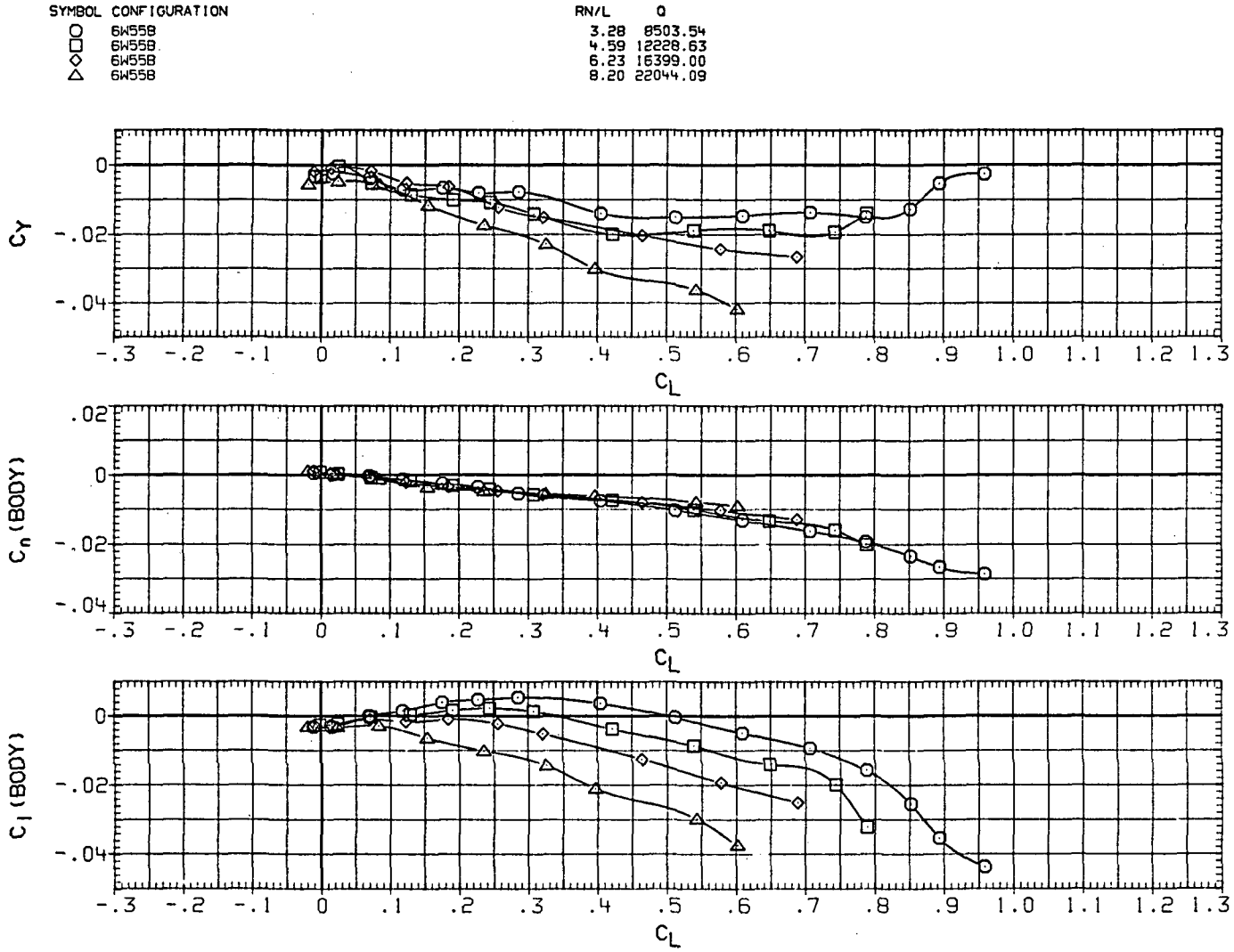


(e) $C_Y$, $C_n$, and $C_l$ vs $C_L$

Figure 29.– Concluded.

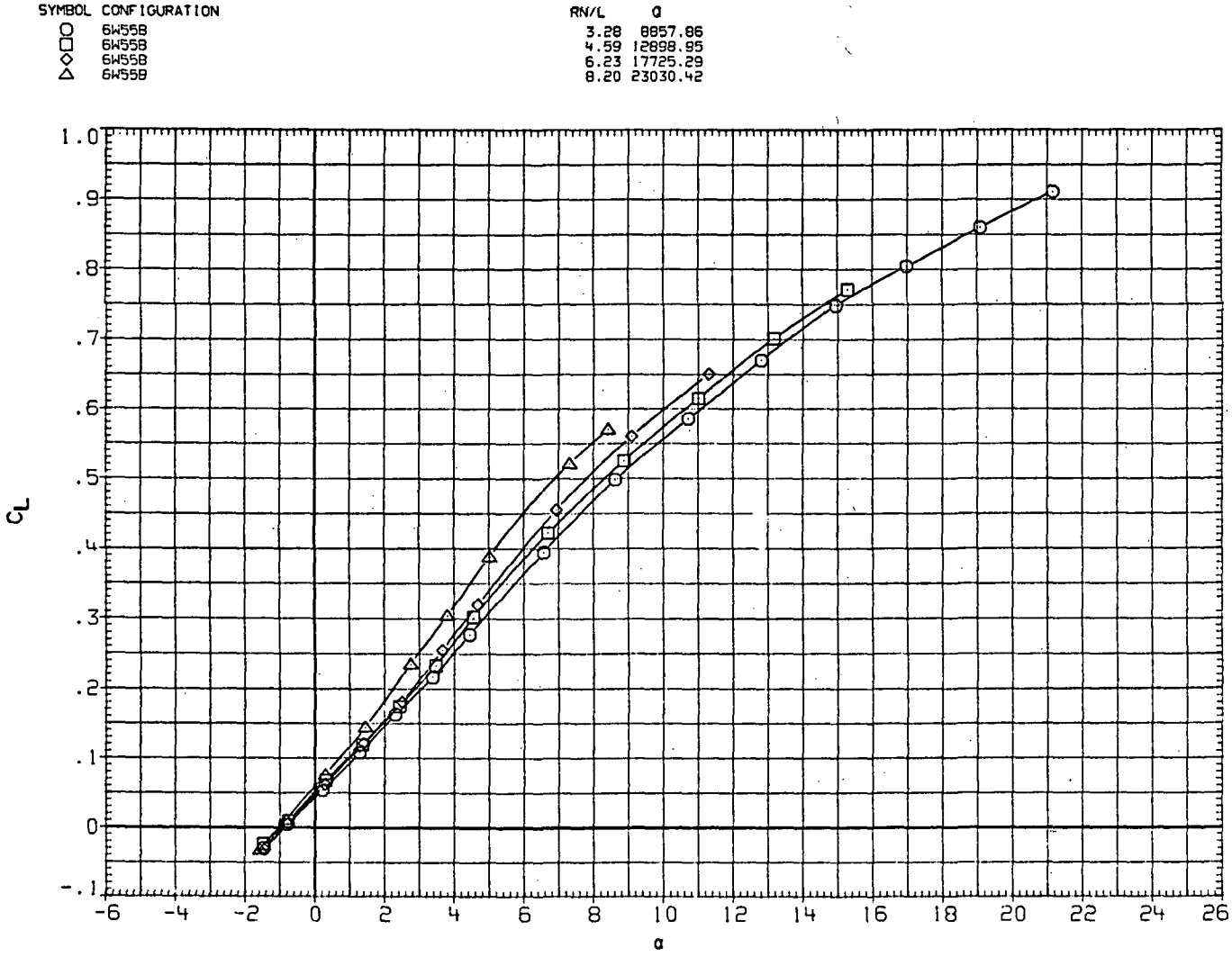


(a) $C_L$ vs $\alpha$

Figure 30.– Flexibility effects due to dynamic-pressure changes on the aerodynamic characteristics of the trapezoidal oblique wing: $\Lambda = 55°, M = 1.2$.

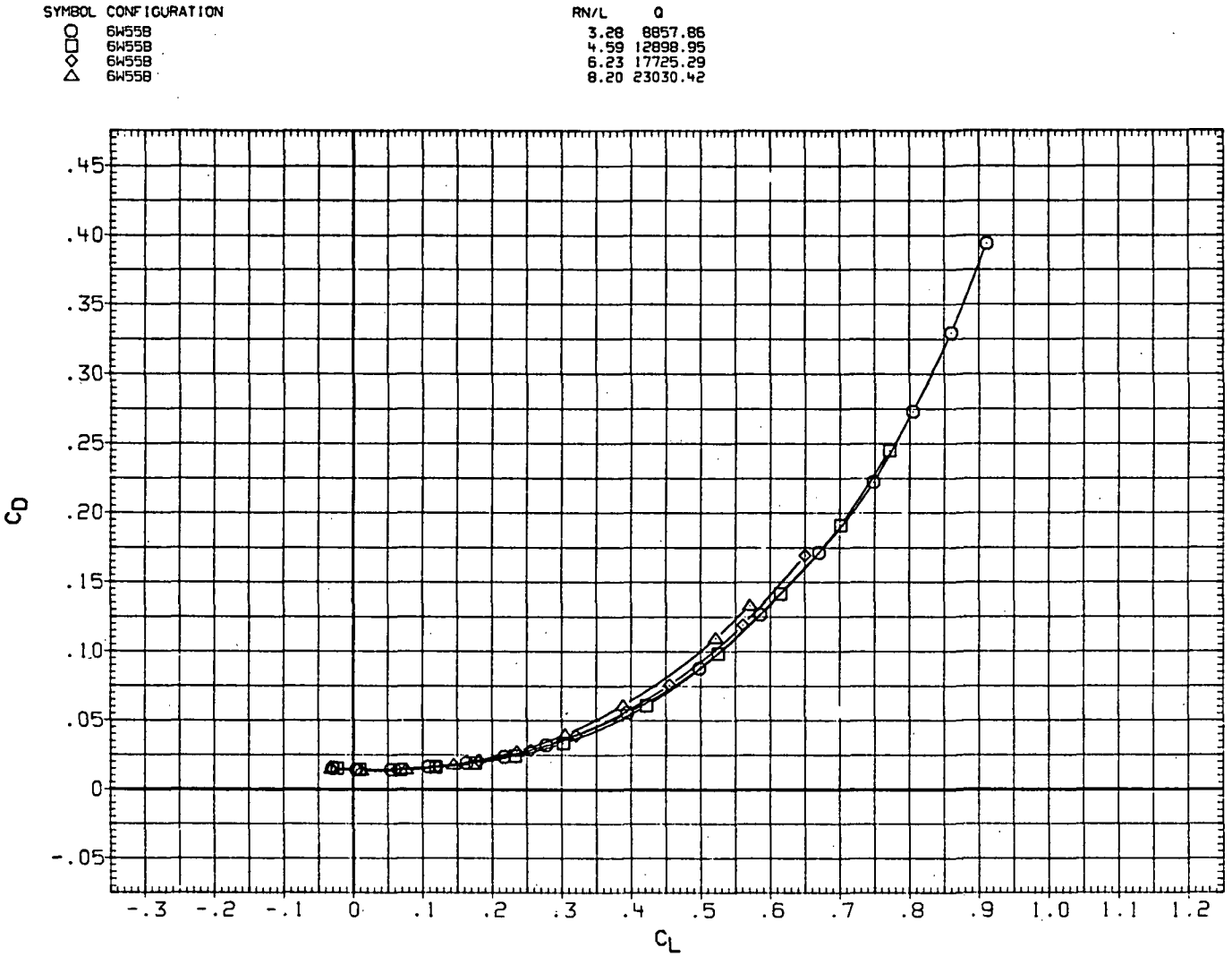


(b) $C_D$ vs $C_L$

Figure 30.– Continued.

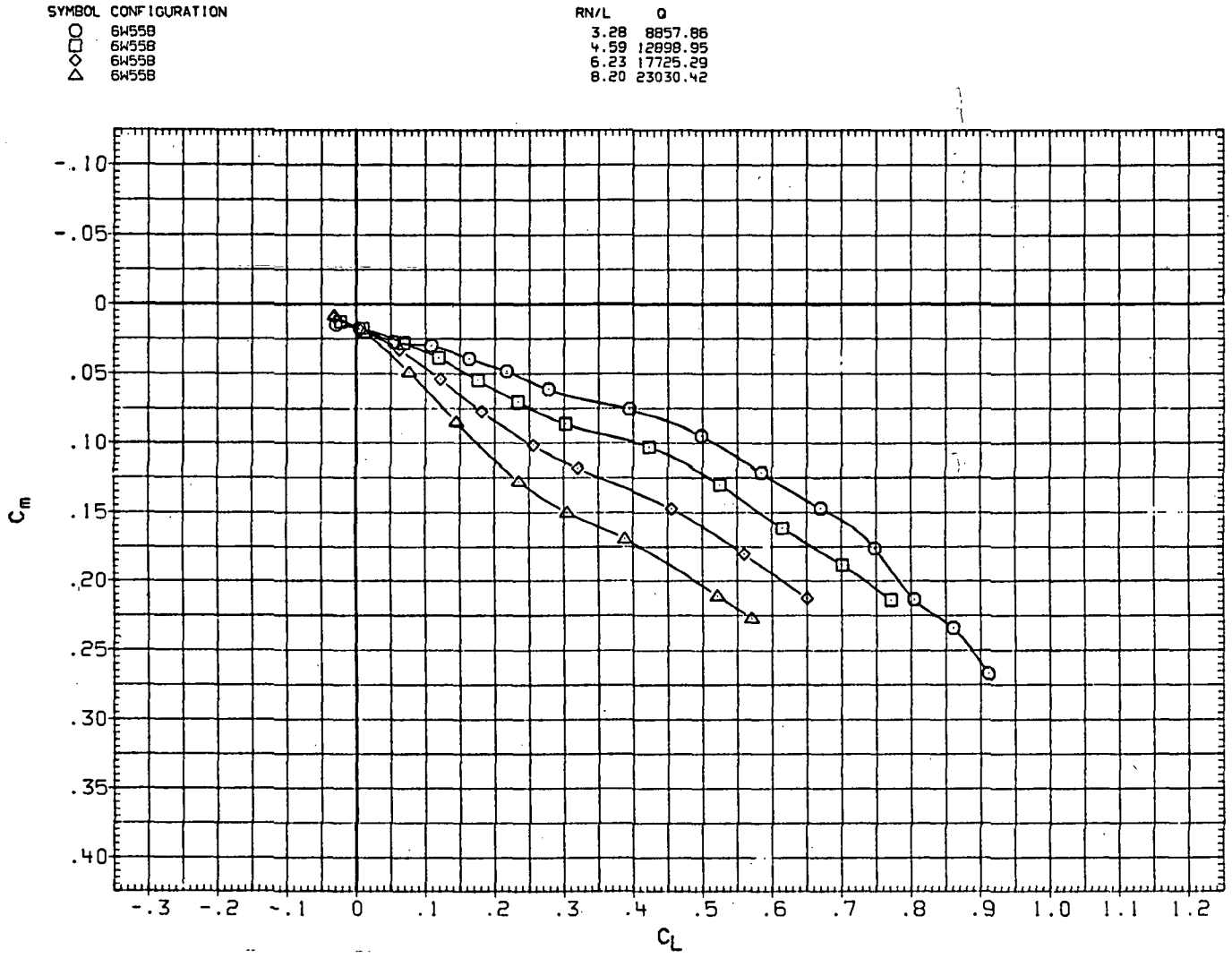


(c) $C_m$ vs $C_L$

Figure 30.– Continued.

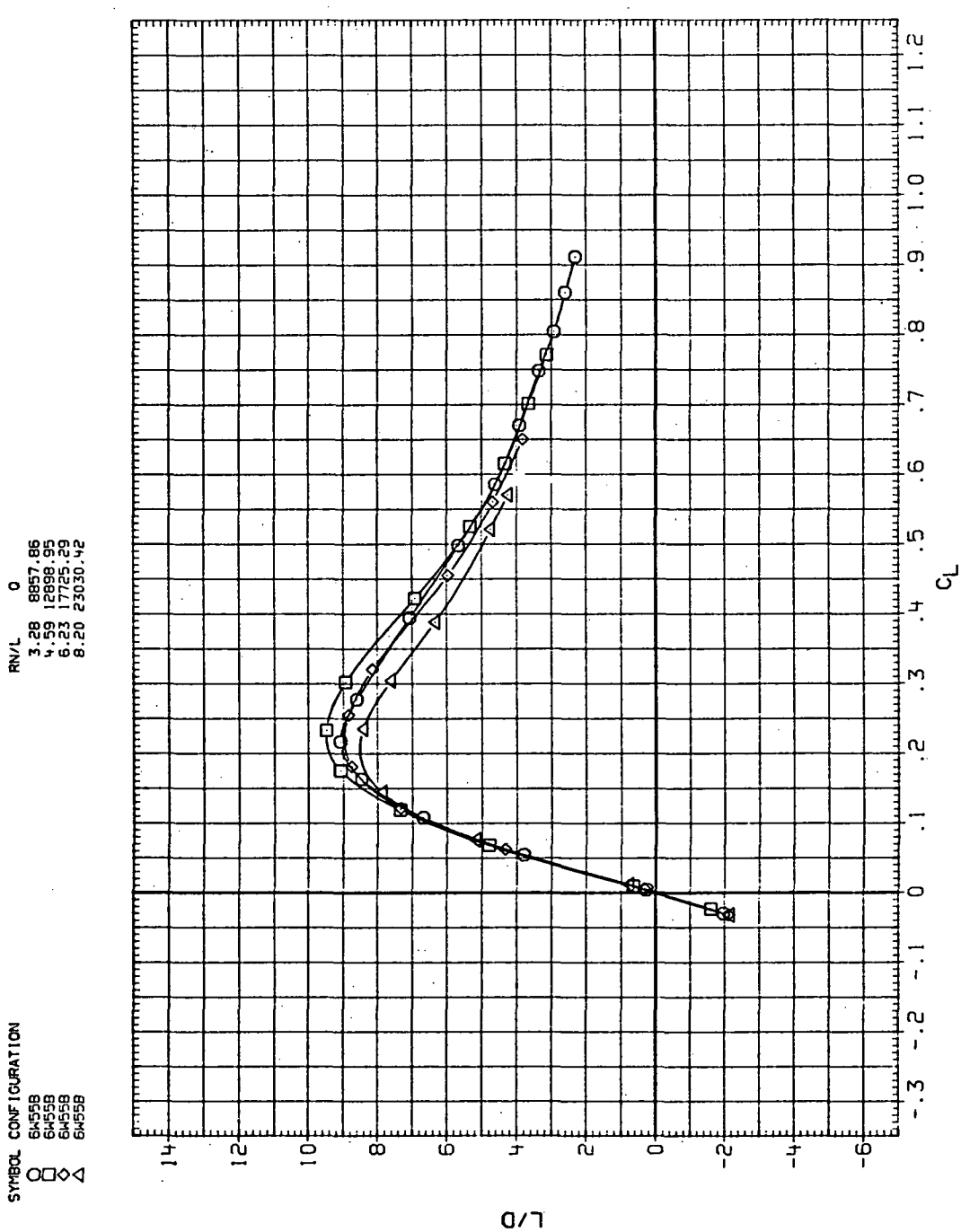


(d) $L/D$ vs $C_L$

Figure 30.– Continued.

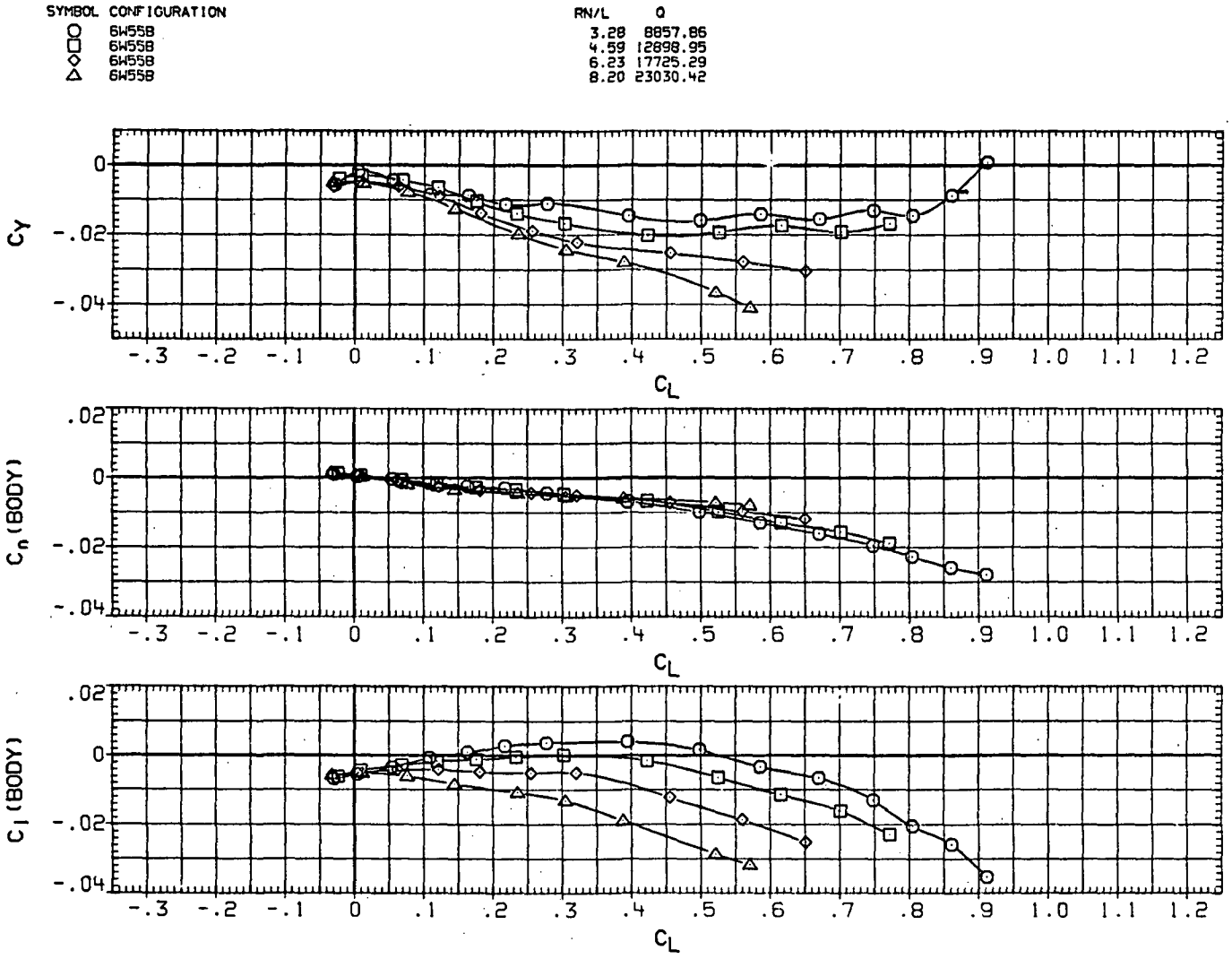


(e) $C_Y$, $C_n$, and $C_l$ vs $C_L$

Figure 30.– Concluded.

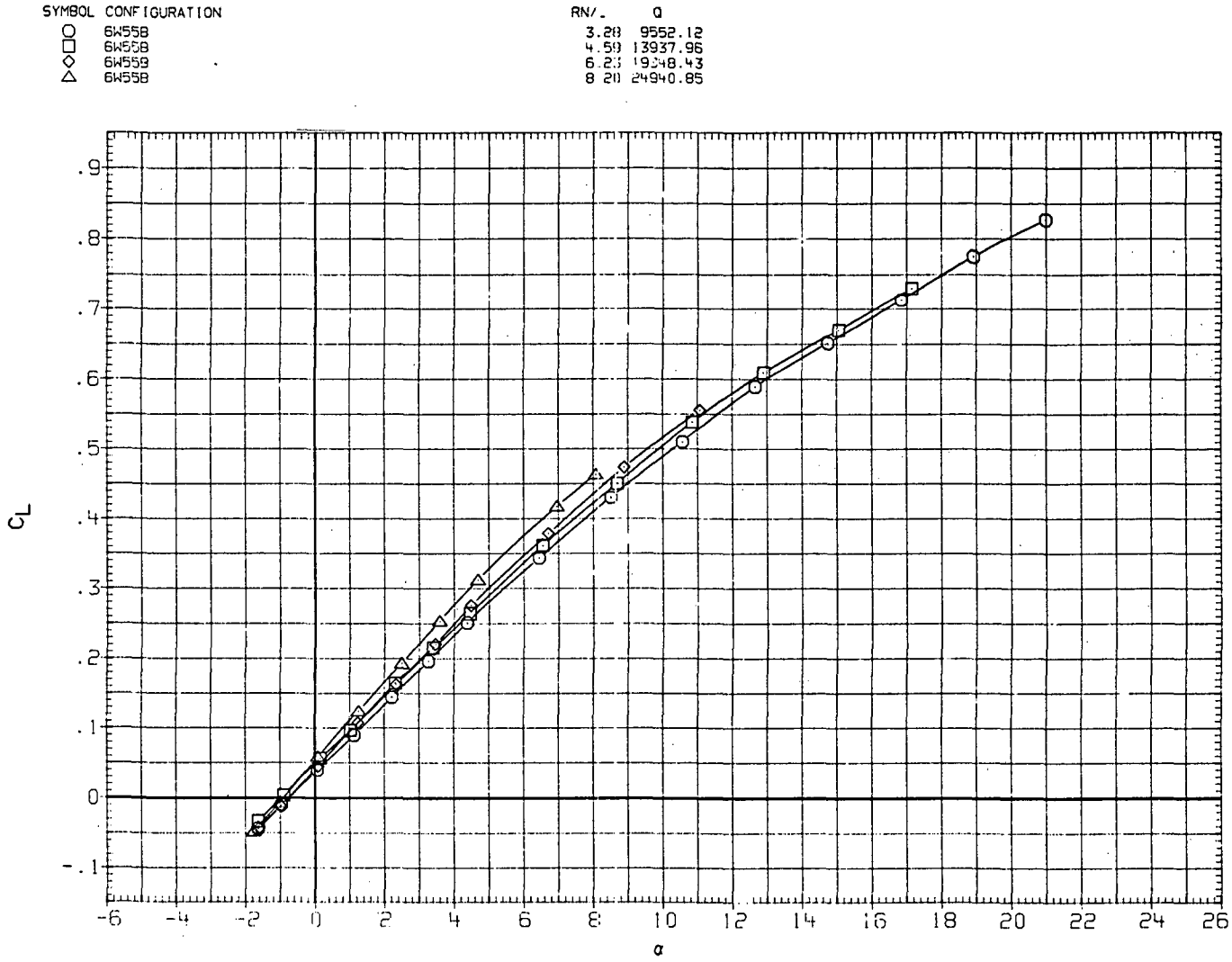


(a) $C_L$ vs $\alpha$

Figure 31.– Flexibility effects due to dynamic-pressure changes on the aerodynamic characteristics of the trapezoidal oblique wing: $\Lambda = 55°, M = 1.6$.

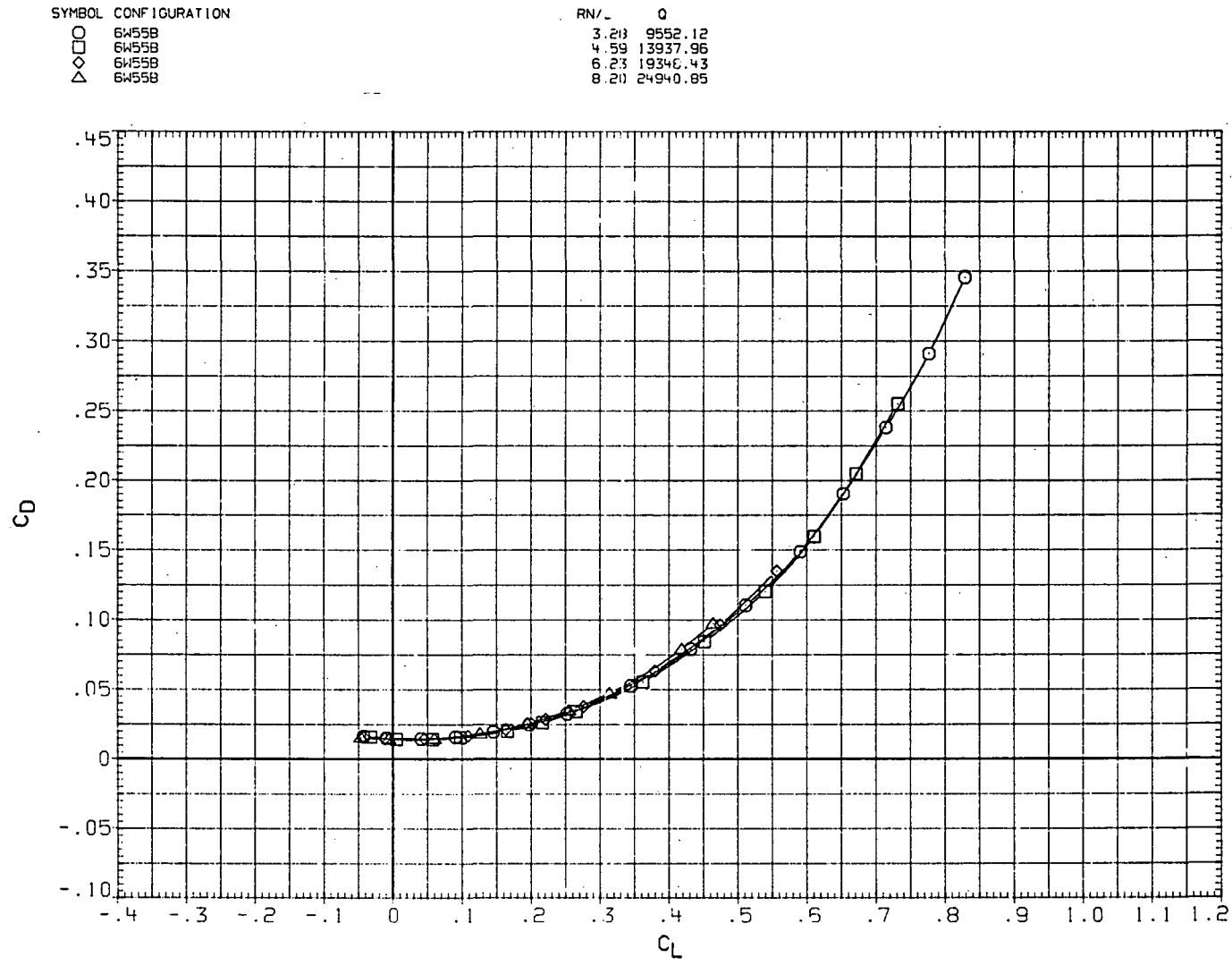


(b) $C_D$ vs $C_L$

Figure 31.– Continued.

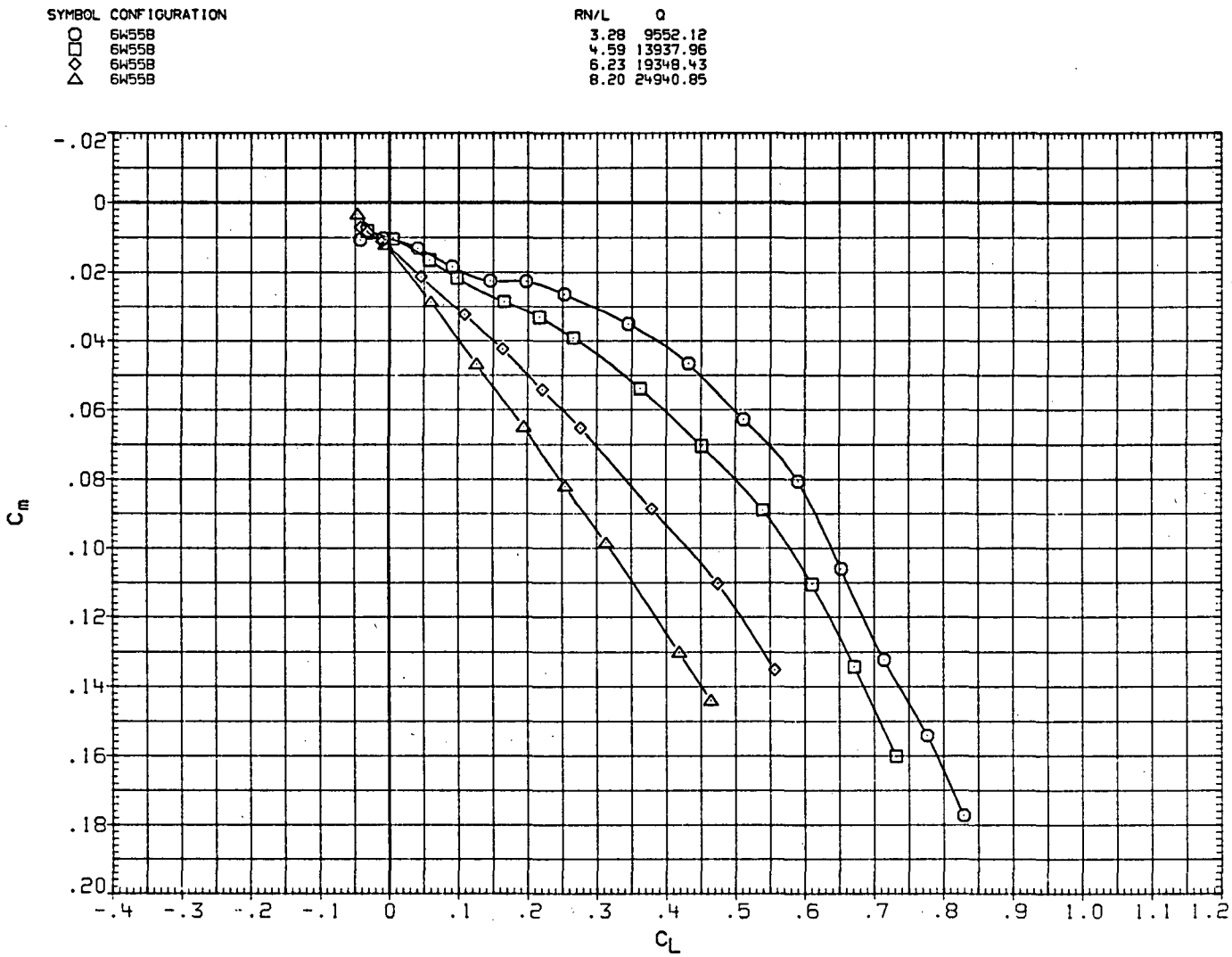


(c) $C_m$ vs $C_L$

Figure 31.– Continued.

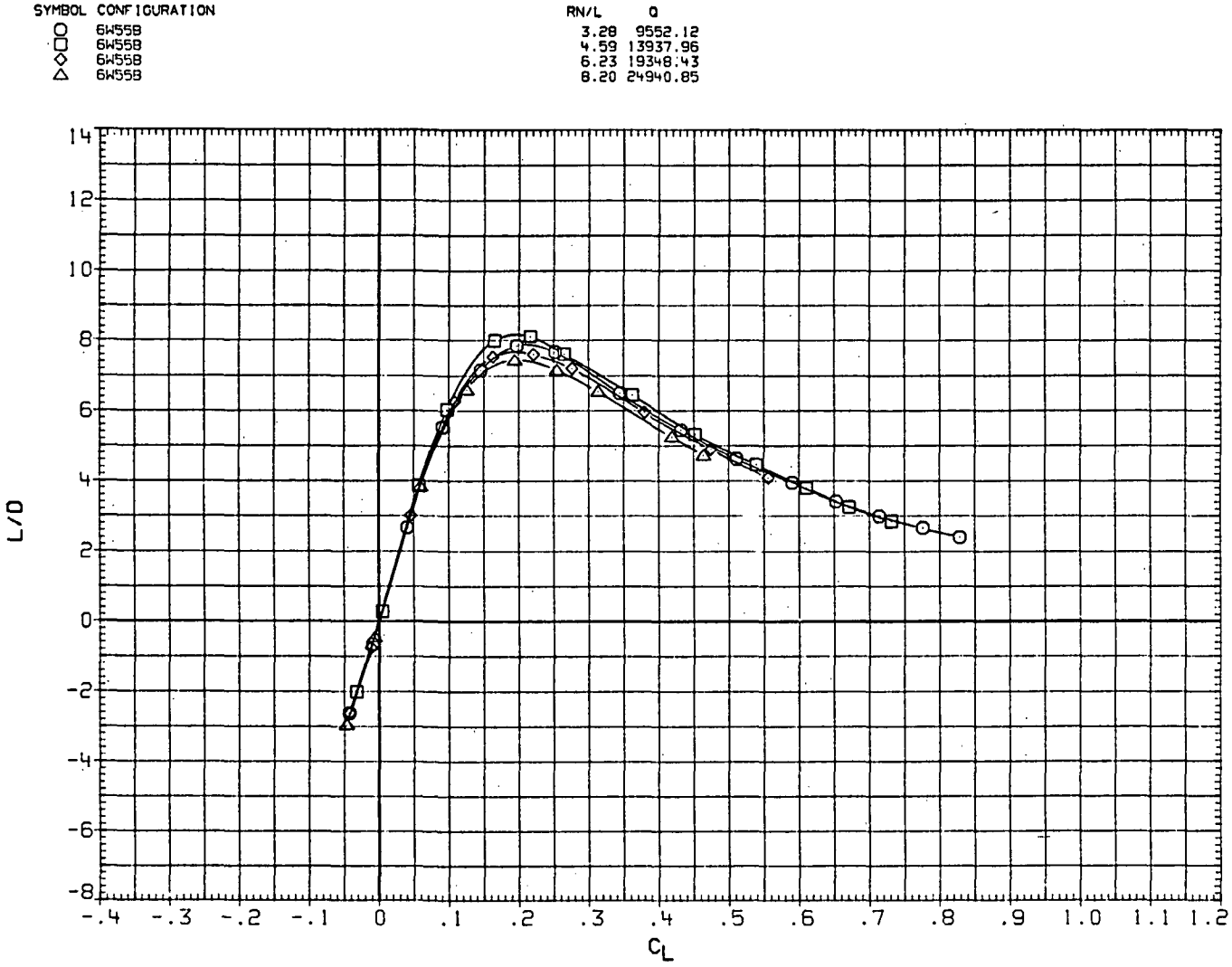


(d) $L/D$ vs $C_L$

Figure 31.– Continued.

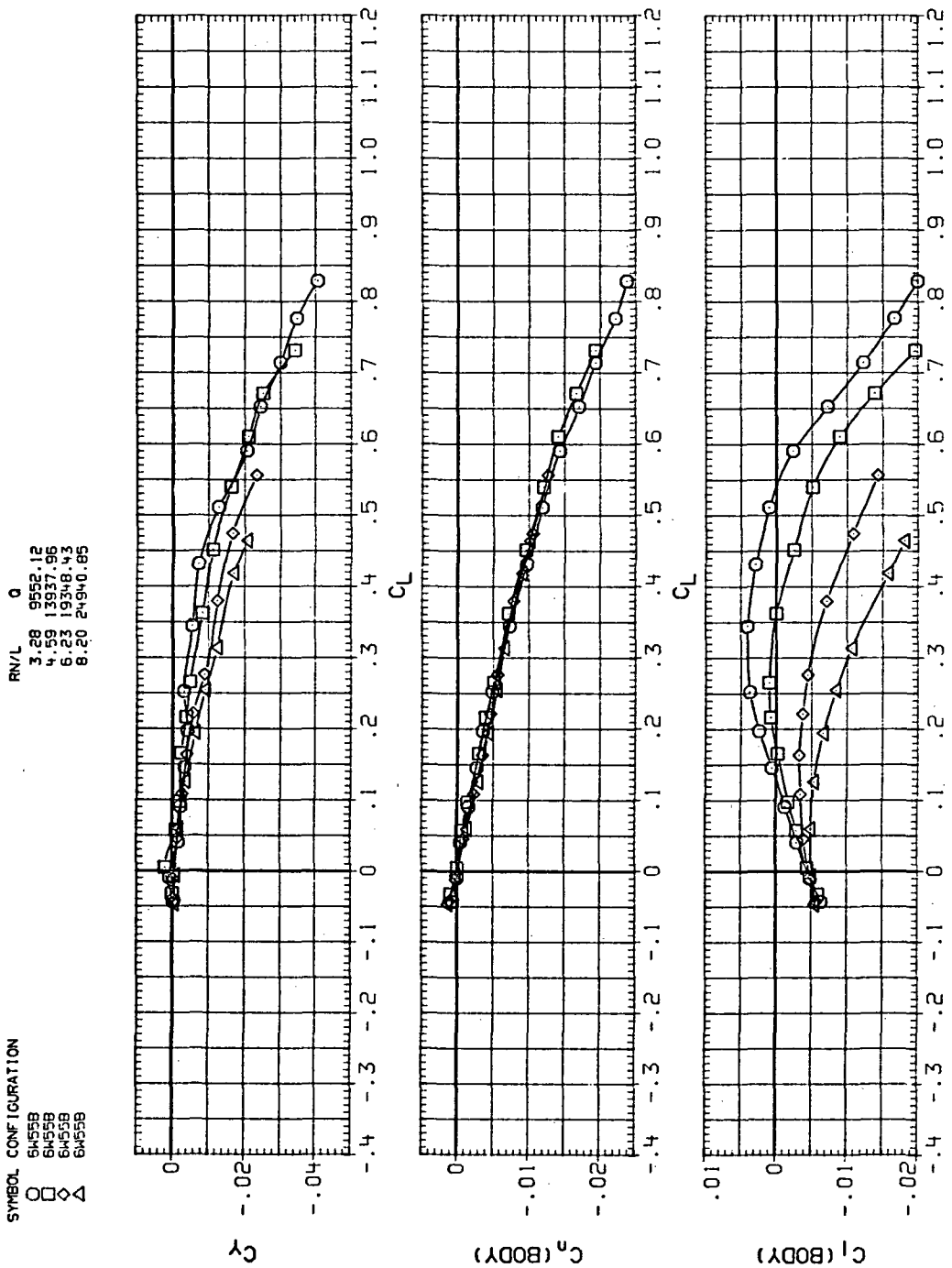


(e) $C_Y$, $C_n$, and $C_l$ vs $C_L$

Figure 31.– Concluded.

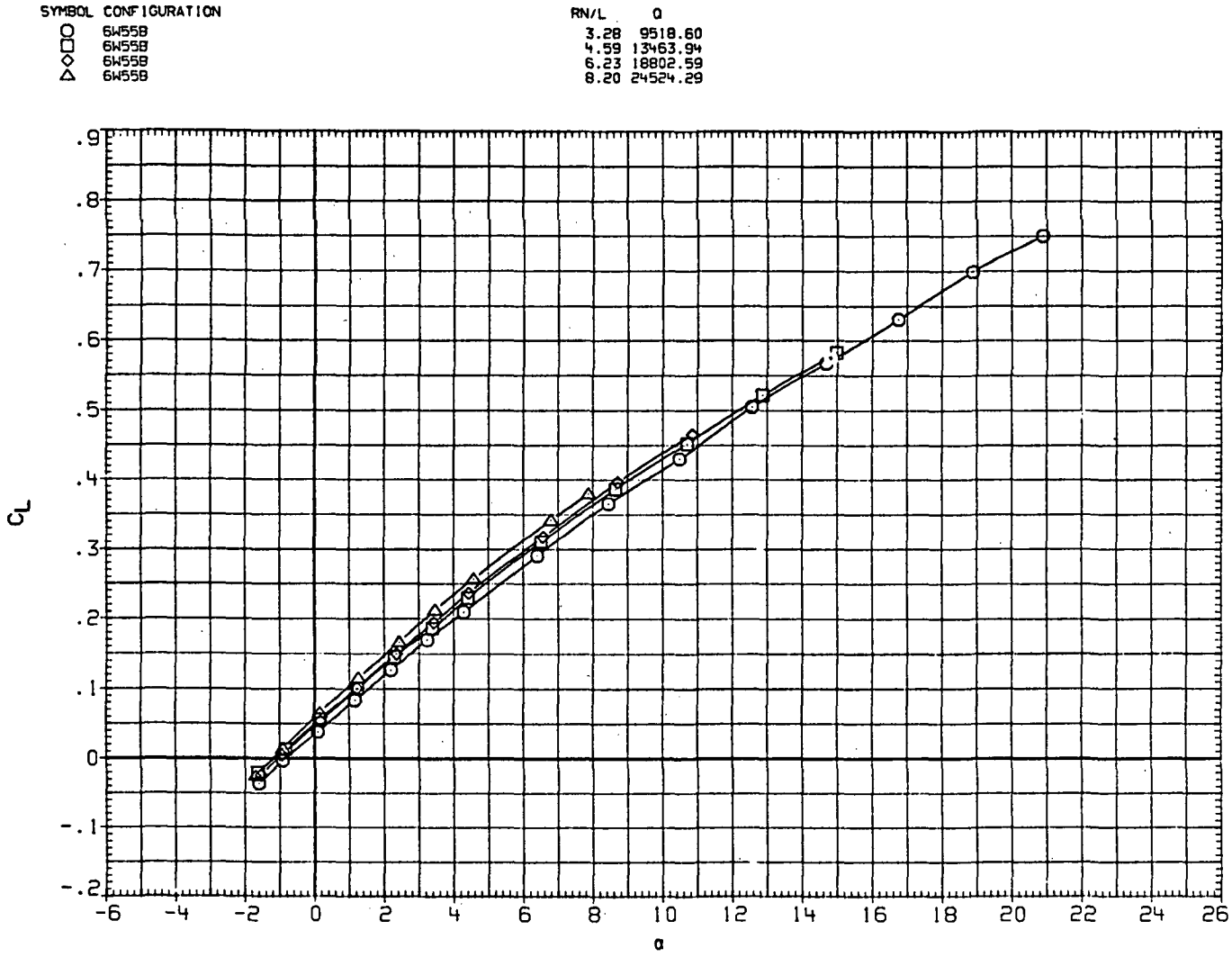


(a) $C_L$ vs $\alpha$

Figure 32.– Flexibility effects due to dynamic-pressure changes on the aerodynamic characteristics of the trapezoidal oblique wing: $\Lambda = 55°, M = 2.0$.

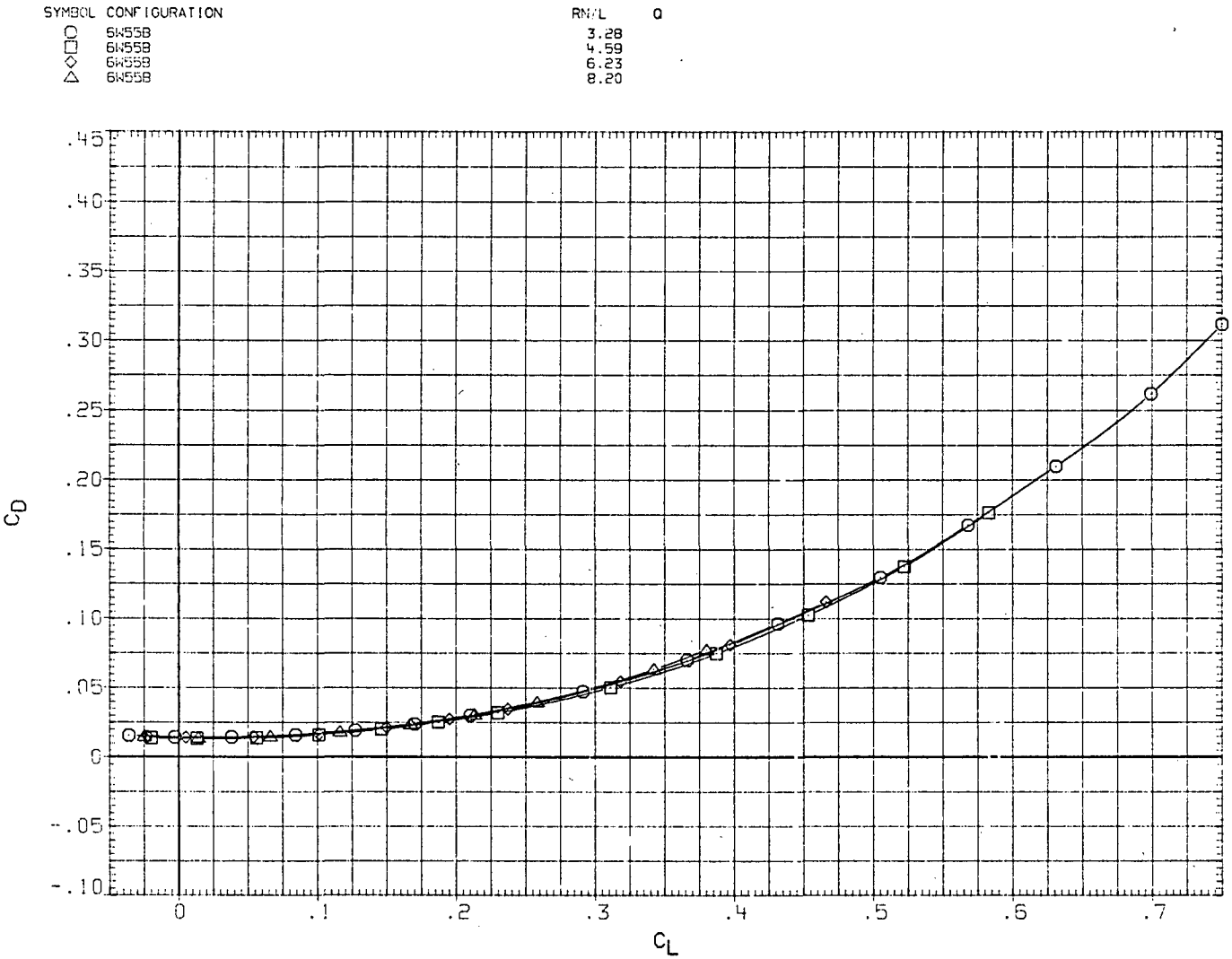


(b) $C_D$ vs $C_L$

Figure 32.– Continued.

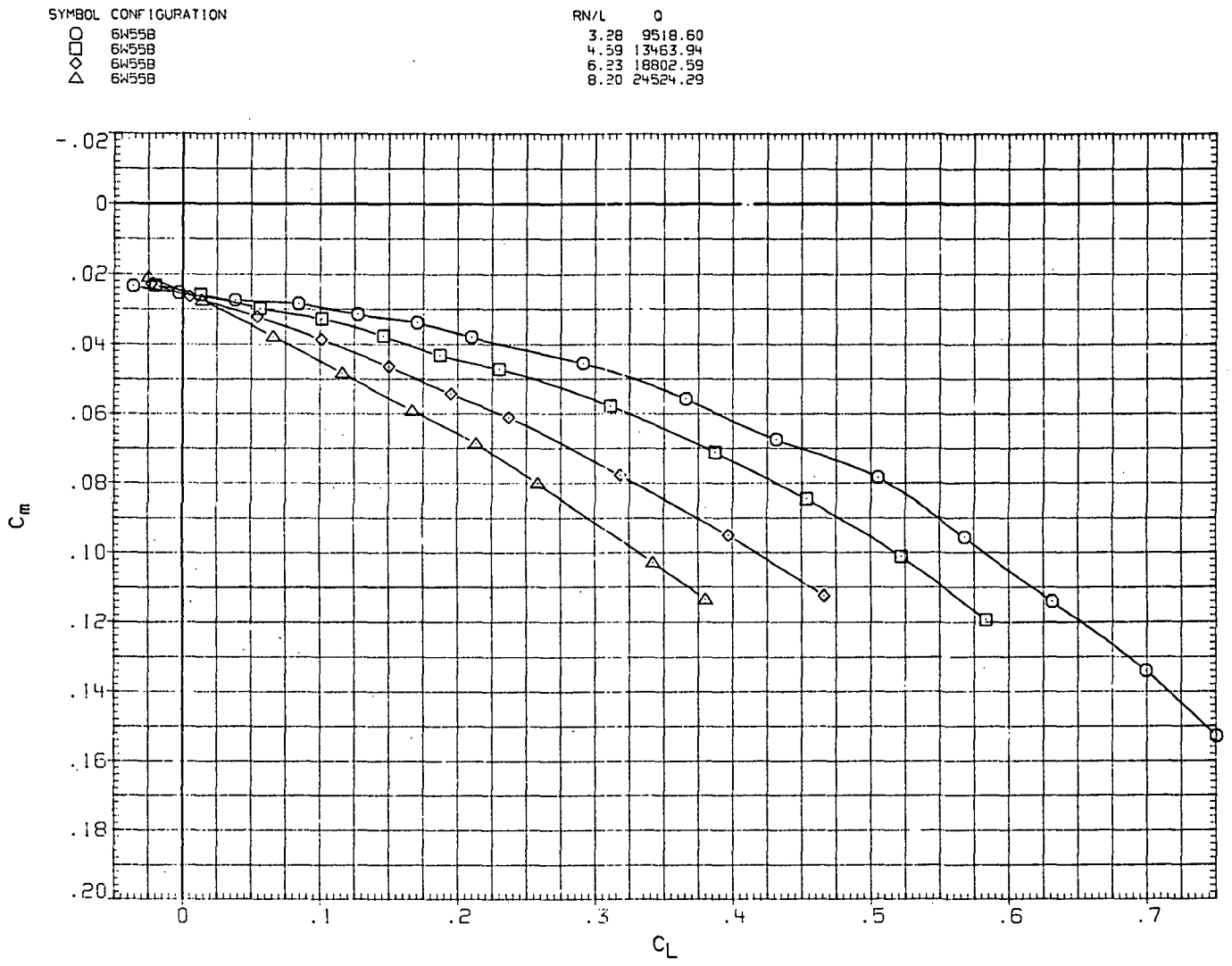


(c) $C_m$ vs $C_L$

Figure 32.– Continued.

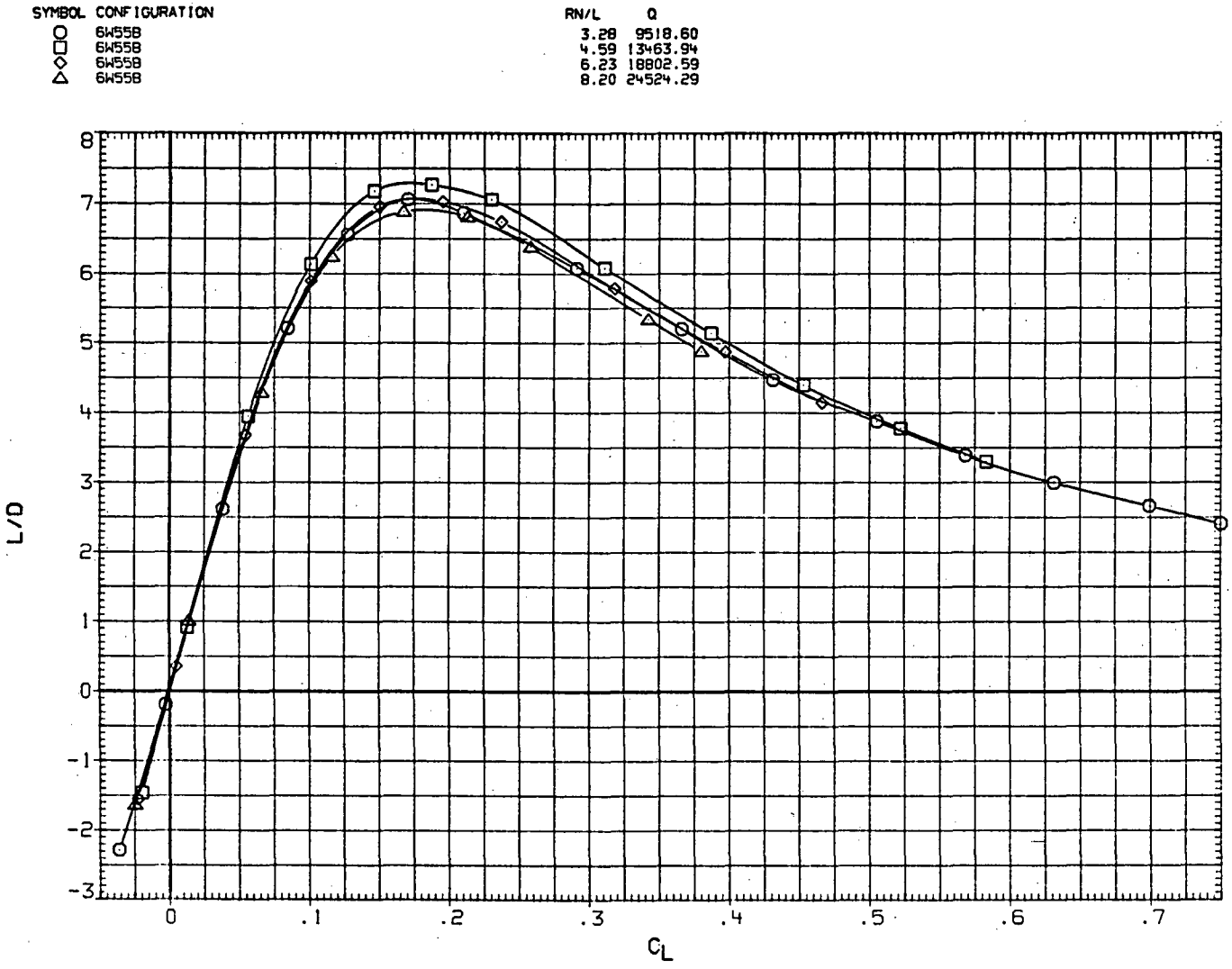


(d) $L/D$ vs $C_L$

Figure 32.– Continued.

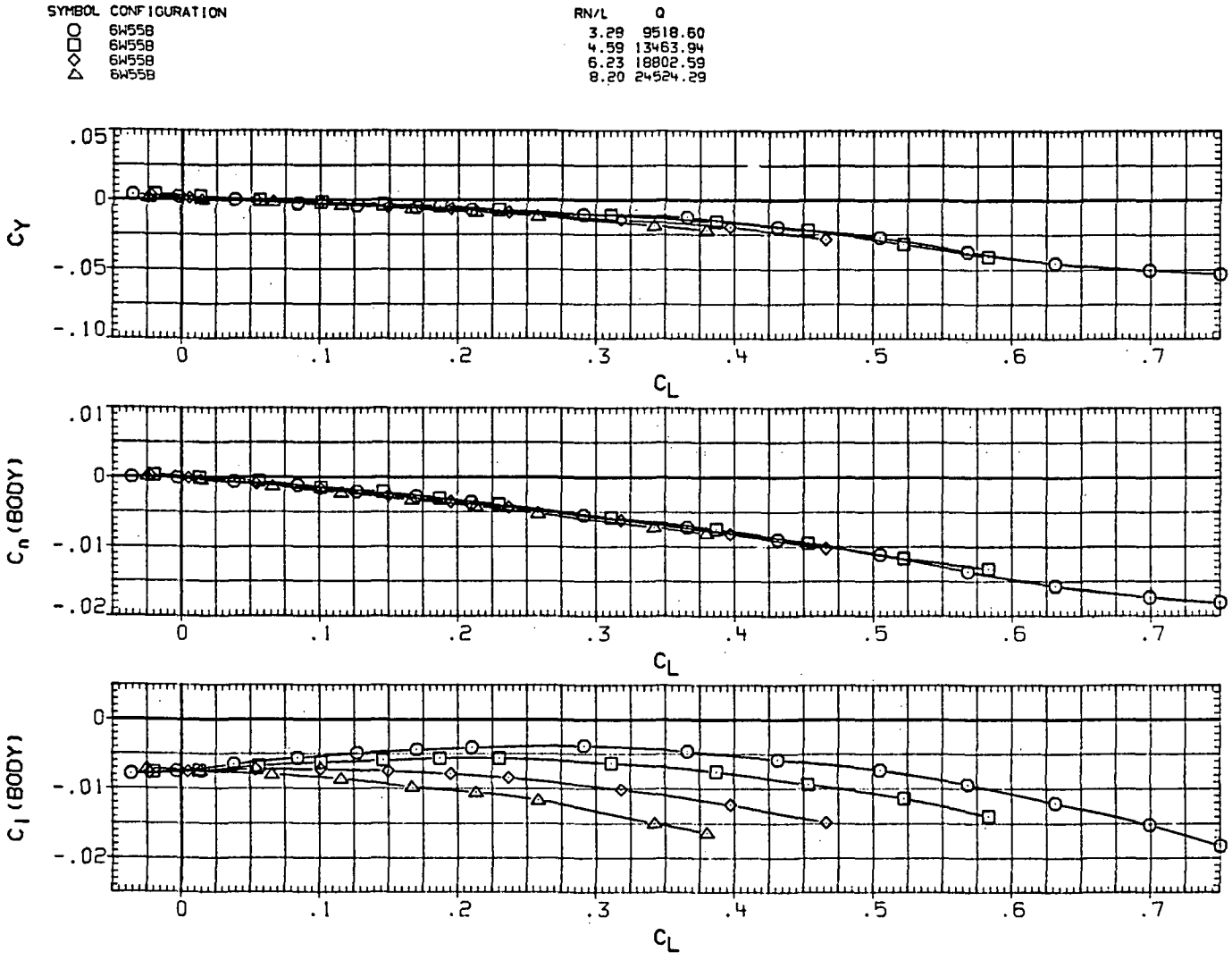


(e) $C_Y$, $C_n$, and $C_l$ vs $C_L$

Figure 32.– Concluded.

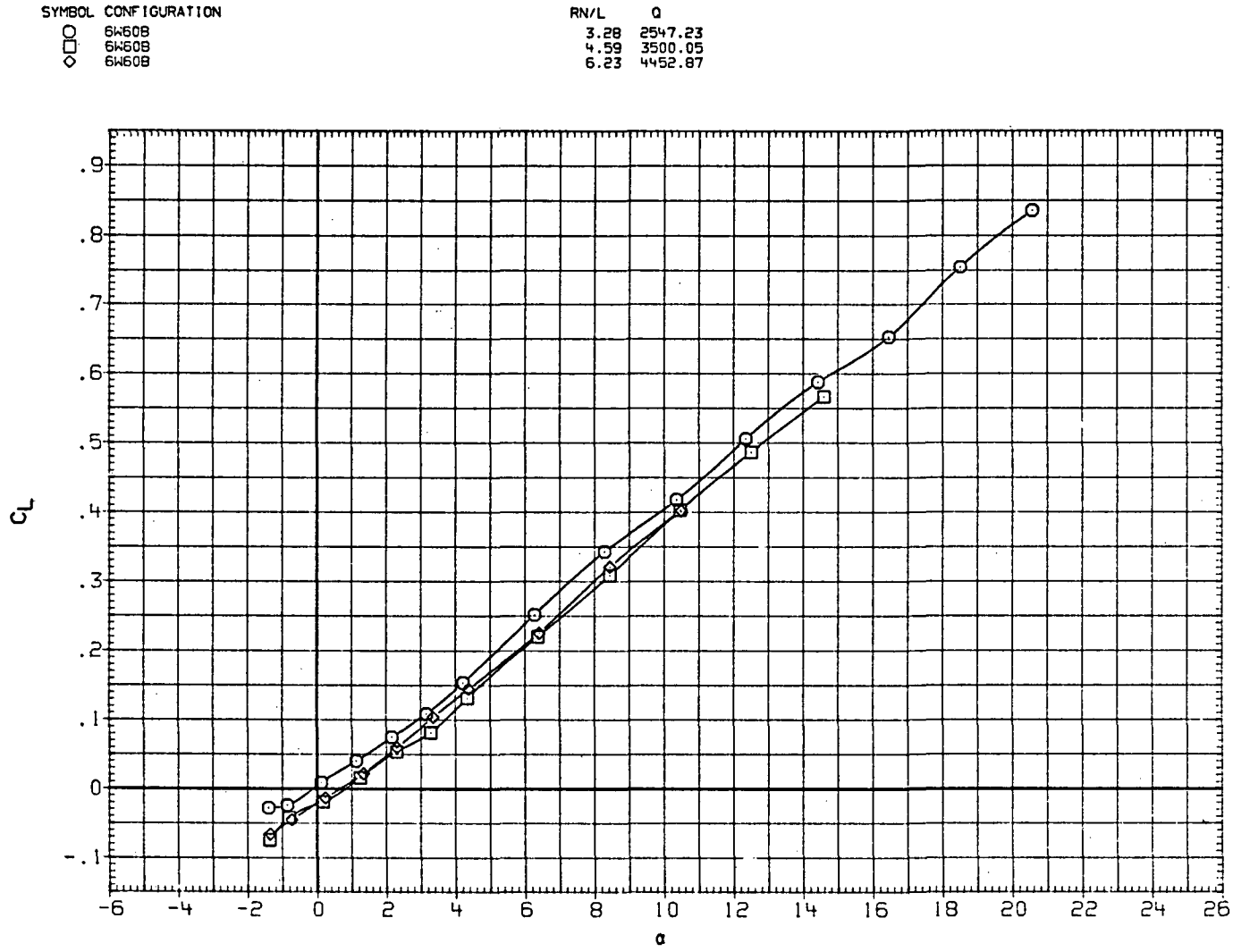


(a) $C_L$ vs $\alpha$

Figure 33.– Flexibility effects due to dynamic-pressure changes on the aerodynamic characteristics of the trapezoidal oblique wing: $\Lambda = 60°, M = 0.25$.

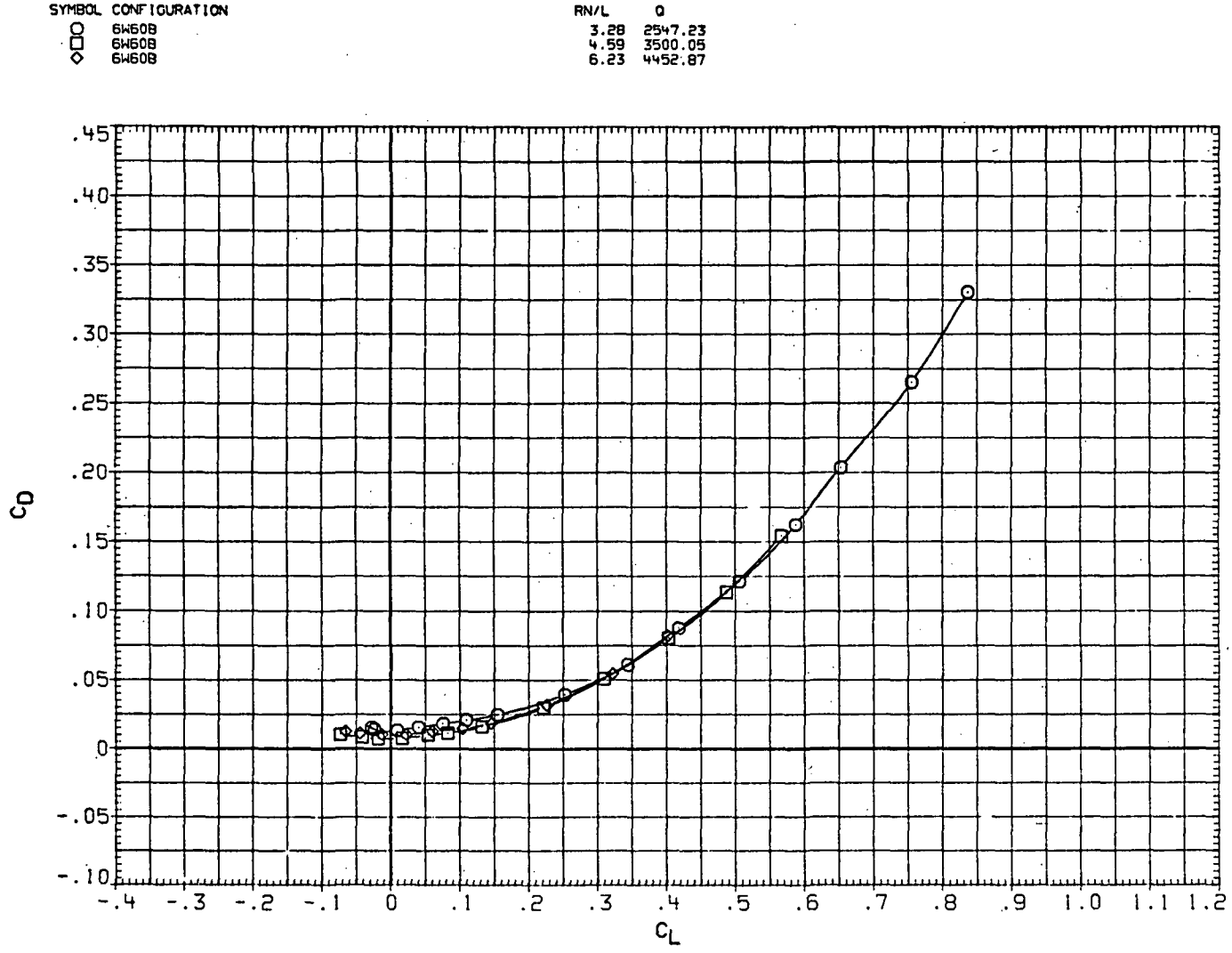


(b) $C_D$ vs $C_L$

Figure 33.– Continued.

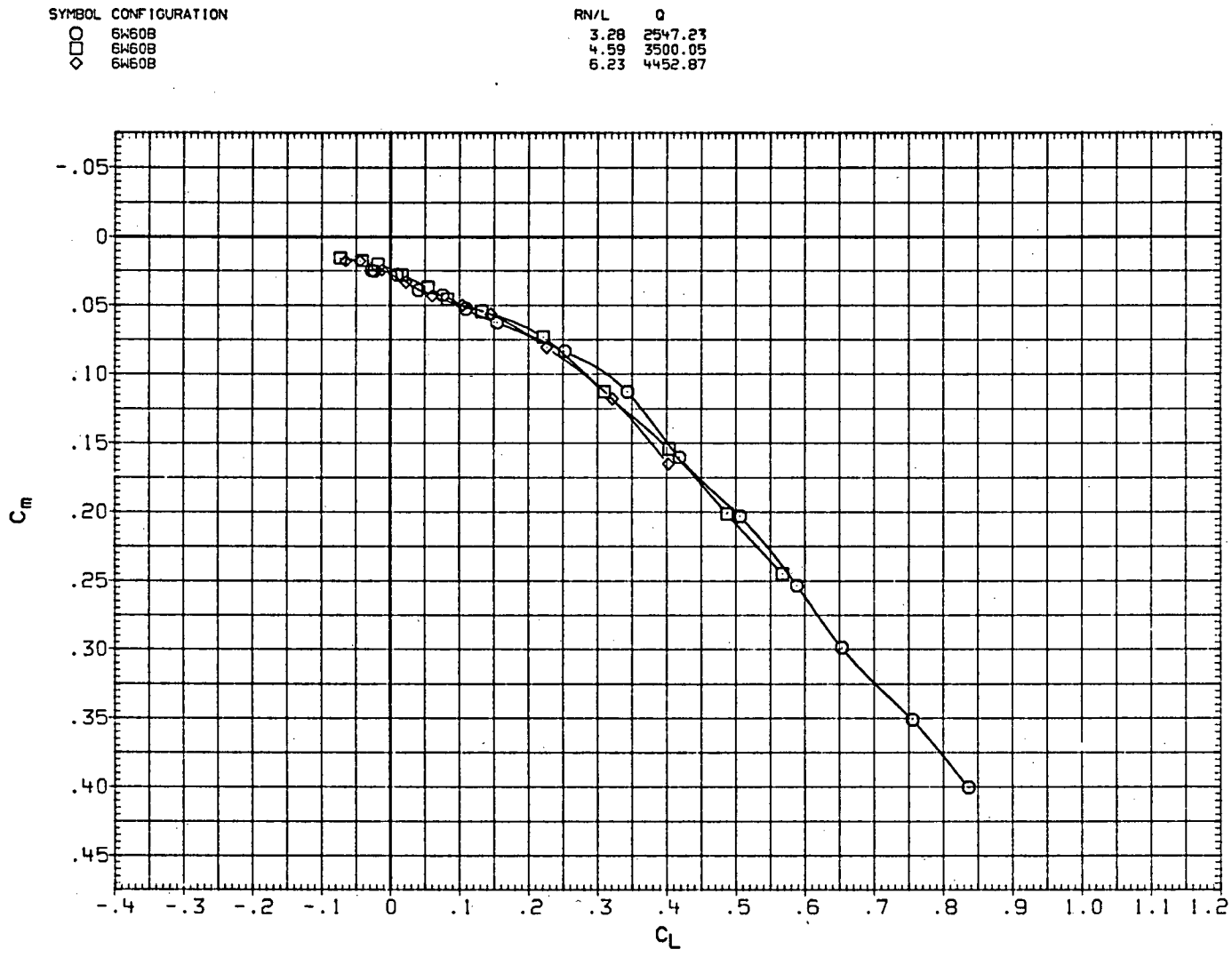


(c) $C_m$ vs $C_L$

Figure 33.– Continued.


(d) $L/D$ vs $C_L$

Figure 33.– Continued.

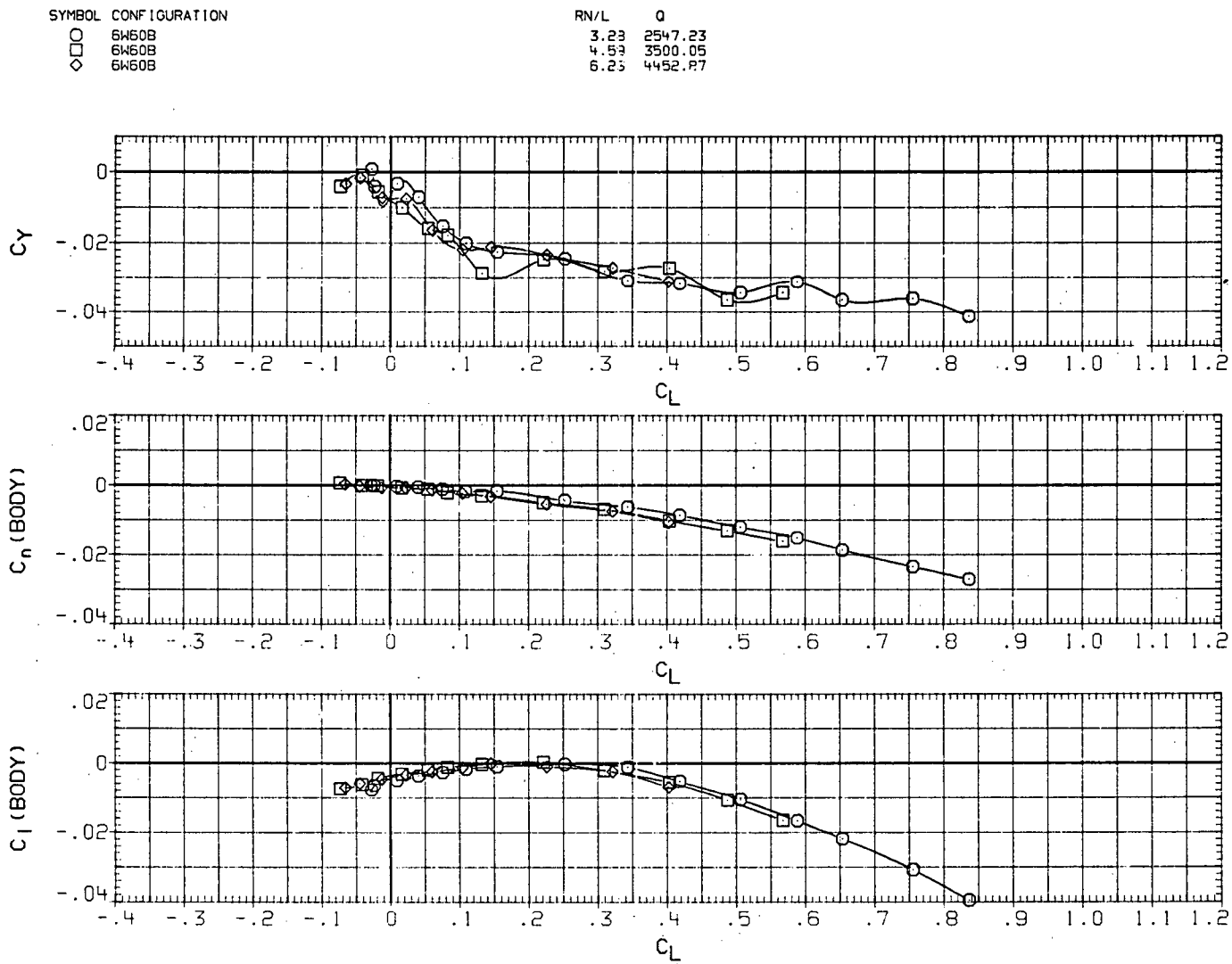


(e) $C_Y$, $C_n$, and $C_l$ vs $C_L$

Figure 33.– Concluded.

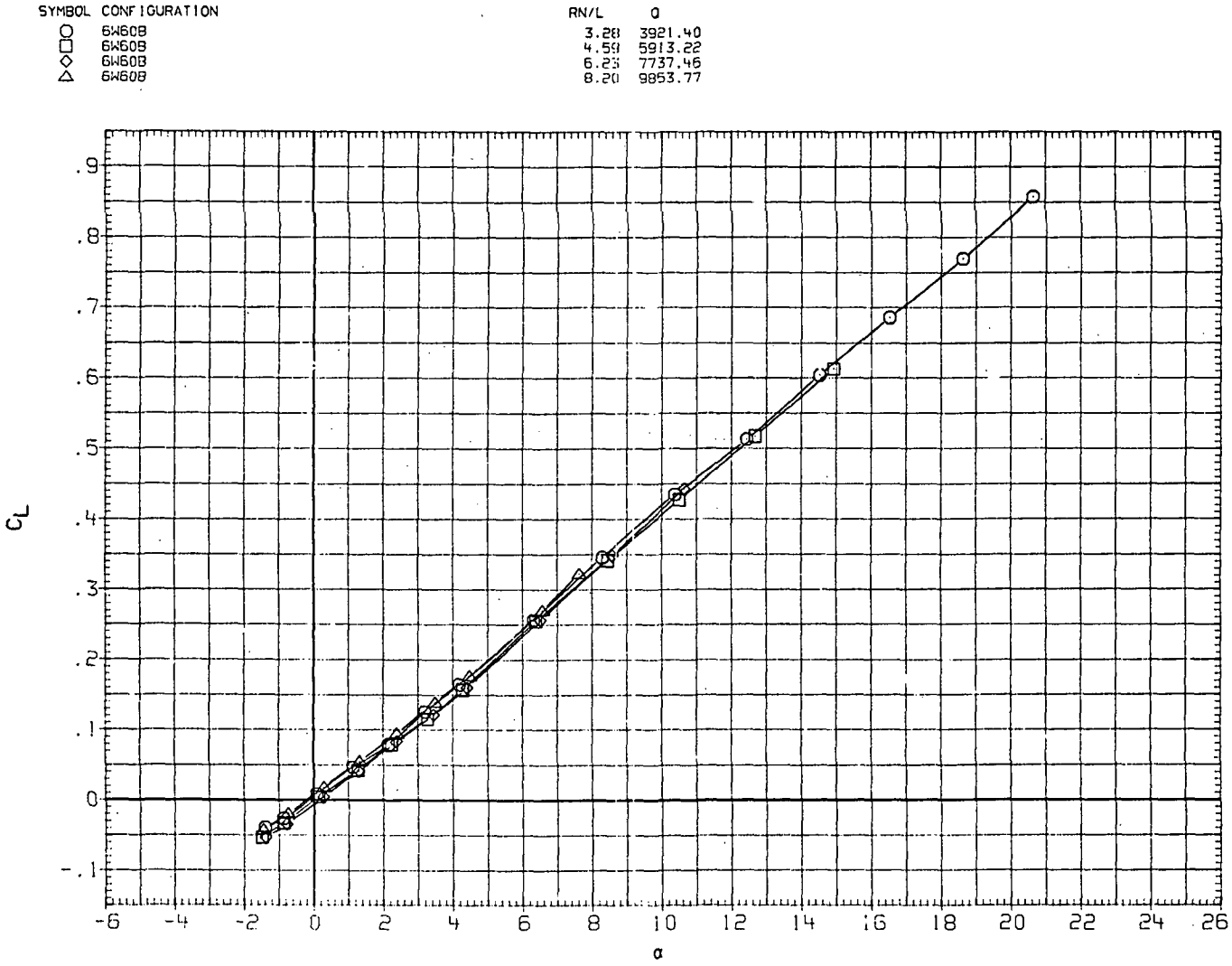


(a) $C_L$ vs $\alpha$

Figure 34.– Flexibility effects due to dynamic-pressure changes on the aerodynamic characteristics of the trapezoidal oblique wing: $\Lambda = 60°$, $M = 0.4$.

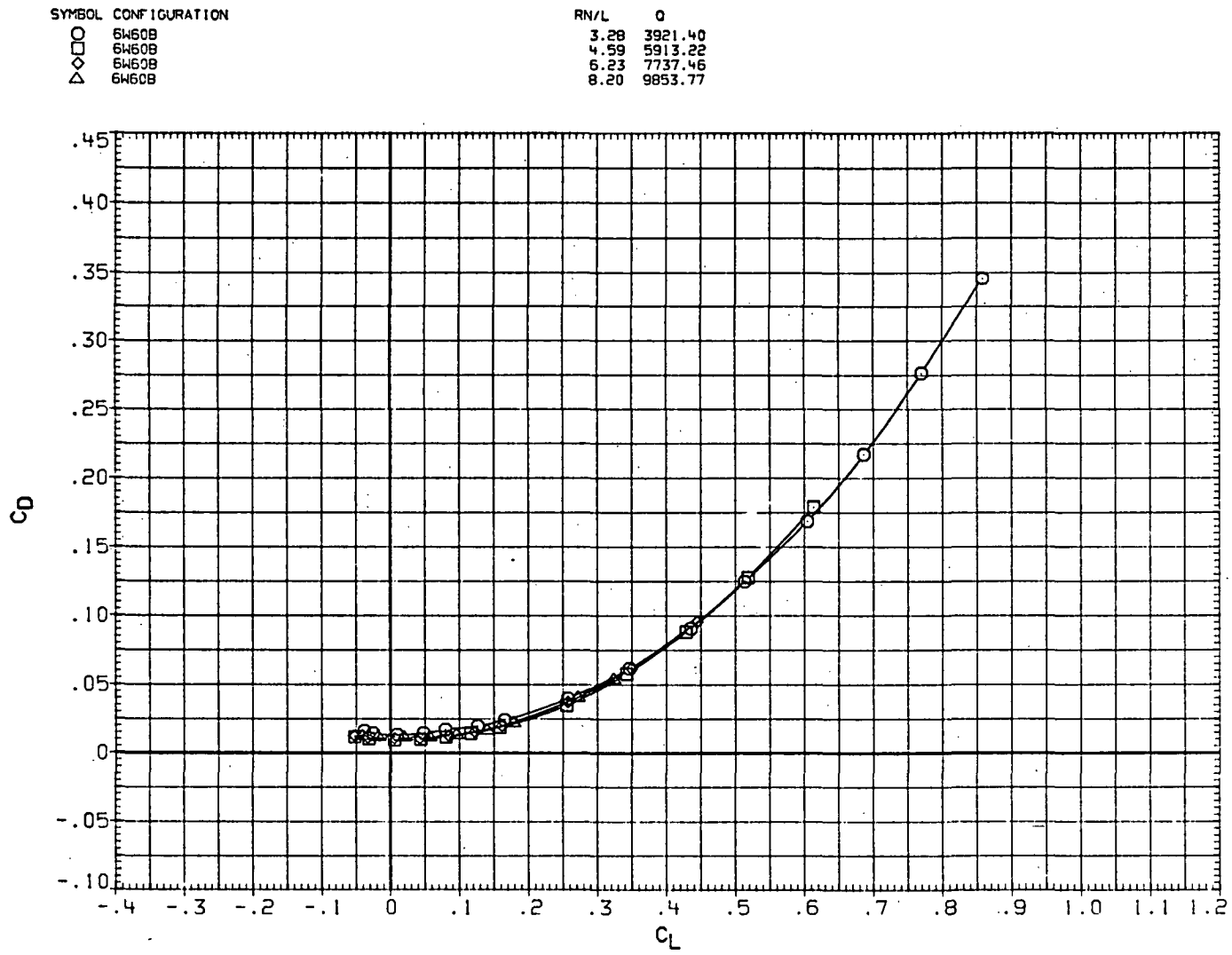


(b) $C_D$ vs $C_L$

Figure 34.– Continued.

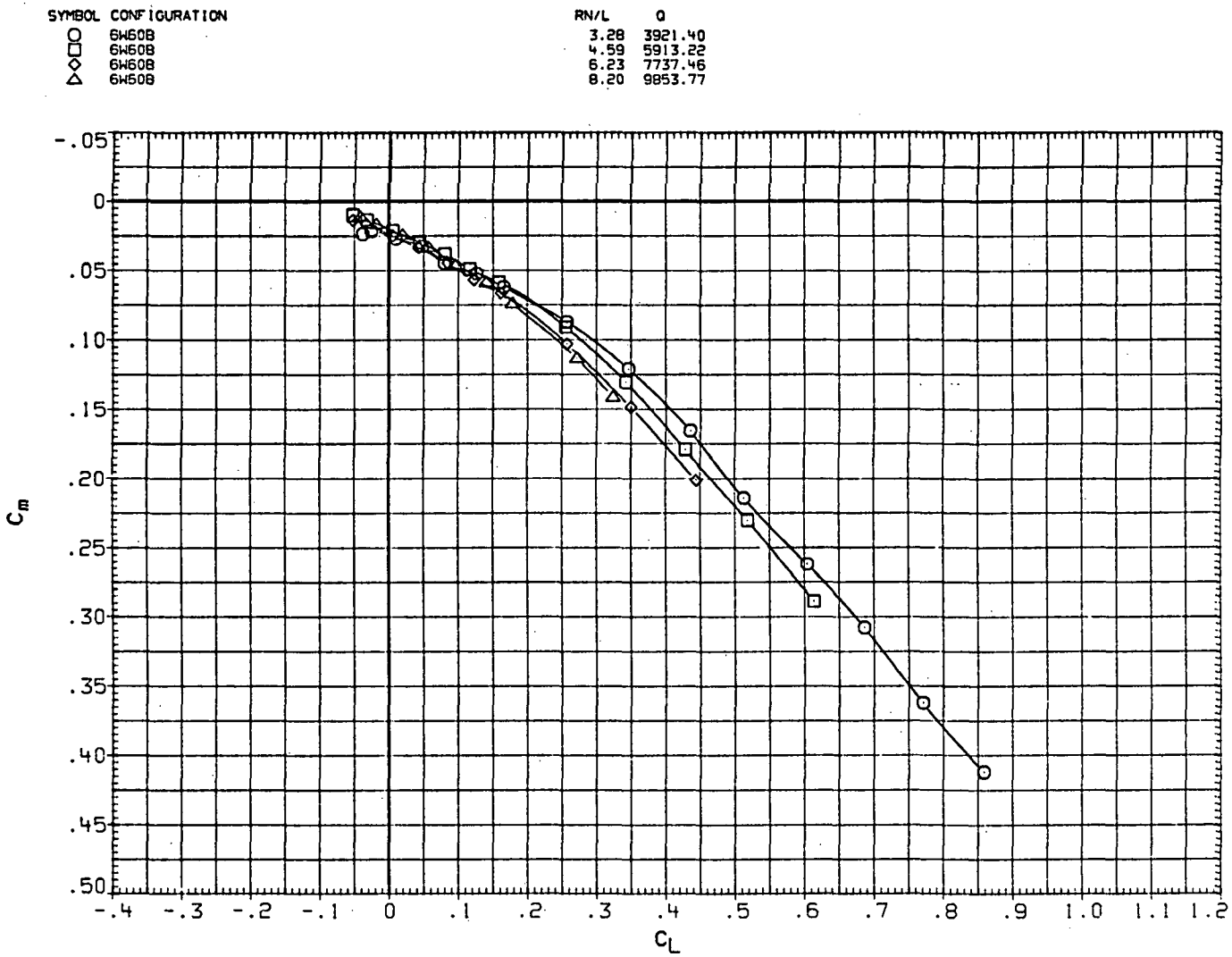


(c) $C_m$ vs $C_L$

Figure 34.– Continued.

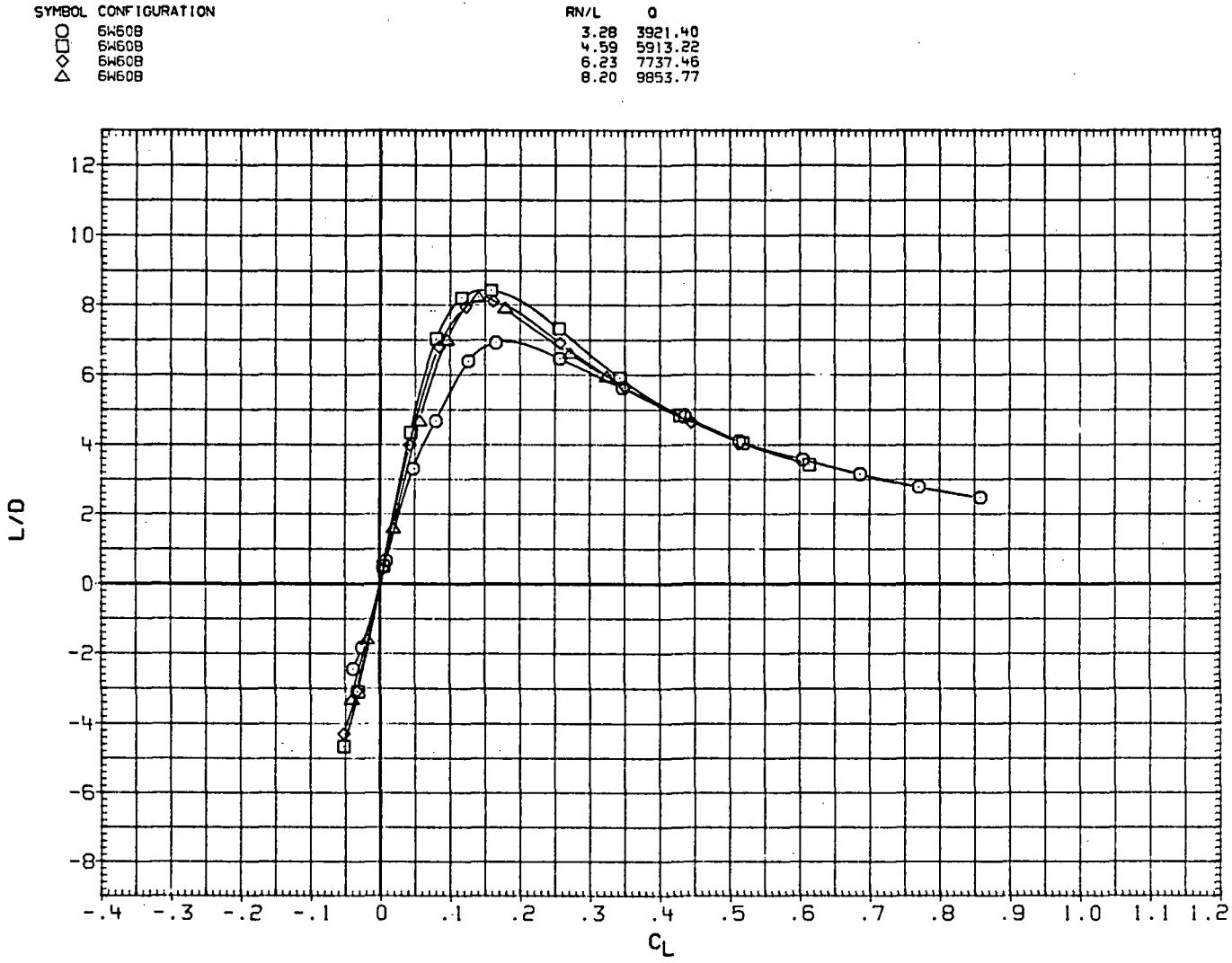


(d) $L/D$ vs $C_L$

Figure 34.– Continued.

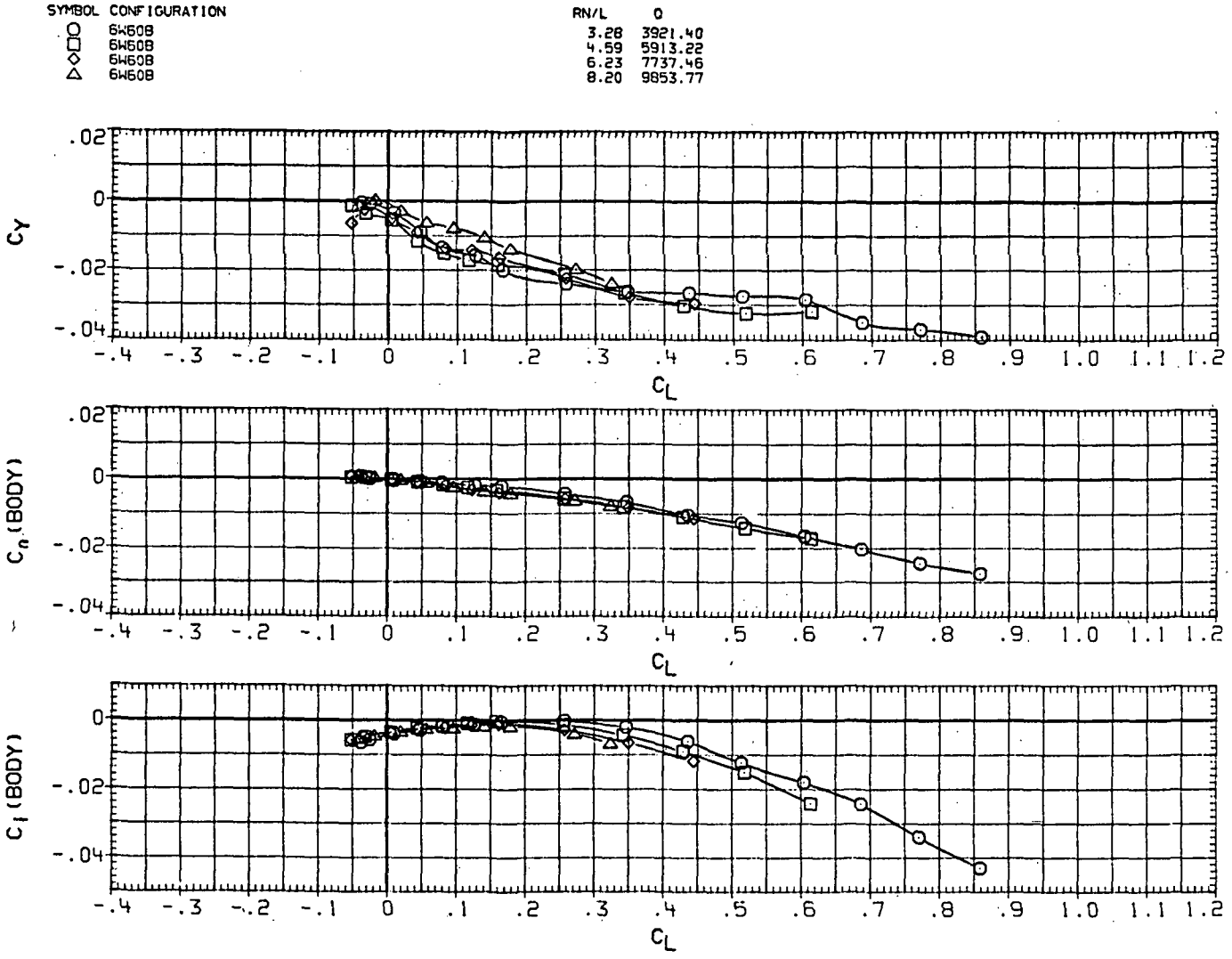


(e) $C_Y$, $C_n$, and $C_l$ vs $C_L$

Figure 34.– Concluded.

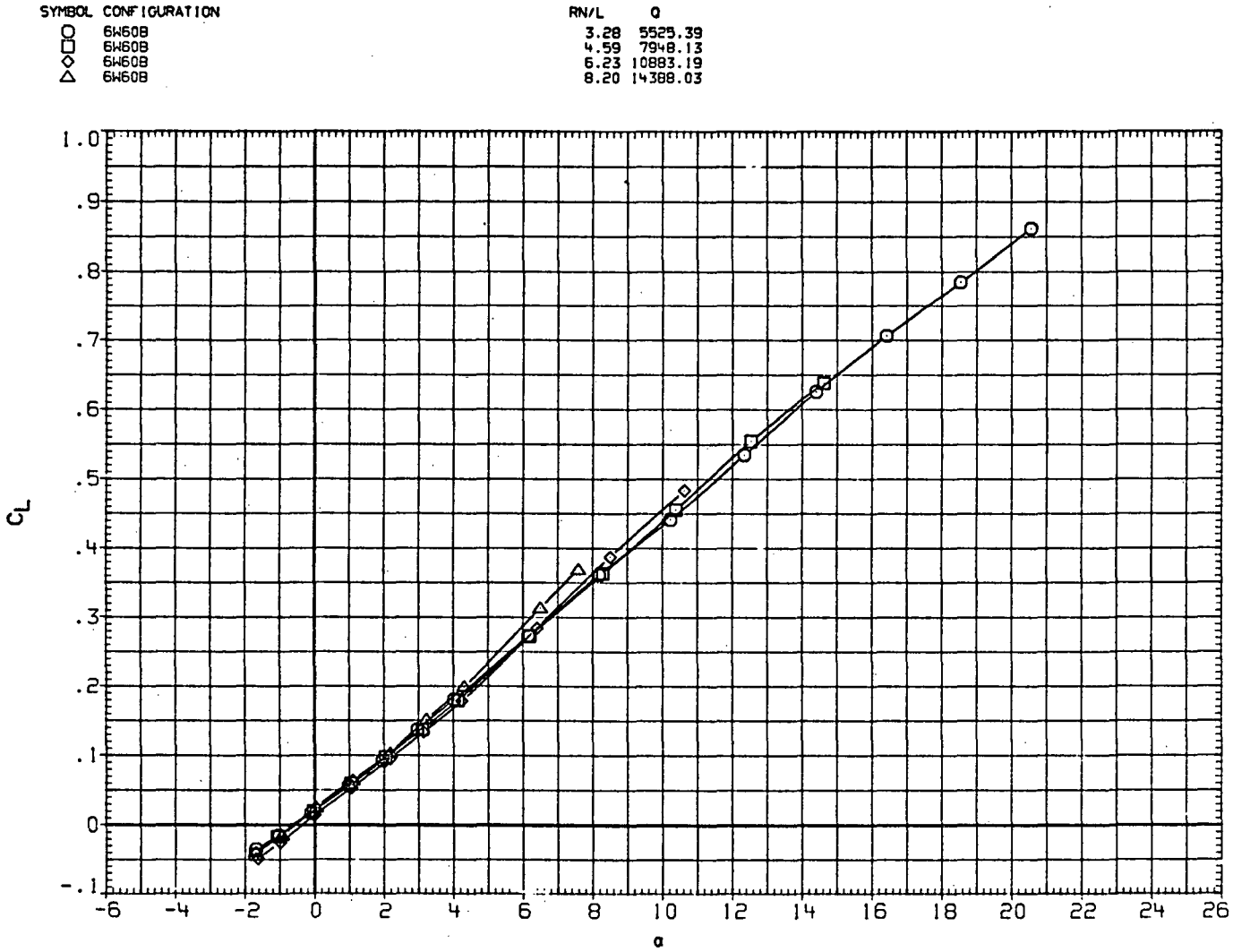


(a) $C_L$ vs $\alpha$

Figure 35.– Flexibility effects due to dynamic-pressure changes on the aerodynamic characteristics of the trapezoidal oblique wing: $\Lambda = 60°, M = 0.6$.

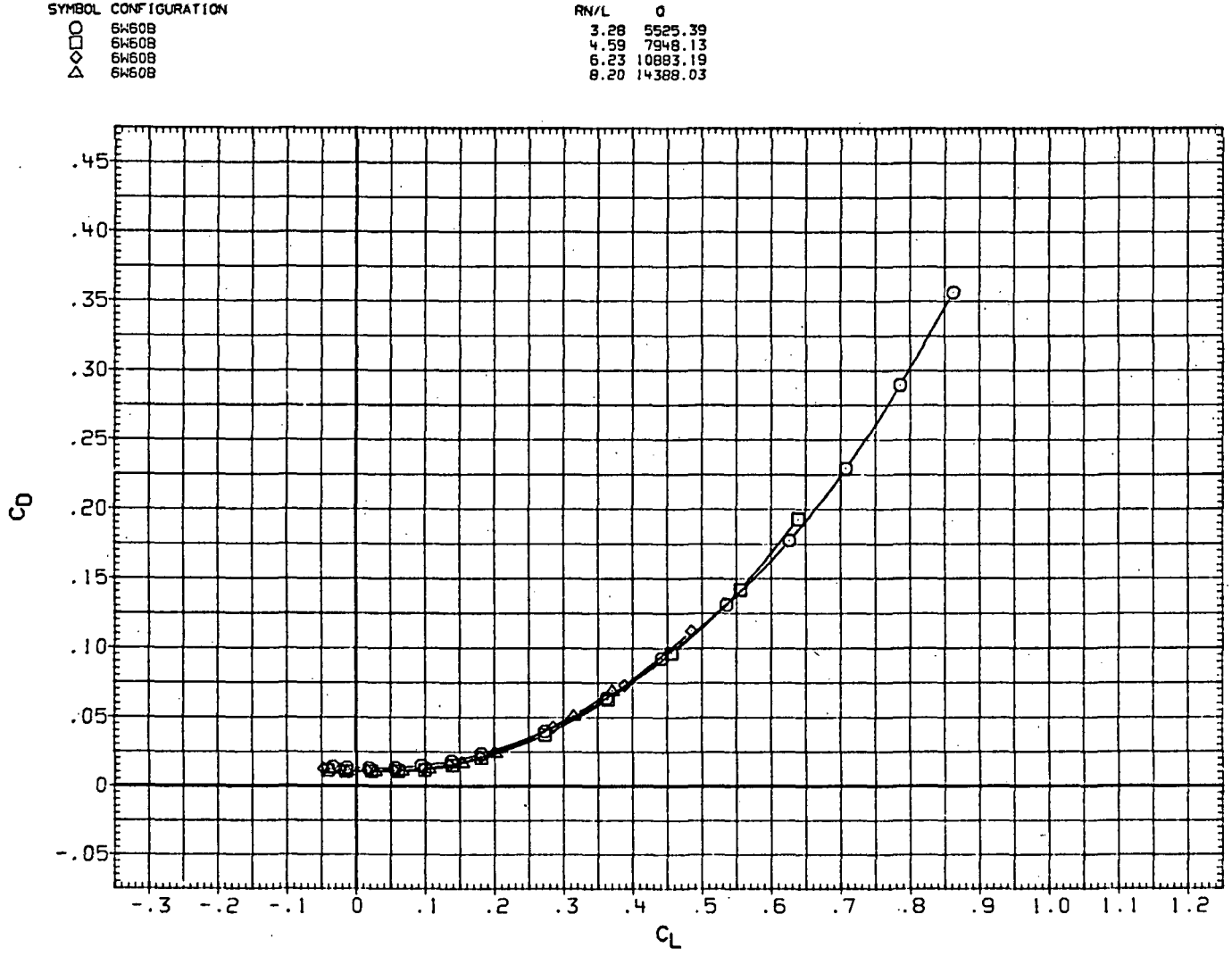


(b) $C_D$ vs $C_L$

Figure 35.– Continued.

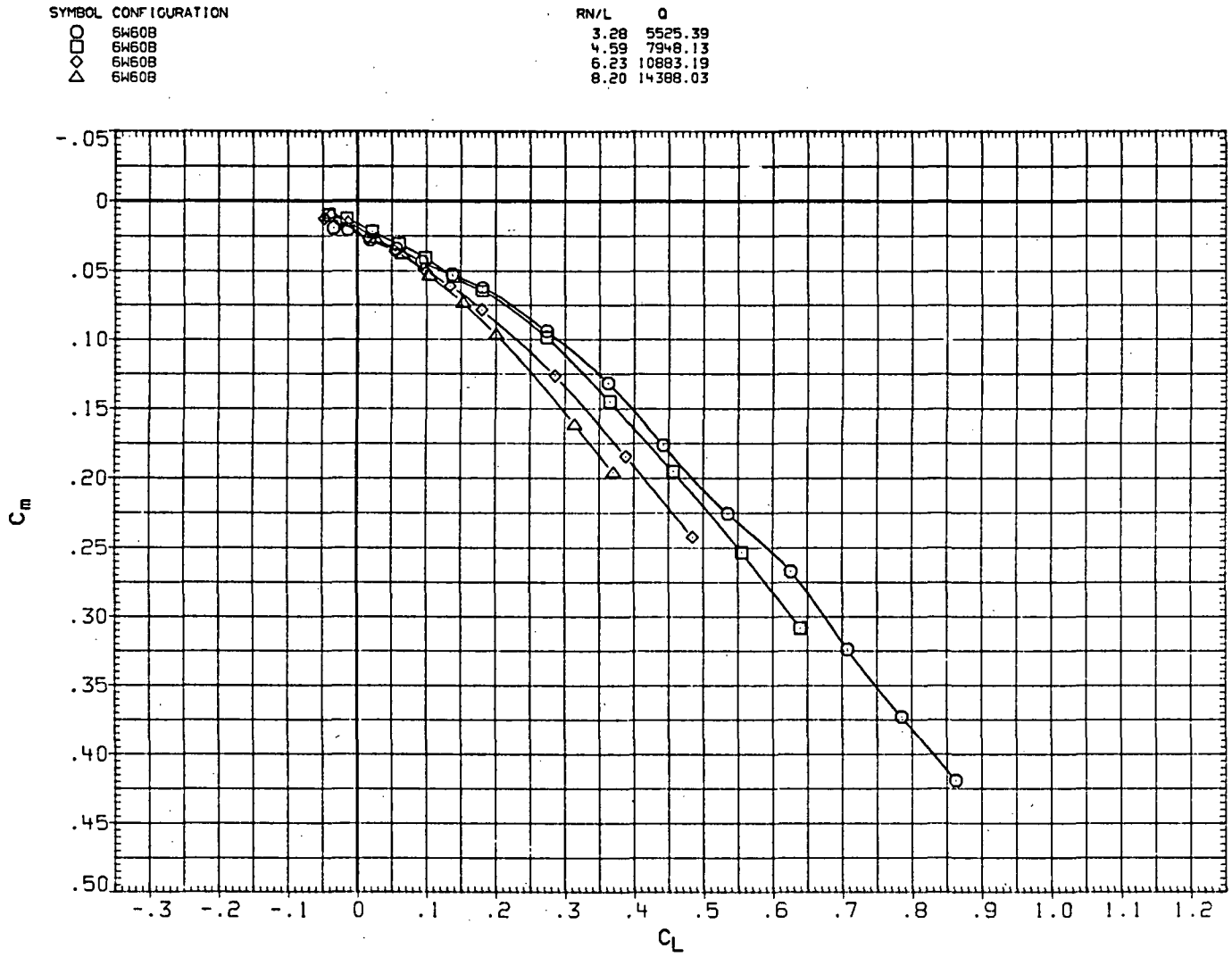


(c) $C_m$ vs $C_L$

Figure 35.– Continued.

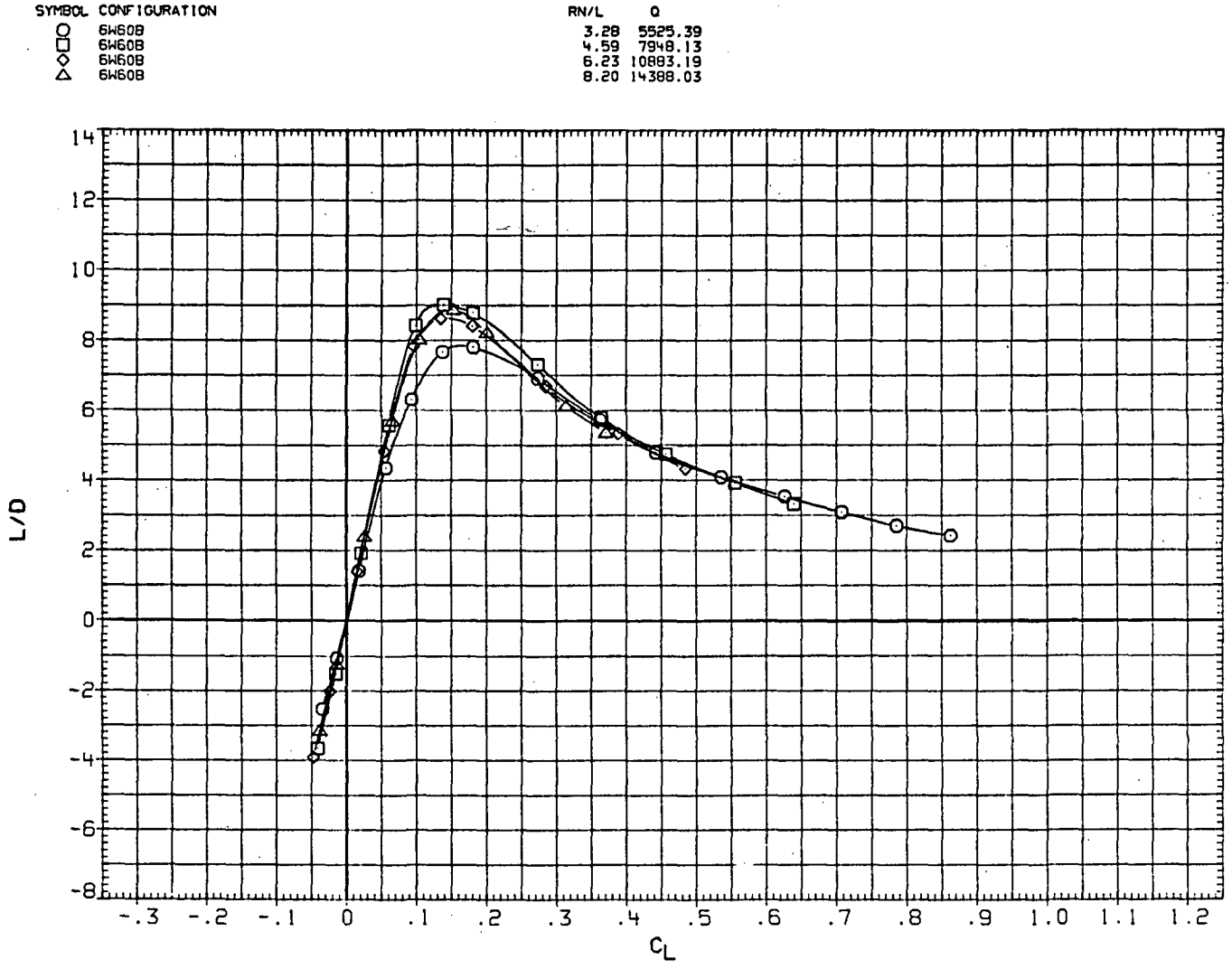


(d) $L/D$ vs $C_L$

Figure 35.– Continued.

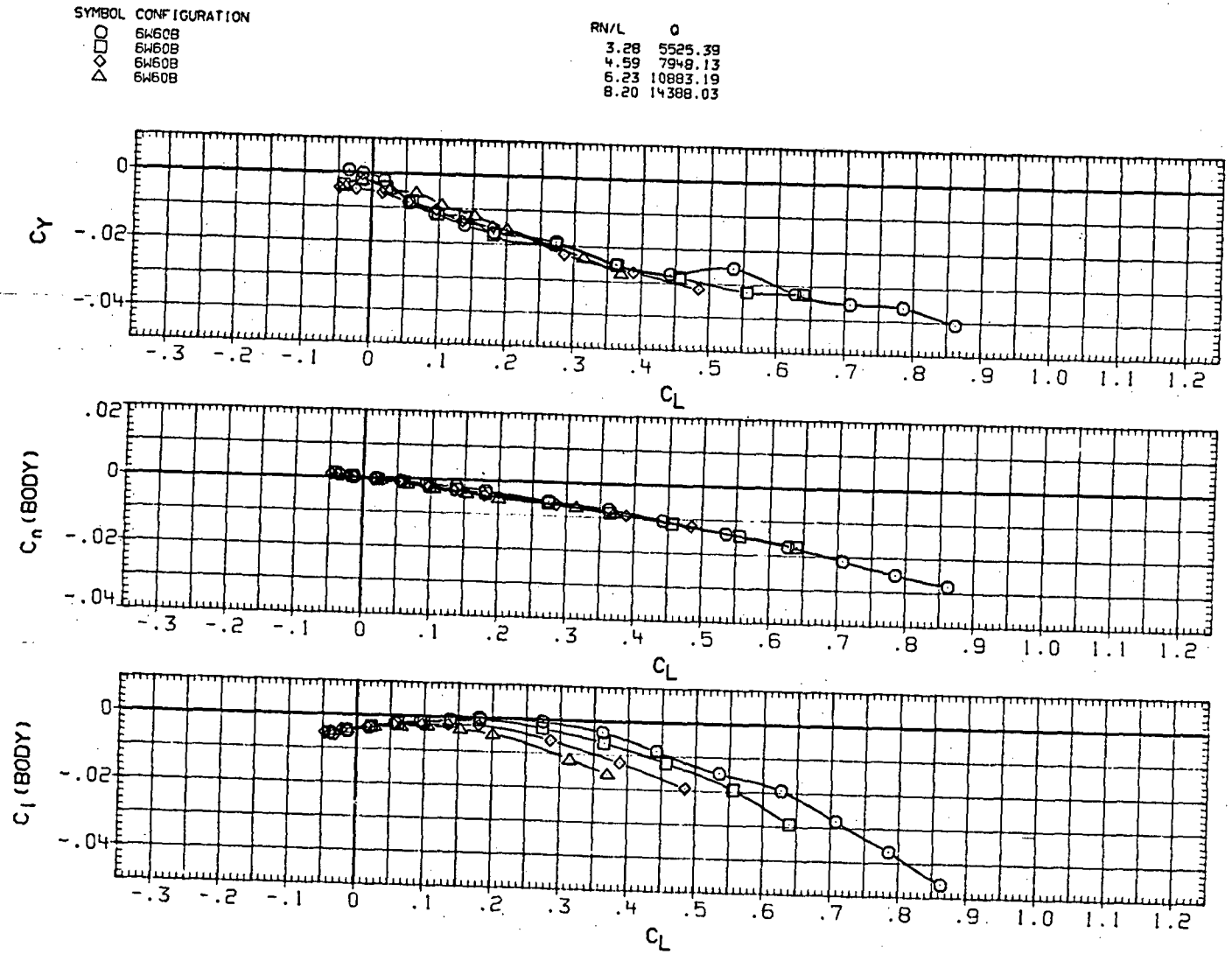


(e) $C_Y$, $C_n$, and $C_l$ vs $C_L$

Figure 35.– Concluded.

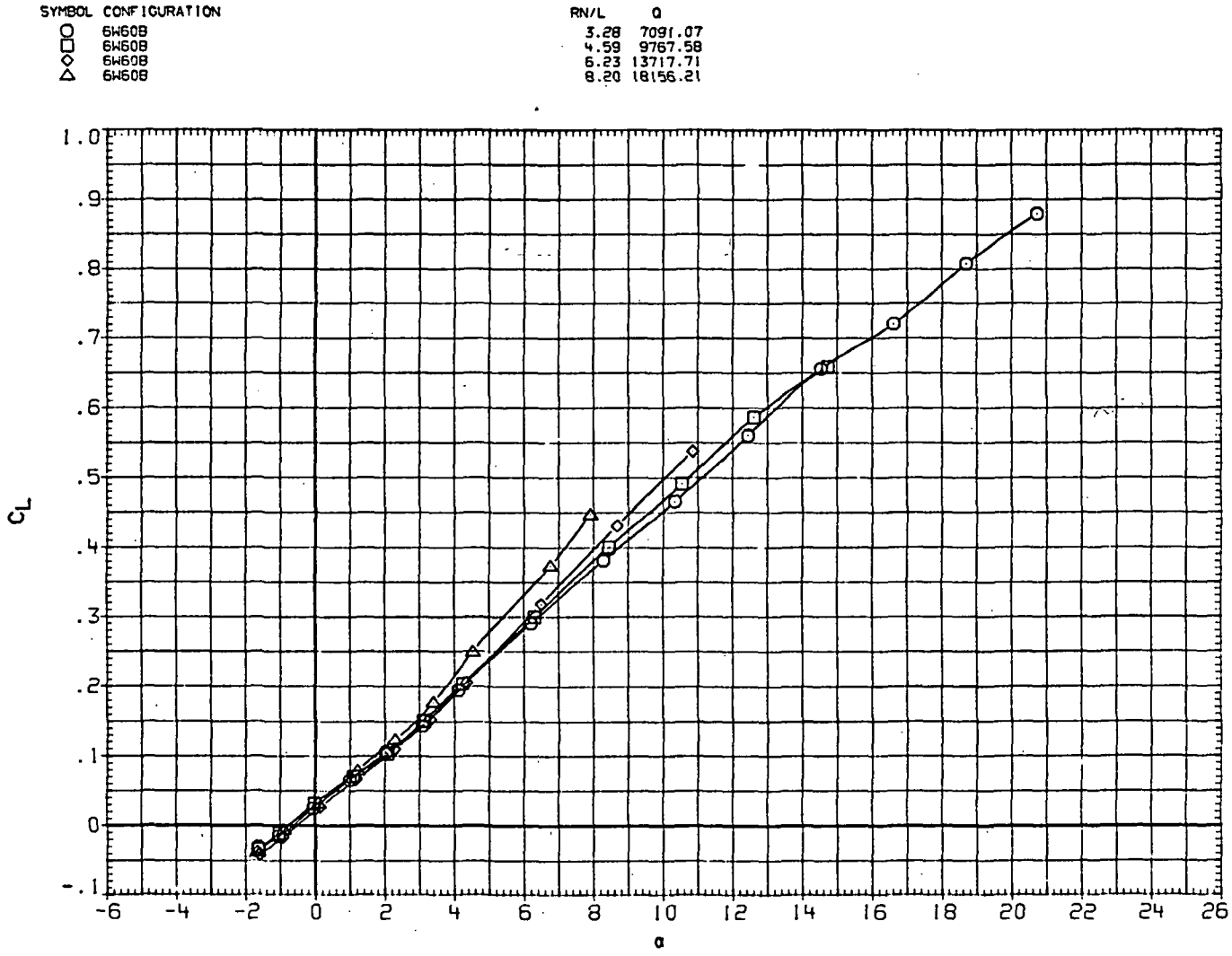


(a) $C_L$ vs $\alpha$

Figure 36.– Flexibility effects due to dynamic-pressure changes on the aerodynamic characteristics of the trapezoidal oblique wing: $\Lambda = 60°, M = 0.8$.

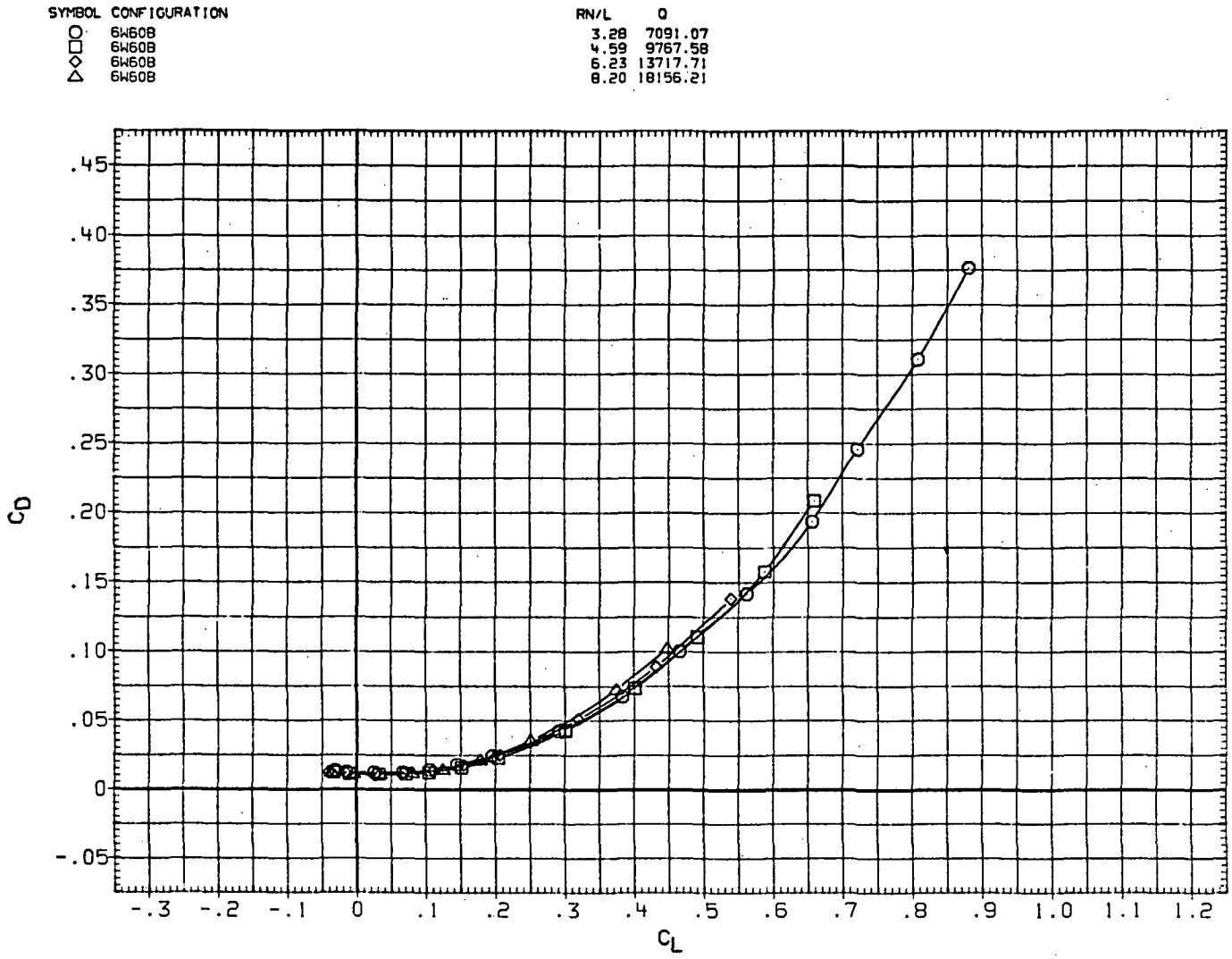


(b) $C_D$ vs $C_L$

Figure 36.– Continued.

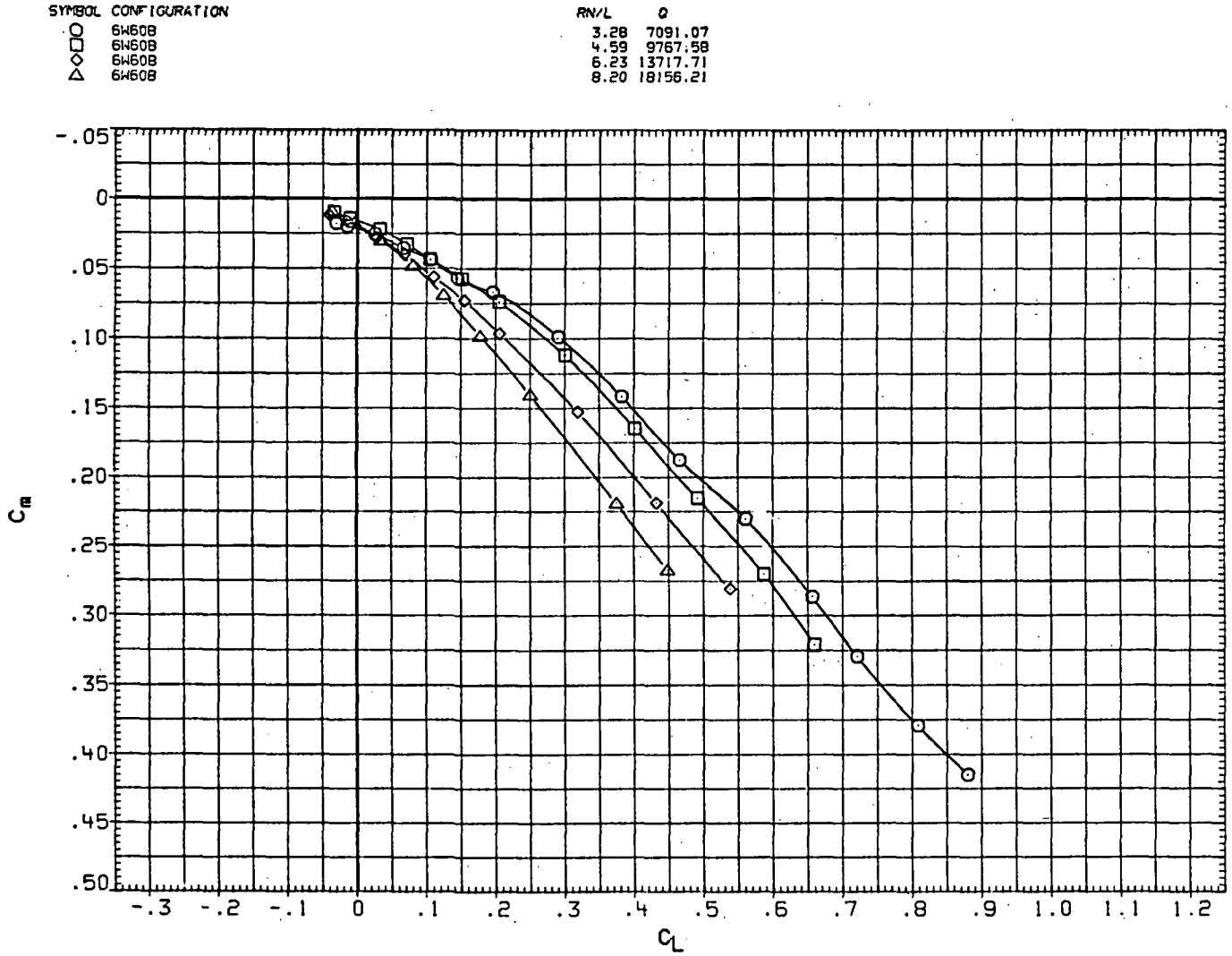


(c) $C_m$ vs $C_L$

Figure 36.– Continued.


(d) $L/D$ vs $C_L$

Figure 36.– Continued.

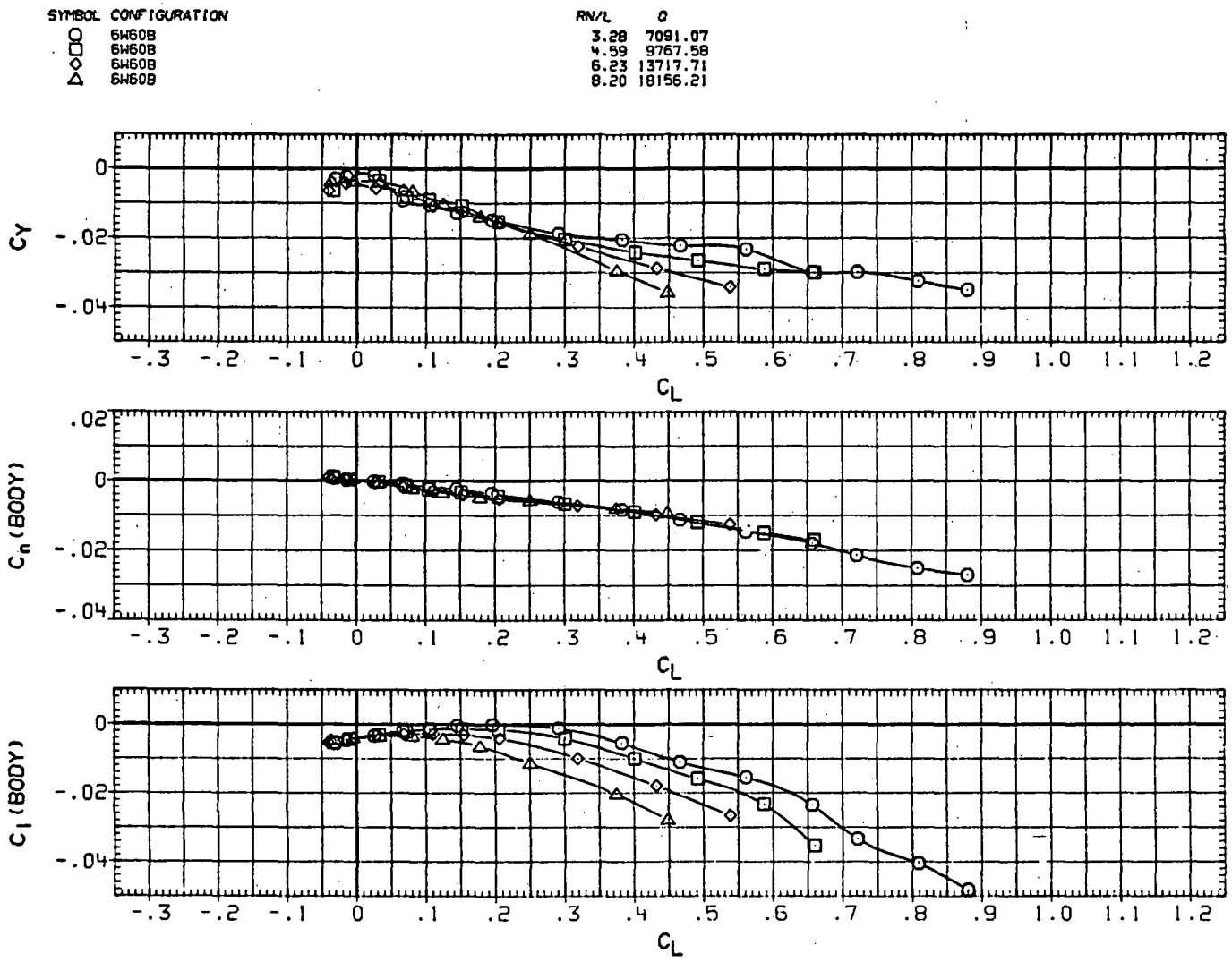


(e) $C_Y$, $C_n$, and $C_l$ vs $C_L$

Figure 36.– Concluded.

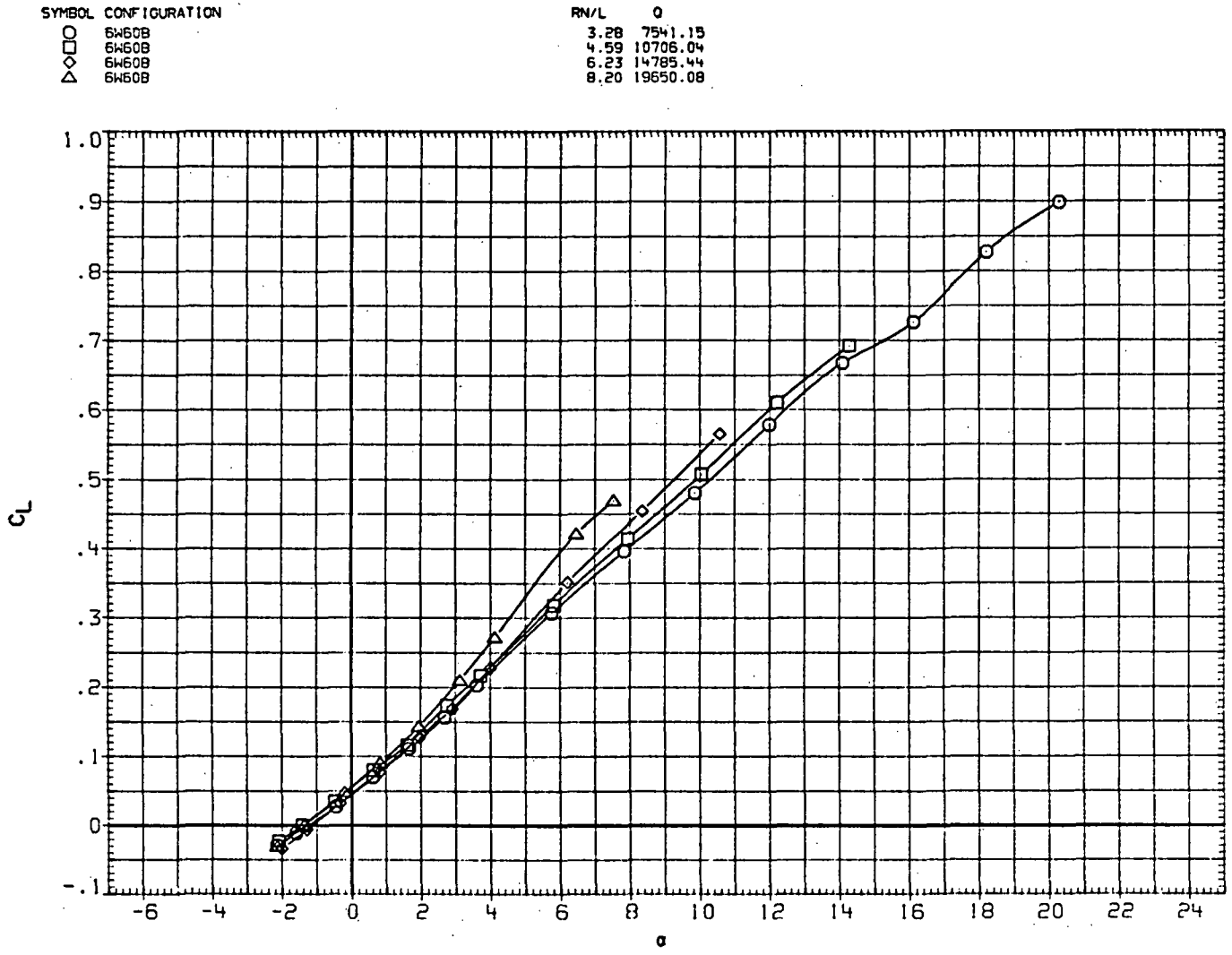


(a) $C_L$ vs $\alpha$

Figure 37.– Flexibility effects due to dynamic-pressure changes on the aerodynamic characteristics of the trapezoidal oblique wing: $\Lambda = 60°, M = 0.9$.

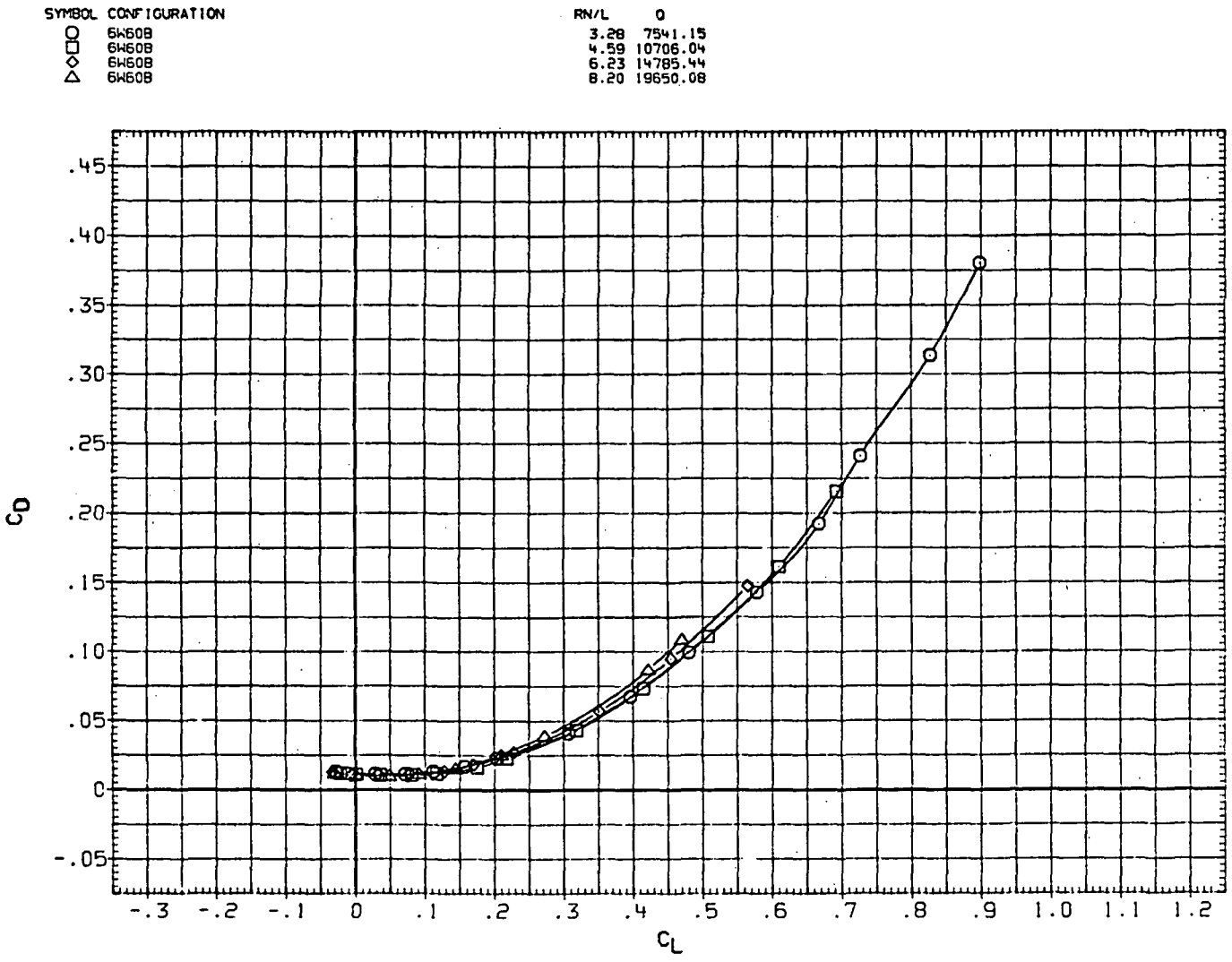


(b) $C_D$ vs $C_L$

Figure 37.– Continued.

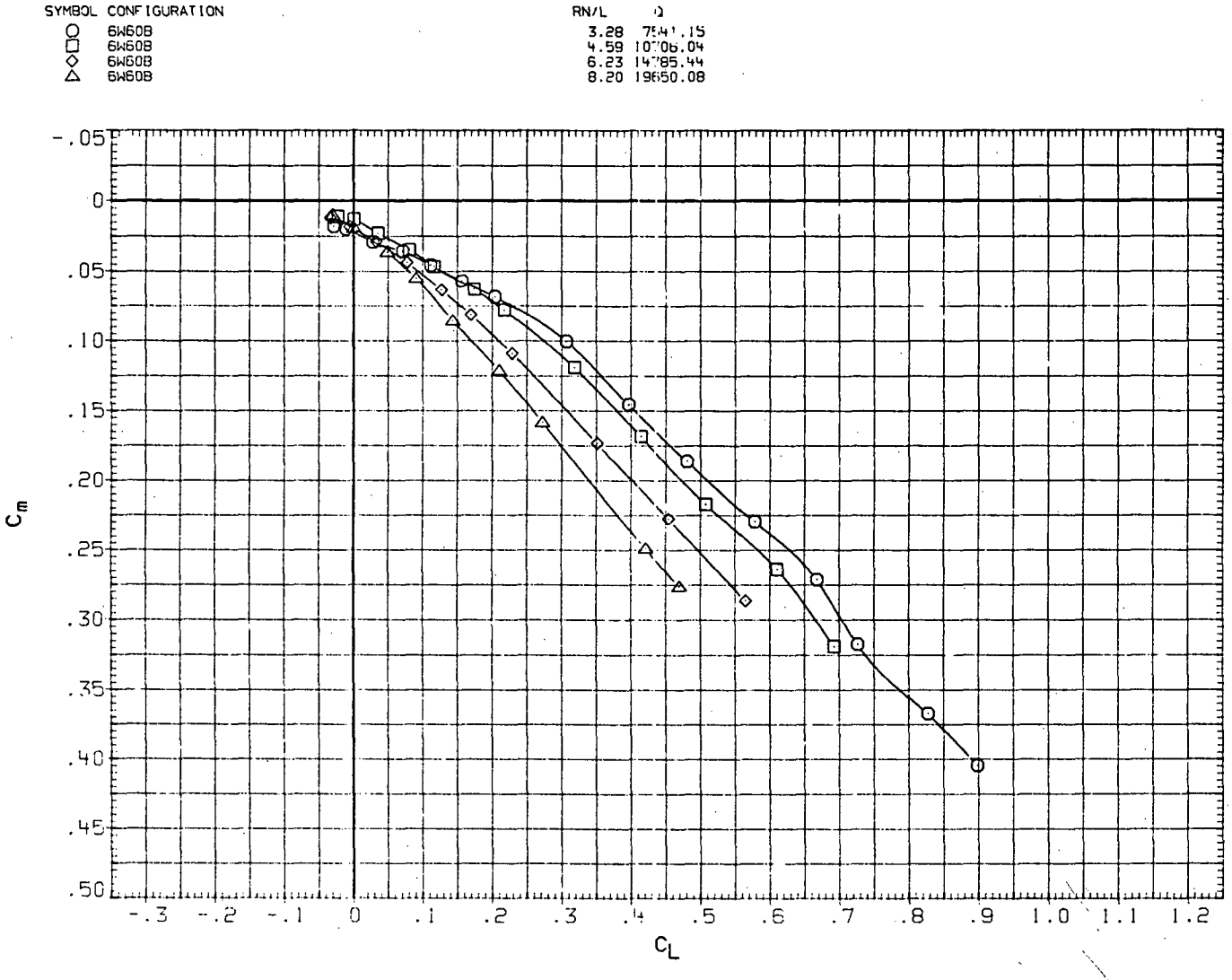


(c) $C_m$ vs $C_L$

Figure 37.– Continued.

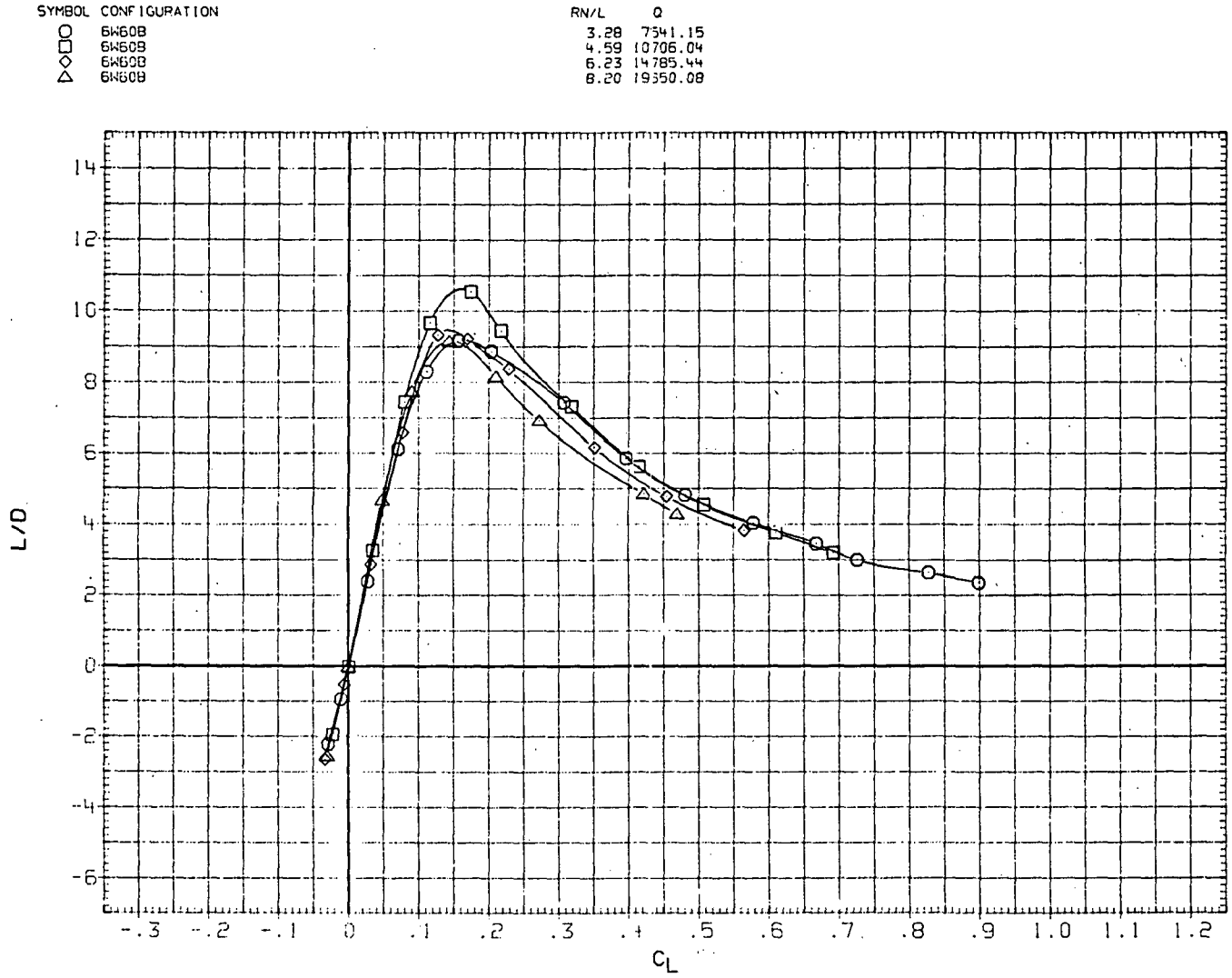


(d) $L/D$ vs $C_L$

Figure 37.– Continued.

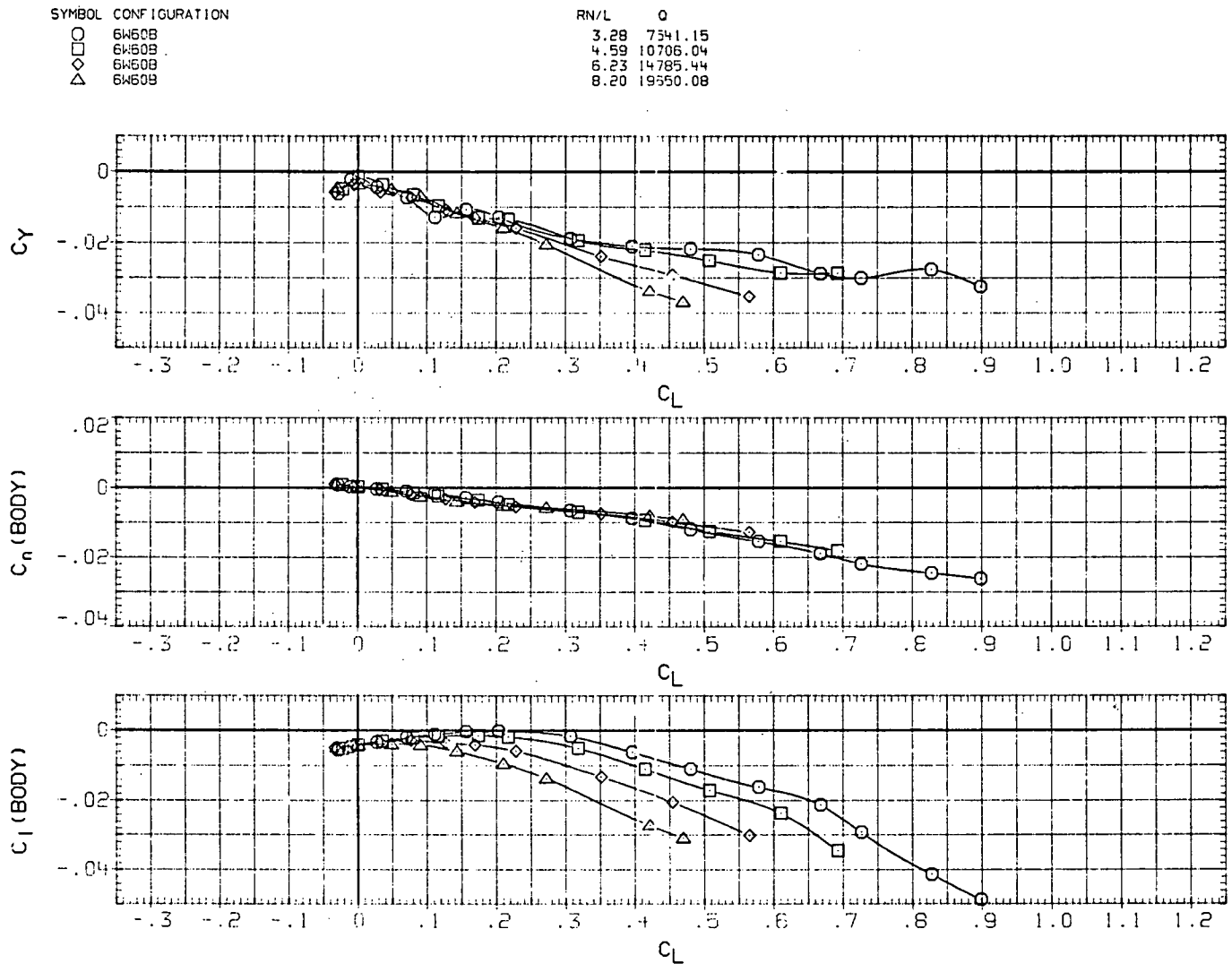


(e) $C_Y$, $C_n$, and $C_l$ vs $C_L$

Figure 37.– Concluded.

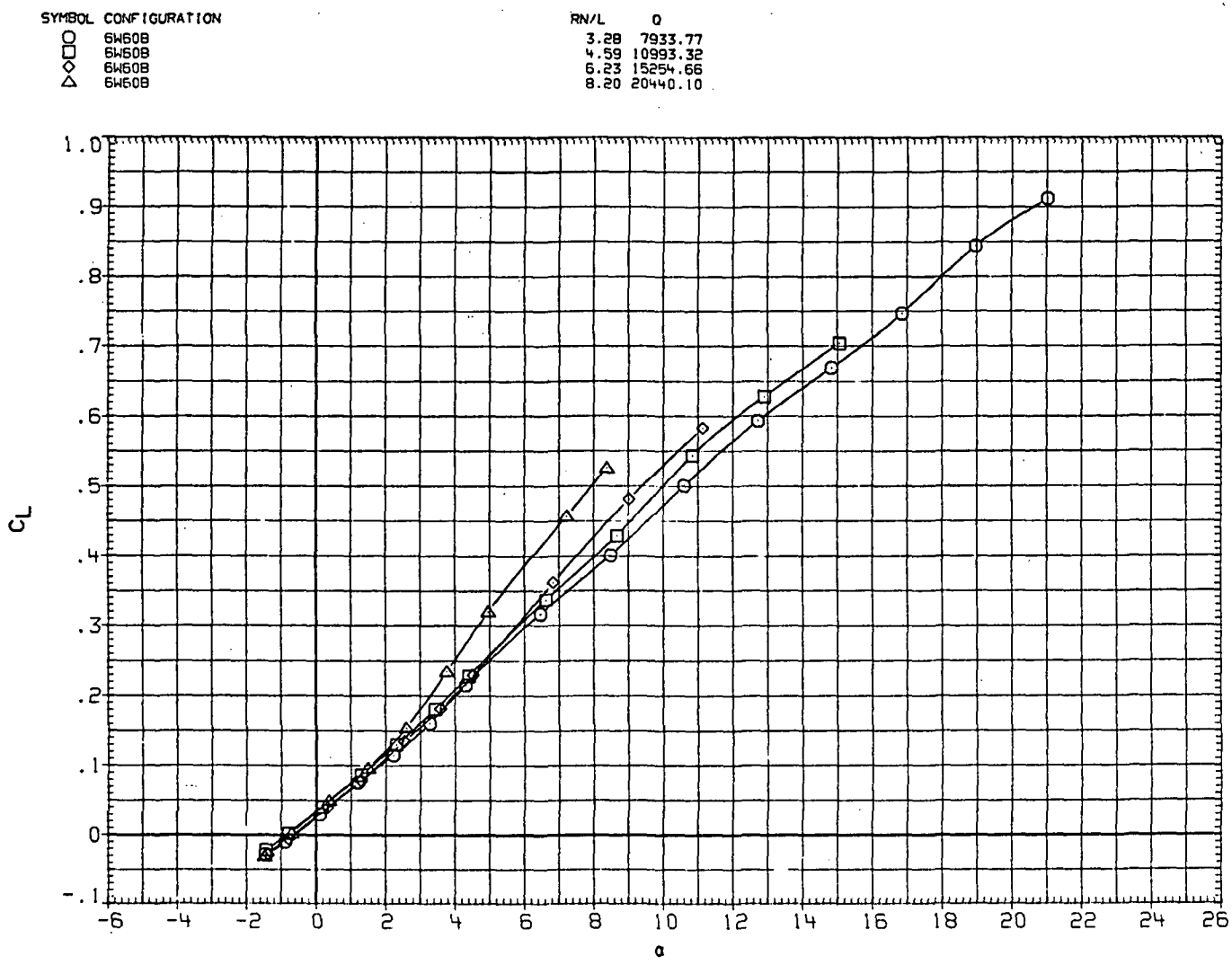


(a) $C_L$ vs $\alpha$

Figure 38.– Flexibility effects due to dynamic-pressure changes on the aerodynamic characteristics of the trapezoidal oblique wing: $\Lambda = 60°, M = 0.95$.

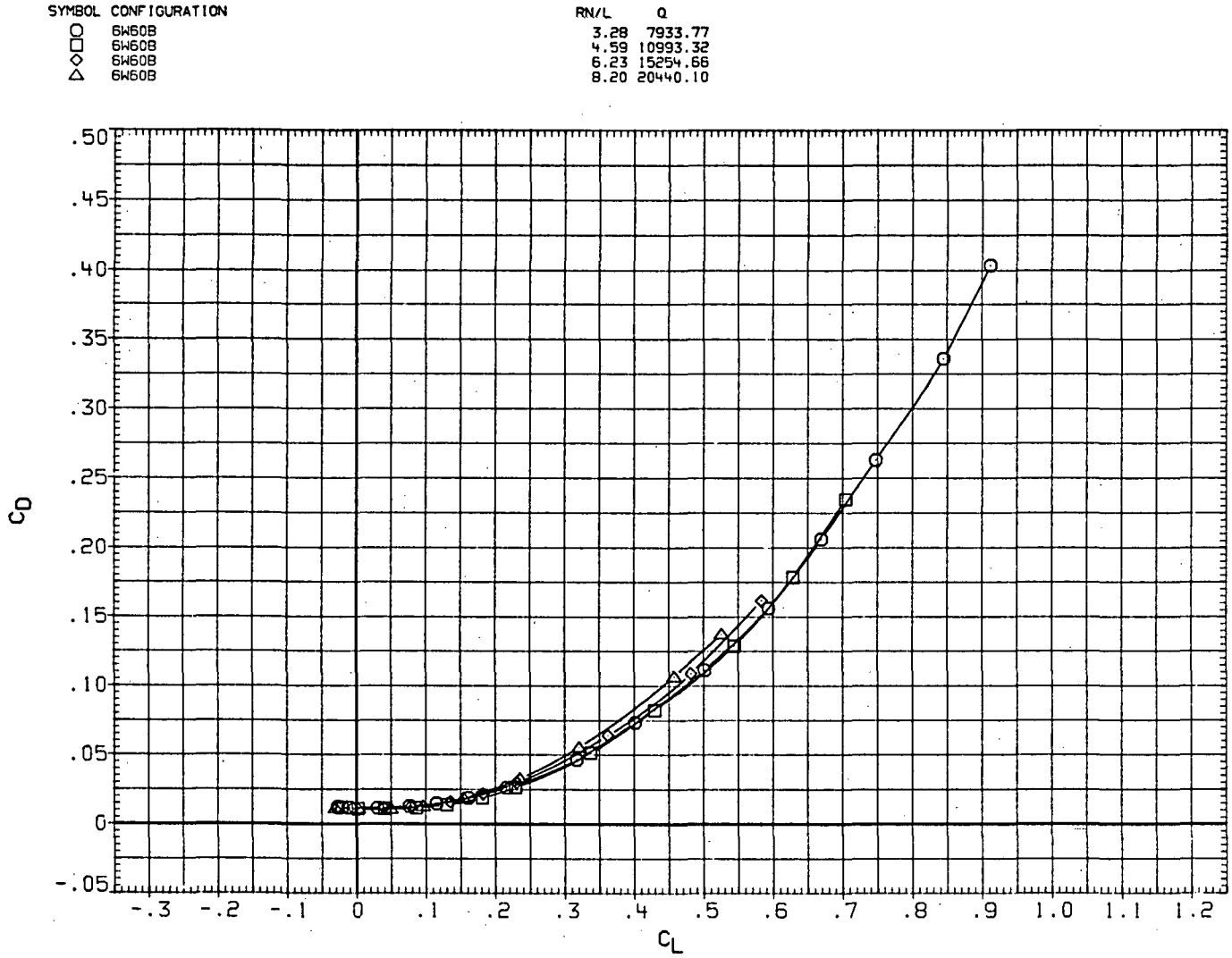


(b) $C_D$ vs $C_L$

Figure 38.– Continued.

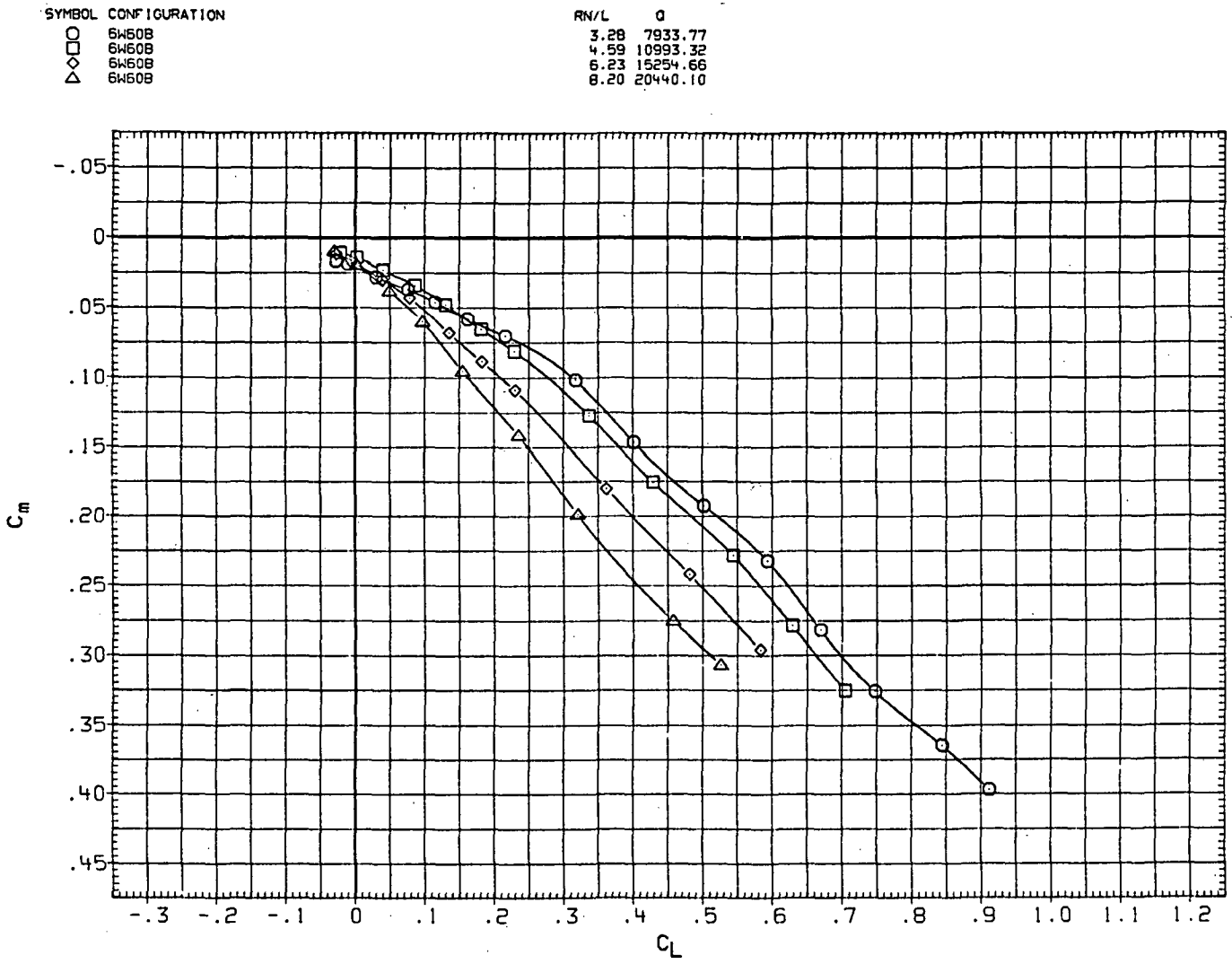


(c) $C_m$ vs $C_L$

Figure 38.– Continued.

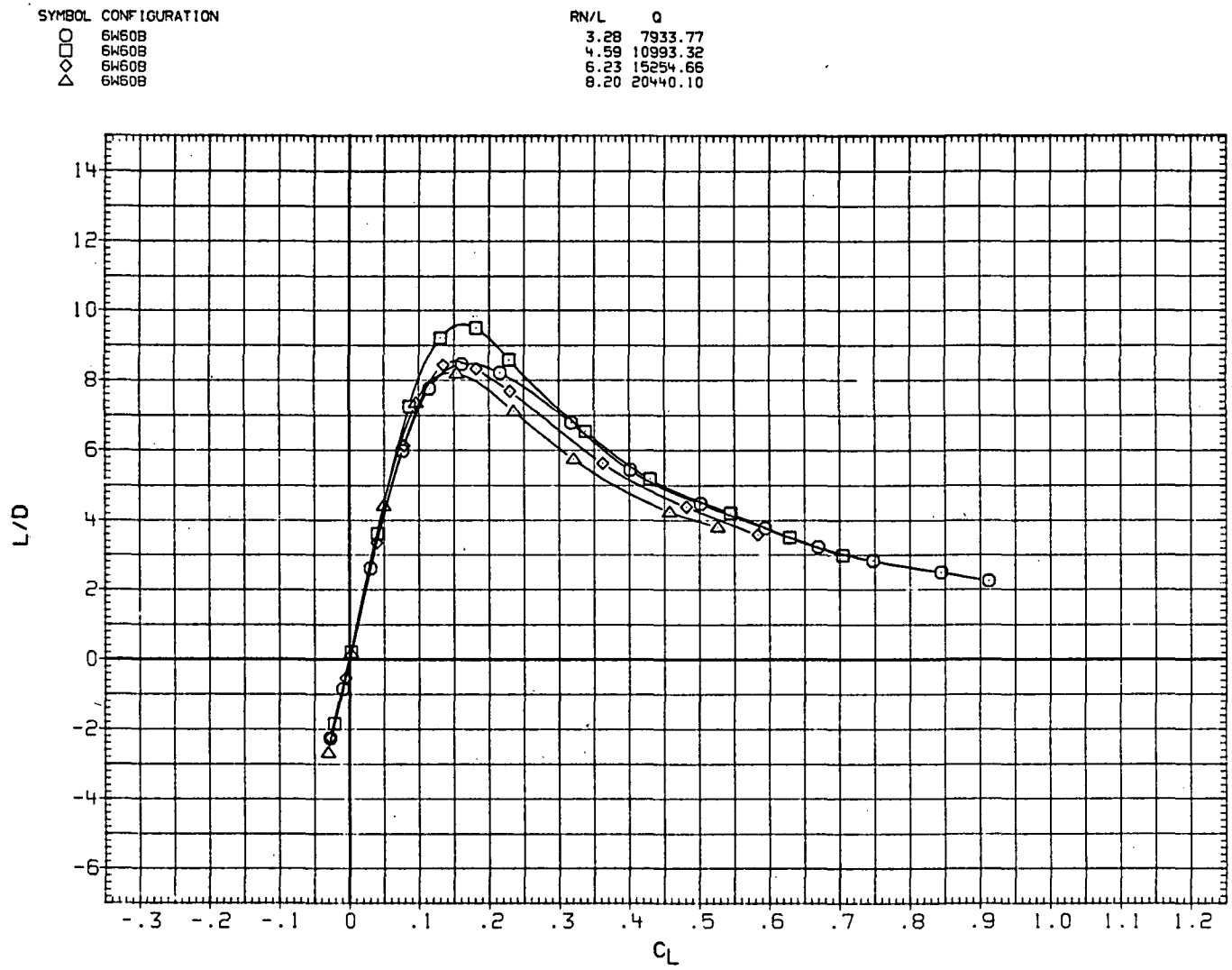


(d) $L/D$ vs $C_L$

Figure 38.– Continued.

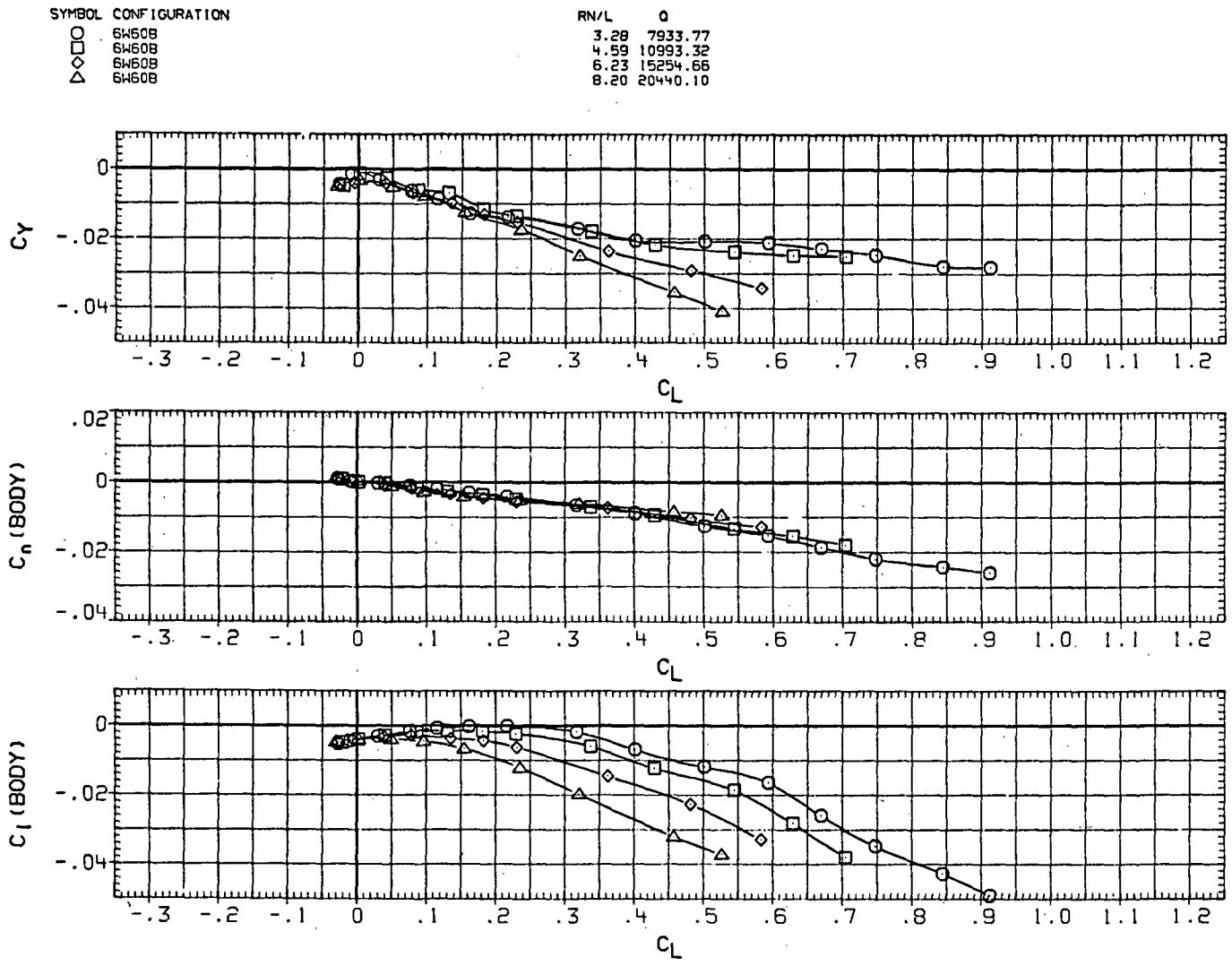


(e) $C_Y$, $C_n$, and $C_l$ vs $C_L$

Figure 38.– Concluded.

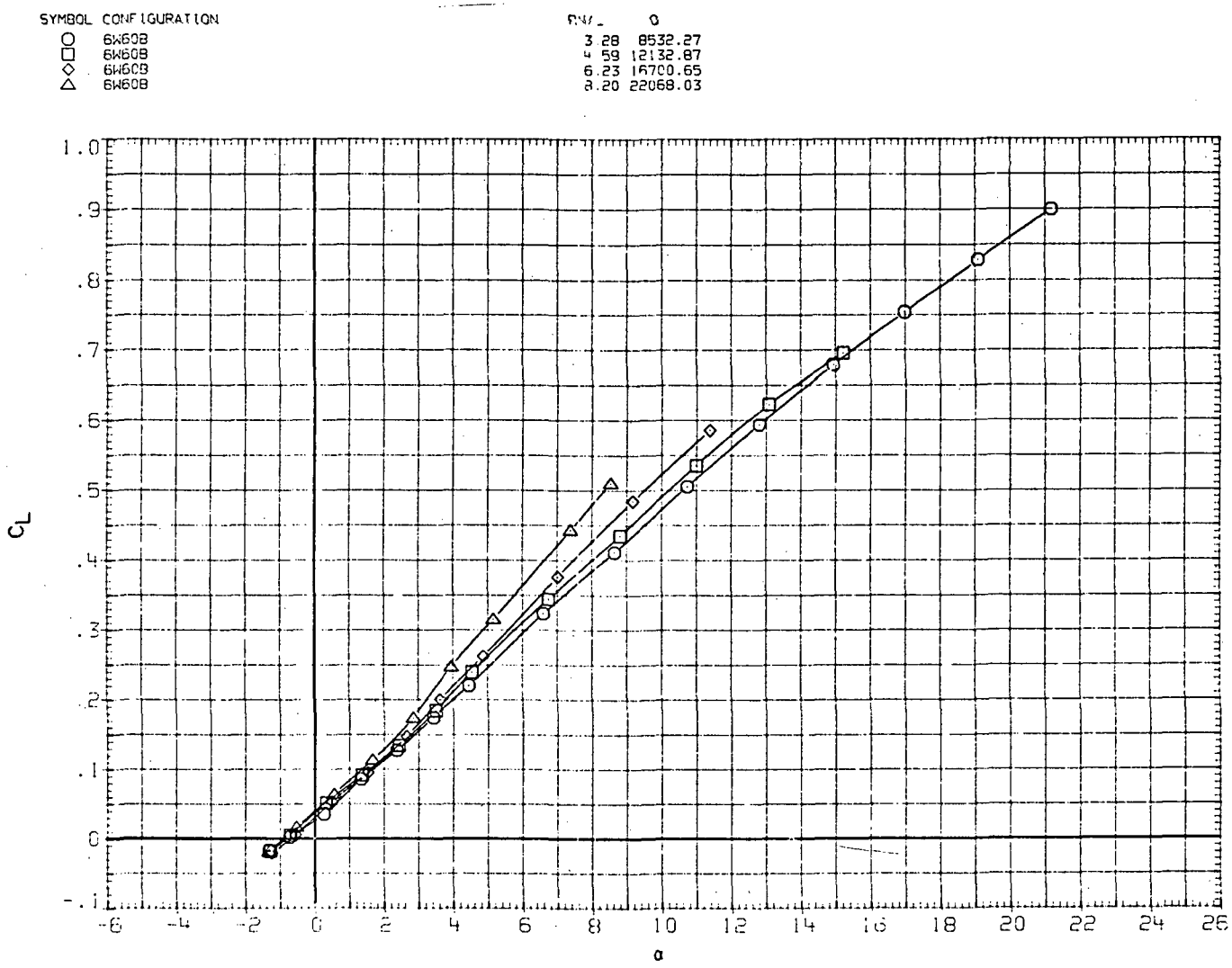


(a) $C_L$ vs $\alpha$

Figure 39.– Flexibility effects due to dynamic-pressure changes on the aerodynamic characteristics of the trapezoidal oblique wing: $\Lambda = 60°, M = 1.1$.

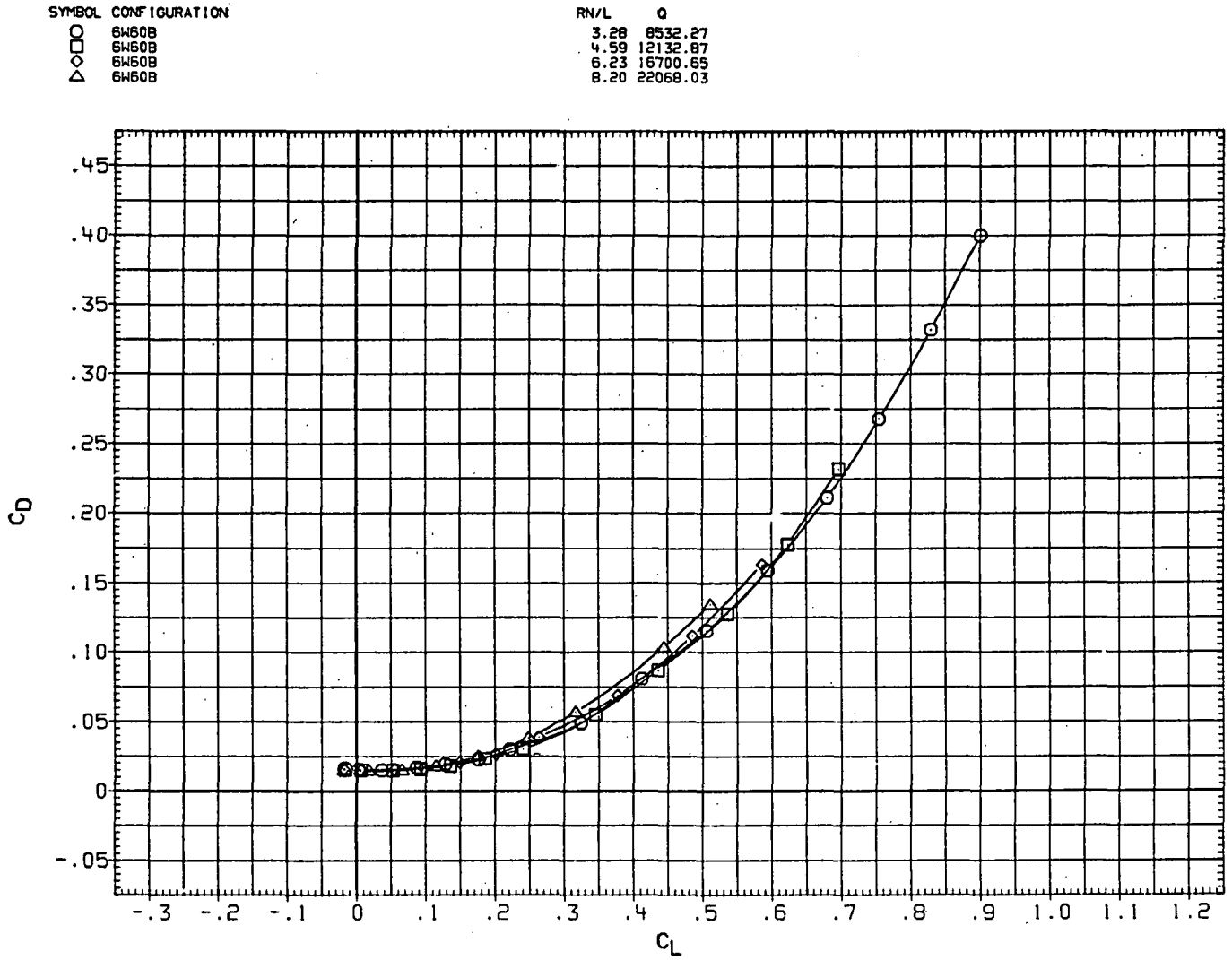


(b) $C_D$ vs $C_L$

Figure 39.– Continued.

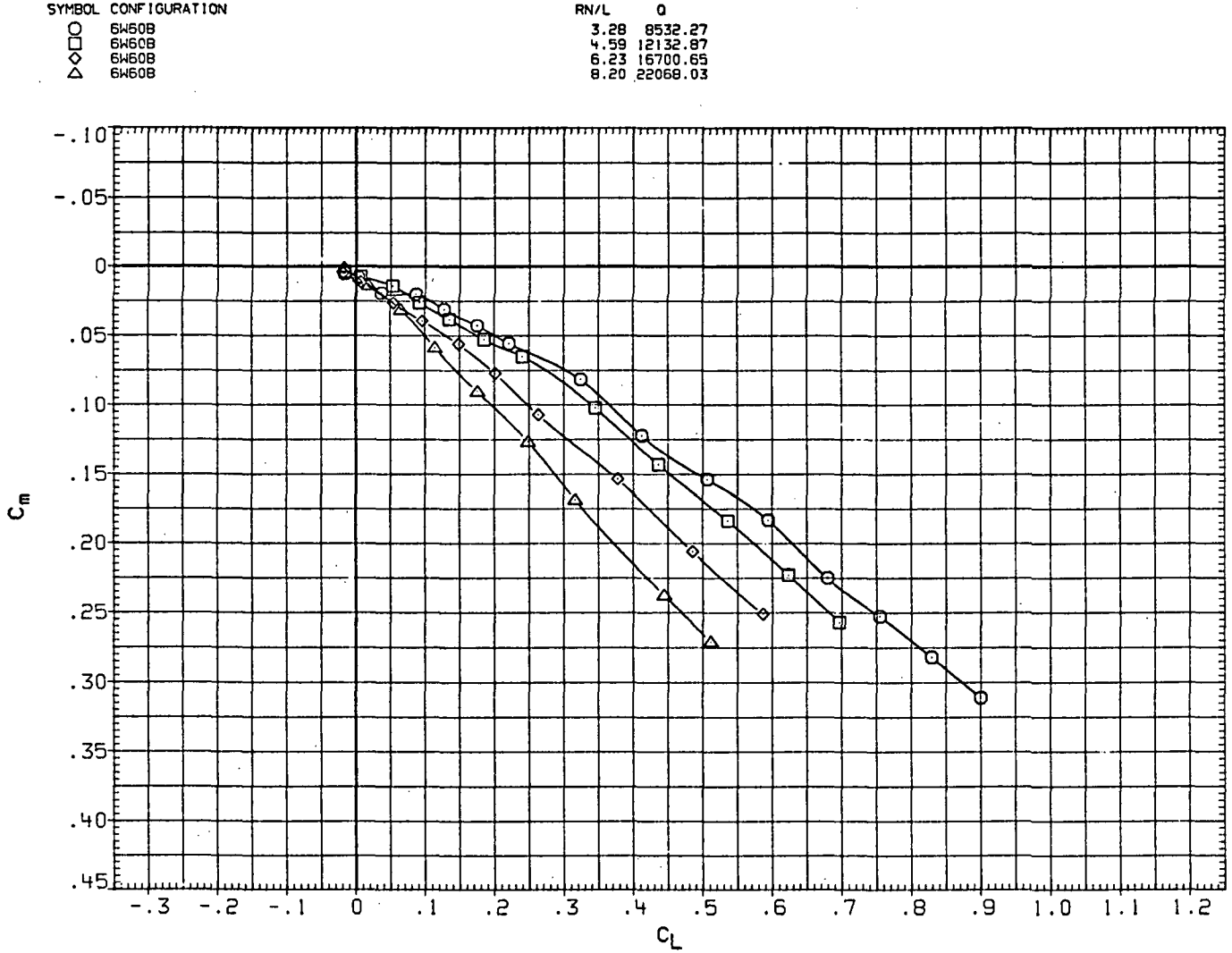


(c) $C_m$ vs $C_L$

Figure 39.– Continued.

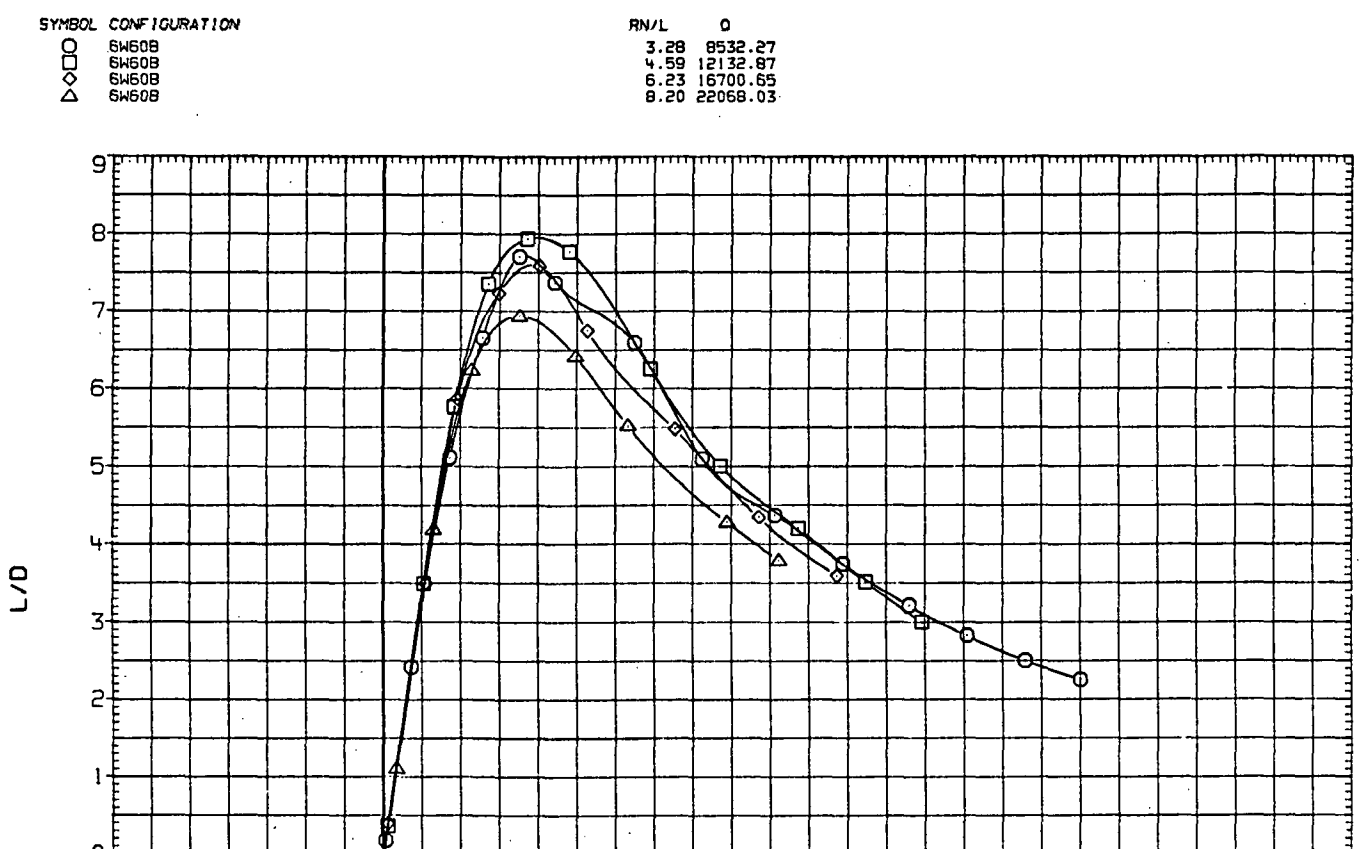


(d) $L/D$ vs $C_L$

Figure 39.– Continued.

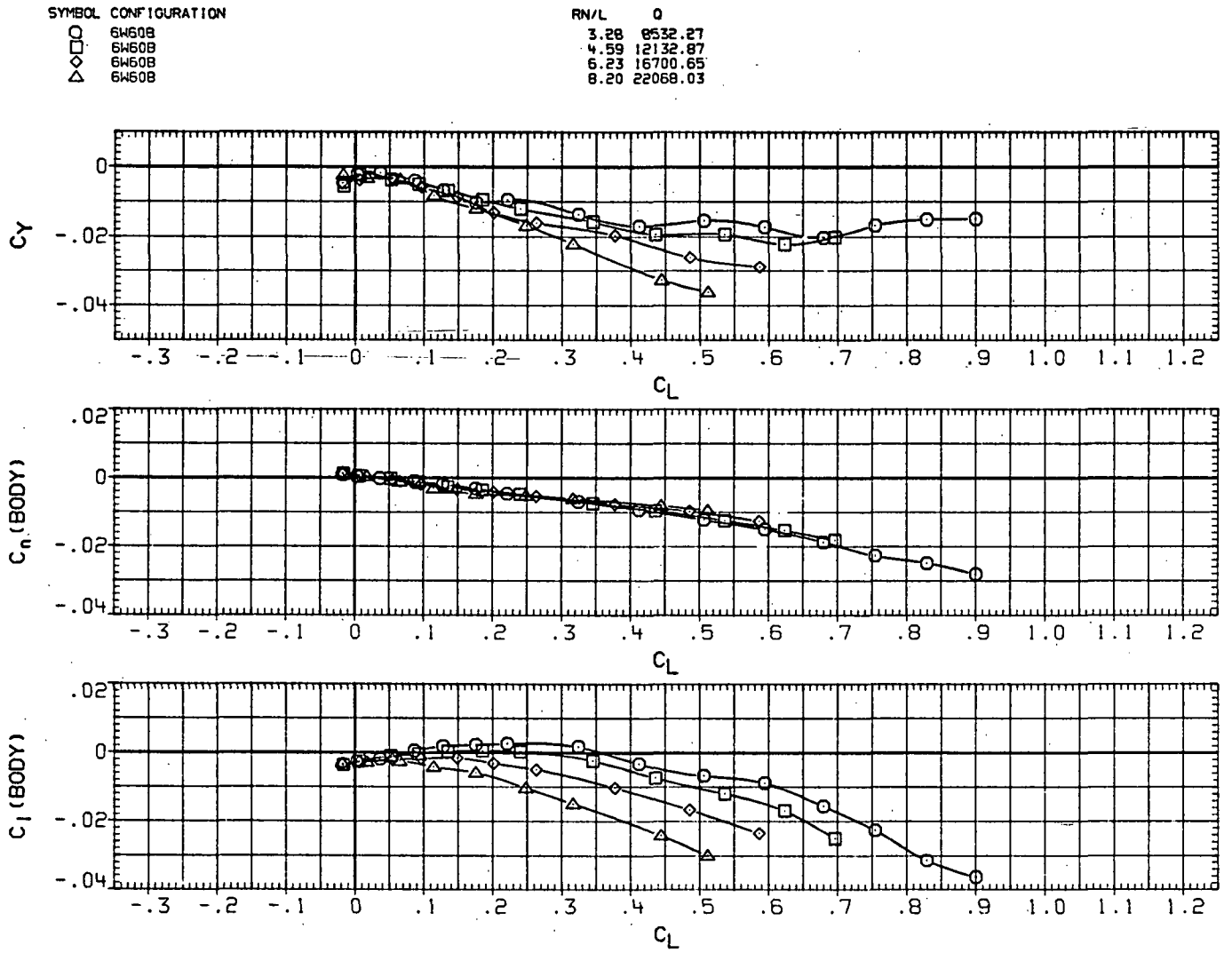


(e) $C_Y$, $C_n$, and $C_l$ vs $C_L$

Figure 39.– Concluded.

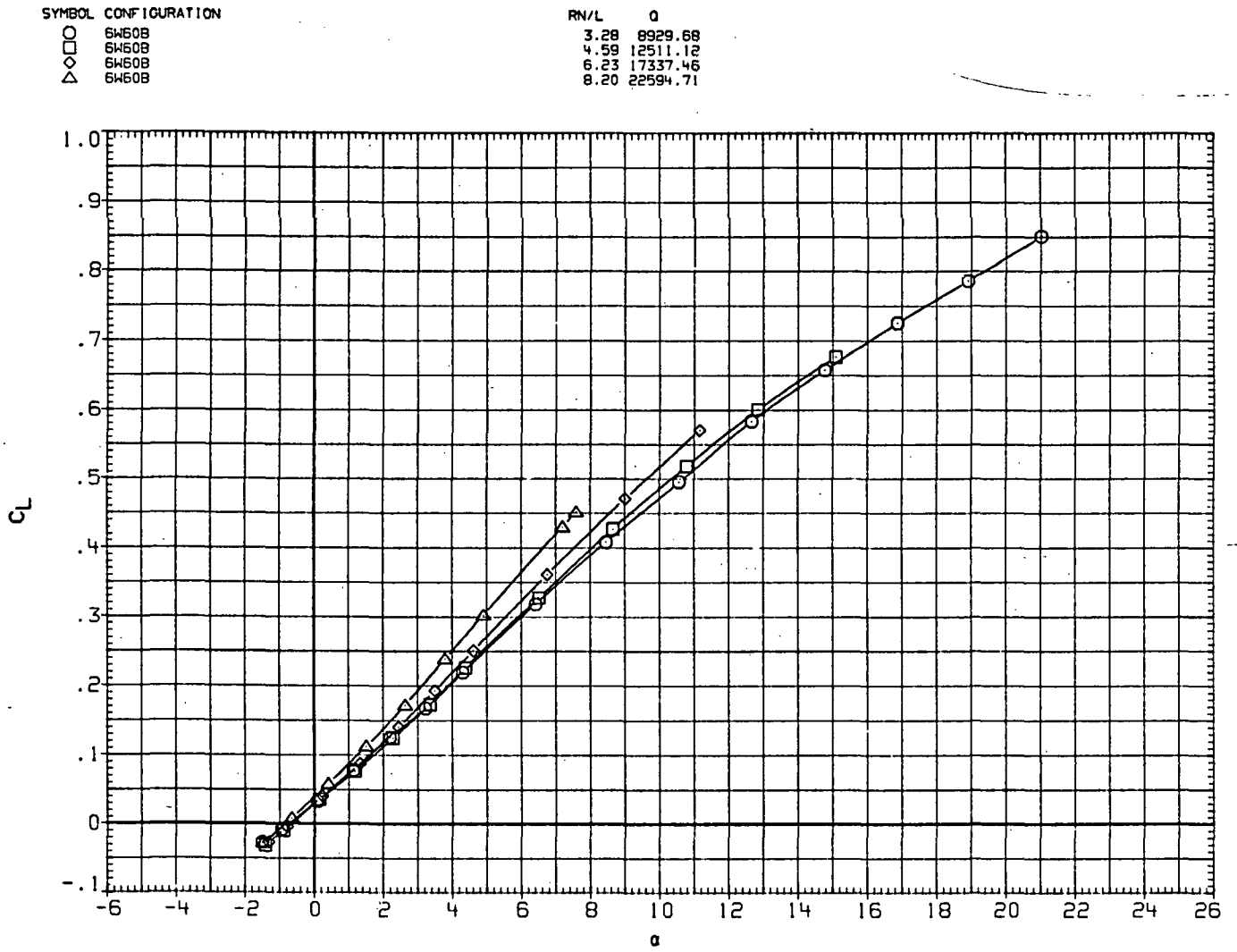


(a) $C_L$ vs $\alpha$

Figure 40.– Flexibility effects due to dynamic-pressure changes on the aerodynamic characteristics of the trapezoidal oblique wing: $\Lambda = 60°, M = 1.2$.

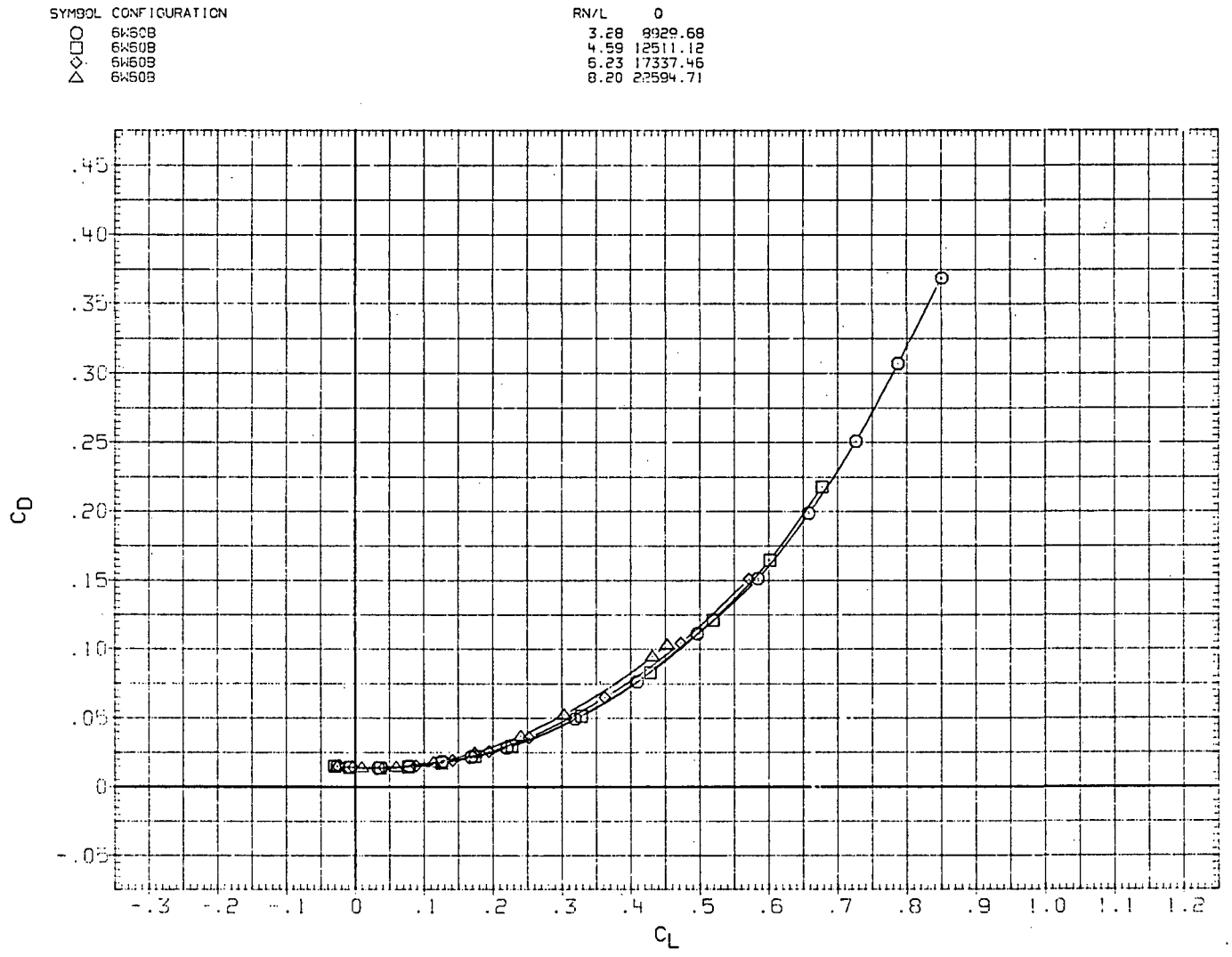


(b) $C_D$ vs $C_L$

Figure 40.– Continued.

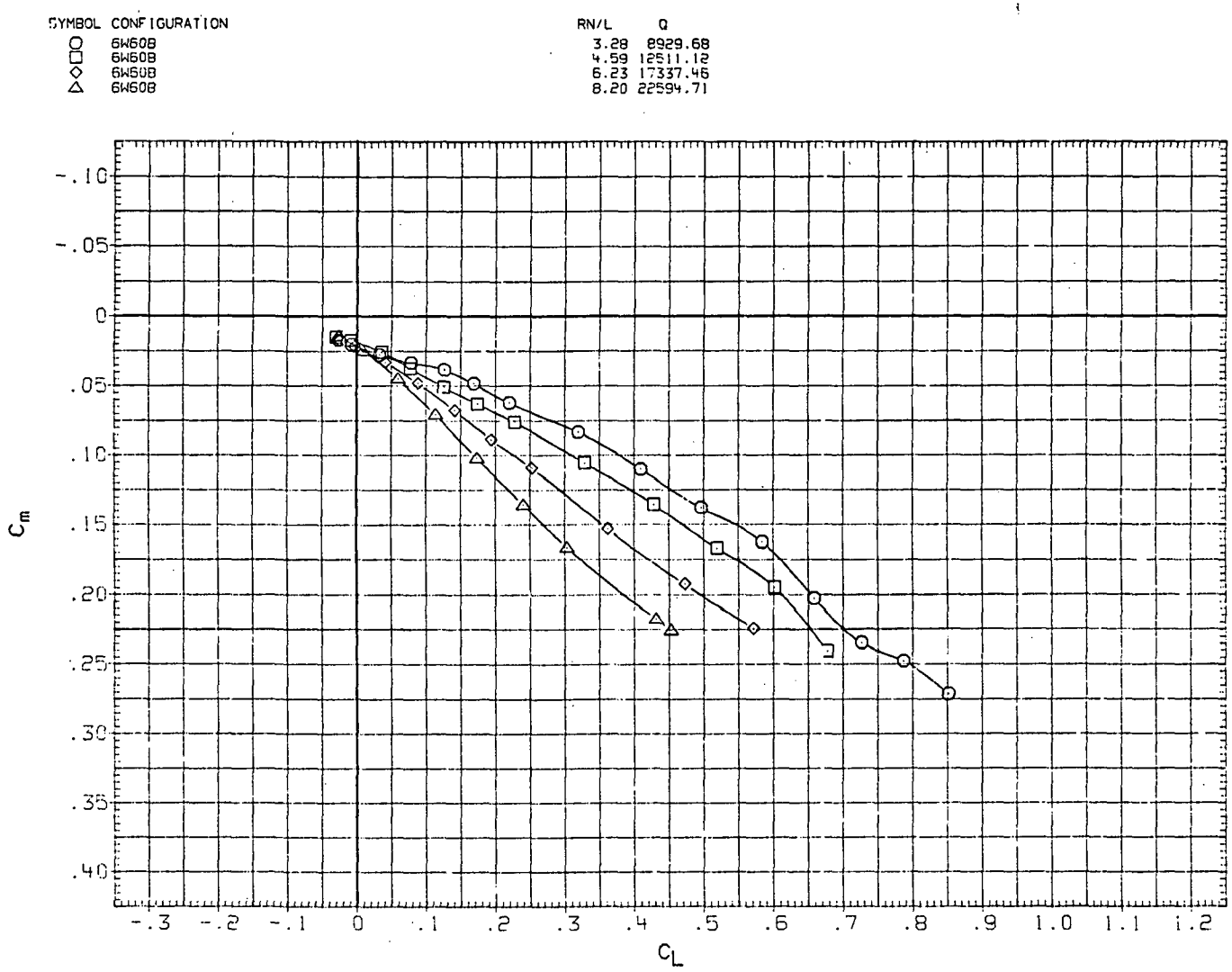


(c) $C_m$ vs $C_L$

Figure 40.– Continued.


(d) $L/D$ vs $C_L$

Figure 40.– Continued.

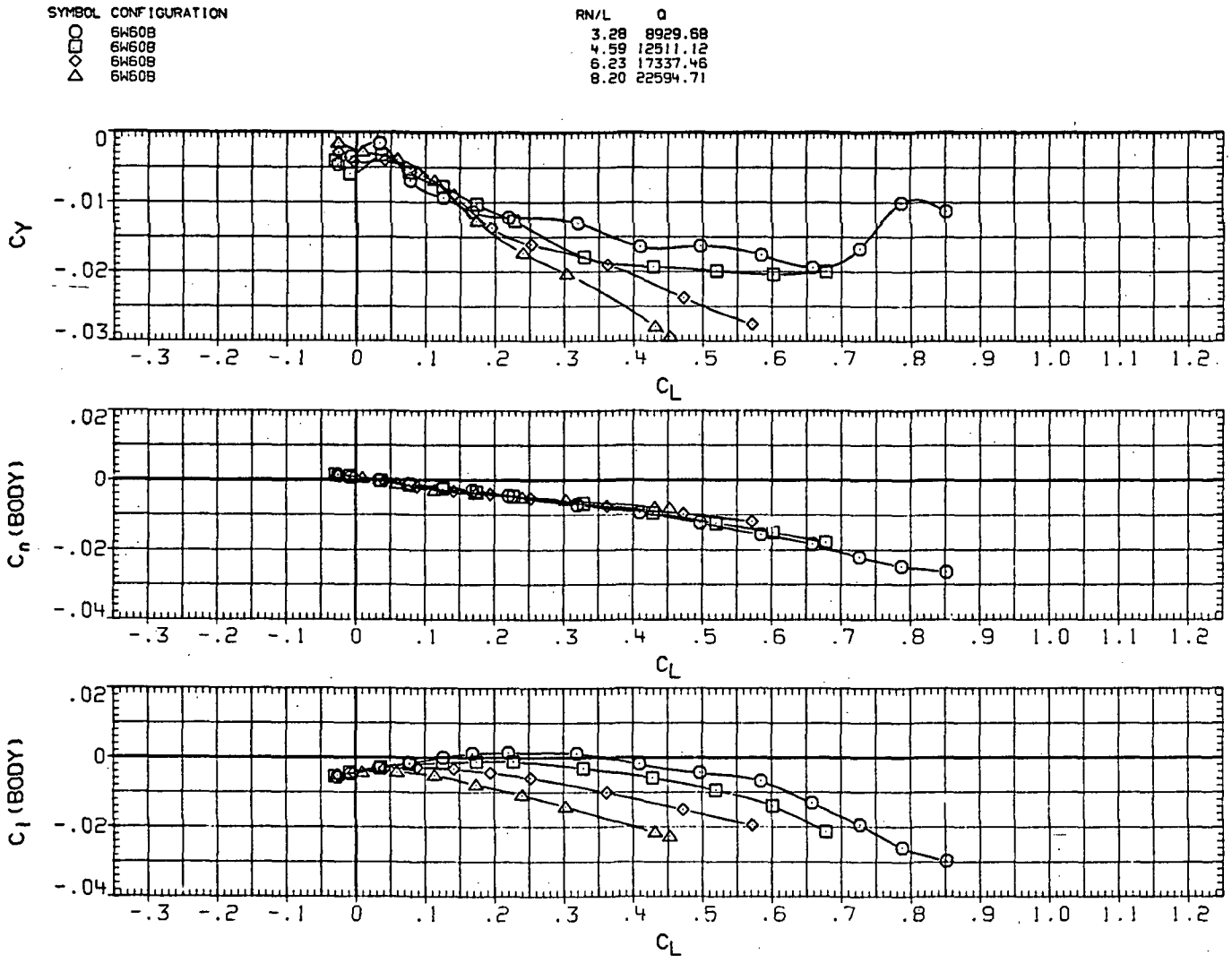


(e) $C_Y$, $C_n$, and $C_l$ vs $C_L$

Figure 40.– Concluded.

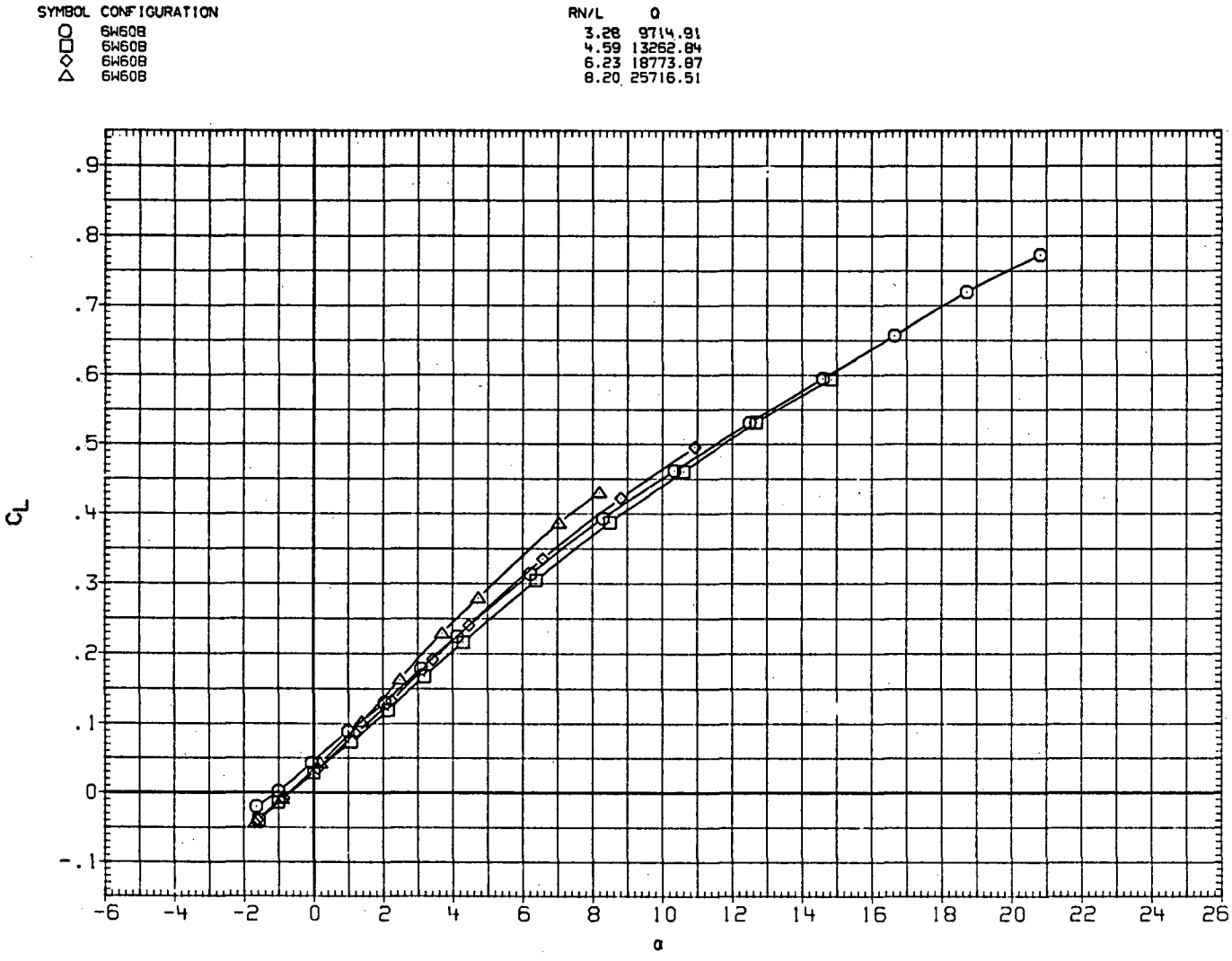


(a) $C_L$ vs $\alpha$

Figure 41.– Flexibility effects due to dynamic-pressure changes on the aerodynamic characteristics of the trapezoidal oblique wing: $\Lambda = 60°, M = 1.6$.

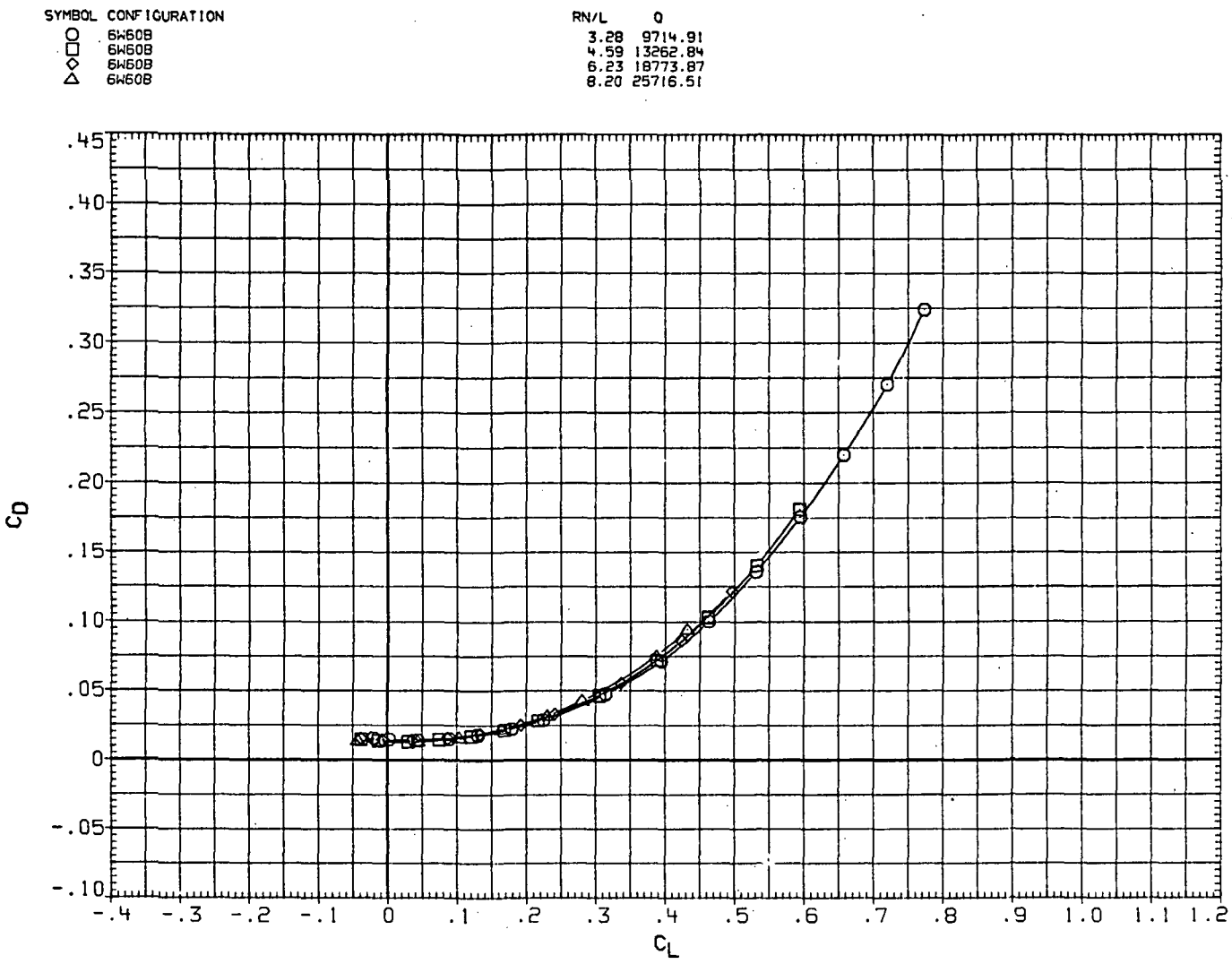


(b) $C_D$ vs $C_L$

Figure 41.– Continued.

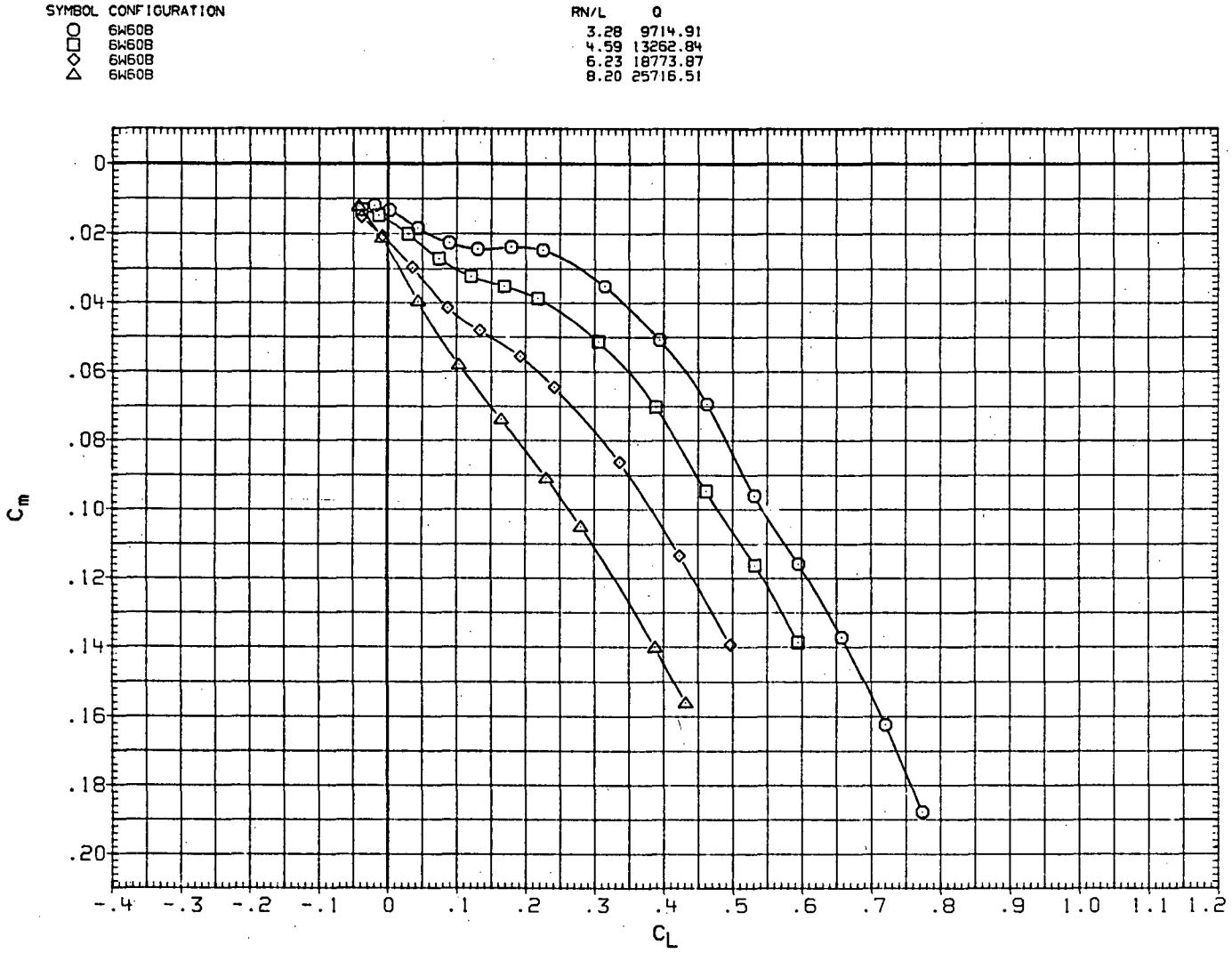


(c) $C_m$ vs $C_L$

Figure 41.– Continued.

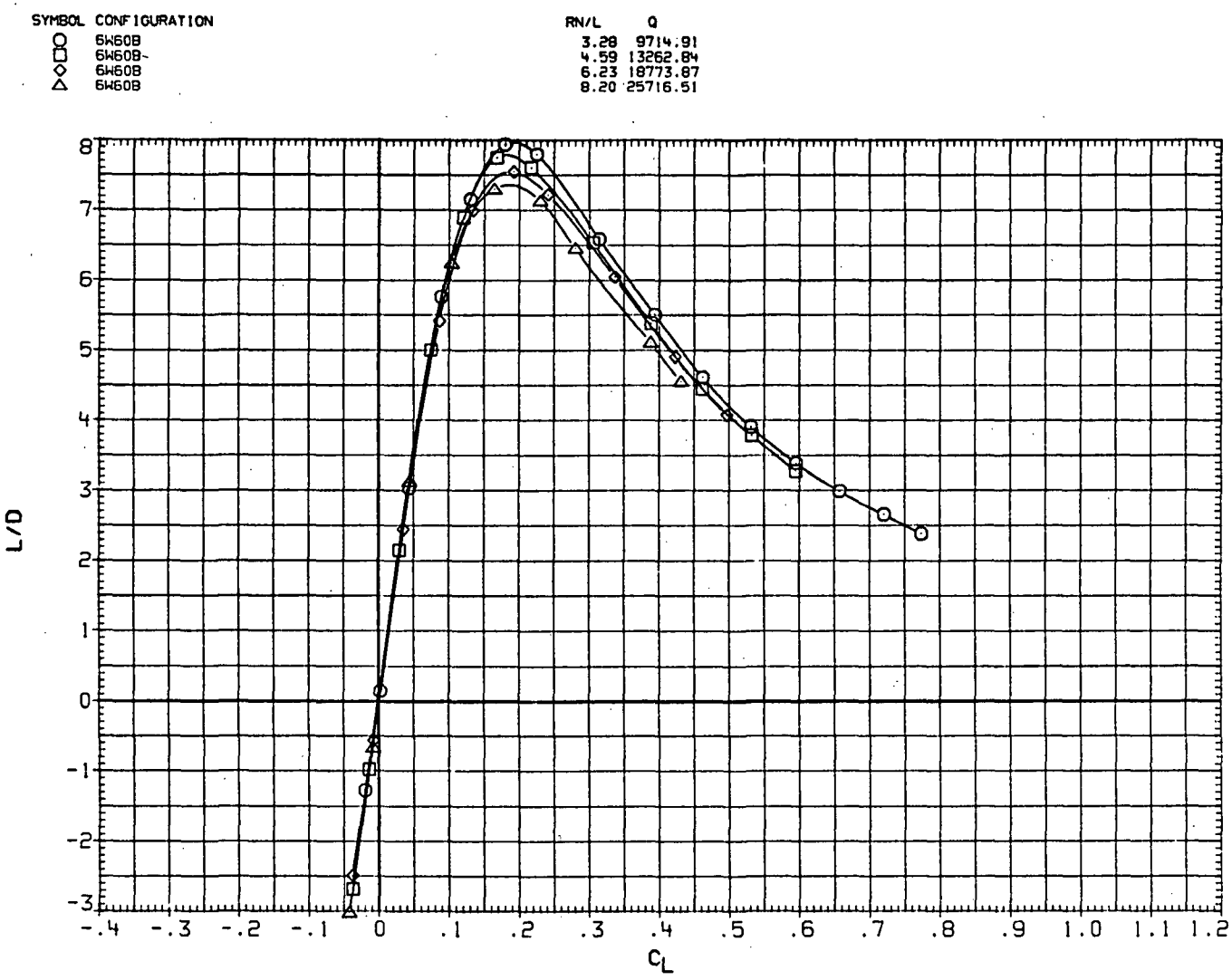


(d) $L/D$ vs $C_L$

Figure 41.– Continued.

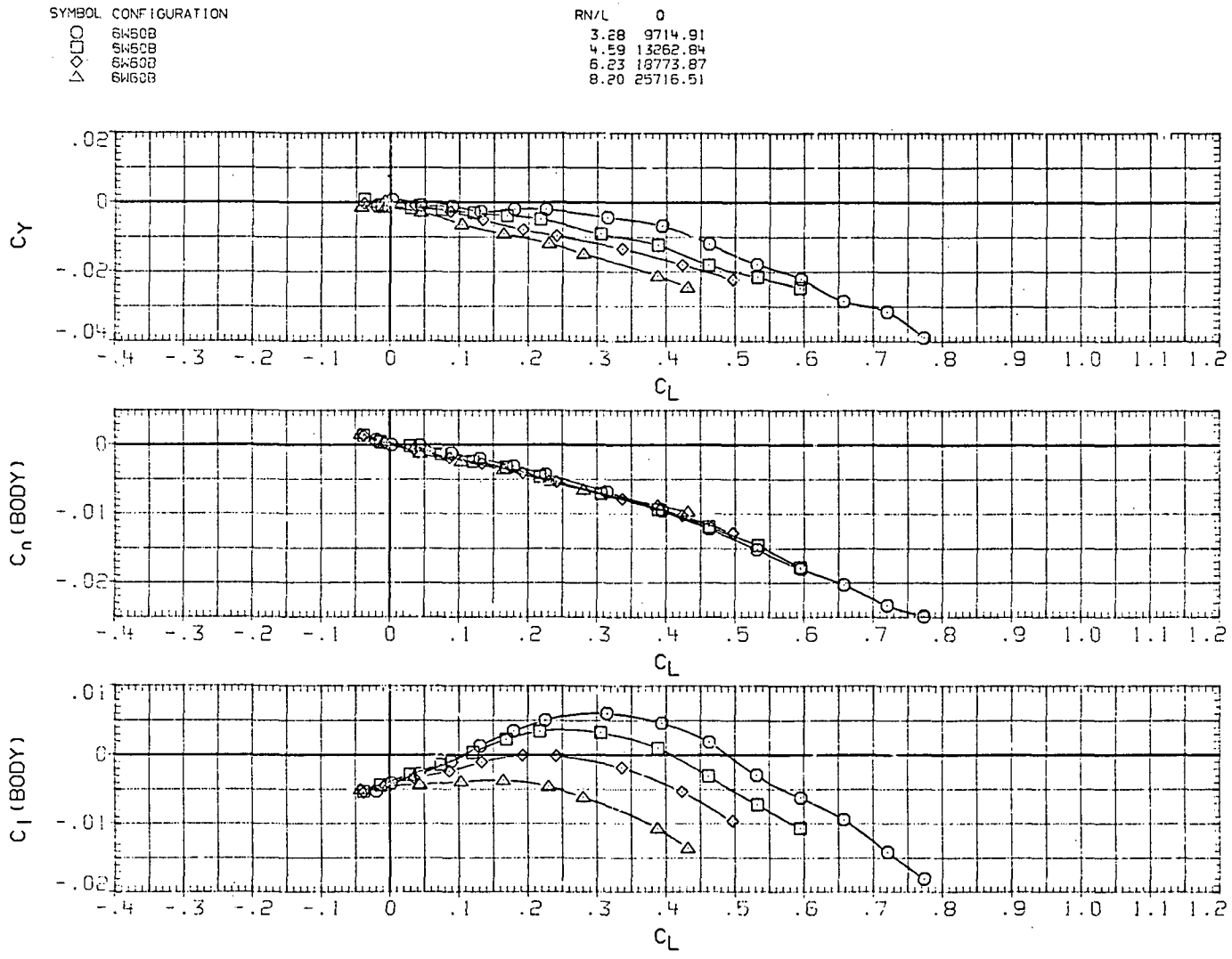


(e) $C_Y$, $C_n$, and $C_l$ vs $C_L$

Figure 41.– Concluded.

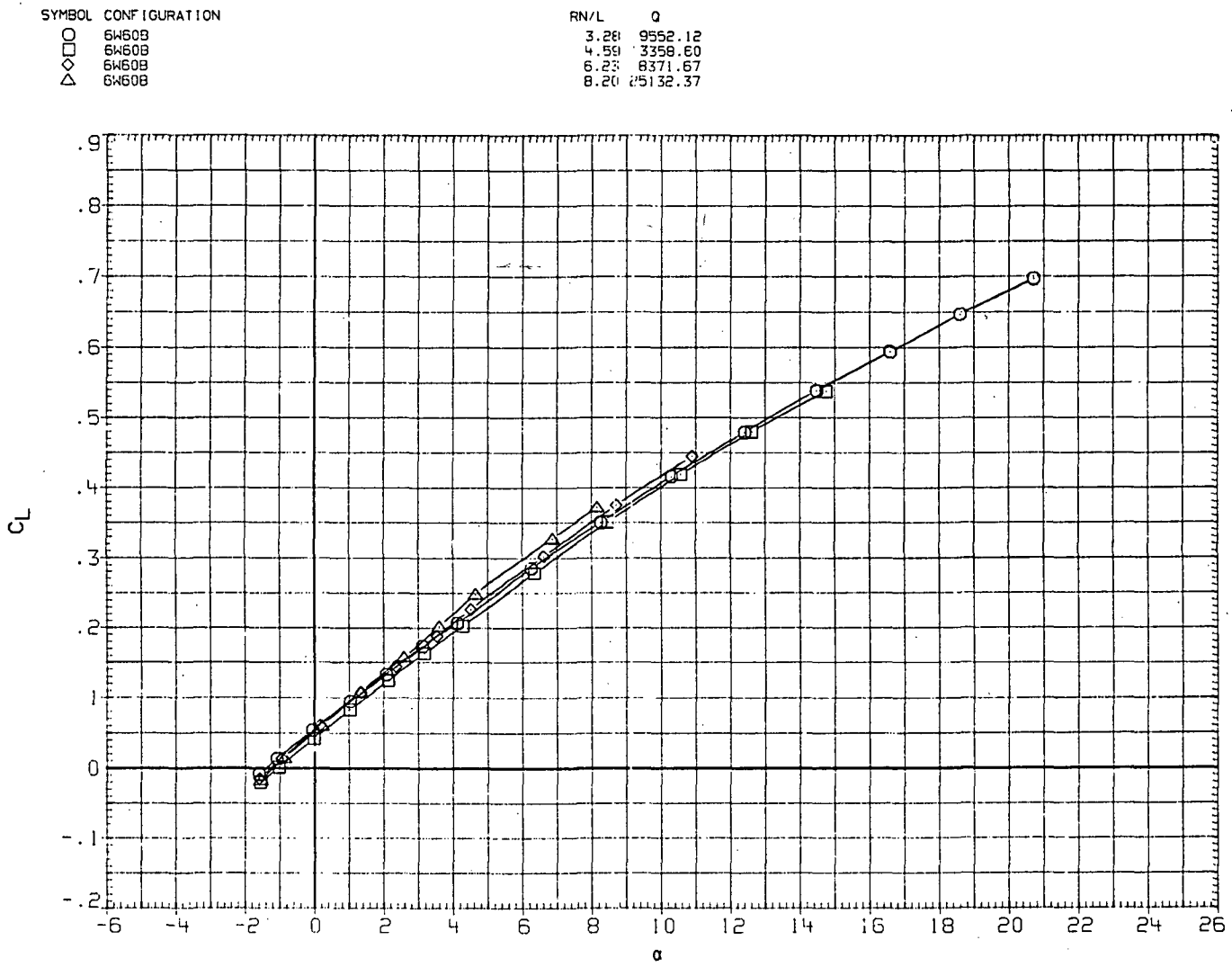


(a) $C_L$ vs $\alpha$

Figure 42.– Flexibility effects due to dynamic-pressure changes on the aerodynamic characteristics of the trapezoidal oblique wing: $\Lambda = 60°$, $M = 2.0$.

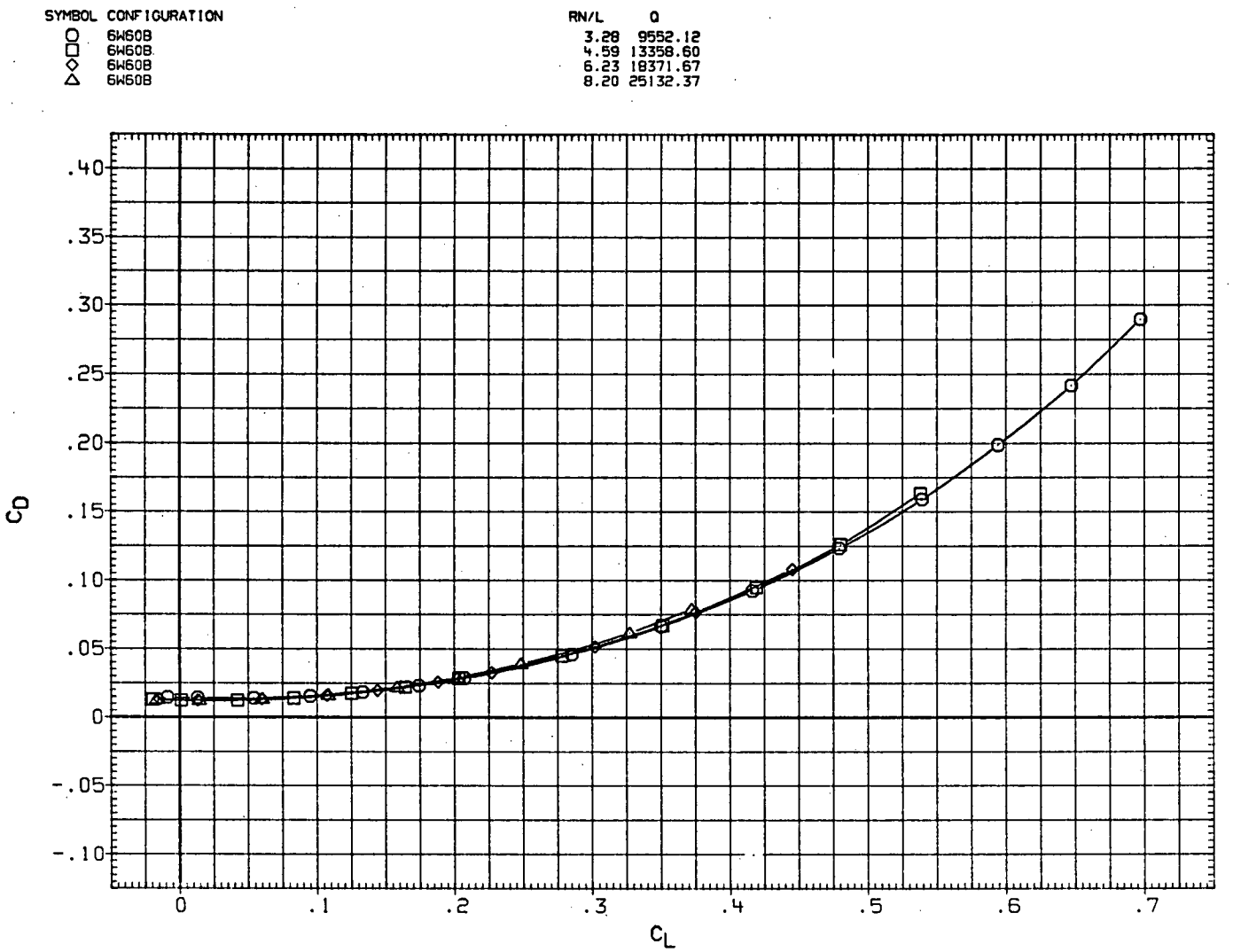


(b) $C_D$ vs $C_L$

Figure 42.– Continued.

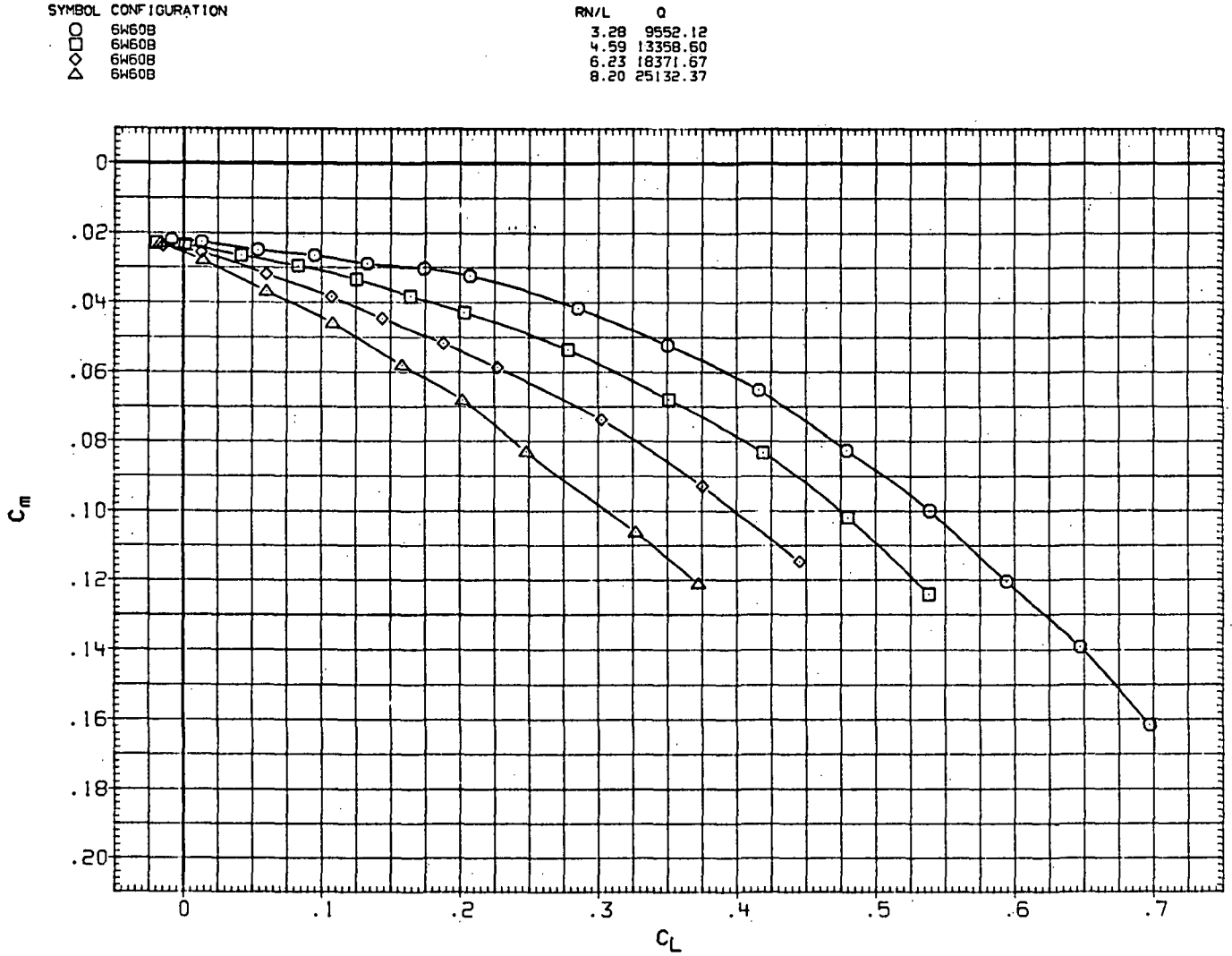


(c) $C_m$ vs $C_L$

Figure 42.– Continued.


(d) $L/D$ vs $C_L$

Figure 42.– Continued.

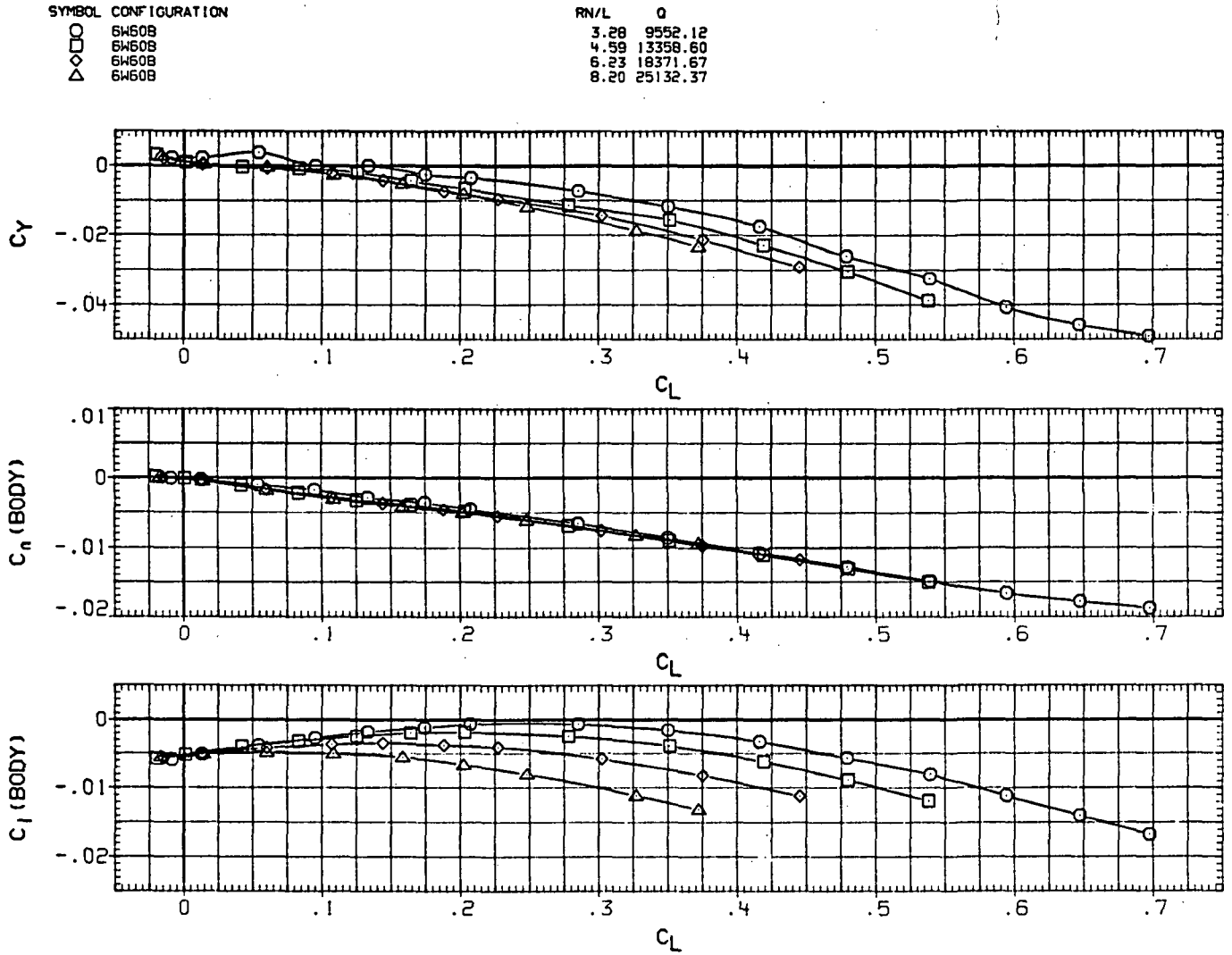


(e) $C_Y$, $C_n$, and $C_l$ vs $C_L$

Figure 42.– Concluded.

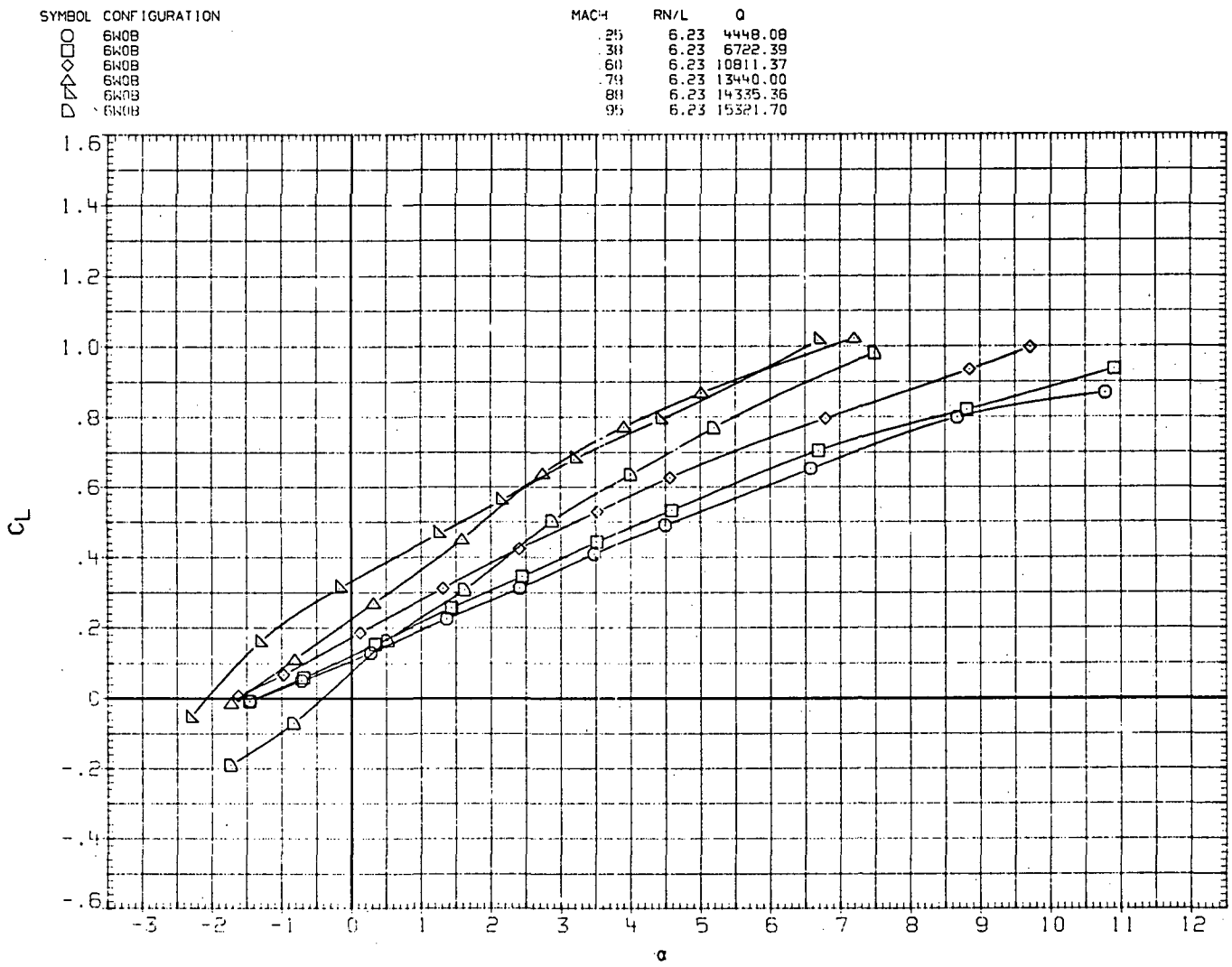


(a) $C_L$ vs $\alpha$

Figure 43.– Effect of Mach number on the aerodynamic characteristics of the trapezoidal oblique wing: $\Lambda = 0$.

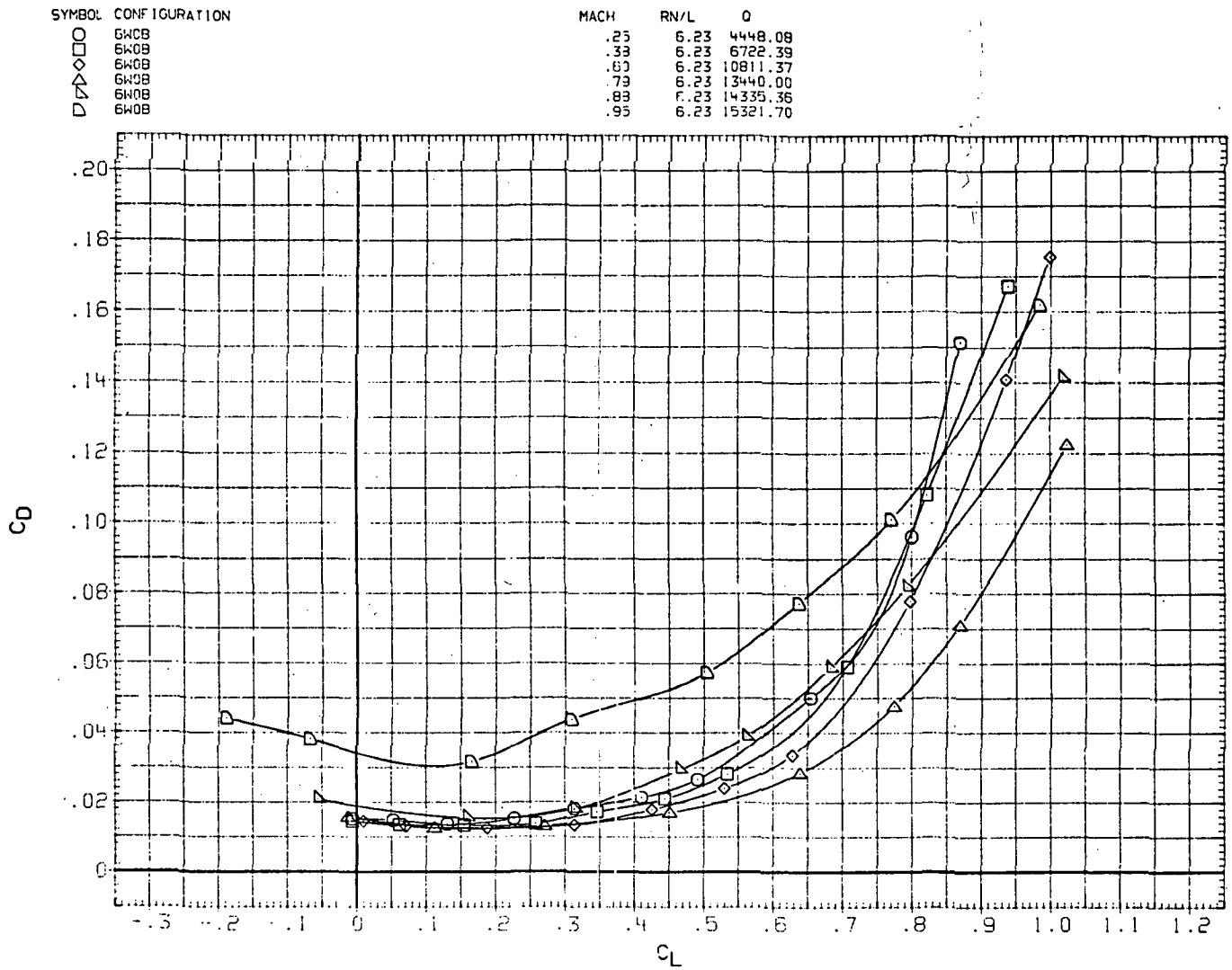


(b) $C_D$ vs $C_L$

Figure 43.– Continued.

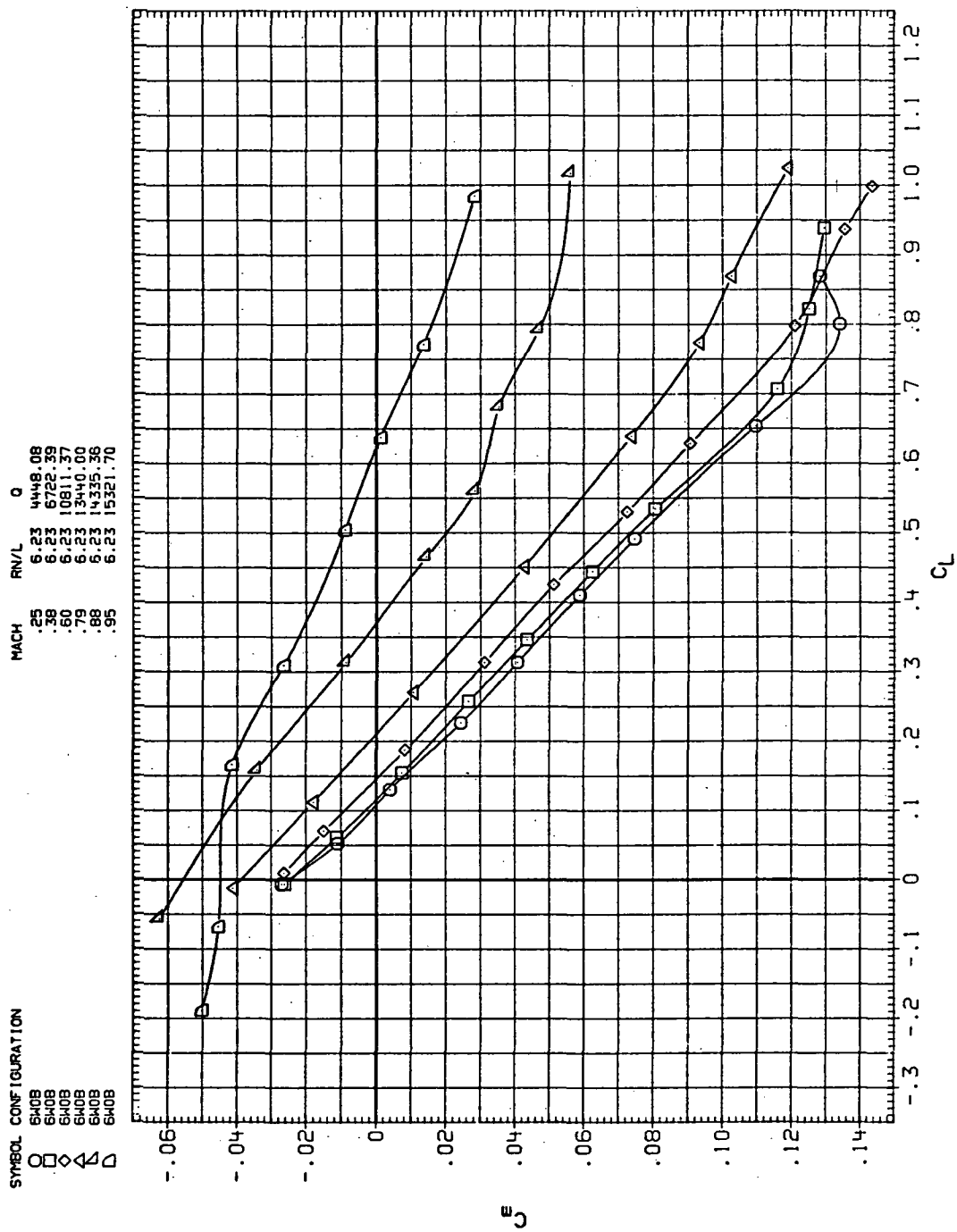


(c) $C_m$ vs $C_L$

Figure 43.– Continued.

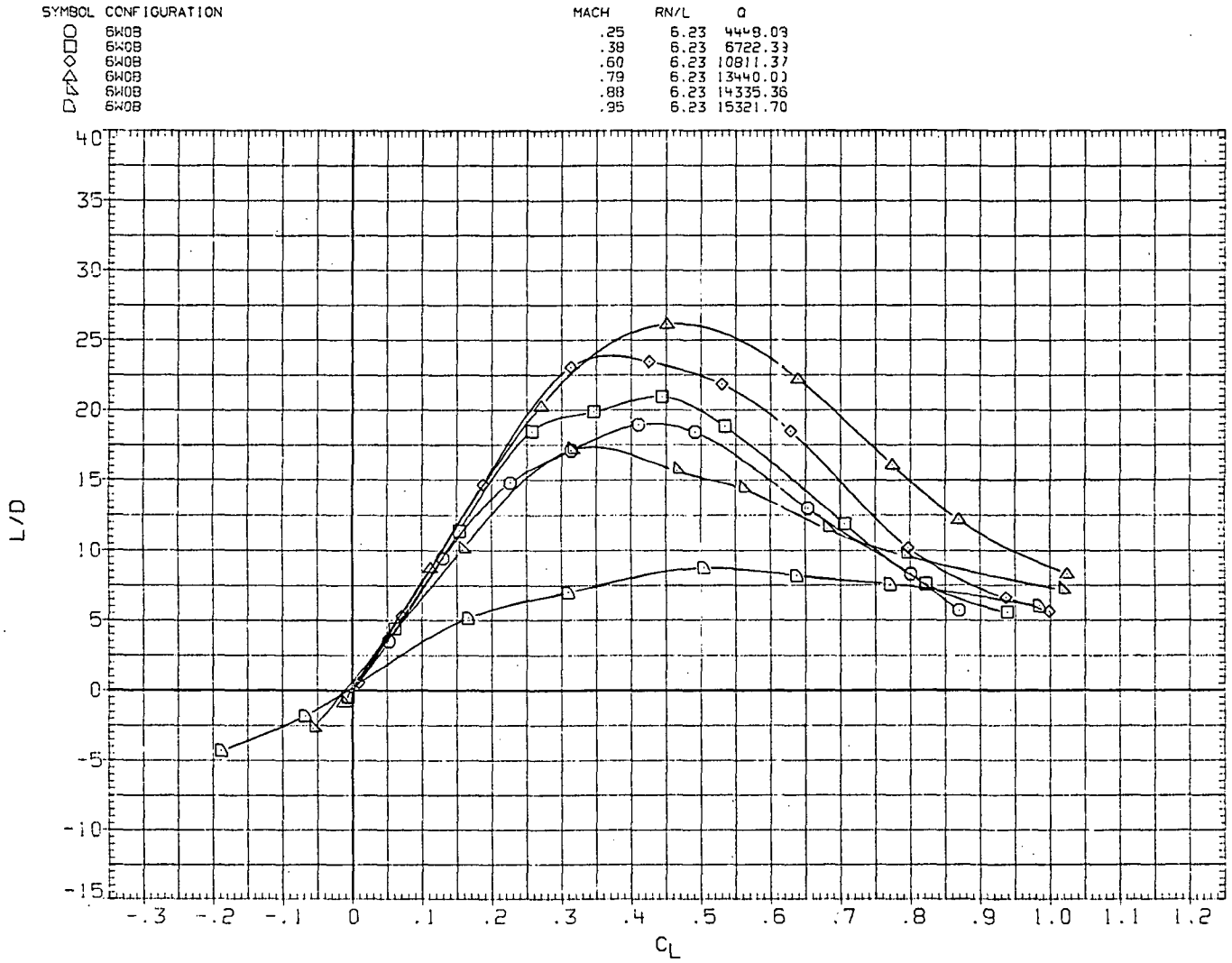


(d) $L/D$ vs $C_L$

Figure 43.– Continued.

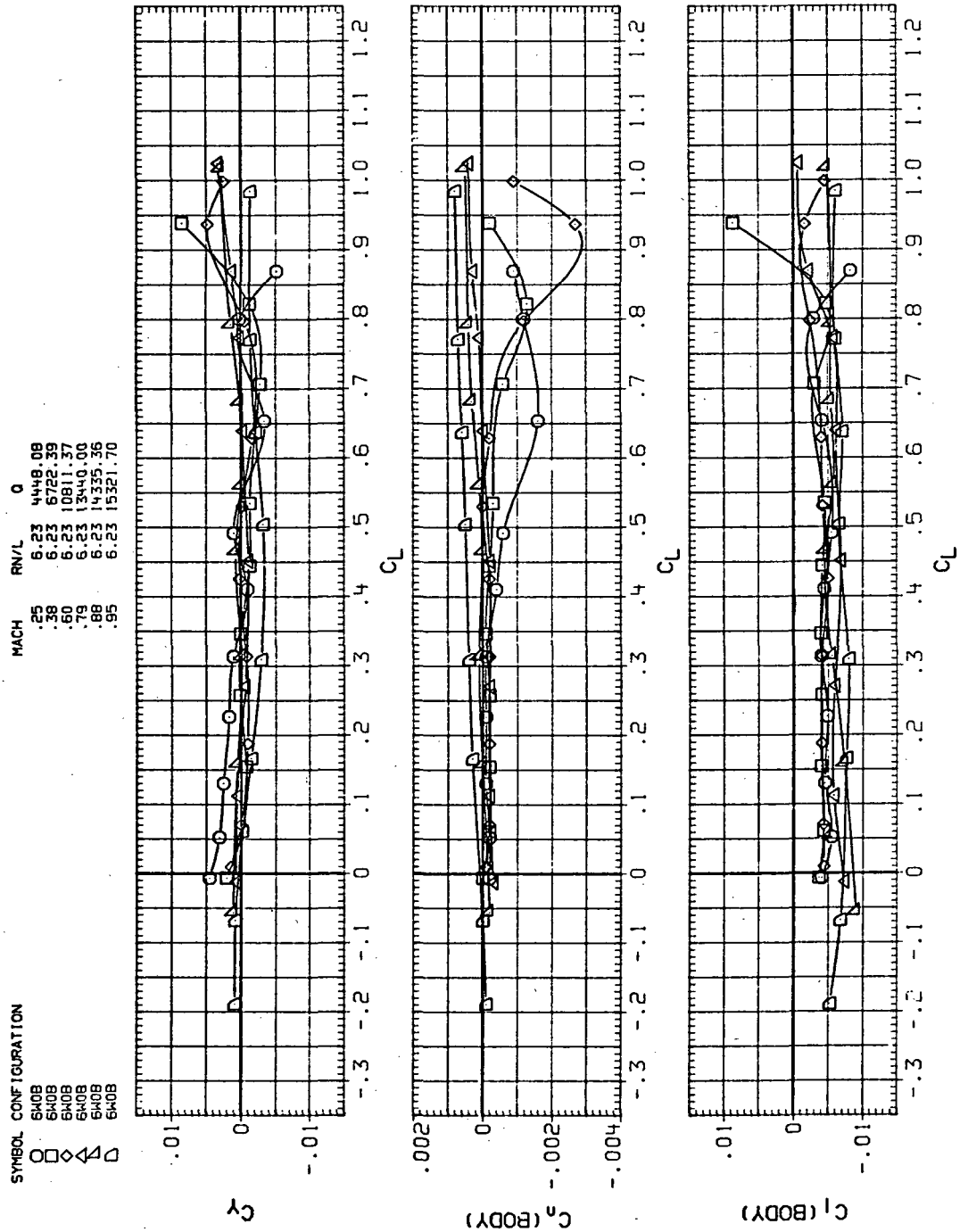


(e) $C_Y$, $C_n$, and $C_l$ vs $C_L$

Figure 43.– Concluded.

NATIONAL AERONAUTICS AND SPACE ADMINISTRATION
WASHINGTON, D.C. 20546

OFFICIAL BUSINESS
PENALTY FOR PRIVATE USE $300

SPECIAL FOURTH-CLASS RATE BOOK

POSTAGE AND FEES PAID
NATIONAL AERONAUTICS AND SPACE ADMINISTRATION
451

U.S.MAIL

POSTMASTER : If Undeliverable (Section 15 Postal Manual) Do Not Retu

*"The aeronautical and space activities of the United States shall be conducted so as to contribute . . . to the expansion of human knowledge of phenomena in the atmosphere and space. The Administration shall provide for the widest practicable and appropriate dissemination of information concerning its activities and the results thereof."*

—NATIONAL AERONAUTICS AND SPACE ACT OF 1958

# NASA SCIENTIFIC AND TECHNICAL PUBLICATIONS

TECHNICAL REPORTS: Scientific and technical information considered important, complete, and a lasting contribution to existing knowledge.

TECHNICAL NOTES: Information less broad in scope but nevertheless of importance as a contribution to existing knowledge.

TECHNICAL MEMORANDUMS: Information receiving limited distribution because of preliminary data, security classification, or other reasons. Also includes conference proceedings with either limited or unlimited distribution.

CONTRACTOR REPORTS: Scientific and technical information generated under a NASA contract or grant and considered an important contribution to existing knowledge.

TECHNICAL TRANSLATIONS: Information published in a foreign language considered to merit NASA distribution in English.

SPECIAL PUBLICATIONS: Information derived from or of value to NASA activities. Publications include final reports of major projects, monographs, data compilations, handbooks, sourcebooks, and special bibliographies.

TECHNOLOGY UTILIZATION PUBLICATIONS: Information on technology used by NASA that may be of particular interest in commercial and other non-aerospace applications. Publications include Tech Briefs, Technology Utilization Reports and Technology Surveys.

***Details on the availability of these publications may be obtained from:***

**SCIENTIFIC AND TECHNICAL INFORMATION OFFICE**

**NATIONAL AERONAUTICS AND SPACE ADMINISTRATION**

**Washington, D.C. 20546**